IDENTIFICATION AND SYNTHESIS OF SMALL MOLECULES IN CAENORHABDITIS ELEGANS

A Dissertation

Presented to the Faculty of the Graduate School

Of Cornell University

In Partial Fulfillment of the Requirements for the Degree of

Doctor of Philosophy

By

Russell Nicholas Burkhardt

December 2021

IDENTIFICATION AND SYNTHESIS OF SMALL MOLECULES IN CAENORHABDITIS ELEGANS

Russell Nicholas Burkhardt, Ph.D.

Cornell University 2021

Due to its high homology to higher animals, *Caenorhabditis elegans* has become one of the most important model organisms for human biology. It has become the model of choice for studying development, aging, and diabetes. Whereas *C. elegans* genetics and physiology have been studied extensively, its metabolome has remained largely uncharacterized. However, recent studies indicate that yet unidentified small molecules may be involved in regulating almost every aspect of *C elegans*' life history.

This dissertation presents contributions to the collective knowledge of small molecules that are associated with organismal development and sex. We began our investigations with a comprehensive comparison of the metabolome of male nematodes, which are present as a small minority in a population of *C. elegans* and, with that of the dominant sex, the hermaphrodites. Next, through the use of mutant animals, we investigated which male-specific compounds are derived from the male germline and which compounds are derived from the male soma, and how production of these compounds is tied to development and aging. One of the compounds we identified was nacq#1, which increases the rate of sexual development and reproduction in hermaphrodites at the expense of a shortened lifespan. In addition to nacq#1, we found five additional classes of compounds, as well as other individual small molecules, that are enriched in or specific to males. In addition, we contributed new chemical tools to investigate the biology of a known class of molecules called dafachronic acids (dafa#s) which are responsible for

continued development of *C. elegans*. Through isotopic labeling we probed the metabolism of known dafachronic acids to find potentially more active ligands as well as degradation products.

BIOGRAPHICAL SKETCH

Russell Nicholas Burkhardt was raised in State College, PA and graduated as a National Merit Scholar from the State College Area High School in 2011. Russell then attended the Rochester Institute of Technology as an Honors Student, where he joined the lab of Dr. Jeremy Cody after completing his first quarter. In Dr. Cody's lab Russell worked on natural product synthesis of bioactive alkaloids, becoming a GlaxoSmithKline Summer Research Follow. During the summer of 2013 Russell worked in the lab of Dr. Peter Baran at Juniata College studying the interactions of coordination compounds in red wine. The following summer he was a summer student intern at the National Institutes of Health's National Institute on Drug Abuse, studying selective ligands for the dopamine D4 receptor. In 2011, Russell graduated from RIT to pursue his Ph.D. at Cornell University in the Department of Chemistry and Chemical Biology. At Cornell, Russell joined the lab of Dr. Frank Schroeder and was selected to participate in the Chemistry Biology Interface program at Cornell.

This dissertation is dedicated to my parents, Russell and Marlene, who,

through their love and support, made me the man I am today,

and my sister Sara, who showed me that through hard work anything is possible.

ACKNOWLEDGMENTS

Special Committee Chair and Advisor: Professor Frank C. Schroeder

Special Committee: Professor Brett Fors and Professor Hening Lin

Collaborating Researchers: Dr. Alex Artyukhin, Dr. Joshua A. Baccile, Dr. Bennett Fox, Dr. Pooja Gudibanda, Dr. Maximillian Helf, Dr. Hanno A. Ludewig, Ezra Pak-Harvey, Dr. Pedro Rodrigues, Marco Sanchez-Ayala, Dr. Ying Zhang.

Core Facilities: Dr. Ivan Keresztes, Gary Horvath

Organizations: Department of Chemistry and Chemical Biology of Cornell University, the Boyce Thompson Institute

Funding: Boyce Thompson Institute, Chemistry Biology Interface Training Program (T32GM008500), Cornell University, NSF MRI award CHE-1531632

TABLE OF CONTENTS

LIST OF ABBREVIATIONS

AcOH……Acetic Acid

DCM……Dichloromethane

DMT……*N*,*N*-dimethyltryptamine

DMW……*N*,*N*-dimethyltryptophan

EtOAc……Ethyl Acetate

fem……Feminization

glp……Germline Proliferation

him……High Incidence of Males

HPLC……High Performance Liquid Chromatography

HRMS……High Resolution Mass Spectrometry

KO……Knockout

m/z……Mass-to-Charge Ratio

MeOH……Methanol

MID……Male-Induced Demise

mog……Masculinization of Germline

MS……Mass Spectrometry

MS2……Tandem Mass Spectrometry

NMR……Nuclear Magnetic Resonance

OE……Overexpression

PDDA……Population Density-Dependent Acceleration of aging

SAM……*S*-adenosylmethionine

s.e.m……Standard Error of Means

UHPLC……Ultra-High Performance Liquid Chromatography

VLCPUFA……Very Long Chain Polyunsaturated Fatty Acid

PREFACE

Caenorhabditis elegans, a free-living nematode, has become one of the most well-studied model organisms for biomedical research. Originally proposed for study by Sidney Brenner in 1963, its transparent body, ease of maintenance, and genetic tractability quickly made it popular among biologists and chemists alike[1]. The popularity of *C. elegans* resulted in it becoming the first multicellular organism to have its genome sequenced in 1998[2]. Despite a vast period of evolutionary divergence, a significant majority of proteins in *C. elegans* have a human homolog, making it an ideal candidate for studying many aspects of human health, from the impact of caloric restriction to diabetes, aging, and neurodegenerative diseases[3,4,5]. Despite the wide range of phenotypes relevant to human health research that can be investigated with *C. elegans*, a key aspect affecting many health-relevant pathways has been largely ignored until recent years – sex. As *C. elegans* predominantly exists as a self-replicating hermaphrodite, males, and the impact of sex-specific differences on physiology, were often overlooked. However, accumulating evidence from human and model studies in other organisms, including *C. elegans*, indicates that the different sexes may respond in completely different manners in many biological contexts[6,7].

While the genetic differences between males and hermaphrodites is only in the absence of a second copy of the X chromosome in males, differences in gene expression are pervasive and have been studied extensively through transcriptomics and proteomics[8]. Moreover, preliminary studies by our lab and others have begun to investigate the differences in small molecules and their corresponding responses, and this work aims to expand on these differences in an untargeted manner[9,10].

Preview of Chapters

Chapter 1: Characterization of the male metabolome

In Chapter 1 we discuss our methodology for the identification of differences between metabolomes of males and hermaphrodites. Through comparative analysis of mass spectrometric (MS) data obtained for small molecule extracts of males and hermaphrodites using the MetaboSeek platform, we detected a large number of compounds that are present in greater quantities in males than in hermaphrodites and vice versa. Among these are over 200 compounds that are at least 2-fold enriched in males with a p-value of less than 0.05. Further, using sex mutants in which the germline is specifically male or female, we classified these compounds into metabolites derived from the male germline and those derived from the male soma.

Chapter 2: Identification of a male pheromone that shortens lifespan

This second chapter focuses on the characterization of a small molecule that is involved in the phenomenon of male-induced demise (MID). The presence of male *C. elegans* has been shown to shorten the lifespan of hermaphrodites[11]. Using activity-guided fractionation, UHPLC-HRMS/MS, NMR, and chemical synthesis, we identified the structure of a metabolite, named nacq#1, that is largely responsible for MID. nacq#1, a conjugate of the amino acid glutamine and decatrienoic acid, represents a new type of signaling molecule mediating lifespan, reproductive maturation, and other aspects of development. This chapter includes a detailed description of the enantioselective synthesis of nacq#1 and its quantification at different time points during the lifecycle of hermaphrodites and males.

Chapter 3: β-methyl lipids are enriched in males

The third chapter presents a class of unique β-methyl decanoic acid derivatives, the bemeth#s, that are enriched in males. With the presence of a β-methyl group, bemeth#1 cannot be degraded through normal β-oxidation and must instead go through α-oxidation, consistent with most of the identified compounds also containing an α-hydroxyl group. As such, these compounds were initially found during the investigations of a methyltransferase (F13D12.9), which is responsible for the β-methyl branch, and hydroxyacyl-CoA-lyase (*hacl-1*), which would further oxidize the compounds for chain shortening[12]. In addition to α-hydroxylation we demonstrated that bemeth#-family metabolites are further oxidized or conjugated to amino acids, which are enriched in males to different extents at different time points during their life cycle.

Chapter 4: Identification of other new classes of male-enriched metabolites

In the fourth chapter we describe identification of several other classes of male-enriched compounds, derived from diverse metabolic pathways. This includes a class of nucleoside-derivatives, the panglu#s, in which nucleobases are conjugated to glucose rather than ribose or deoxyribose as in canonical nucleosides. We further identified a number of ascarosides incorporating gluconucleosides similar to those observed in the panglu#s. In addition to these gluconucleoside-conjugated ascarosides, we find that the ascaroside ascr#1, and several of its derivatives, are also male-enriched. A derivative of *S*-adenosylmethionine (SAM), a novel tryptophan derivative reminiscent of the psychoactive drug dimethyltryptamine (DMT), and a series of very long-chain polyunsaturated fatty acids (VLCPUFAs) round out the male-enriched compounds discussed in this chapter.

Chapter 5: Investigation of dafachronic acid metabolism

Chapter 5 discusses the metabolism of dafachronic acids (dafa#s), bile acid-like ligands of the nuclear hormone receptor DAF-12, a homolog of mammalian FXR, that regulate the development of *C. elegans* to reproductive maturity[13]. Based on the hypothesis that previously identified dafa#s may be further activated into more active ligands, we developed several methods for investigating the metabolism of dafa#s, beginning with a functionalized derivative for protein interactions. In addition, we also synthesized a stable-isotope labeled dafachronic acid to track possible activation and degradation.

REFERENCES

(1) Brenner, S. The Genetics of Caenorhabditis Elegans. *Genetics* **77**: 71-94. **1974**.

(2) The C. elegan Sequencing Consortium. Genome Sequence of the Nematode *C. elegans*: A Platform for Investigating Biology. *Science* **282**: 2012-2018. **1998**.

(3) Lai, C. H., *et al.* Identification of novel human genes evolutionarily conserved in Caenorhabditis elegans by comparative proteomics. *Genome Res.* **10**:703-713. **2000**.

(4) Lakowski, B. and Hekimi, S. The genetics of caloric restriction in *Caenorhabditis elegans*. *Proc. Natl. Acad. Sci.* **95**: 13091-13096. **1998**.

(5) Morcos, M. and Hutter, H. The model Caenorhabditis elegans in diabetes mellitus and Alzheimer's disease. *J. Alzheimer's Dis.* **16**: 897-908. **2009**.

(6) Liggett, M. R., Hoy, M. J., Mastroianni, M., Mondoux, M. A. High-glucose diets have sex-specific effects on aging in *C. elegans*: toxic to hermaphrodites but beneficial to males. *Aging* **7**: 283-287. **2015**.

(7) Honjoh, S., *et al.* The Sexual Dimorphism of Dietary Restriction Responsiveness in *Caenorhabditis elegans*. *Cell Reports* **21**: 3646-3652. **2017**.

(8) Albritton, S. E., *et al*. Sex-Biased Gene Expression and Evolution of the X Chromosome in Nematodes. *Genetics* **197**: 865-883. **2014**.

(9) Izrayelit, Y., *et al*. Targeted metabolomics reveals a male pheromone and sex-specific ascaroside biosynthesis in *C. elegans*. *ACS Chem Biol.* **7**: 1321-1325. **2012**.

(10) Ludewig, A. H., Artyukhin, A. B, Aprison, E. Z., Rodrigues, P. R., Pulido, D. C., Burkhardt, R. N., Panda, O., Zhang, Y. K., Gudibanda, P., Ruvinsky, I., Schroeder, F. C. An excreted small molecule promotes *C. elegans* reproductive development and aging. *Nature Chem Biol.* **15**: 838-845. **2019**.

(11) Maures, T. J., *et al*. Males shorten the life span of *C. elegans* hermaphrodites via secreted compounds. *Science* **31**: 541-544. **2014**.

(12) Helf, M. J., Fox, B. W., Artyukhin, A. B., Zhang, Y. K., Schroeder, F. C. Comparative metabolomics with Metaboseek reveals functions of a conserved fat metabolism pathway in *C. elegans*. *Submitted August 2021*.

(13) Mahanti, P., *et al.* Comparative metabolomics reveals endogenous ligands of DAF-12, a nuclear hormone receptor, regulating C. elegans development and lifespan. *Cell Metabolism* **19**: 73-83. **2014**.

CHAPTER 1

CHARACTERIZATION OF THE MALE METABOLOME

Contributions and Acknowledgements

This research presented in this chapter will result in submission of a manuscript prepared by Russell N. Burkhardt (RNB) and Dr. Frank Schroeder (FCS). This research was performed with input and assistance from others in the Schroeder Lab (Cornell University, Ithaca, NY) and the Lee Lab (Cornell University, Ithaca, NY). Experiments were designed by RNB with input from FCS, Dr. Bennett Fox (BF), and Dr. Amaresh Chaturbedi (AC). Cultures of *C. elegans* for metabolomic analysis were grown by RNB and AC. Metabolomic analysis was performed by RNB. Synthesis for compound confirmation was performed by RNB and Brian Curtis (BC).

Abstract

Whereas phenotypic, genetic, and transcriptomic differences between the sexes in *C. elegans* and other model systems have been extensively studied, little is known about the *chemical* differences. *Caenorhabditis elegans* provides an excellent model for such studies as large populations can readily be grown in the laboratory with under well-controlled conditions. We employed untargeted comparative metabolomics based on UHPLC-HRMS analysis to investigate the chemical differences between male and hermaphrodite *C. elegans*. Through comparison of the *C. elegans* wildtype strain N2, which are >99% hermaphrodites, and the male-rich *him-5(e1490)* strain, over 200 metabolites that were more than 2-fold enriched in males were detected, including compounds from all branches of primary metabolism. Among these 200+ compounds are lipids, nucleoside-sugar conjugates, and modified amino acids, including many compounds with new or unusual structures, which are discussed in later chapters. These compounds were further examined in mutants which possess a male (*fem-3(q20)*) or female (*fem-2(b245)*) germline, or no germline at all (*glp-4(bn2)*). In addition, we monitored their production throughout development and adulthood in both N2 and *him-5* cultures. Our results indicate that not only do the sexes have different body plans and gene expression profiles but have vastly different metabolomes.

1.1 Introduction

C. elegans has been used extensively as a model organism for organismal biology, including aging and development[1]. Most of this research has focused on the predominant sex of *C. elegans*, self-fertile hermaphrodites, which make up over 99% of the population under laboratory conditions whereas the much less abundant males have been studied only to a very limited extent[2]. Beyond the anatomical and behavioral differences, "maleness" has been

described in several manners. The genetic differences between hermaphrodites and males are relatively small as in *C. elegans* sex is the result of chromosomal dosing, where males have a single X chromosome and hermaphrodites have two copies[3]. Delving a layer deeper, it has been shown that there are stark transcriptomic differences between the sexes, with nearly 6000 transcripts being expressed at higher levels in males and roughly the same being more abundantly expressed in hermaphrodites[4]. Despite these numerous and obvious differences between the sexes, only recently have studies concerning the role sex plays in general physiology, including metabolism, begun to arise in the field[5,6].

Even with the relatively small number of papers addressing sex-specific differences in general physiology, i.e., differences not directly related to reproductive functions, there is growing evidence that there are major sex-specific differences in metabolism, disease response, and aging-associated changes. As one of the most "well-researched" organisms for longevity and aging, it has recently been demonstrated that, in *C. elegans*, much of what has been shown to be beneficial for increased lifespan of hermaphrodites may actually be harmful for males. Dietary restriction, which in many organisms has been shown to increase lifespan, is one such example. While it is well-documented that various forms of dietary restriction increase lifespan, recent research has shown that *C. elegans* males receive no benefit and may, in fact, under some starvation regimens, experience shortened lifespans[7].

While it is clear that there are significant differences in phenotypic responses between the sexes, the molecular signals and pathways responsible for these phenomena are poorly understood. Some of the earliest studies into the chemical differences between *C. elegans* hermaphrodites and males focused on a well characterized class of signaling molecules, the ascarosides[5]. As pheromones, the ascarosides contribute to many developmental and behavioral

responses, including dauer induction, attraction, and repulsion[8]. For example, ascr#3, one of the most abundant secreted ascarosides by hermaphrodites, acts as a deterrent or dispersal signal, whereas the chemically very similar ascr#10, one of the most abundant secreted ascarosides by males, acts as an attractant. However, even among ascarosides, as perhaps the most well-studied signaling molecules in *C. elegans*, only a select few have been quantified separately in males and hermaphrodites[5]. The relative abundances of most other metabolites, any of which represent compounds whose chemical structures have not yet been determined, have never been studied in a sex-specific manner. Moreover, it is unclear whether there are any strictly sex-specific metabolites in *C. elegans*, e.g. compounds that only males make, but are completely absent in hermaphrodites.

As one additional example, it has been shown that the phenomenon of Male-Induced Demise (MID) is not primarily the result of physical interactions during mating but is largely mediated by small molecules[9]. One such molecule, which is the subject of Chapter 2, is nacq#1, a compound derived from the amino acid glutamine conjugated to a unique polyunsaturated fatty acid[10].

The identification of nacq#1 was the result of activity-guided fractionation in search of small molecules possibly responsible for MID. Throughout the process of identifying nacq#1 and investigating its biosynthesis, it became apparent that there is a large number of sex-specific differences between the metabolomes of males and hermaphrodites, and that many compounds that are more abundant in males have escaped previous metabolomic analysis. In this work we use an untargeted UHPLC-MS-based comparative metabolomics approach to parse the *C. elegans* metabolome and characterize what it is to chemically be a male.

1.2 Designing an approach to dissect the metabolome

One reason for the relatively scant investigation into the male metabolome is their low abundance in populations of the wildtype laboratory strain. Under laboratory conditions, the "Bristol N2" strain introduced by Sydney Brenner consists almost entirely of hermaphrodites which self-fertilize to produce what are essentially genetic clones of themselves[2]. During conventional culture of N2 nematodes, males rarely emerge, and hardly to a level suitable for metabolomic analysis. Through heat-shock, an approximately six-hour incubation at 35°C of L4 larvae, meiotic disruption can result in a small number of sperm that lack an X chromosome (A0)[11]. Fertilization of a normal AX ovum with A0 sperm can then result in generation of a small number of male nematodes. From this point on, sexual reproduction between a hermaphrodite and a male can result in increased numbers of males, in theory up to 50% (1:1 AX:A0 sperm). The issue with relying on this process for generating large populations of males, however, is that sexual reproduction must occur on solid media rather than liquid media, which limits the number of worms that can be grown and makes preparing samples of ≥10,000 worms as needed for in-depth metabolomic studies unfeasible.

Starting in the late 1970's a number of mutants were described which, without sexual reproduction, constitutively feature a high incidence of males (*him* mutants)[12,13,14]. While multiple *him* strains exist, each with a mutation in a different gene, their viability and population makeup can vary drastically[13]. Perhaps the most useful, and commonly used, of these *him* strains is *him-5(e1490)*, which carries a mutation in a protein believed to be involved in double strand breaks in DNA during meiosis. This mutation, although unclear how, results in an increased likelihood of nondisjunction of X chromosomes during meiosis. Cultures of *him*-5 animals typically yield approximately 35% (and in our hands up to 50%) males with no known

phenotypic anomalies[12]. By using this mutant we can efficiently grow liquid cultures with large numbers of males. These cultures can then be used to obtain not only endo-metabolome samples (worm body extracts) but also exo-metabolome samples (extracts of spent media containing excreted metabolites) (Figure 1.1). Comparisons between these metabolomes of male-enriched cultures and those of conventional wildtype (N2) cultures can then be used as a starting pointto uncover chemical differences between males and hermaphrodites.

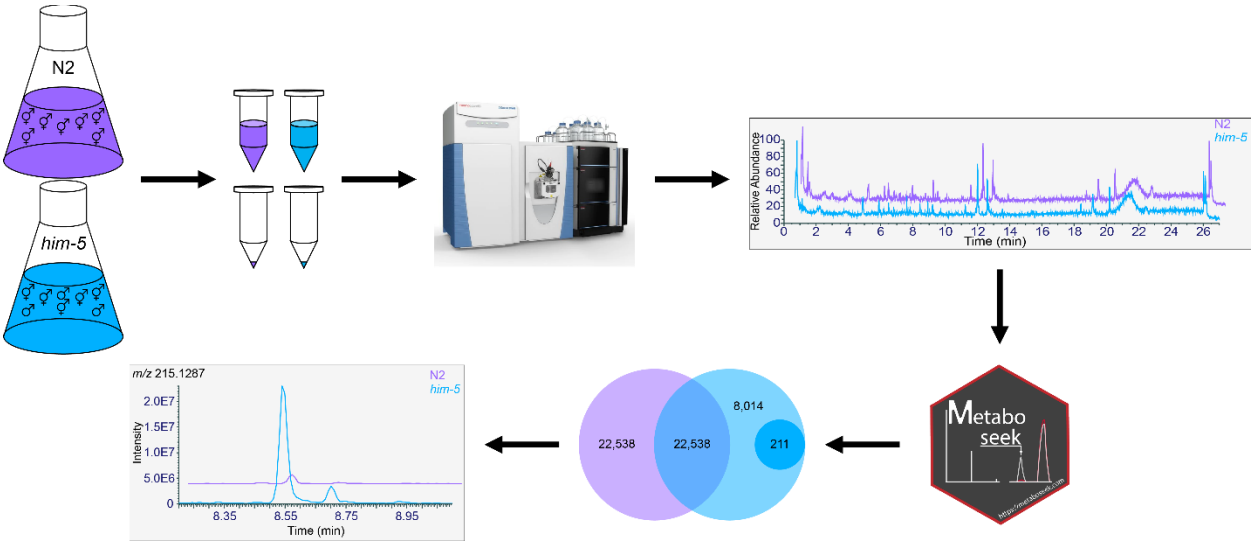

Figure 1.1 | Metabolomics Pipeline. Liquid cultures of synchronized wildtype hermaphrodites (N2) and male-enriched mutants (*him-5*) are grown to adulthood. The media (exo-metabolome) and worm bodies (endo-metabolome) are separated, extracted, and concentrated for UHPLC-HRMS analysis. Collected data is analyzed through the MetaboSeek analytics platform and manually curated to identify significantly differential compounds.

For detection of compounds in the metabolome samples, we employed ultra-high-performance liquid chromatography coupled to a high-resolution Orbitrap mass spectrometer (UHPLC-HRMS) (Figure 1.1). One benefit of HRMS is that the increased resolution often permits unambiguous determination of the chemical formulae of detected compounds from a single injection through the high-accuracy of *m/z* detection (up to 480,000 at *m/z* 300, using one of the spectrometers used for this study) which can resolve the fine structure of isotope patternsup to *m/z* 600. The data obtained from the UHPLC-HRMS analysis of the metabolomic

samples is then fed into the comparative metabolomics platform, MetaboSeek, which provides a comprehensive toolset for the initial structural characterization of newly discovered metabolites[15]. Our analysis of the exo- and endo-metabolomes of N2 and *him-5* cultures yielded 110,184 significant features, unique pairs of mass-to-charge (*m/z*) ratios and retention times. Applying a 2-fold differential filter to these 110,184 mass spectrometric features MetaboSeek returns 8,225 compounds at least 2-fold more abundant in the male-enriched *him-5* cultures and 22,538 MS features that are at least 2-fold more abundant in N2 cultures. Manual analysis of these male-enriched features to remove isotopes, adducts, and fragments reduced the 8,225 features enriched in *him-5* to 210 unique peaks that are up-regulated in male-enriched in *him-5* cultures, and approximately 300 compounds enriched in wildtype N2 over *him-5* (Figure 1.1). Following comparative analysis of the UHPLC-HRMS data, we acquired MS2 fragmentation spectra for all differential metabolites.

1.3 Germline and somatic origins of male-enriched compounds

Like in other species, the germline and reproductive systems differ between the sexes in *C. elegans*, however as they are a male-hermaphrodite species rather than a male-female species, both sexes produce sperm. Hermaphrodites produce a much smaller amount of sperm than males and do not have the accompanying male somatic sex organs and lack other male-specific body plan features. To determine which of the male-enriched compounds we detected are directly associated with the male germline versus the rest of the male body (the male *soma*) we examined a series of temperature-sensitive germline mutants. *fem-3(q20)* gain-of-function mutants, like hermaphrodites, possess a hermaphrodite soma, but unlike hermaphrodites have a masculinized germline that produces an increased amount of sperm and no eggs[16]. Conversely, *fem-2(b245)*

loss-of-function, have a hermaphrodite soma and maintain egg production but, lack sperm[17,18]. Another germline mutant we selected for study, the *glp-4(bn2)* loss-of-function strain, maintains a hermaphrodite-like soma but develops no germline at 25°C (Figure 1.2a,b)[19].

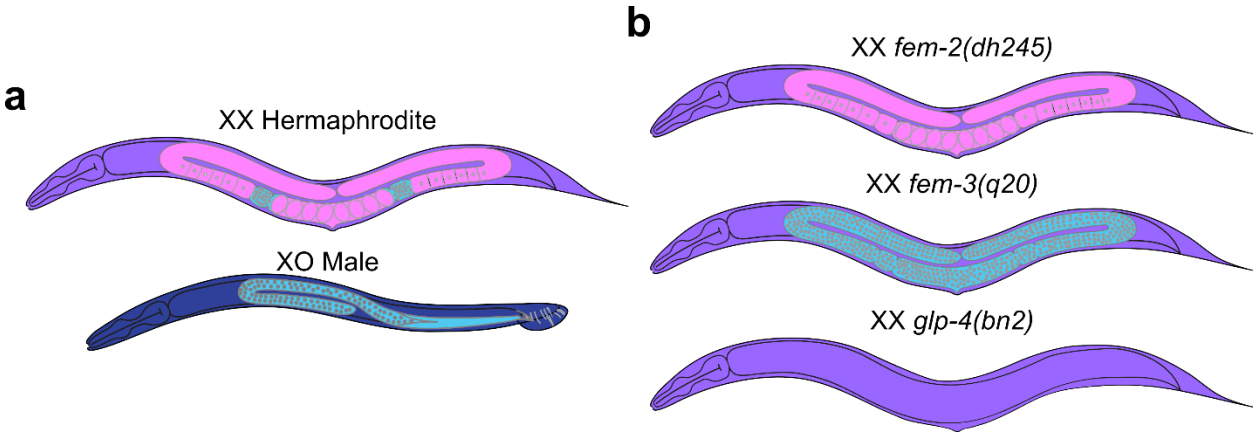

Figure 1.2 | Elucidating the origin of male-enriched compounds. a. Hermaphrodites have both female (pink) and male (light blue) germlines and a hermaphrodite soma (purple) while males have only a male germline and a male soma (dark blue). **b.** *fem-2(b245)* feminized worms have a hermaphrodite body but only a female germline. *fem-3(q20)* masculinized mutants have a hermaphrodite body but poses only a male germline that produces an increased amount of sperm. *glp-4(bn2)* mutants have a hermaphrodite body but do not develop a germline.

Enrichment of metabolites in *fem-3* (OE) relative to *fem-2* (KO), *glp-4* (KO), and/or N2 would indicate they are associated with the male germline. Conversely, if a metabolite is increased in *him-5* male-enriched cultures but not in *fem-3* (OE) cultures, this indicates that it is likely associated specifically with the presence of a male soma. We observed that 23 of the male-enriched compounds previously identified are also up-regulated in *fem-3* (OE) cultures, indicating that they are associated with a male germline, whereas the remaining 187 may be soma-dependent. Profiling *fem-3* (OE)-enriched metabolites also led us to recognize additional male-enriched compounds that were missed in the initial comparison of *him-5* vs. wildtype metabolomes, which added 11 compounds to our list of male-enriched compounds.

While this method enabled detection of a large number of male germline-dependent compounds, our approach neglects that physical and chemical interactions between males and

hermaphrodites may alter their metabolism. In *him-5* cultures, the increased numbers of males are interacting with hermaphrodites in the culture. In *fem-3* (OE) cultures, however, all worms have male germlines with no potential sensory feedback from fertile or gravid worms. Therefore, we performed two additional comparisons. In one experiment, we compared a small sample of pure hand-picked males against pure hand-picked hermaphrodites, which should reveal any compounds that are the result of male-hermaphrodite interactions. In this comparison, 65 of the male enriched-compounds identified from the *him-5*-N2 comparison were detectable in the smaller sample, and 21 of those compounds were also increased in pure males, indicating their production is independent of hermaphrodites, while increased production of the other 46 may be dependent on interactions with hermaphrodites. The remaining 145 compounds not detected in pure males may be present but were produced in quantities too small to detect, given the small sample size (Figure 1.3). Similarly, 19 of the 101 *fem-3* (OE)-enriched compounds that were detectable in the pure male samples were also upregulated in pure males, 1 of which was not upregulated in the *him-5* cultures, indicating that under these experimental conditions they are only produced in the absence of hermaphrodites (Figure 1.3b).

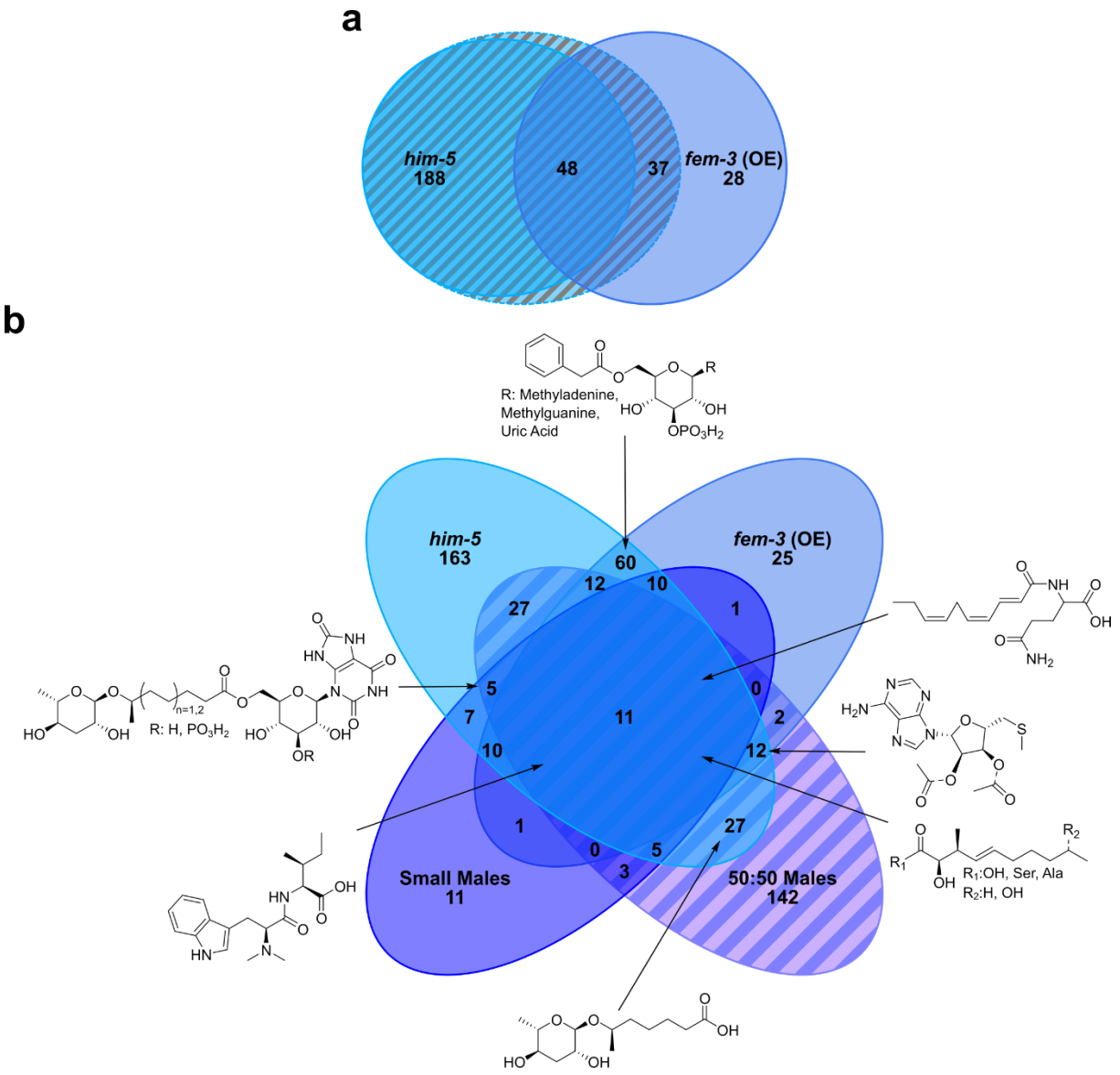

Figure 1.3 | Compounds overlap between samples. a. Male-enriched compounds overlap between young adult *him-5* (light blue) or after one day of adulthood (striped light blue) liquid cultures with *fem-3* (OE) liquid cultures. **b.** Compound overlap between *him-5* at 1 day of adulthood, *fem-3* (OE), and hand-picked males (dark blue). More complete information on compounds, including molecular formulae or *m/z*, identity (if known), and fold-changes for *him-5*, *fem-3* (OE), and small hand-picked males can be found in Supplemental Tables 1.1, 1.2, and 1.3.

In a second verification experiment, to further investigate whether the increase in abundance in any metabolites resulted from male-hermaphrodite interactions, we compared a 1:1 mixture of males and hermaphrodites, grown on plates (generated via heat shock), with control plates of hermaphrodites. Of the 160 male-enriched compounds found in *him-5* that were not

upregulated in *fem-3* (OE) cultures, 34 were detected and 32 were also upregulated in the 1:1 mixture of males and hermaphrodites (Figure 1.3b). Similarly, the one *fem-3* (OE)/pure male-enriched compounds that was not enriched in the *him-5* cultures was also not enriched in the 1:1 samples, indicating it is either produced only in the absence of hermaphrodites or is metabolized by hermaphrodites.

1.4 The effect of aging on the male metabolome

In most animals, metabolism undergoes profound changes during development and throughout adult life. In men, the classic example is testosterone – production of testosterone is relatively small in childhood, spikes during puberty, slightly declines into the thirties, then is roughly constant[20]. Knowledge of the developmental stages at which different compounds are produced in *C. elegans* will provide a basis for elucidating their biological functions and biosyntheses. To this end, we examined the exo-metabolome of *him-5* cultures by collecting the expended media during different time periods throughout larval development and adulthood. Specifically, we collected media containing excreted metabolites during the L1 to early L4 stages (38 h post L1 arrest), from L4 to young adulthood (YA) stage (38-52 h), from YA to gravid adult stage (52-72 h) and then for every day of adulthood until the worm bodies were harvested (Figure 1.4a)[21].

1.4.1 Examination of a known male-increased metabolite

Previous studies showed that production of the ascaroside ascr#10 is increased in males relative to hermaphrodites, and that this compound is partially responsible for the accelerated aging of hermaphrodites in the presence of males[10]. The original work reporting ascr#10 as a male-upregulated metabolite was based on the analysis of mixed-stage *him-5* cultures, containing animals at different larval stages and ages of adulthood. In these *him*-5 cultures, ascr#10 was

found to be about 3-fold upregulated. In our analyses of YA-stage *him*-5 cultures, ascr#10 was not significantly upregulated when compared to wildtype cultures (Figure 1.4b). Similarly, ascr#10 levels in young adult cultures of germline-masculinized *fem-3* (OE) mutants were not increased relative to wildtype (Figure 1.4b). We then examined ascr#10 production by different developmental stages as well as by older adults. We found that barely any ascr#10 is produced during the four larval stages (L1-L4), and that production increases dramatically during the L4-YA time window. Levels of ascr#10 continue to increase through the third day of full adulthood up to a level of about 9-fold above WT levels after 144 hours, after which they begin to decline (Figure 1.4c). Although apparently germline-independent as it is produced at similar levels in cultures of animals with or without a male germline, ascr#10 production appears to align with sperm production, though further investigation would be required to state so conclusively[22].

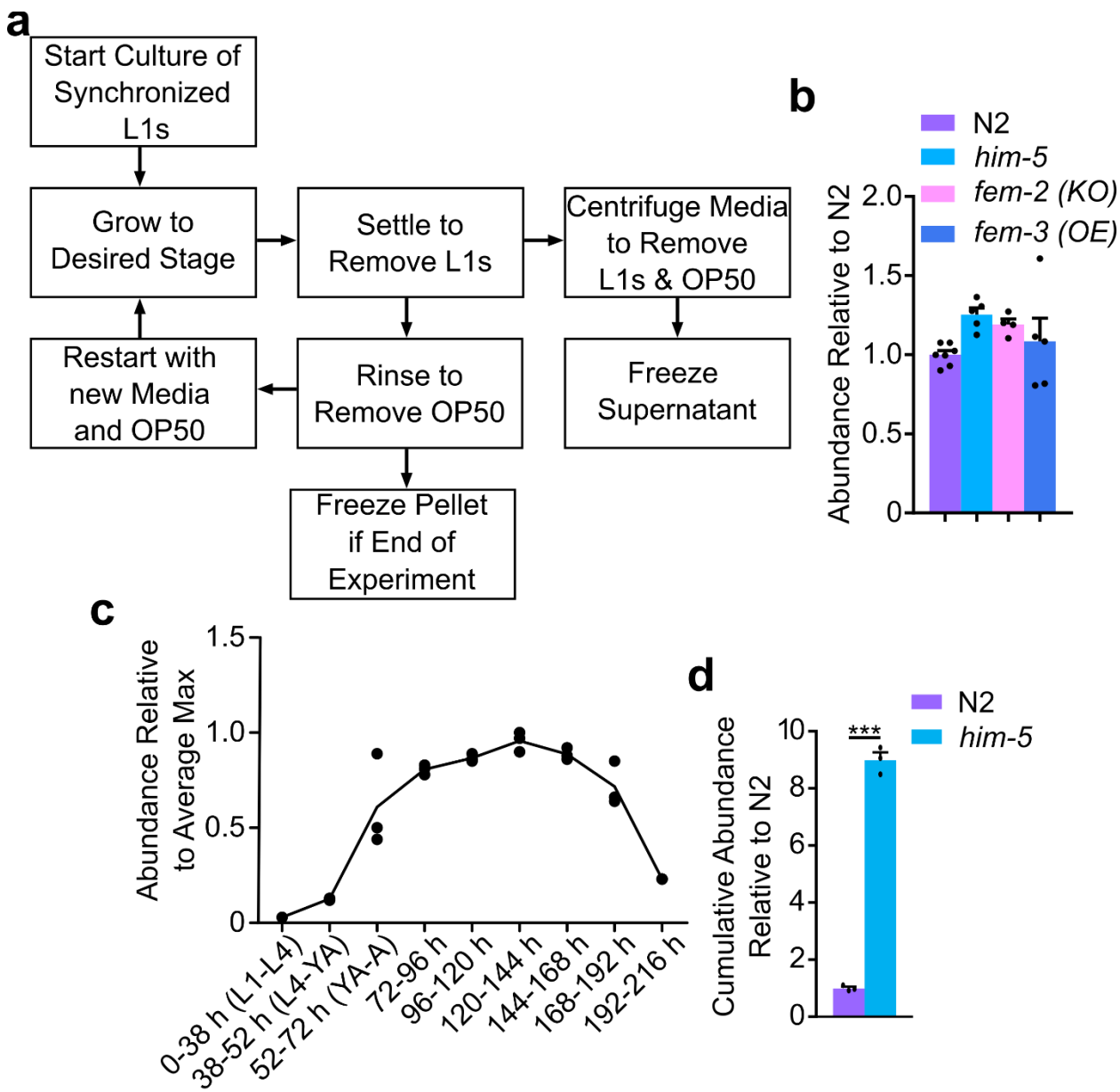

Figure 1.4 | Production of ascr#10. **a.** Aging studies were performed by growing synchronized L1 larvae to a desired timepoint (i.e,. after all worms have grown to the L4 stage), settling the culture to remove any new progeny that may be present, rinsing the animals to remove bacteria, and then restarting the culture with fresh media and bacteria. The supernatant from the settle was then centrifuged to remove bacteria and remaining worms and then frozen until extraction. **b.** Quantification of ascr#10 in *him-5*, *fem-2* (KO), and *fem-3* (OE) relative to abundance in N2. **c.** UHPLC-HRMS quantification of ascr#10 in exo-metabolome samples of *him-5* cultures during development and adulthood scaled to the maximum average measured intensity. **d.** Cumulative excretion of ascr#10 was determined by summation of ascr#10 abundances from 0-144 h. ***, $p<0.0005$.

1.6 A foreword to the following chapters

Most of the male-enriched metabolites we detected in this Chapter represent novel metabolites that have not previously been described. In the next three Chapters, we describe the elucidation of the structures of many of the most abundant male-enriched compounds, which revealed compounds with origins in diverse parts of primary metabolism, including fatty acid, amino acid, and nucleoside metabolism. Identification and biological activity of one of the first male-enriched compound identified, nacq#1, is described in Chapter 2[10]. In Chapter 3 we identify a family of male-enriched lipids that are the product of a novel β-methyltransferase and processed by α-oxidation, the β-methyl acids (bemeth#s)[15,23]. In Chapter 4 we examine a variety of other compounds that are enriched in males, including the phenylacetyl-gluconucleosides (panglu#s), gluconucleoside-conjugated ascarosides (uglas#s), a unique dimethyl-tryptophan-isoleucine dipeptide, and ascr#1 derivatives.

References

(1) Morcos, M. and Hutter, H. The model Caenorhabditis elegans in diabetes mellitus and Alzheimer's disease. *J. Alzheimer's Dis.* **16**: 897-908. **2009**.

(2) Brenner, S. The Genetics of Caenorhabditis Elegans. *Genetics* **77**: 71-94. **1974**.

(3) Hodgkin, J. Sex Determination in the Nematode *C. elegans*: Analysis of TRA-3 Suppressors and Characterization of FEM Genes. *Genetics.* **114**: 15-52. **1986.**

(4) Albritton, S. E., Kranz, A., Rao, P., Kramer, M., Dieterich, C., Ercan, S. Sex-Based Gene Expression and Evolution of the X Chromosome in Nematodes. *Genetics* **197**: 865-883. **2014.**

(5) Izrayelit, Y., Srinivasan, J., Campbell, S. L., Jo, Y., von Reuss, S. H., Genoff, M. C., Sternberg, P. W., Schroder, F. C. Targeted metabolomics reveals a male pheromone and sex-specific ascaroside biosynthesis in *C. elegans*. *ACS Chem. Biol.* **7**: 1321-1325. **2012.**

(6) Liggett, M. R., Hoy, M. J., Mastroianni, M., Mondoux, M. A. High-glucose diets have sex-specific effects on aging in *C. elegans*: toxic to hermaphrodites but beneficial to males. *Aging* **7**: 283-287. **2015.**

(7) Honjoh, S., Ihara, A., Kajiwara, Y., Yamamoto, T., Nishida, E. The Sexual Dimorphism of Dietary Restriction Responsiveness in *Caenorhabditis elegans*. *Cell Reports* **21**: 3646-3652. **2017.**

(8) von Reuss, S. H., Srinivasan, J., Yim, J. J., Judkins, J. C., Sternberg, P. W., Schroder, F. C. Comparative metabolomics reveals biogenesis of ascarosides, a modular library of small molecule signals in *C. elegans*. *JACS* **134**: 1817-1824. **2012.**

(9) Maures, T. J., Booth, L. N., Benayoun, B. A., Izrayelit, Y., Schroeder, F. C., Brunet, A. Males Shorten the Life Span of *C. elegans* Hermaphrodites via Secreted Compounds. *Science* **31**: 541-544. **2014.**

(10) Ludewig, A. H., Artyukhin, A. B., Aprison, E. Z., Rodrigues, P. R., Pulido, D. C., Burkhardt, R. N., Panda, O., Zhang, Y. K., Gudibanda, P., Ruvinsky, I., Schroeder, F. C. An excreted small molecule promotes *C. elegans* reproductive development and aging. *Nature Chem. Biol.* **15**: 838-845. **2019.**

(11) Hodgkin, J. Male Phenotypes and Mating Efficiency in *Caenorhabditis elegans.* *Genetics* **103**: 43-64. **1983.**

(12) Hodgkin, J., Brenner, S. Mutations Causing Transformation of Sexual Phenotype in the Nematode *Caenorhabditis elegans. Genetics* **86**: 275-287. **1977.**

(13) Hodgkin, J., Horvitz, H. R., Brenner, S. Nondisjunction Mutants of the Nematode *Caenorhabditis elegans. Genetics* **91**: 67-94. **1979.**

(14) Hodgkin, J. More Sex-Determination Mutants of *Caenorhabditis elegans*. *Genetics* **96**: 649-664. **1980.**

(15) Helf, M. J., Fox, B. W., Artyukhin, A. B., Zhang, Y. K., /Schroeder, F. C. Comparative metabolomics with Metaboseek reveals functinos of a conserved fat metabolism pathway in *C. elegans. Submitted August 2021*.

(16) Barton, M. K., Schedl, T. B., Kimble, J. Gain-of-Function Mutations of *fem-3*, a Sex-Determination Gene in *Caenorhabditis elegans. Genetics* **115**: 107-119. **1987.**

(17) Hodgkin, J. Sex Determination in the Nematode *C. elegans*: Analysis of *TRA-3* Suppressors and Characterization of *FEM* genes. *Genetics* **114**: 15-52. **1986.**

(18) Hansen, D., Pilgrim, D. Molecular Evolution of a Sex Determination Protein: FEM-2 (PP2C) in Caenorhabditis. *Genetics* **149**: 1353-1362. **1998.**

(19) Rastogi, S., Borgo, B., Pazdernik, N., Fox, P., Mardis, E. R., Kohara, Y., Havranek, G., Schedl. *Caenorhabditis elegans glp-4* Encodes a Valyl Aminoacyl tRNA Synthetase. *G3* **5**: 2719-2728. **2015.**

(20) Kelsey, T. W., Li, L. Q., Mitchel, R. T., Whelan, A., Anderson, R. A. A Validated Age-Related Normative Model for Male Total Testosterone Shows Increasing Variance but No Decline after Age 40 Years. *PLOS ONE* **9**: e109346. **2014.**

(21) Byerly, L., Cassada, R. C., Russell, R. L. The life cycle of the nematode *Caenorhabditis elegans. Dev. Biol* **51**: 23-33. **1976.**

(22) Chou, W., Lin, Y., Lee, Y. Short-term starvation stress at young adult stages enhances meiotic activity of germ cells to maintain spermatogenesis in aged male *Caenorhabditis elegans*. *Aging Cell* **18**: e12930. **2019.**

(23) Fox, B. W., *et al. In preparation*.

CHAPTER 2

AN EXCRETED SMALL MOLECULE PROMOTES *C. ELEGANS* REPRODUCTIVE DEVELOPMENT AND AGING

Contributions and Acknowledgments

This chapter is the result of collaborative work of several members of the Schroeder Lab (Cornell University, Ithaca, NY) and the Ruvinsky Lab (Northwestern University, Evanston, Illinois). The project was the culmination of research on population density-dependent acceleration of aging by Dr. Hanno Ludewig (HAL) and the natural product identification work of Dr. Alexander Artyukhin (ABA), who designed the experiments with Dr. Frank Schroeder (FCS) and Dr. Ilya Ruvinsky (IR). This work led to the publication in *Nature Chemical Biology* (Ludewig, H. A., *et al*.). Russell N. Burkhardt (RNB) contributed to the synthesis of the newly identified male-specific metabolite nacq#1 and the determination of its stereochemistry, to the relative quantification of metabolites in different sexes and at different developmental stages, as well as to the characterization of *fat-1(ok2323)*, *fat-2(wa17)*, and *daf-22(ok693)* mutants. This Chapter is based on sections of the *Nature Chemical Biology* paper that relate to these contributions.

Abstract

Excreted small-molecule signals can bias developmental trajectories and physiology in diverse animal species. However, the chemical identity of these signals remains largely obscure. Here we report identification of an unusual *N*-acylated glutamine derivative, nacq#1, that accelerates reproductive development and shortens lifespan in *Caenorhabditis elegans*. Produced predominantly by *C. elegans* males, nacq#1 hastens onset of sexual maturity in hermaphrodites by promoting exit from the larval dauer diapause and by accelerating late larval development. Even at picomolar concentrations, nacq#1 shortens hermaphrodite lifespan, suggesting a trade-off between reproductive investment and longevity. Unlike ascaroside pheromones, which are restricted to nematodes, fatty acylated amino acid derivatives similar to nacq#1 have been reported from humans and invertebrates, suggesting that related compounds may serve signaling functions throughout metazoa.

2.1 Introduction

Interorganismal small-molecule signaling has been implicated in regulating multiple aspects of animal biology[1]. In addition to shaping behaviors on relatively short timescales, chemosocial signals can also modulate gene expression programs that regulate development and physiology. These longer-lasting changes often occur in response to chemical messages from particularly salient emitters, such as potential mates and competitors. For example, *Drosophila melanogaster* males exposed to female sex pheromones showed complex physiological changes consistent with expectation of mating[2]. In mice, sexually mature males produce a small-molecule signal that induces earlier onset of the first estrus in peripubescent females[3]. Previous studies in *C. elegans* demonstrated that individuals of both sexes excrete as-yet-unidentified signals that alter development: *C. elegans* hermaphrodites develop faster on hermaphrodite-conditioned

plates or following exposure to trace quantities of male-excreted metabolites (Fig. 2.1a)[4,5]. Accelerated progression through larval development in response to small-molecule signals from other individuals in a population appears to be in direct opposition to larval arrest of development at the dauer stage, which is triggered by harsh environmental conditions in combination with excreted pheromones called ascarosides[6–8]. The ability to modify the rate of development in response to environmental conditions may be particularly important to short-lived animals in ephemeral boom-and-bust habitats[9]. Notably, the ability to accelerate development in response to male and hermaphrodite signals appears to come at a cost—both of these treatments reduce hermaphrodite lifespan[4,10–12] (Fig. 2.1a), mirroring the effect of female sex pheromones on longevity of Drosophila males[3]. Similar effects of chemical signals on developmental time and longevity have been observed in divergent species raising the possibility that at least some of the underlying mechanisms are conserved among metazoa. However, little is known regarding the chemical nature of the signal(s) and the regulatory pathways that implement their effects. In this study, we identified an excreted small molecule, nacq#1 (**2.1**), that promotes sexual maturation of *C. elegans* hermaphrodites by modulating conserved signaling pathways. nacq#1 is an *N*-acylated glutamine that belongs to a class of small molecules found in diverse animal lineages, unlike the previously described ascarosides, which appear to be largely restricted to nematodes. Our findings expand the repertoire of known metabolites that specifically alter development and physiology in members of the same species. Because nacq#1 is predominantly present in male excretions, our results contribute to a better understanding of the sexual dimorphism of metabolism, particularly with respect to excreted signaling compounds. Finally, the availability of a pure molecule that potently alters development and

lifespan offers a new tool for the study of mechanisms that regulate development and longevity in response to social signals.

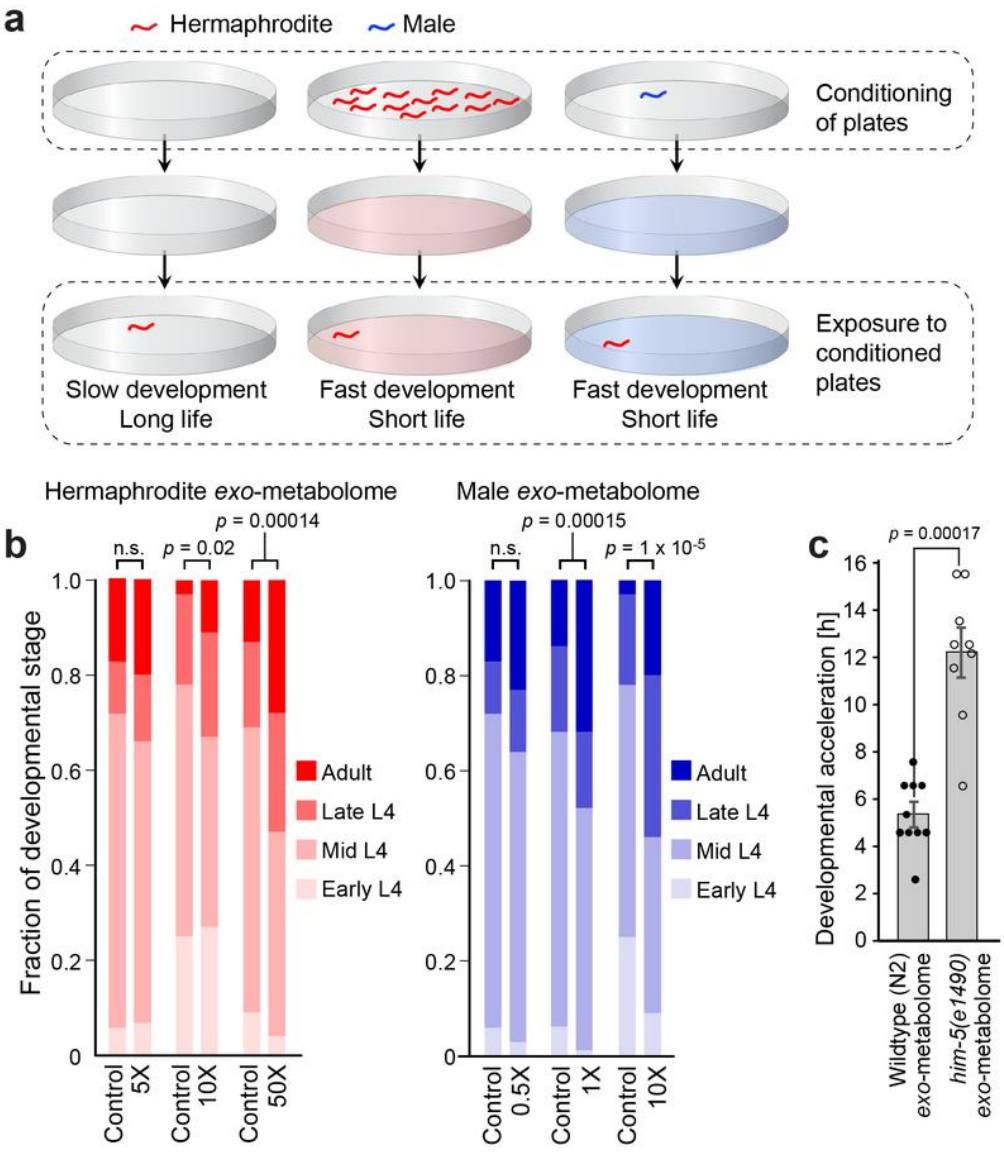

Fig. 2.1 Excreted small molecules accelerate development in *C. elegans*. a. Schematic of preconditioning experiments: worms on plates conditioned by single males or groups of hermaphrodites develop faster and have a shorter lifespan than worms raised on non-conditioned plates[4,5,11]. **b.** Developmental progression of N2 hermaphrodites grown on plates conditioned with exo-metabolomes of N2 hermaphrodites or males (n= 5 biologically independent samples, where each replicate was one plate with ~30 animals). **c.** Developmental acceleration, measured by the onset of egg laying, in daf-22 hermaphrodites exposed to wild-type (N2; >99% hermaphrodites) and him-5 (~30% males) exo-metabolome (n= 10 worms for N2 and n= 9 worms for him-5). Data are presented as mean ± s.e.m. and testing for significance was performed using a $\chi 2$ test or two-tailed t test. n.s., not statistically significant

2.2 Excreted metabolites accelerate development and aging

In pursuit of the specific molecule(s) that accelerate *C. elegans* development and aging, we first compared the properties of the male- and hermaphrodite-excreted products. Analyses of hermaphrodite development on plates conditioned by exo-metabolomes (Fig. 2.1b) revealed that male excretions were approximately tenfold more potent than those of hermaphrodites. Accordingly, exo-metabolomes from *him-5* cultures, which contain >30% males, were more potent at accelerating sexual maturation than extracts of wild-type cultures, which are >99% hermaphrodite (Fig. 2.1c). *daf-22* males, which are defective in peroxisomal β-oxidation (pβO), accelerate hermaphrodite development as effectively as wild-type males[5], indicating that the active compound is likely not an ascaroside pheromone, as these are pβO dependent[13,14]. Similarly, the hermaphrodite-excreted product was daf-22-independent (Supp. Fig. 2.2)[4]. These results suggest that developmental acceleration and lifespan shortening are likely caused by a metabolite that is excreted in higher quantities by males than by hermaphrodites and does not belong to known families of *C. elegans* pheromones.

2.3 Identifying nacq#1 via comparative metabolomics

To determine the chemical identity of the acceleration signal, we pursued a two-pronged approach, combining comparative metabolomics with activity-guided fractionation. To identify metabolites that are excreted in greater amounts by males, we compared the exo-metabolomes from wild-type cultures and *him-5* cultures (Fig. 2.2a). High-resolution HPLC–MS using the XCMS platform[15,16] revealed more than 20 compounds that were at least threefold enriched in him-5 cultures relative to wild-type cultures and thus represented plausible candidates for the acceleration signal. We then fractionated the *him-5* metabolome, using the onset of egg laying to measure developmental acceleration[4] (Supp. Fig. 2.2). For this assay, we used *daf-22* worms,

because this mutant does not produce ascaroside pheromones[13], which may antagonize the activity of the acceleration signal[4]. The activity-guided fractionation revealed three active fractions, which were analyzed for the presence of metabolites enriched in *him-5* cultures. The two most abundant *him-5*-enriched compounds were detected in the most robustly active fraction, fraction 13, but not in adjacent inactive fractions, fraction 12 and fraction 14 (Fig. 2.2b), and thus were selected as the most likely candidates for the acceleration signal. Tandem MS analysis suggested that these compounds represent two isomeric fatty acylated amino acid derivatives that do not correspond to any previously reported metabolites (Fig. 2.2c and Supp. Fig. 2.3). Following isolation of the compounds via preparative HPLC, we determined their structures via NMR spectroscopic analysis, which revealed *cis* and *trans* isomers of a triply unsaturated ten-carbon fatty acid attached to the amino acid glutamine. The absolute configuration of the glutamine moiety was determined using Marfey's reagent (Supp. Fig. 2.4). We named the *cis* and *trans* isomers nacq#1 (*N*-acyl glutamine #1) and nacq#2 (**2.2**), respectively (Fig. 2.2c). nacq#1 isomerizes into nacq#2 under physiological conditions, suggesting that nacq#1 is the primary biosynthetic product.

To see how production and excretion of this development-accelerating signaling molecule is reflected in development and adulthood, we preformed HPLC–MS analysis of endo-metabolomes (worm body extracts) and exo-metabolomes of worms at various timepoints corresponding to major developmental shifts and days of adulthood. The first developmental timepoint chosen represented adolescence and encompasses the L1 to L4 larval stages, followed by the pubescent-like L4-young adult molt, and the transition from young adulthood to gravid reproductive maturity. This assay showed that in N2 hermaphrodites nacq#1 production commences around the time of the transition from L4 larva to young adult, approximately corresponding to sexual maturity, and declines shortly thereafter (Fig. 2.2c and Supp. Fig. 2.5a,b).

Similar analysis of exo- and endo-metabolomes of aging *him*-5 animals showed that, while nacq#1 production in males also begins around the L4-young adult transition, peak production does not occur for several days, after which it declines (Fig. 2.2b). Moreover, similarly to dauer pheromones such as ascr#3 (**3**), nacq#1 was primarily found in the exo-metabolome, as would be expected for an interorganismal signaling molecule (Supp. Fig. 2.5a). In line with the estimate from functional assays of total exo-metabolomes (Fig. 2.1b), we found that males excreted approximately tenfold more nacq#1 than hermaphrodites (Fig. 2.2e), and that this compound was about threefold more abundant in male-enriched *him-5* mutant cultures (>30% male) than in wild-type cultures (Supp. Fig. 2.5c).

Examination of nacq#1 levels in cultures of *fem-2* (KO), *fem-3* (OE), and *glp-4* (KO) animals relative to N2 revealed further insight into its origins. In cultures of germline-feminized *fem-2* (KO) mutants and germline-null *glp-4* (KO) animals excrete virtually no nacq#1 whereas germline-masculinized *fem-3* (OE) produce over 15-times as much nacq#1 as N2 animals (Fig. 2.2e). In additional experiments we showed that cultures of 50:50 mixture males:hermaphrodites excrete three times as much nacq#1 as pure hermaphrodite cultures as was observed in the comparison of N2 and *him-5* cultures (2.2f). Amounts of nacq#1 in the endo-metabolome of adult N2 and *him-5* males are also observed to be several hundred-fold greater than are present in the endo-metabolome of N2 hermaphrodites (2.2g).

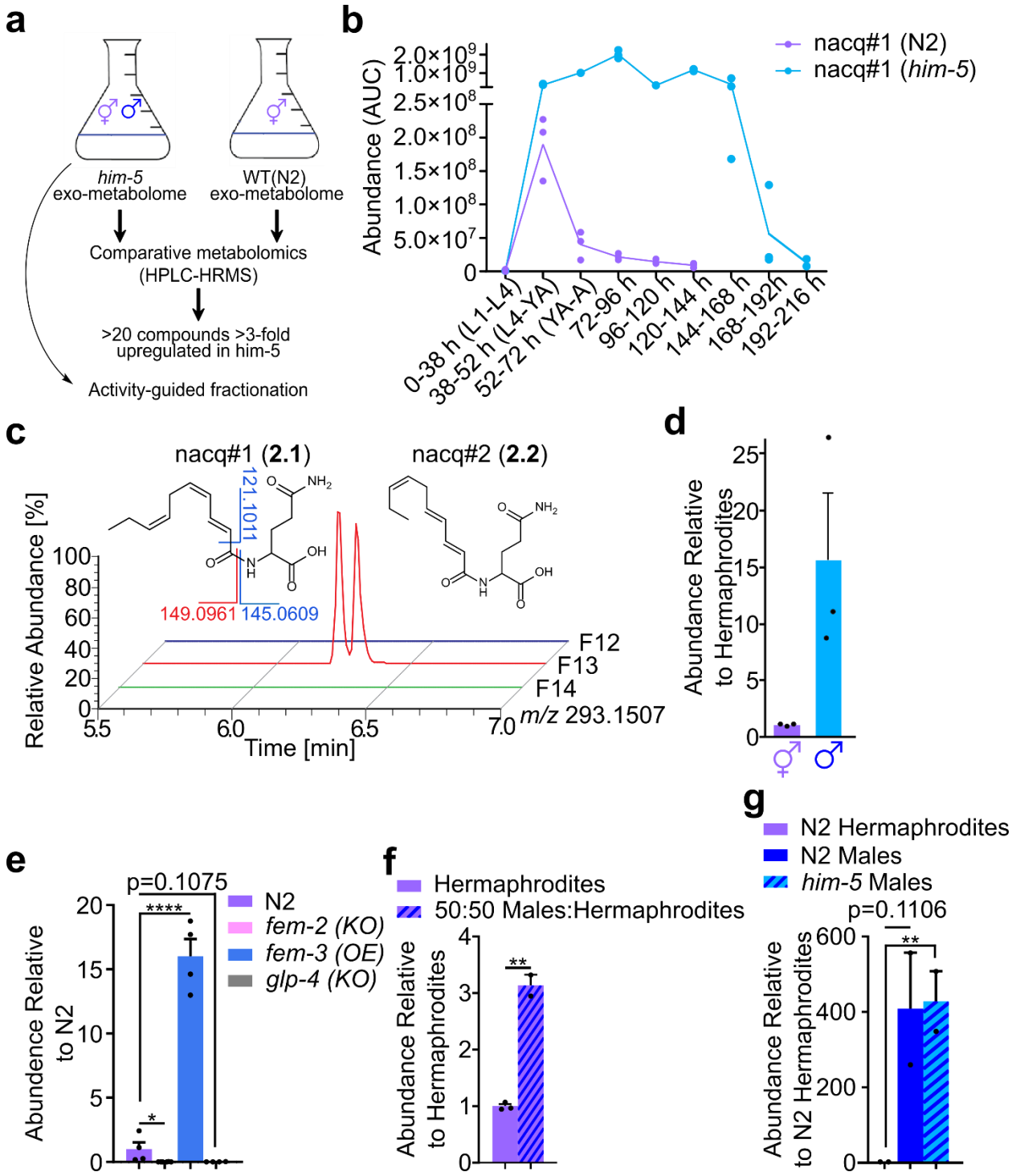

Fig. 2.2 Identification of nacq#1, a signaling molecule primarily produced by males. **a.** Experimental set up for comparative metabolomics with male-enriched *him-5* and wildtype N2 worm cultures. **b.** UHPLC-MS-based quantification of nacq#1 in the exo-metabolomes collected during different time intervals of N2 and *him-5(e1490)*, corresponding to different developmental stages and points in adulthood. **c.** Ion chromatograms comparing HPLC fractions 12, 13 and 14 for *m/z* 293.1506 revealing presence of nacq#1 and nacq#2 in fraction 13 (this fractionation was performed once). **d.** Relative amounts of nacq#1 excreted by hermaphrodites and males. **e.** Relative amounts of nacq#1 in N2 and germline mutants. **f.** Relative amounts of nacq#1 in cultures of hermaphrodites and 50:50 males:hermaphrodites. **g.** Relative amounts of nacq#1 in the endo-metabolome of N2 hermaphrodites, males, and *him*-5 males. *, p≤0.05; **, p≤0.005; ****, p≤0.00001. Error bars represent mean ± s.e.m.

Given that nacq#1 incorporates an omega-3 polyunsaturated fatty acid, we asked whether its biosynthesis requires the fatty acid desaturases FAT-2 and FAT-1, which are required for the introduction of omega-6 and omega-3 double bonds in *C. elegans*, respectively (for example, in the conversion of oleic acid (**4**) to linoleic acid (**5**) and α-linolenic acid (**6**) (Fig. 2.3a)). nacq#1 production was largely abolished in *fat-1* and *fat-2* mutant worms (Fig. 2.3b), indicating that nacq#1 biosynthesis proceeds via longer-chained polyunsaturated fatty acids. Furthermore, consistent with the observation that developmental acceleration by male- and hermaphrodite-derived exo-metabolomes is not dependent on the ascaroside biosynthetic enzyme DAF-22 (Supp. Fig. 2.1), nacq#1 biosynthesis was not affected by loss of *daf-22* in the wild-type (Fig. 2.3b) or *him-5* mutant background (Supp. Fig. 2.5c)[4,5]. We confirmed that biosynthesis of ascaroside pheromones, for example the dauer pheromone component ascr#3, was abolished in *daf-22* mutants (Fig. 3b). Furthermore, we found that nacq#1 biosynthesis was not strongly affected by nutritional conditions (Supp. Fig. 2.6).

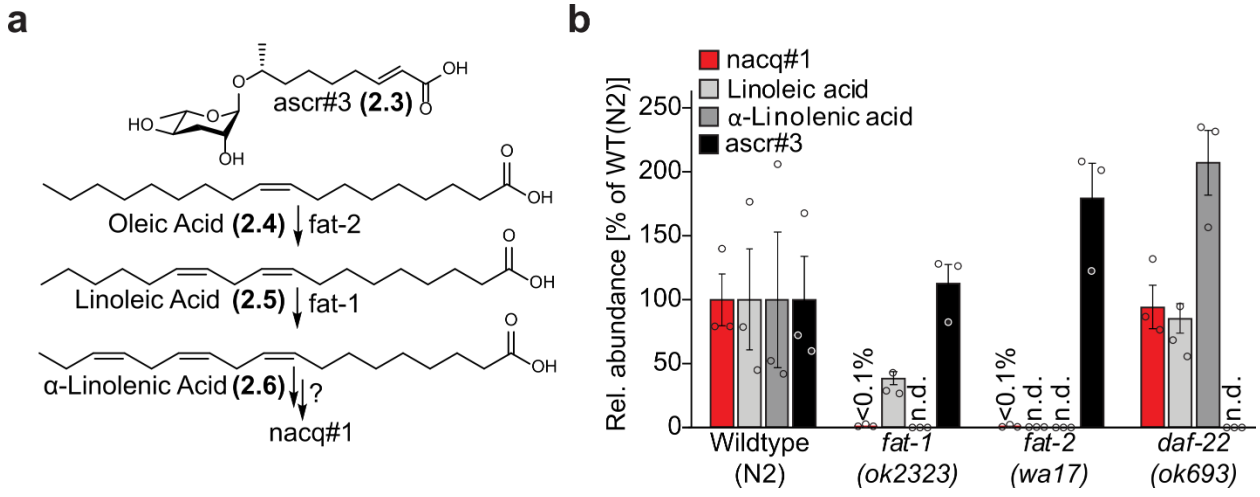

Fig. 2.3 Origin of the unsaturated lipid moiety in nacq#1| a. Chemical structures of compounds in **b** and enzymatic roles of *fat-1* and *fat-2*. **b.** HPLC-MS-based quantification of nacq#1, linoleic acid, α-linolenic acid, and ascr#3 in the *exo*-metabolomes of wildtype (N2), *fat-1(ok2323)*, *fat-2(wa17)*, and *daf-22(ok693)* worms (n = 3 biologically independent samples). Error bars represent mean ± s.e.m.

2.4 nacq#1 accelerates development and shortens lifespan

To explore the biological properties of nacq#1, we developed a short synthesis that provided access to pure nacq#1 and related compounds (Fig. 2.4). Tosylation of (*Z*)-hex-3-en-1-ol (**2.7**) was followed by conversion to the corresponding phosphonium iodide salt (**2.9**). The triply unsaturated fatty acid chain in nacq#1 was then formed by the Wittig reaction between salt **2.9** and aldehyde (**2.8**). Acidic hydrolysis of the resulting ester yielded *(2E,4Z,7Z)*-decatrienoic acid (**2.10**). Acid **2.10** was then coupled to L-glutamine *t*-butyl ester followed by acidic deprotection to furnish synthetic nacq#1 that was used for all subsequent biological experiments. First, we confirmed that synthetic nacq#1 at picomolar to low nanomolar concentrations accelerated reproductive development, by measuring the onset of egg laying (Fig. 2.5a and Supp. Fig. 2.7a) and the age at which adult morphology was attained (Supp. Fig. 2.7b,c). Higher concentrations of nacq#1 were less effective, resulting in a bell-shaped dose–response curve, as is the case for responses to other small-molecule signals in *C. elegans* and other species[17,18,19]. Hermaphrodites produced on the order of 16 femtomoles of nacq#1 per individual during the transition from L4 to young adult, corresponding to accumulation of picomolar concentrations of nacq#1 on conditioned plates, which is consistent with the range of active concentrations observed for synthetic nacq#1. In contrast, neither nacq#2 nor the free fatty acid (nacq#1 without glutamine) was active at any of the tested concentrations (Supp. Fig. 2.8). Similarly, the most abundant male-enriched ascaroside, ascr#10 (**11**), did not by itself accelerate larval development in hermaphrodites, nor did it synergize with nacq#1 (Supp. Fig. 2.9)[20]. Male-excreted compounds shorten the last larval stage (L4), and we found that synthetic nacq#1 also specifically accelerated this stage of development (Supp. Fig. 2.5b)[4]. Given the relatively modest extent of acceleration— approximately 2–3 h or approximately 3–5% of the total egg-to-egg developmental time—we tested whether there was any impact on the

onset of reproduction. Hermaphrodites raised in the presence of nacq#1 on average produced roughly 30% more offspring during the first day of egg laying (Fig. 2.5e), which is a notable advantage for a species with a fast boom-and-bust life cycle[21].

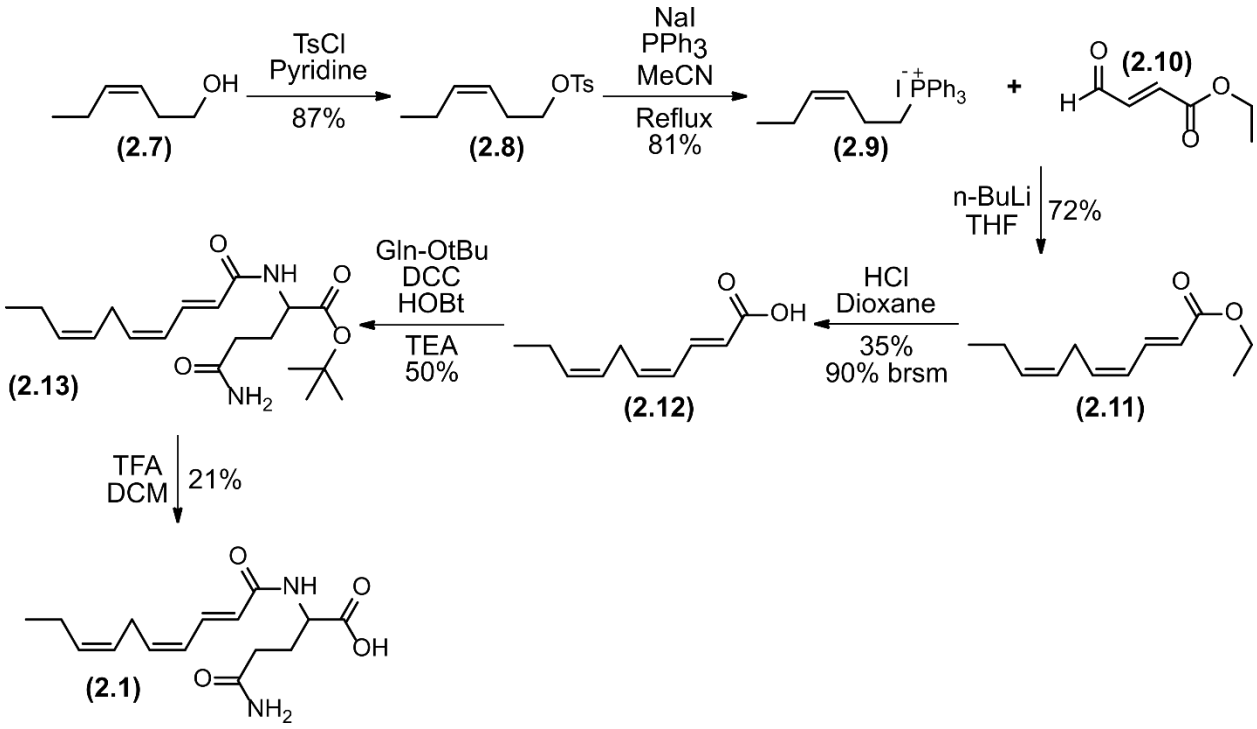

Fig. 2.4 | Synthesis of nacq#1 and related molecules.

Next, we asked whether nacq#1 could also explain the observation that the presence of males[10–12] and, under some conditions, high population density shorten the lifespan of hermaphrodites[4]. Previous studies had shown that the lifespan-shortening effect of the male exo-metabolome is at least partly dependent on the ascaroside biosynthetic enzyme DAF-22, implicating as one factor the ascaroside ascr#10, which is excreted at much higher levels by males than by hermaphrodites[11,12,20]. To test whether nacq#1 affects hermaphrodite lifespan, we used a single-worm assay that largely prevented the potentially confounding exposure of test animals to excreted metabolites from other worms. We found that exposure to picomolar concentrations of nacq#1 significantly reduced lifespan from 16.3 days to 13.6 days (Fig. 2.4b), similarly to the

lifespan shortening observed for hermaphrodites exposed to male exo-metabolome[11]. In contrast, nacq#1 had little effect in lifespan assays conducted at higher population density.

Because males produce much more nacq#1 than hermaphrodites (Fig. 2.2d), our results suggest that individual males and hermaphrodites at high population density produce sufficient quantities of nacq#1 (and possibly additional substances) to shorten hermaphrodite lifespan. However, singled hermaphrodites and groups of hermaphrodites have a similar lifespan in aging assays set up with worms as young adults or L4 larvae[4,12,22]. Combined with our finding that nacq#1 is excreted by hermaphrodites primarily during the transition from the L4 larval stage to young adults but later in adulthood by males (Fig. 2.2b), these results indicate that lifespan is determined not only by population density during adulthood, but also by the social conditions and associated exposure to nacq#1 and other pheromones experienced by larvae between hatching and the onset of adulthood.

Next, we assessed the effects of nacq#1 and ascr#10, both of which are produced in larger quantities by males, on hermaphrodite lifespan. We confirmed that ascr#10 shortens hermaphrodite lifespan and found that the lifespan-shortening effects of ascr#10 and nacq#1 were additive at low concentrations (Fig. 2.5c and Supp. Fig. 2.10), indicating that they may act via partly independent molecular mechanisms. Notably, nacq#1 shortened hermaphrodite lifespan significantly at concentrations as low as 1 pM, to a degree that was similar to the lifespan-shortening effect of ascr#10 at 4 nM. Because nacq#1 is active at lower concentrations than ascr#10, and given that males excrete similar amounts of ascr#10 and nacq#1, the effect of nacq#1 on hermaphrodite lifespan may outweigh that of ascr#10 under natural conditions; however, ascarosides are chemically much more stable than nacq#1, and the spatial and temporal deposition of these compounds by males differ slightly (Fig. 2.4d)[20,23]. Neither metabolite is excreted at

appreciable quantities as larvae, but both are produced robustly in adulthood. While nacq#1 excretion ceases after a few days ascr#10 is excreted at a roughly constant level throughout all days of adulthood examined.

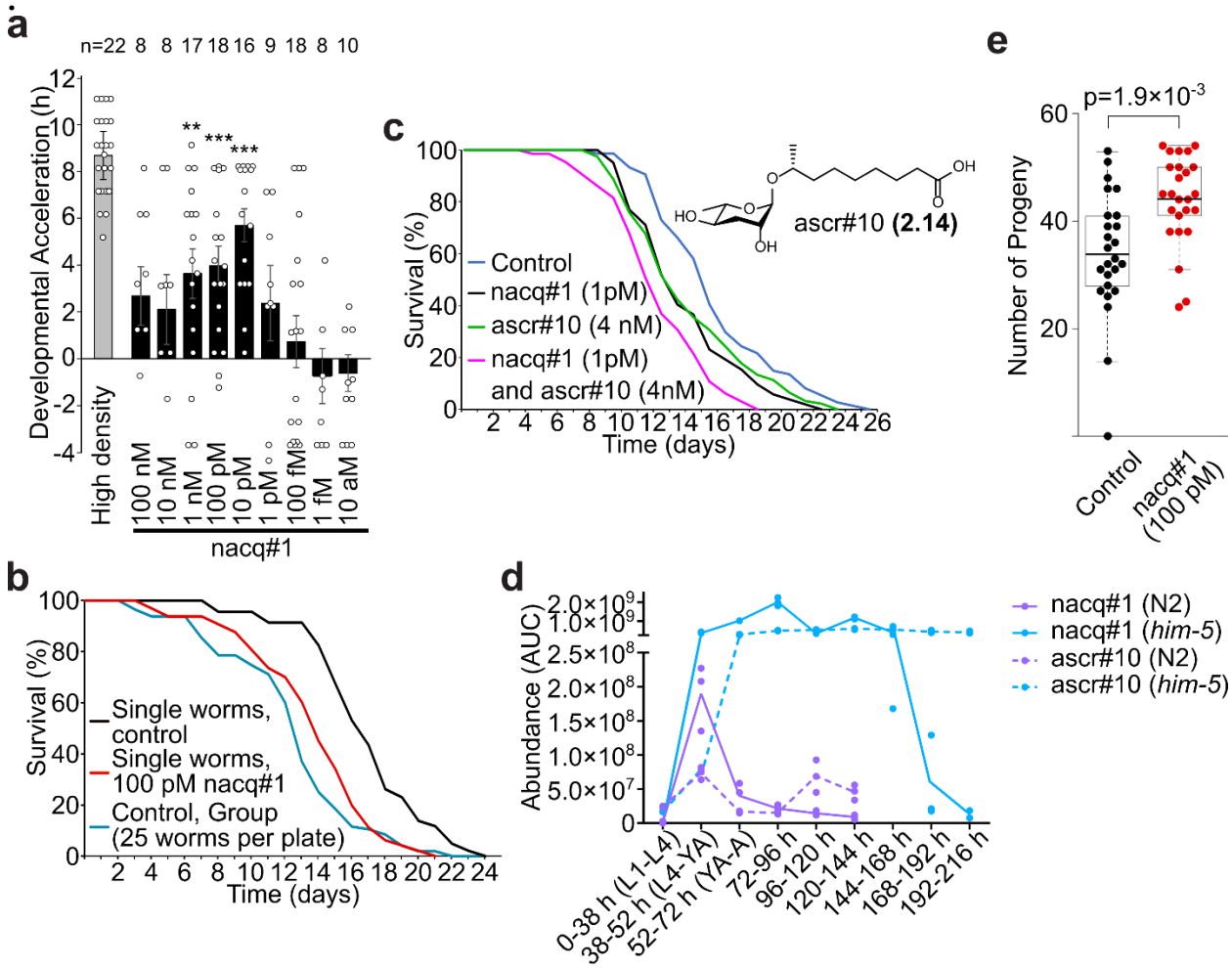

Fig. 2.5 Biological properties of nacq#1. a. Developmental acceleration assays measuring the onset of egg laying in daf-22 worms exposed to nacq#1 (numbers of worms tested for each condition as indicated). **b.** Survival of groups of hermaphrodites (25 worms per plate; blue) and singled hermaphrodites (1 worm per plate) in the presence (red) or absence (black) of nacq#1. Assays were repeated three times for grouped worms and six times for singled worms. **c.** Survival of singled hermaphrodites on plates containing nacq#1, ascr#10 or both compounds. Assays were repeated five times. **d.** UHPLC-MS-based quantification of nacq#1 in the exo-metabolomes collected during different time intervals of N2 and *him-5(e1490)*, corresponding to different developmental stages and points in adulthood. **e.** Progeny production during the first day of reproduction. Each dot represents the offspring of one parent (n=25 (control) and n=21 (nacq#1) worms per time point. Data are presented as mean ± s.e.m. **, p≤0.005; ***, p≤0.0005.

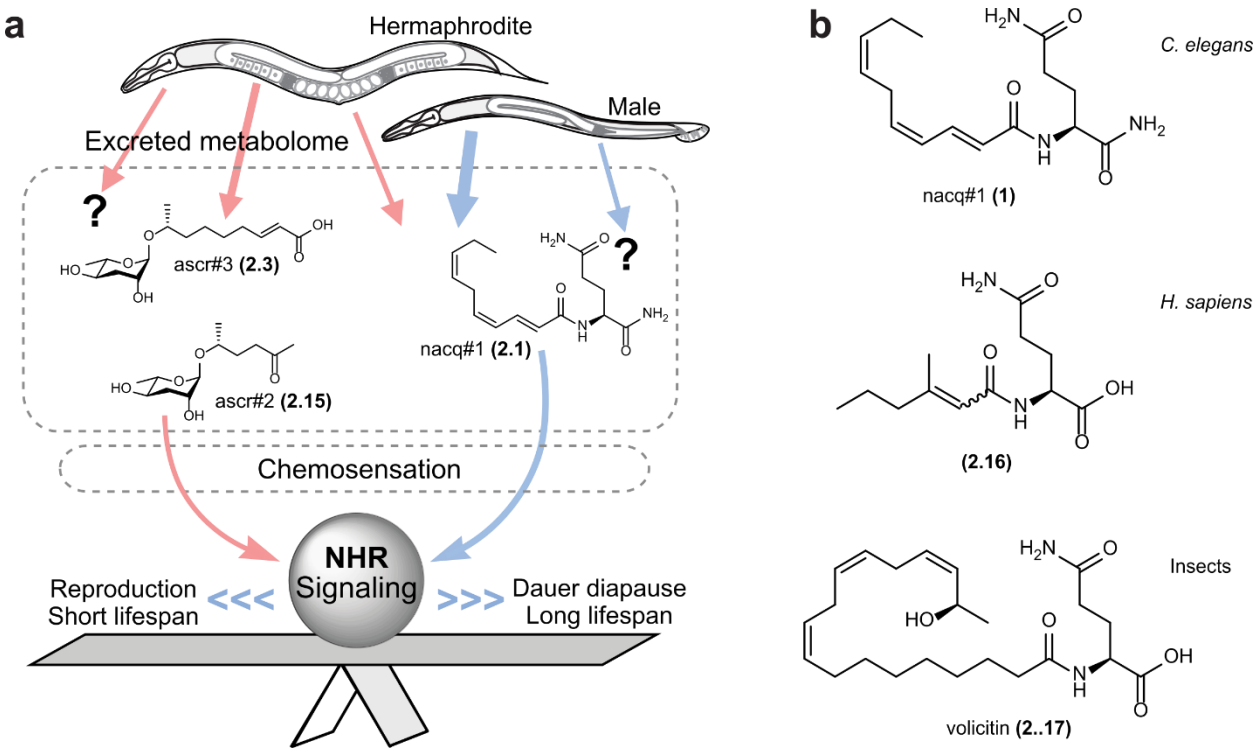

Fig. 2.6 nacq#1 signals via conserved signaling pathways. **a.** Competing small-molecule signals regulate development via NHR signaling. **b.** Chemical structures of N-acyl amino acids similar to nacq#1 identified from other phyla.

2.5 Discussion

Males and, to a lesser extent, hermaphrodites excrete a small molecule signal, nacq#1, that antagonizes diapause and accelerates development, hastening sexual maturation, but at the expense of a reduced lifespan (Fig. 2.6a). Because of the associated costs, reproductive commitment may be singularly attuned to signals from potential mates and competitors. In natural habitats, *C. elegans* are often found as developmentally arrested, dispersing dauer larvae[9]. A small molecule excreted upon reaching sexual maturity, nacq#1, may indicate that sufficient resources are available to exit the dauer stage and resume reproductive development. nacq#1 further accelerates sexual maturation in larvae that are already developing into adults. This latter role of nacq#1, predominantly produced by males after reaching full adulthood, is reminiscent of the signal

produced by sexually mature male mice that induces earlier onset of the first estrus in peripubescent females[3]. These parallels suggest that signals excreted primarily by males modulate similar developmental processes in divergent animal lineages. Overall, our findings present a picture of a pull–push system of small-molecule signals that fine-tune development and longevity in response to changing social environments by modulating conserved gene regulatory networks (Fig. 2.6a). The chemical structure of nacq#1 suggests parsimonious use of simple building blocks from primary metabolism—the amino acid glutamine and an unusual triply unsaturated ten-carbon fatty acid that could be derived from canonical omega-3 fatty acids, for example eicosapentaenoic or linolenic acid. Notably, unusual fatty acylated glutamines have been reported from multiple animal phyla. For example, a compound featuring an uncommon branched acyl moiety, *N*-3-methyl-2-hexenoylglutamine (**13**), occurs in human sweat[24] (Fig. 2.6b). It is unclear whether these human metabolites serve a biological function, as may be suggested by the otherwise uncommon fatty acid moieties. In addition, amino acid derivatives of long-chain fatty acids have been implicated in intra- and interorganismal signaling in vertebrates and invertebrates, for example volicitin (**14**)2[5,26,27,28]. Our discovery of nacq#1 as a regulator of development and lifespan *in C. elegans* suggests that related small molecules may serve signaling functions throughout metazoa.

References

(1) von Reuss, S. H. & Schroeder, F. C. Combinatorial chemistry in nematodes: modular assembly of primary metabolism-derived building blocks. *Nat. Prod. Rep.* **32**: 994-1006. **2015**.

(2) Gendron, C. M., *et at*. *Drosophila* life span and physiology are modulated by sexual perception and reward. *Science* **343**: 544-548. **2014**.

(3) Vandenbergh, J. G. Male odor accelerates female sexual maturation in mice. *Endocrinology* **84**: 658-660. **1969**.

(4) Ludewig, A. H. *et al.* Larval crowding accelerates *C. elegans* development and reduces lifespan. *PLoS Genet.* **13**: e1006717. **2017**.

(5) Aprison, E. Z. and Ruvinsky, I. Sexually antagonistic male signals manipulate germline and soma of *C. elegans* hermaphrodites. *Curr. Biol.* **26**: 2827-2833. **2016**.

(6) Ludewig, A. H. and Schroeder, F. C. in *WormBook* (ed. The *C. elegans* Research Community) **2015**.

(7) Schroeder, F. C. Modular assembly of primary metabolic building blocks: a chemical language in *C. elegans*. *Chem. Biol.* **22**: 7-16. **2015**.

(8) Butcher, R. A. Small molecule pheromones and hormones controlling nematode development. *Nat. Chem. Biol.* **13**: 577-586. **2017**.

(9) Frezal, L. and Feliz, M. A. *C. elegans* outside the Petri dish. *eLife* **4**: e05849. **2015**.

(10) Shi, C. and Murphy, C. T. Mating induces shrinking and death in *Caenorhabditis* mothers. *Science* **343**: 536-540. **2014**.

(11) Maures, T. J. *et al.* Males shorten the life span of *C. elegans* hermaphrodites via secreted compounds. *Science* **31**: 541-544. **2014**.

(12) Shi, C., Runnels, A. M., Murphy, C. T. Mating and male pheromone kill *Caenorhabditis* males through distinct mechanisms. *eLife* **6**: e23493. **2017**.

(13) Artyukhin, A. B. *et al*. Metabolomic "dark matter" dependent on peroxisomal β-oxidation in *Caenorhabditis elegans. JACS* **140**: 2841-2852. **2018**.

(14) Von Reuss, S. H. *et al.* Comparative metabolomics reveals biogenesis of ascarosides, a modular library of small molecule signals in *C. elegans. JACS* **134**: 1817-1824. **2012**.

(15) Forsber, E. M., *et al*. Data processing, multi-omic pathway mapping, and metabolite activity analysis using XCMS Online. *Nat. Protoc.* **13**: 633-651. **2018**.

(16) Tautenhahn, R., Bottcher, C., Neumann, S. Highly sensitive feature detection for high resolution LC/MS. *BMC Bioinformatics* **9**: 504. **2009**.

(17) Pungaliya, C., *et al*. A shortcut to identifying small molecule signals that regulate behavior and development in *Caenorhabditis elegans. Proc. Natl Acad. Sci.* **106**: 7708-7713. **2009**.

(18) Aprison, E. Z. & Ruvinsky, I. Counteracting ascarosides act through distinct neurons to determine the sexual identity of *C. elegans* pheromones. *Curr. Biol.* **27**: 2589-2599. **2017**.

(19) He, J., *et al*. Distinct signals conveyed by pheromone concentrations to mouse vomeronasal organ. *J. Neurosci.* **30**: 7473-7483. **2010**.

(20) Izrayelit, Y., *et al.* Targeted metabolomics reveals a male pheromone and sex-specific ascaroside biosynthesis in *Caenorhabditis elegans. Genetics* **7**: 1321-1325. **2012**.

(21) Schulenburg, H. and Felix, M. A. The natural biotic environment of *Caenorhabditis elegans*. *Genetics* **206**: 55-86. **2017**.

(22) Gems, D. & Riddle, D. L. Genetic, behavioral and environmental determinants of male longevity in *Caenorhabditis elegans. Genetics* **154**: 1597-1610. **2000**.

(23) Srinivasan, J. et al. A blend of small molecules regulates both mating and development in *Caenorhabditis elegans. Nature* **454**: 1115-1118. **2008**.

(24) Butcher, R. A., Fujita, M., Schroeder, F. C. & Clardy, J. Small-molecule pheromones that control dauer development in *Caenorhabditis elegans. Nat. Chem. Biol.* **3**: 420-422. **2007**.

(25) Jeong, P. Y. et al. Chemical structure and biological activity of the *Caenorhabditis elegans* dauer-inducing pheromone. *Nature* **433**: 541-545. **2005**.

(26) Ludewig, A. H. et al. Pheromone sensing regulates *Caenorhabditis elegans* lifespan and stress resistance via the deacetylase SIR-2.1. *Proc. Natl Acad. Sci.* **110**: 5522-5527. **2013**.

(27) Golden, J. W. & Riddle, D. L. A pheromone influences larval development in the nematode *Caenorhabditis elegans. Science* **218**: 578-80. **1982**.

(28) Hu, P. J. in WormBook (ed. The *C. elegans* Research Community) **2007**.

(29) Kenyon, C. The plasticity of aging: insights from long-lived mutants. *Cell* **120**: 449-460. **2005**.

(30) Kaplan, F. et al. Ascaroside expression in *Caenorhabditis elegans* is strongly dependent on diet and developmental stage. *PLoS ONE* **6**: e17804. **2011**.

(31) Fielenbach, N. & Antebi, A. *C. elegans* dauer formation and the molecular basis of plasticity. *Genes Dev.* **22**: 2149-2165. **2008**.

(32) Mangelsdorf, D. J. et al. The nuclear receptor superfamily: the second decade. *Cell* **83**: 835-839. **1995**.

(33) Antebi, A., Yeh, W. H., Tait, D., Hedgecock, E. M. & Riddle, D. L. daf-12 encodes a nuclear receptor that regulates the dauer diapause and developmental age in *C. elegans. Genes Dev.* **14**: 1512-1527. **2000**.

(34) Ludewig, A. H. et al. A novel nuclear receptor/coregulator complex controls *C. elegans* lipid metabolism, larval development, and aging. *Genes Dev*. **18**: 2120-2133. **2004**.

(35) Magner, D. B. et al. The NHR-8 nuclear receptor regulates cholesterol and bile acid homeostasis in *C. elegans. Cell Metab.* **18**: 212-224. **2013**.

(36) Tondamal, M., Witting, M., Schmitt-Kopplin, P. & Aguilaniu, H. Steroid hormone signalling links reproduction to lifespan in dietary-restricted *Caenorhabditis elegans. Nat. Commun.* **5**: 4879. **2014**.

(37) 7. Bargmann, C. I. & Horvitz, H. R. Control of larval development by chemosensory neurons in *Caenorhabditis elegans. Science* **251**: 1243-1246. **1991**.

(38) Schackwitz, W. S., Inoue, T. & Tomas, J. H. Chemosensory neurons function in parallel to mediate a pheromone response in *C. elegans. Neuron.* **17**: 719-728. **1996**.

(39) Alcedo, J. & Kenyon, C. Regulation of *C. elegans* longevity by specifc gustatory and olfactory neurons. *Neuron.* **41**: 45-55. **2004**.

(40) Apfeld, J. & Kenyon, C. Regulation of lifespan by sensory perception in *Caenorhabditis elegans. Nature* **402**: 804-809. **1999**.

(41) Park, D. et al. Interaction of structure-specifc and promiscuous G-proteincoupled receptors mediates small-molecule signaling in *Caenorhabditis elegans. Proc. Natl Acad. Sci.* **109**: 9917-9922. **2012**.

(42) Maglich, J. M. et al. Comparison of complete nuclear receptor sets from the human, *Caenorhabditis elegans* and *Drosophila genomes. Genome Biol.* **2**: research0029.7-0029.7. **2001**.

(43) Wollam, J. & Antebi, A. Sterol regulation of metabolism, homeostasis, and development. *Annu. Rev. Biochem.* **94**: 355-382. **2011**.

(44) Gems, D. & Partridge, L. Genetics of longevity in model organisms: debates and paradigm shifts. *Annu. Rev. Physiol.* **75**: 624-644. **2013**.

(45) Maklakov, A. A. & Immler, S. The expensive germline and the evolution of ageing. *Curr. Biol.* **26**: R577-R586. **2016**

(46) Kuhn, F. & Natsch, A. Body odour of monozygotic human twins: a common pattern of odorant carboxylic acids released by a bacterial aminoacylase from axilla secretions contributing to an inherited body odour type. *J. R. Soc. Interface* **6**: 377-392. **2009**.

(47) Long, J. Z. et al. The secreted enzyme PM20D1 regulates lipidated amino acid uncouplers of mitochondria. *Cell* **166**: 424-435. **2016**.

(48) Long, J. Z. et al. Ablation of PM20D1 reveals N-acyl amino acid control of metabolism and nociception. *Proc. Natl Acad. Sci.* **115**: E6937-E6945. **2018**.

(49) Schmelz, E. A., Engelberth, J., Alborn, H. T., Tumlinson, J. H. & Teal, P. E. A. Phytohormone-based activity mapping of insect herbivore-produced elicitors. *Proc. Natl Acad. Sci.* **106**: 653-657. **2009**.

(50) Weiss, L. C. et al. Identifcation of *Chaoborus* kairomone chemicals that induce defences in *Daphnia. Nat. Chem. Biol.* **14**: 1133-1139. **2018**.

CHAPTER 3

β-METHYL LIPIDS ARE ENRICHED IN MALES

Contributions and Acknowledgments

The work presented here intersects with several other research projects in the Schroeder lab. The first β-methyl lipids were discovered by Dr. Maximillian Helf (MH) during his studies of the methyltransferase F13D12.9 and were then found to be dependent on α-oxidation by Dr. Alex Artyukhin (AA). This chapter focuses on the discovery by RNB that β-methyl lipids are dramatically enriched in males and that they represent a large and structurally diverse family of compounds. Further, this chapter reports the enantioselective synthesis for several important members of the β-methyl family of lipids and their biological activity. MH, Dr. Bennett W. Fox (BWF), AA, RNB, and Dr. Amaresh Chaturbedi (AC) contributed *C. elegans* samples. Metabolomic analysis was performed by RNB and BWF. Part of the syntheses of racemic bemeth#1 and bemeth#23 was performed by Dr. Frank C. Schroeder (FCS) and YZ. Stereoselective synthesis was performed by RNB. Biological assays referred to in this Chapter were performed by BWF and AC.

Abstract

Among the classes of male-enriched metabolites discovered from the work outlined in Chapter 1, analysis of MS2 spectra revealed a large number of putative derivatives of β-methyl decanoic acid (bemeth#s). This included the mono- and dihydroxylated derivatives (bemeth#23 and bemeth#31), whose production had previously been shown to depend on a putative methyltransferase, F13D12.9. In this work, we developed a stereoselective synthesis that established the absolute configuration of the putative parent compound, β-methyl-4*E*-decanoic acid (bemeth#1), and its derivatives. In addition, we here identified three amino acid conjugates (bemeth#71, bemeth#81, and bemeth#91) that are strongly upregulated in males. We further showed that upregulation of bemeth#s depends on the male germline and that production in males is very low until the transition from the L4 larval stage to young adulthood, after which production peaks and then gradually declines. Bioassays with synthetic compounds demonstrate that the parent compound, bemeth#1, strongly activates expression of the fatty acid desaturase FAT-7, likely via the nuclear hormone receptor NHR-49.

3.1 Introduction

During the development of the MetaboSeek metabolomics platform, Dr. Maximilian Helf *et al*. examined the role of a putative methyltransferase, F13D12.9[1]. Differential analysis between wildtype N2 and F13D12.9 mutants (the *C. elegans* homolog of 2-hydroxyphytanoyl-CoA-lyase, HACL1) revealed several metabolites whose production was strictly F13D12.9-dependent. The most abundant of these methyltransferase-dependent compounds, named bemeth#23 ($C_{11}H_{20}O_3$) and bemeth#3.1 ($C_{11}H_{20}O_4$), were isolated and identified by MS2 and 2D NMR as (*E)*-2-hydroxy-3-methyldec-4-enoic acid and (*E*)-(2,9)-dihydroxy-3-methyldec-4-enoic acid, respectively.

In a parallel study, bemeth#23 and bemeth#31 were identified as shunt metabolites accumulating in mutants of *hacl-1*, the *C. elegans* homolog of mammalian 2-hydroxyphytanoyl-CoA-lyase, HACL1, a component of the canonical α-oxidation pathway[2]. Therefore, it was hypothesized that bemeth#23 and bemeth#31 are derived from a putative precursor, (*E*)-3-methyldec-4-enoic acid, bemeth#1, which was subsequently detected in wildtype worms and its structure verified via a simple non-stereoselective synthesis (**3.4**) (Fig. 3.1a). A second non-stereoselective synthesis confirmed the planar structure of the monohydroxylated shunt metabolite, bemeth#23, as (*E*)-2-hydroxy-3-methyldec-4-enoic acid (**3.8**) (Fig. 3.1b)[1,3].

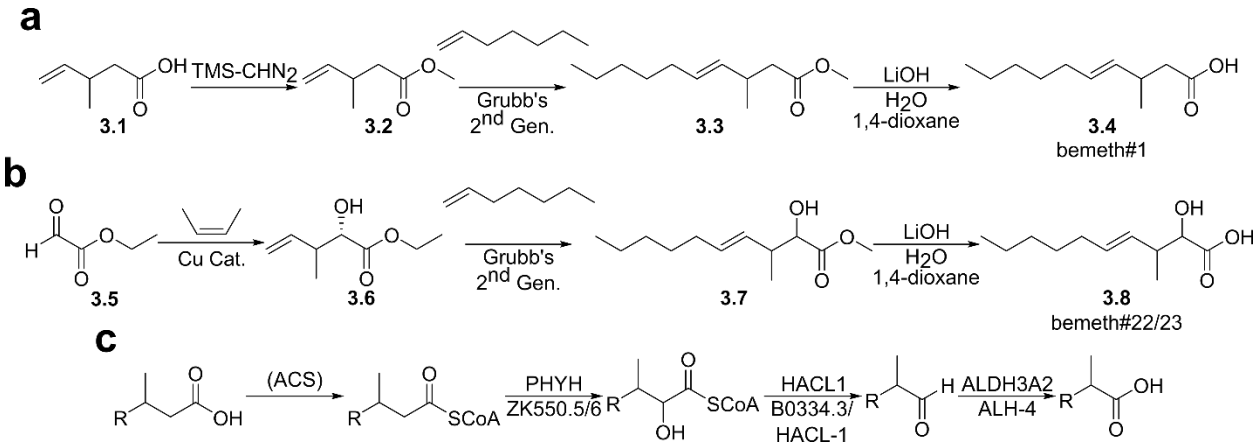

Fig. 3.1 | Previous syntheses and biosynthesis. a. Non-stereoselective synthesis of bemeth#1 performed by Dr. Frank Schroeder. **b.** Non-selective synthesis of a mixture of bemeth#22 and bemeth#23 performed by Dr. Ying Zhang. **c.** α-oxidation of β-methyl lipids in *C. elegans* is proposed to occur in a manner homologous to the human pathway. PHYH, HACL1, and ALDH3A2 are human proteins and ZK550.5/6, HACL-1, and ALH-4 are their corresponding *C. elegans* homologs.

In this Chapter, we show that males produce greatly increased amounts of the bemeth#1 family of compounds. In addition to the previously characterized bemeth#1 derivatives, our differential analysis of N2 and *him-5* revealed a number of additional male-upregulated compounds whose MS2 spectra suggested that they also represent bemeth#1 derivatives (*vide infra*). Increased amounts of these putative bemeth#1 derivatives were further observed in the metabolomes of pure male cultures, 1:1 mixtures of males and hermaphrodites, and in

masculinized *fem-3* (OE) animals whereas putative bemeth#1 derivatives were undetectable in *fem-2* (KO) and *glp-1* (KO) metabolomic extracts. The second part of this Chapter describes development of an enantioselective synthesis that provided access to the enantiomers of the parent compound, (3*R*,*E*) and (3*S*,*E*)-3-methyldec-4-enoic acid, enabled determination of the stereochemistry of naturally occurring derivatives, and provided samples for bioassays.

3.2 Males produce increased amounts of bemeth# family metabolites

Untargeted comparison of the exo-metabolomes of male-enriched *him-5* cultures and wildtype as described in Chapter 1 uncovered nine compounds that appeared to represent derivatives of a C_{11} carboxylic acid and were upregulated from 3- to 24-fold in male or masculinized cultures (Fig. 3.3a). Biosynthesis of all nine compounds was found to be abolished in mutants of the methyltransferase F13D12.9, indicating that these metabolites feature a β-methyldecanoic acid backbone. Analysis of the MS2 spectra yielded fragments consistent with those of the previously identified bemeth#1 family compounds, e.g. bemeth#22/23 and bemeth#31/32[3]. For example, bemeth#22 (*m/z* 199.1340, $C_{11}H_{20}O_3$, 12.62 min), fragments to yield a glyoxylate fragment (*m/z* 72.9935) characteristic of the α-hydroxylation pattern in 2-hydroxy-3-methyldec-4-enoic acid (bemeth#23), representing a diagnostic fragment for the α-hydroxylated members of the bemeth family of compounds. Neutral losses of formic acid and H_2O, in addition to retention time matching with a synthetic standard from a non-stereoselective synthesis, confirmed the identity of the compound as bemeth#23 (**3.8**)[4]. In addition to bemeth#22 and bemeth#23 we observed two more compounds of the same molecular formula of similar retention times that do not fragment in the same way as bemeth#22 and bemeth#23 (Supp. Fig. 3.19). Despite their difference in MS2 fragmentation their dependence on F13D12.9 verifies that they are β-methyl compounds, perhaps α-keto compounds or products of double bond migration.

In addition, two dihydroxylated bemeth#-derivatives, named bemeth#31 and bemeth#32, were detected among the male enriched metabolites. bemeth#31 and bemeth#32 (*m/*z 215.1287, $C_{11}H_{20}O_4$, 8.54 min) are two of nearly a dozen features of the same mass and similar retention times in the *C. elegans* metabolome, of which only bemeth#31 and bemeth#32 are enriched in males. Similar to bemeth#23, the MS2 spectra of bemeth#31 and bemeth#32 showed a glyoxylate fragment and are consistent with the previously established structure of (*E*)-(1,9)-dihydroxy-3-methyldec-4-enoic acid for bemeth#31 (**3.9**) (Fig. 3.2b)[3]. The MS2 spectra of bemeth#32, which elutes slightly later than bemeth#31 on a reverse-phase column, are similar to those of bemeth#31, indicating that it likely represents a diastereomer of bemeth#31 (Fig. 3.2c). Additional male-enriched metabolites that appear to be related include a compound at *m/z* 213.1134 ($C_{11}H_{18}O_3$, 8.52 min) that fragments nearly identically to the previously published bemeth#31, suggesting that it may represent the corresponding ketone, (*E*)-2-hydroxy-9-keto-3-methyldec-4-enoic acid (bemeth#41, **3.11).** In addition, we detected a putative diacid, (*E*)-2-hydroxy-3-methyldec-4-endioic acid (bemeth#61, **3.12**), likely representing an oxidation product of the diol bemeth#33 (**3.10**), which themselves are not enriched in males, as it fragments to produce the glyoxylate fragment, neutral losses of CO_2, H_2O, CO_2+H_2O, and a double loss of CO_2. Interestingly, although we observed an increase in a putative oxidation product of bemeth#33, we did not see an increase in bemeth#33 at any point in development or adulthood (Supp. Fig. 3.9).

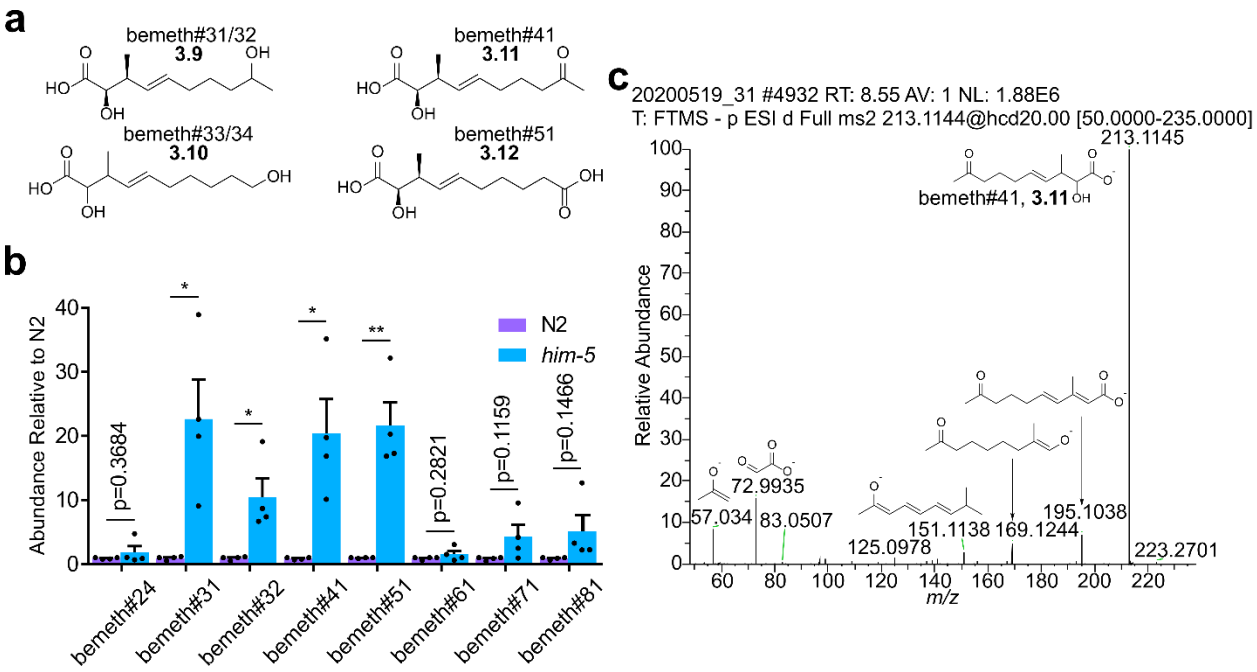

Fig. 3.2 | bemeth#s upregulated in *him-5*. a. The previously identified bemeth#31 and bemeth#32 (**3.9**, chirality of the ω-1 position was not determined) are enriched in males, as are the further oxidized ketone (**3.11**) and diacid (**3.12**). **b.** The oxidized bemeth# acids are significantly enriched in *him-5* cultures over N2, ranging from 9- to 24-fold increases in abundance. **c.** The (ω-1)-ketone bemeth#41 yields the diagnostic glyoxylate fragment (m/z 72.9935) and fragments in a manner like bemeth#3.1 with one additional degree of unsaturation. Data are presented as mean ± s.e.m. *, p≤0.05; **, p≤0.005.

3.2.1 Amino acid conjugates of bemeth#s

Although not initially observed in the comparison of N2 and *him*-5 exo-metabolomes, comparative analysis of exo-metabolome samples of WT and germline-masculinized *fem-3* (OE) worms revealed three compounds that appeared to represent amino acid conjugates of bemeth#23 (Fig. 3.3). Based on their MS2 spectra (*vide infra*) and given that their production is dependent on the methyltransferase, F13D12.9 (Fig. 3.1c), which is required for the biosynthesis of all known bemeth# family compounds, we concluded that these compounds were additional members of the bemeth# family[3]. These putative amino acid conjugates were 7- to 47-fold increased in *fem-3* (OE) over N2 and were also found to be even more enriched in the exo-metabolome of aging *him-5* cultures (Fig. 3.5f). The first such conjugate, bemeth#71 (*m/z* 270.1708, $C_{14}H_{25}NO_4$), fragments to produce an ion at *m/z* 88.0409 ($C_3H_6NO_2^-$) suggesting alanine, a loss of CO_2, as well as C_{10}

species at *m/z* 153.1295 and 155.1420 which are found in the MS2 spectrum of bemeth#23 (Supp. Fig. 3.1 and 3.6). Conjugation of alanine to bemeth#23 to form an amide would also explain the absence of the diagnostic glyoxylate fragment present in the MS2 spectra of other members of the bemeth# family. A second conjugate, bemeth#81 (*m/z* 286.1656, $C_{14}H_{25}NO_5$), fragments similarly to bemeth#7 but instead produces ions suggesting dehydroalanine (*m/z* 86.0240) and serine (*m/z* 104.0348) and was thus assigned as the serine conjugate of bemeth#23.

The third conjugate, bemeth#91 (*m/z* 268.1551, $C_{14}H_{23}NO_4$), also appears to be a serine conjugate, however it appears to be attached to a doubly unsaturated version of bemeth#1, likely the 2,4-diene. bemeth#91 produces the same dehydroalanine and serine fragments as bemeth#81 in addition to fragments corresponding to the doubly unsaturated aliphatic chain, $C_{11}H_{15}O^-$ (*m/z* 163.1139) and $C_{10}H_{15}^-$ (*m/z* 135.1189) (Supp. Fig. 3.8).

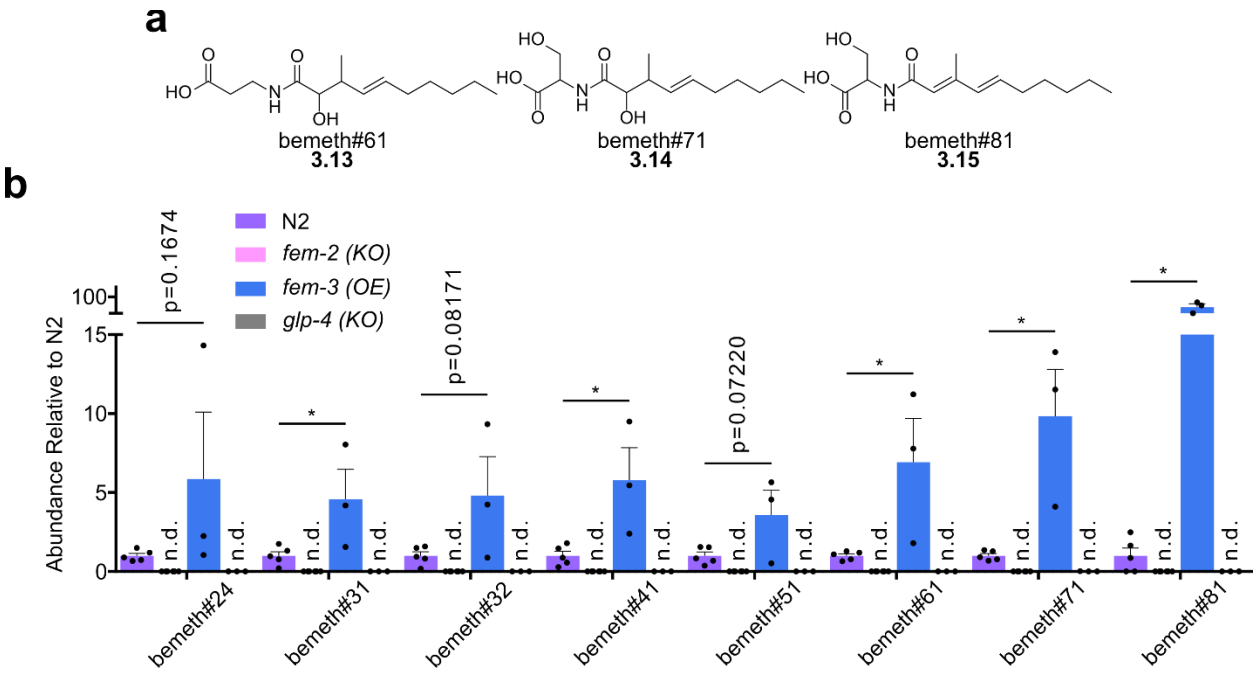

Fig. 3.3 | bemeth# enrichment in *fem-3* (OE) germline mutants. **a.** Members of the bemeth# family are found conjugated to amino acids. **b.** UHPLC-MS quantifiaction of members of the bemeth# family in *fem-2* (KO), *fem-3* (OE), and *glp-4* (KO) relative to the average abundance found in N2. Data are presented as mean ± s.e.m. * p≤0.05.

3.2.2 Enrichment of bemeth#s is observed in all male samples

In 50:50 cultures of males:hermaphrodites we see that bemeth#s are enriched in a manner similar to cultures of *him-5* mutants. In this case, while bemeth#24, bemeth#41, and bemeth#51 are undetectable, we observe a significant increase in the amino-acid conjugated bemeth#s that was not observed in *him*-5 cultures harvested as young adults (Fig. 3.4b). In hand-picked cultures of N2 and *him-5* males relative to N2 hermaphrodites the amino-acid conjugated bemeth#s were even more enriched than in *fem-3* (OE) samples, over 200-fold enriched, although with only two replicates statistical significance cannot be assessed (Fig. 3.4a). As in the 50:50 male:hermaphrodite cultures we observed enrichment of bemeth#31 and bemeth#32 in hand-picked males, whereas bemeth#24, bemeth#41, and bemeth#51 were below the limits of detection.

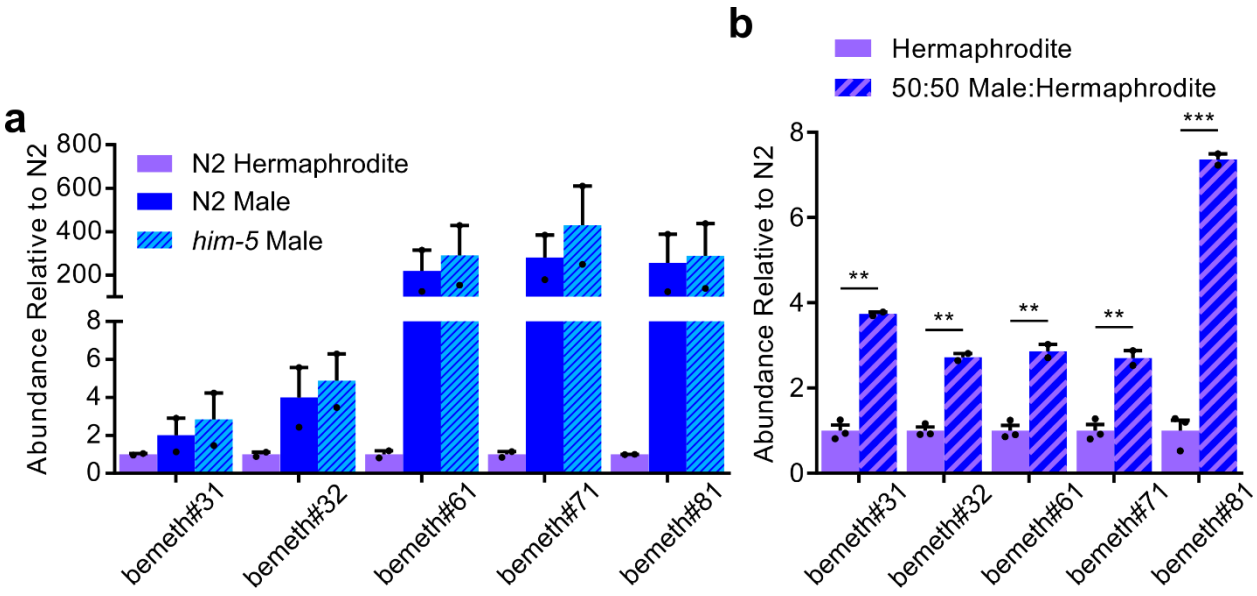

Fig. 3.4 | Presence of bemeth#s in smaller cultures. Quantification of the detected bemeth#s in hand-picked N2 hermaphrodites, N2 males, and *him-5* males (**a**) and hermaphrodite and male-enriched N2 cultures (**b**) presented relative to the levels of N2 hermaphrodites. Data are presented as mean ± s.e.m. **, p≤0.005; ***, p≤0.0005.

3.2.3 Increased production of bemeth#s is dependent on the male germline

Next we compared the relative abundances of bemeth#24-bemeth#81 in our set of germline mutants, including *fem*-2 (KO), *fem-3* (OE), and *glp-4* (KO). We found that production of all characterized bemeth#s we examined was abolished in *glp-4* (KO) mutants, which lack the entire germline, as well as in *fem*-2 (KO) mutants, which have a feminized germline that lacks sperm. As in *him-5* animals, we saw no increase in the abundance of the putative progenitor of the class, bemeth#1[1,3]. The mono-hydroxylated bemeth#24 was slightly enriched in *fem-3* (OE) but this increase did not reach statistical significance. The dihydroxylated acids, bemeth#31 and bemeth#32, and the further oxidized bemeth#41 and bemeth#51, were all significantly increased in *fem-3* (OE) over N2 (Fig. 3.3b). The amino acid conjugates, bemeth#61, bemeth#71, and bemeth#81, while not significantly increased in *him-5* cultures (Fig. 3.2b), were increased significantly in *fem-3* (OE) cultures. Since the production of bemeth#s was abolished in animals lacking sperm and increased 4- to 47-fold in the germline-masculinized *fem-3* (OE) worms, which produce elevated levels of sperm, bemeth# production may be associated with sperm production in the male germline.

3.2.4 Production of bemeth#-family metabolites is starvation- and lifestage-dependent

To assess whether lifestage and nutritional conditions affect production of the male-enriched compounds of the bemeth# family, we analyzed exo and endo-metabolomic samples from animals at various life stages, from the larval stages (L1-L4) to six days of adulthood, or with an abundance or absence of food.

We found that production of 3-methyldec-4-enoic acid (bemeth#) derivatives in wildtype hermaphrodites was generally low during larval stages L1-L4 under well-fed conditions and

increases markedly during the transition to adulthood in hermaphrodites and drops off after that (Fig. 3.4b). In contrast, production of bemeth#-family metabolites remained high and roughly constant at least through six days of adulthood in *him-5* mutants (Fig. 3.4c).

Amino acid conjugates, interestingly, did not follow the same pattern as free β-methyl acids. Like nacq#1, the amino acid conjugates peaked early in adulthood and production decreased throughout life in roughly the same pattern for N2 and *him-5* cultures. While no significant difference in abundance of bemeth#61, bemeth#71, and bemeth#81 was observed in *him-5* cultures harvested as young adults, production of these bemeth#s was most prominent in mature adults, where we saw male-enrichment (Fig. 3.2b, 3.4d, e, f).

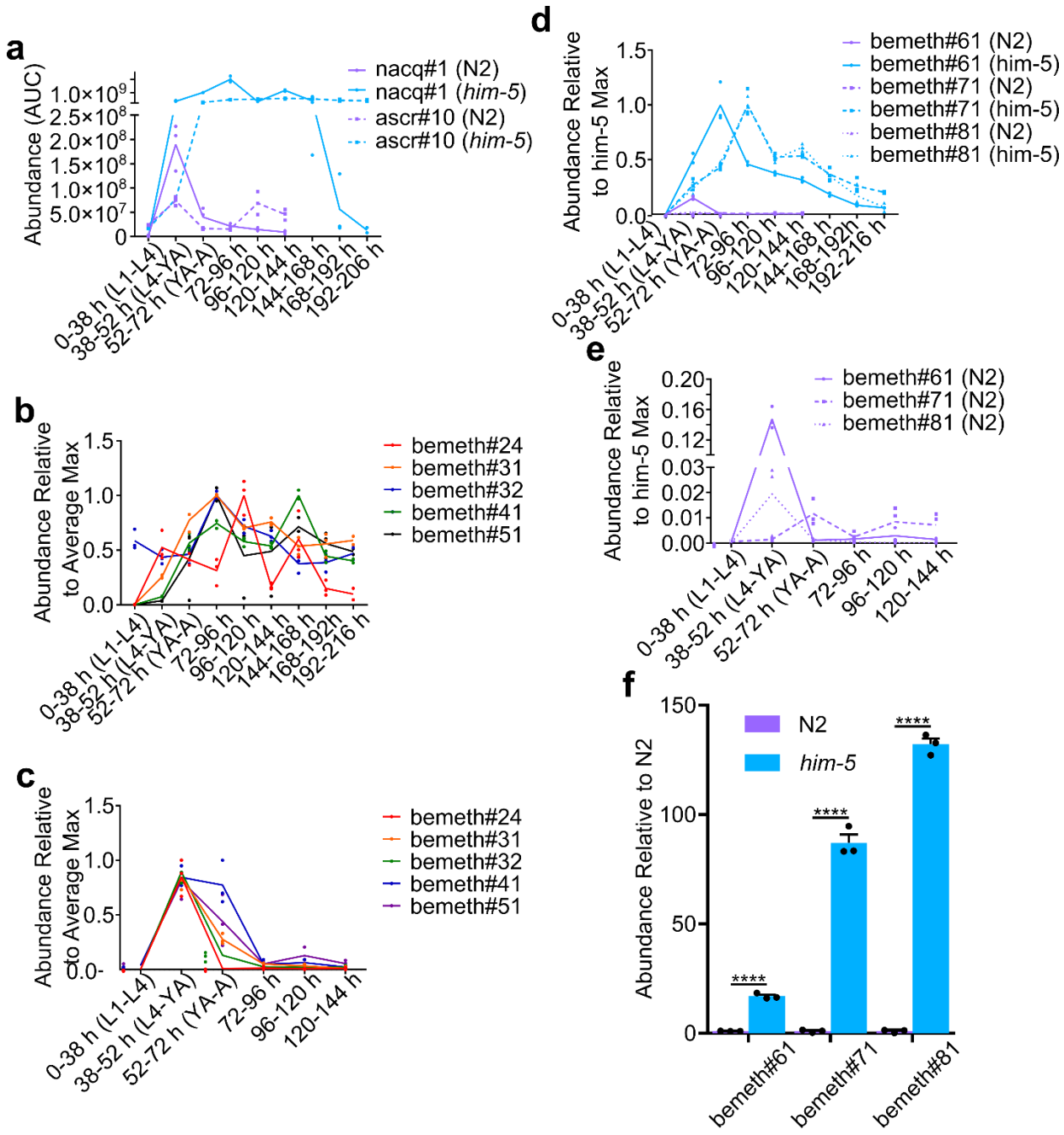

Fig. 3.5 | Age-dependent production of male-enriched metabolites in N2 and *him-5*. **a.** nacq#1 and ascr#10 production quantified by UHPLC-MS. **b,c.** Quantification of free β-methyl lipids in *him-5* (**b**) and N2 (**c**) relative to the average maximum intensity of each bemeth#. **d.** Amino acid conjugated bemeth# quantification in *him-5* and N2 relative to the average maximum intensity of each bemeth# in *him-5*. **e.** A blow-up of the baseline of (**d**) to show N2 levels. **f.** Cumulative excretion of bemeth#61, bemeth#71, and bemeth#81 by N2 and *him-5* from 0-144 h. Data are presented as mean ± s.e.m. ****, p≤0.0001.

3.3.1 Stereospecific synthesis of bemeth#s

In order to determine the absolute configuration and to provide pure samples for bioassays, we developed an enantioselective synthesis of bemeth#1, bemeth#23, and the amino acid conjugates. With the γ-δ unsaturation present in bemeth#1, we envisioned a Claisen rearrangement of vinyl ether **3.20** that would yield a readily oxidized aldehyde (Fig. 3.5b). In the 1960's Paquette and Eizember used an analogous reaction using the vinyl ether of (*E*)-hept-2-en-4-ol (**3.16**, Fig. 3.5a)[6]. The required vinyl ether (**3.20**) could be easily obtained from the corresponding alcohol, which in turn could be prepared via a Grignard reaction with crotonaldehyde (**3.21**).

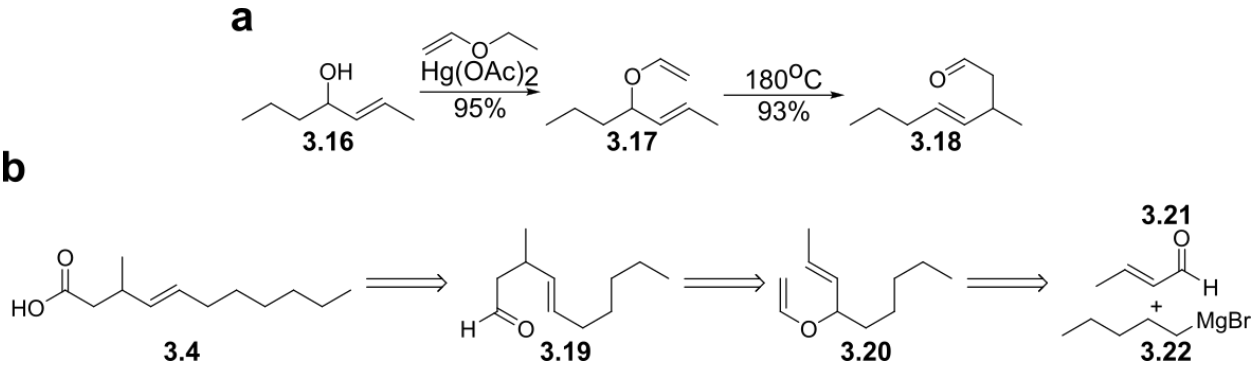

Fig. 3.6 | Retrosynthesis of bemeth#1. a. Paquette and Eizember used an analogous approach to generate aldehyde 3.22 from hept-2-en-4-ol[6]. **b.** bemeth#1 could be obtained via the corresponding aldehyde, obtained via Claisen rearrangement of a vinyl ether derived from a Grignard reaction of crotonaldehyde and pentylmagnesium bromide.

Beginning with crotonaldehyde as envisioned, a Grignard reaction with pentylmagnesium bromide yielded racemic (*E*)-4-hydroxy-non-2-ene (**3.23**) (Fig. 3.6)[7]. With this α-β-unsaturated alcohol in hand, chiral resolution via Sharpless epoxidation produced the (*R*) or (*S*) enantiomers ((*R*)- and (*S*)-**3.24**) respectively with up to 88.8% ee as determined by Mosher derivatization (Supp. Fig. 3.12)[8]. Subsequently, we converted the two enantiomers of **3.24** into the corresponding vinyl ethers (**(*R*)-** and **(*S*)-3.20**), which sets the stage for the Claisen rearrangement[6]. Literature precedent for such a Claisen made no mention of the level of retention of enantiomeric purity; however, the reaction mechanism suggests that no loss of enantiomeric purity should occur, and

thus Claisen rearrangement of **(*S*)-3.20** should selectively produce aldehyde **(*R*)-3.19** (Fig. 3.7a)[6]. Chlorite oxidation of the aldehyde then yielded (*R*)- or (*S*)-bemeth#1 (***(R)*-3.4**), while retaining most enantiomeric purity through the Claisen rearrangement and oxidation, as determined via derivatization with (*R*)-2,2,2,-trifluoro-1-phenethylamine, which revealed an ee up to 65.6% (Supp. Fig. 3.13)[9].

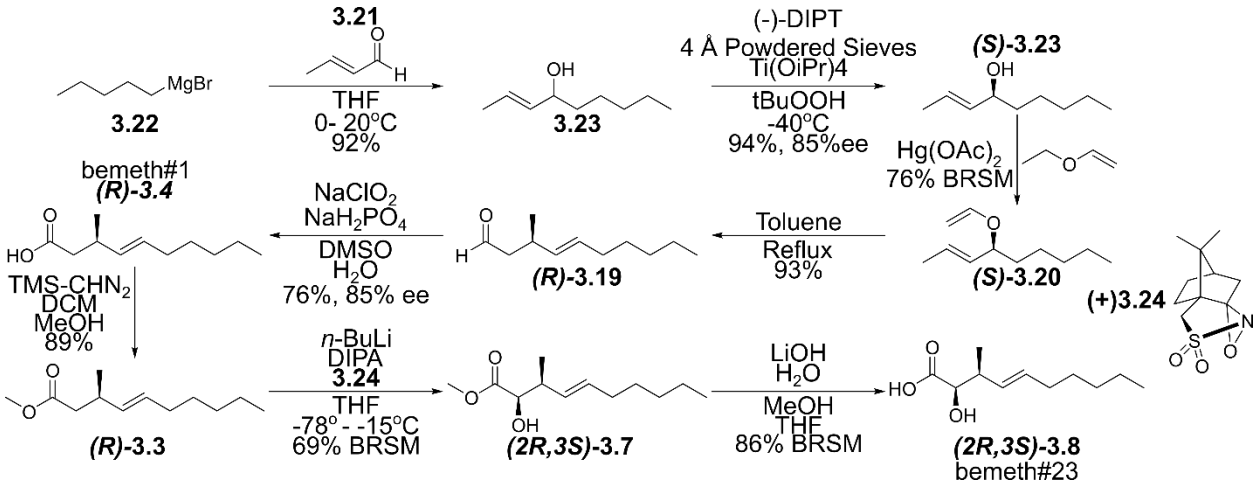

Fig. 3.7 | Synthesis of bemeth#1 and bemeth#23.

As described above, a previous synthesis of bemeth#23 produced mixtures of four different stereoisomers, and the configuration of the naturally occurring isomers was not conclusively assigned; however, it was proposed that the major naturally occurring compound was *syn* with respect to the 2-hydroxyl and 3-methyl groups[4]. Based on these preliminary studies, we used *(R)*-bemeth#1 to prepare the corresponding methyl ester (**(*R*)-3.3**) using TMS-diazomethane. Subsequently, α-hydroxylation of the methyl ester was achieved via Davis oxidation, with the substitution of the original Davis oxaziridine for a camphor-derived alternative (**(+)3.24),** resulting in the stereoselective formation of alcohol **(2*R*,3*S*)-3.7**[10]. Deprotection of the ester (**(2*R*,3*S*)-3.7)** with lithium hydroxide yielded bemeth#23 (**(2*R*,3*S*)-3.8)** with a d.r. of 67.8% (Supp. Fig. 3.14).

Mixtures of steroisomers of the putative amino acid conjugates bemeth#61 (**3.13**) and bemeth#71 (**3.14**) were then formed via EDC coupling of bemeth#23 with alanine or serine (Fig. 3.7b).

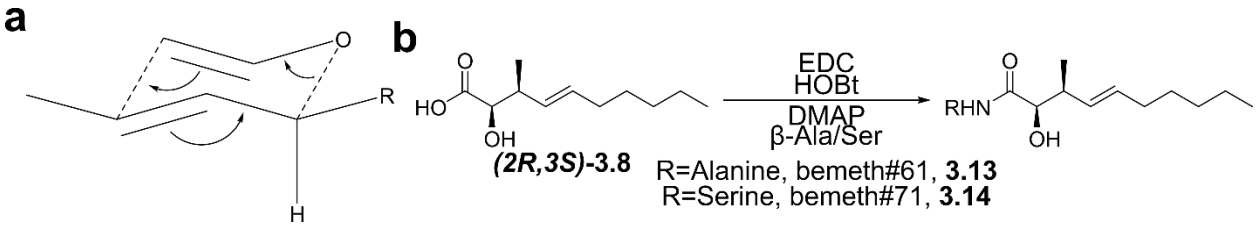

Fig. 3.8 | Origin of chirality and amino acid conjugation. a. The preference for maintaining the R group in the equatorial position leads to the chirality being conferred to the methyl group-bearing carbon. **b.** EDC coupling of amino acids with bemeth#23 yields bemeth#61 or bemeth#71.

3.3.2 Confirmation of compound structures

The stereochemistry of natural bemeth#1 was determined through inference from two separate sources. The first piece of information was determination of the absolute configuration of bemeth#23, which also indicated that bemeth#1 is of the (*R*) configuration.

Previous work on bemeth#23 suggested that the orientation of the 3-hydroxyl and 2-methyl groups is *syn*, thus bemeth#23 should have either (2*R*,3*S*) or (2*S*,3*R*) configuration. Mosher derivatization of a mixture of synthetic (2*R*,3*S)*- and *(*2*S*,3*R)*- bemeth#23 with (*R*)-MTPA yielded a mixture of two fractions, **fx 12** and **fx 13**, which represent two diastereomers, fx 13 co-eluting with the predominant naturally isolated bemeth#23 with (*R*)-MTPA. By comparing the ^{1}H NMR shifts of fx 12 and fx 13, and considering that (*R*)-MTPA was used in this reaction, we derived the stereochemistry of the natural product as follows (Fig. 3.9 and Supp. Fig. 3.15)[4].

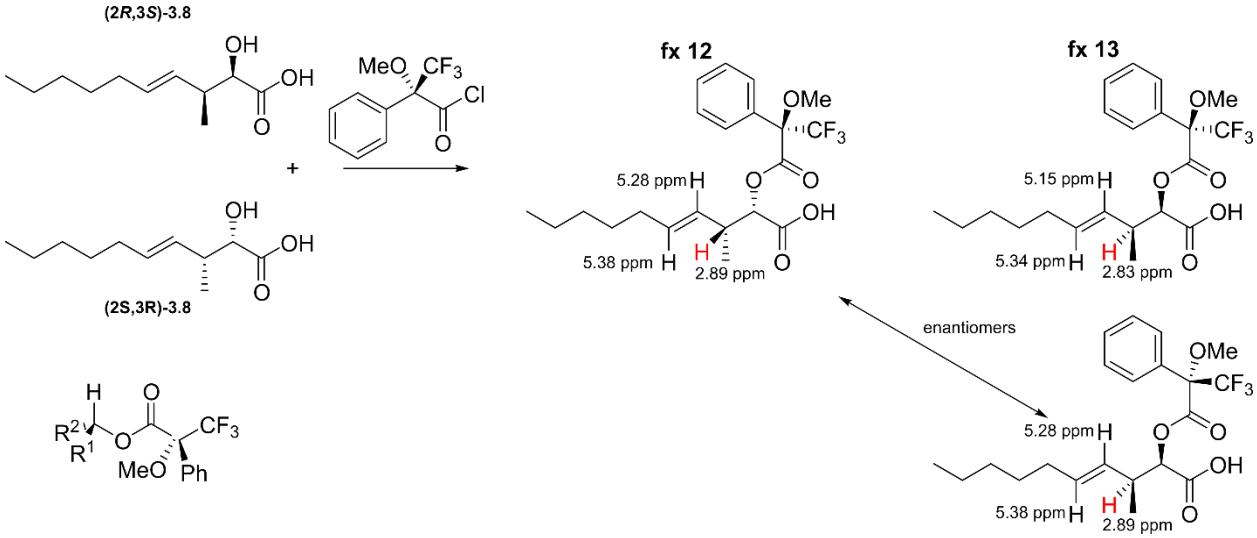

Fig. 3.9 | Determination of chirality of bemeth#23. Fraction 13, which was shown to co-elute with a derivatized synthetic sample of the natural isomer (synthesized by Dr. Kitty Zhang), was found to be (2*R*,3*S*), indicating that bemeth#23 is (2*R*,3*S*,*E*)-2-hydroxy-3-methyldec-4-enoic acid[4]. NMR spectra are visible in Supp. Fig. 3.16.

If we first assume that fx 12 represents the coupling of the compound with (*R*)-MTPA, fx 13 will represent the diastereomer. Under this assumption, the average δ^{SR} (δ_S- δ_R) is -0.08, which assigns the aliphatic chain of bemeth#23 as R^2, making fx 12 (*R*)-MTPA-(2*S*,3*R*)-bemeth#23[4,11]. This, in turn, makes fx 13 "(*S*)"-MTPA-(2*S*,3*R*)-bemeth#23, or (*R*)-MTPA-(2*R*,3*S*)-bemeth#23.

Alternately, if we assign fx 13 as coupling with *(R)*-MTPA, fx 12 would be the reaction with "(*S*)"-MTPA. This, now, results in the value of δ^{SR} now being 0.08, assigning the compound in fx 13 (*R*)-MTPA-(2*R*,3*S*)-bemeth#23. This, like our first calculation, results in the major natural isomer of bemeth#23, which co-elutes with fx 13, to be (2*R*,3*S*,*E*)-2-hydroxy-3-methyldec-4-enoic acid. This assignment was supported by the bioactivity assays described below, which found (*R*,*E*)-3-methyldec-4-enoic acid to be the more active ligand.

Synthetic bemeth#71 co-elutes with the natural sample and fragments in a near identical fashion, which confirmed that bemeth#8 is the serine conjugate of bemeth#23 (Fig. 3.9 and

Supp. Fig. 3.18). The structure of bemeth#61 however was rejected through comparison to a mixture of synthetic standards (Supp. Fig. 3.17). While initial injections of the natural compound and synthetic standards looked promising, additional co-injections of the two samples revealed that the retention times were not perfectly aligned, indicating that bemeth#61 is not the alanine conjugate of bemeth#23, meaning bemeth#61 is either the β-alanine or sarcosine conjugate. As sarcosine production is SAM-dependent, D_3-methionine labeling should yield a D_6-labeled bemeth#23 of *m/z* 292.2034, which is not observed, indicating that bemeth#61 is the conjugate of bemeth#23 and β-alanine (Supp. Fig. 3.11)[12]. Furthermore, while comparison of MS2 spectra revealed a common fragment corresponding to alanine (*m/z* 88.0409), decarboxylation of the synthetic compound was significantly less abundant (Supp. Fig. 3.6).

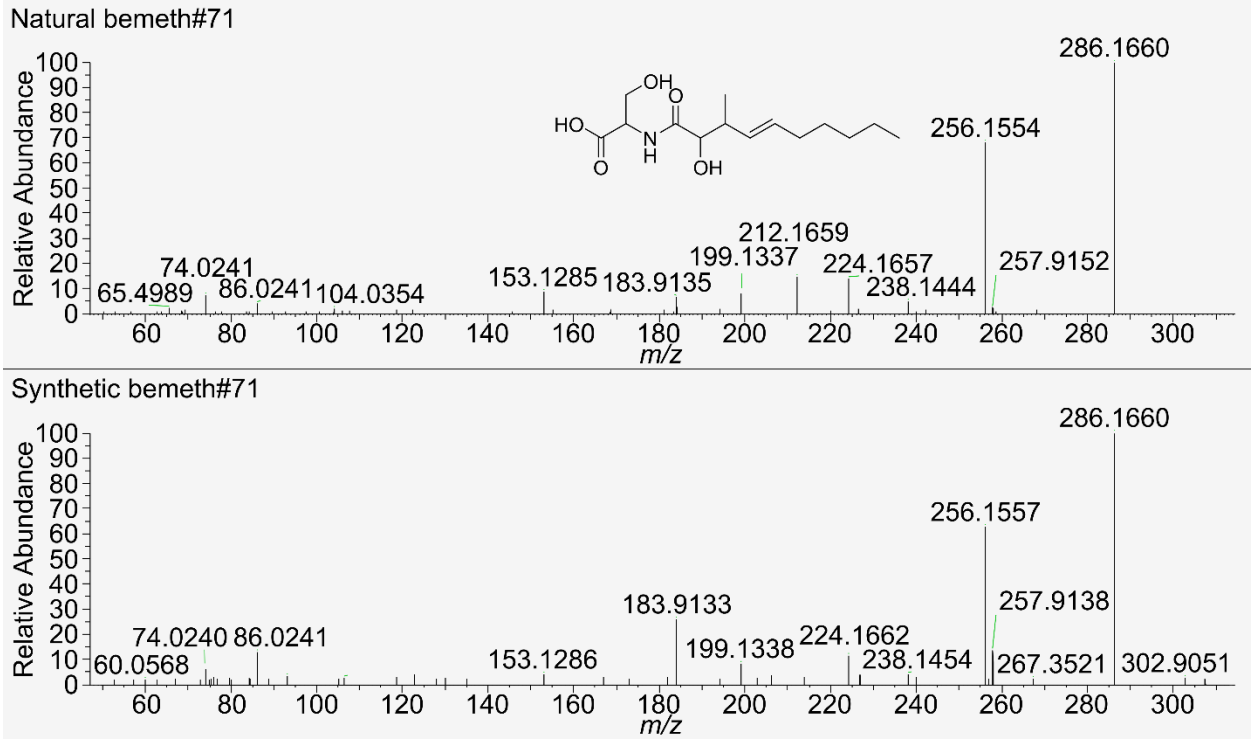

Fig. 3.10 | MS2 validation of bemeth#81. MS2 fragmentation of natural bemeth#71, observed in the exo-metabolome of *fem-3* (OE) cultures, and synthetic bemeth#71.

3.4 Bioactivity of synthetic bemeth#s

Prior research into acyl-CoA-dehydrogenase 11 (ACDH-11) indicated that medium chain fatty acids, C_{10}-C_{12}, induce transcription of FAT-7 through NHR-49[13]. Therefore, we hypothesized that bemeth#1 may represent a ligand of NHR-49. To test this hypothesis we compared activity of undecanoic acid and samples of synthetic bemeth#1 and bemeth#23 in bioassays in which *C. elegans* expressed GFP under a FAT-7 promoter. Feeding of the two enantiomers of bemeth#1 or *n*-undecanoic acid, resulted in significant differences in GFP activation[12]. While the (*R*) enantiomer produced robust GFP fluorescence at even the lowest concentrations used (25 µM), the (*S*) enantiomer and undecanoic acid did not produce similar intensities even at the highest tested concentrations used (100 µM and 500 µM respectively) (Fig. 3.4). The observation that the (*R*) enantiomer is at least 4-times more potent than the (*S*) enantiomer, the (*R*) enantiomer is consistent with our finding that the natural enantiomers of the bemeth# family of compounds have a configuration in the 3 position that corresponds to (3*R*)-configuration in bemeth#1 (priorities of the substituents change e.g. in bemeht#23, result in in a nominal change to (3*S*)). This supports prior experimentation which indicated that natural bemeth#23 is *syn* with respect to the methyl and hydroxyl groups, and later inferred to be (2*R*,3*S*,*E*)-2-hydroxy-3-methyldec-4-enoic acid[4]. α-hydroxylation appears to inactivate bemeth#1, as feeding of bemeth#23 at concentrations up to 300 µM did not induce GFP fluorescence in this assay (Fig. 3.8).

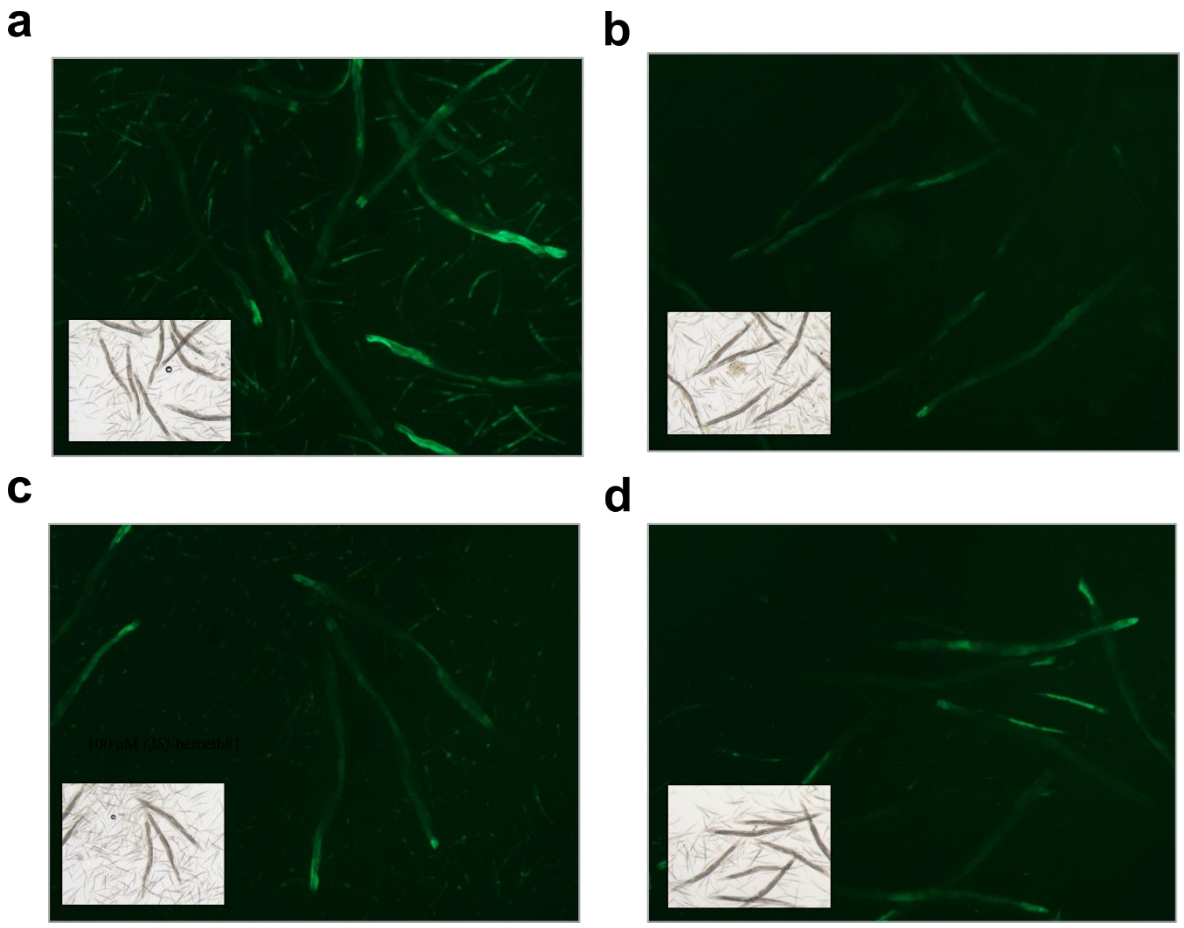

Fig. 3.11 | Feeding of *(E)*-3-methyldec-4-enoic acids to FAT-7::GFP animals. Images of FAT-7::GFP *C. elegans* treated with 50 µM (3*R*)-bemeth#1 (**a**), 100 µM (3*S*)-bemeth#1 (**b**), 300 µM (2*R*,3*S*)-bemeth#23 (**c**), and 500 µM *n*-undecanoic acid (**d**). Taken from images captured by Dr. Bennett W. Fox.

3.5 Discussion

Here we report that a new family of β-methyl lipids, the bemeth#s, are upregulated in male nematodes. We further showed that these compounds are upregulated in wildtype males, not only in genetically altered worms that are used as model systems for maleness. In addition to the previously characterized bemeth#1, bemeth#23, and bemeth#31, we identified 6 additional bemeth#-family compounds enriched in males. These new β-methyl lipids include both further oxidized forms such as bemeth#41 (**3.11**) as well as amino acid conjugates like bemeth#71 (**3.14**). These bemeth#s are not only enriched in true males, but also in masculinized *fem-3* (OE)

animals, whereas they are absent in germline-null *glp-4* (KO) mutants, indicating that they are dependent on the male germline.

Compounds of the bemeth family, much like nacq#1 and ascr#10, not only varied in overall abundances between males and hermaphrodites, but also in the time course of their biosynthesis throughout development and adulthood. In hermaphrodites, nacq#1 reached peak production around the time of young adulthood and quickly drops thereafter, whereas in male-enriched *him-5* cultures production peaked upon full adulthood and continues at high levels for several days (Fig. 3.4a)[5]. Similarly, ascr#10 production was roughly constant in hermaphrodites with a potential peak from between the L4 larval stage and early adulthood, whereas males began producing large quantities after adulthood and continue throughout their remaining adult life (Fig. 3.4a). Production of the β-methyl lipids was also found to be lifestage-dependent, with the majority being produced at roughly constant rates throughout adulthood in males. Hermaphrodites, however, only produced β-methyl lipids in sizeable quantities during young adulthood. The exception to this is the conjugation of amino acids to the β-methyl lipids, which, in both males and hermaphrodites, peaked in early adulthood and decreased thereafter.

Transcriptomics data revealed that F13D12.9, the methyltransferase responsible for the β-methyl branch in the bemeth#s, is expressed in males at levels 23-times higher than in hermaphrodites, consistent with the increased production of bemeth#s in males. As explained in the introduction of this chapter, α-hydroxylation of bemeth#s and further downstream metabolism proceeds via the canonical peroxisomal α-oxidation pathway, and transcriptomic data also indicated upregulation of this pathway in males (Fig. 3.1c). Expression of ZK550.5

and ZK550.6, the putative phytanoyl-CoA-hydroxylases responsible for the α-hydroxylation of bemeth#1, are respectively 11- and 4-fold increased in males over hermaphrodites, whereas expression of *hacl*-1, which performs the next step in α-oxidation, is about twofold increased in males[14]. Interestingly there is no significant difference between levels of *hacl-1* in the two mutants[14].

Finally, we devised a synthetic approach that provides access to individual enantiomers for biological evaluation enable assignment of the absolute configuration of the β-methyl branch in the bemeth# series of compounds, and further clarified that the absolute stereochemistry of bemeth#23 is (2*R*,3*S*). With the availability of synthetic bemeth#1, additional investigations into lipid signaling and regulation become possible. In *C. elegans* NHR-49 does not usually act alone to regulate transcription, and usually heterodimerizes with other NHRs, including NHR-80 which also is responsible for regulation of FAT-7[15,16]. While it is clear that NHR-49 is required for bemeth#1-dependent induction of FAT-7, it is possible that NHR-80, rather than NHR-49, is the target of bemeth#1. This, however, appears unlikely as in humans the NHR-49 homolog, hepatocyte nuclear factor 4 alpha (HNF4α), has been shown to bind a variety of lipids, including dodecanoic acid. While dodecanoic acid is found binding to HNFα, it was found that modified lipids are more commonly bound to HNFα, lending additional support to bemeth#1, with its methylation and unsaturation, being the natural ligand[17]. In addition to further studies of lipid signaling within the worm body, the reason for excretion of hydroxylated and amino acid-conjugated bemeth#s remains unclear and will require further investigation.

References

(1) Helf, M. J., Fox, B. W., Artyukhin, A. B., Zhang, Y. K., Schroeder, F. C. Comparative metabolomics with Metaboseek reveals functinos of a conserved fat metabolism pathway in *C. elegans. Submitted August 2021*.

(2) Kitamura, T., Seki, N., Kihara, A. Phytosphingosine degradation pathway includes fatty acid α-oxidation reactions in the endoplasmic reticulum. *PNAS* **114**: E2616-E2623. **2017.**

(3) Fox, B. W., *et al. In preparation.*

(4) Zhang, Y. K. Synthesis of Nematode Signaling Molecules. *Doctoral dissertation, Cornell University.* **2019.**

(5) Ludewig, A. H., Artyukhin, A. B., Aprison, E. Z., Rodrigues, P. R., Pulido, D. C., Burkhardt, R. N., Panda, O., Zhang, Y. K., Gudibanda, P., Ruvinsky, I., Schroeder, F. C. An excreted small molecule promotes *C. elegans* reproductive development and aging. *Nature Chem. Biol.* **15**: 838-845. **2019.**

(6) Paquette, L. A., Eizember, R. F. Phytochemistry of the *cis*- and *trans*-Bicyclo[6.1.0]nonan-2-ones. *JACS* **91**: 7108-7113. **1969.**

(7) Naef, R., Velluz, A., Jaquier, A. New Volatile Sulfer-Containing Constituents in a Simultaneous Distillation-Extraction Extract of Red Bell Peppers (Capsicum annuum). *J. Ag. Food Chem.* **56**: 517-527. **2008.**

(8) Francke, W., Schroeder, F., Philipp, P., Meyer, H., Sinnwell, V., Gries, G. Identification and synthesis of new bicyclic acetals from the mountain pine beetle, *Dendroctonus ponderosae* Hopkins (Col.:Scol.). *Bioorg. Med. Chem.* **4**: 363-374. **1996.**

(9) Coggins, A. J., Powner, M. W. Prebiotic synthesis of phosphoenol pyruvate by α-phosphorylation-controlled triose glycolysis. *Nat. Chem.* **9**: 310-317. **2017.**

(10) Davis, F. A., Haque, M. S., Ulatowski, T. G., Towson, J. C. Asymmetric Oxidation of Ester and Amide Enolates Using New (Camporylsulfonyl)oxaziridines. *JOC* **51**: 2402-2404. **1986.**

(11) Hoye, T. R., Jeffrey, C. S., Shao, F. Mosher ester analysis for the determination of absolute configuration of sterogenic (chiral) carbinol carbons. *Nat. Protoc.* **2**: 2451-2458. **2007.**

(12) Lee, Y., Lin, T., Lai, S., Liu, M., Lai, M., Chan, N. Structural Analysis of Glycine Sarcosine N-methyltransferase from *Methanohalophilus portucalensis* Reveals Mechanistic Insights into the Regulation of Methyltransferase Activity. *Sci. Rep.* **6**: 38071. **2016.**

(13) Ma, D. K., Li, Z., Lu, A. Y., Sun, F., Chen, S., Rothe, M., Menzel, R., Sun, F., Horvitz, H. R. Acyl-CoA Dehydrogenase Drives Heat Adaptation by Sequestering Fatty Acids. *Cell* **161**: 1152-1163. **2015.**

(14) Albritton, S. E., Kranz, A., Rao, P., Kramer, M., Dieterich, C., Ercan, S. Sex-Based Gene Expression and Evolution of the X Chromosome in Nematodes. *Genetics* **197**: 865-883. **2014.**

(15) Parthare, P. P., Lin, A., Bornfeldt, K. E., Taubert, S., Van Gilst, M. R. Coordinate Regulation of Lipid Metabolism by Novel Nuclear Receptor Partnerships. *PLoS Genet.* **8**: e1002645. **2012.**

(16) Ratnappan, R., Amrit, F. R. G., Chen, S., Gill, H., Holden, K., Ward, J., Yamamoto, K. R., Olsen, C. P., Ghazi, A. Germline Signals Deploy NHR-49 to Modulate Fatty-Acid β-Oxidation and Desaturation in Somatic Tissues of *C. elegans. PLoS Genet.* **10**: e1004829. **2014.**

(17) Dhe-Paganon, S., Duda, K., Iwamoto, M., Chi, Y., Shoelson, S. E. Crystal Structure of the HNF4α Ligand Binding Domain in Complex with Endogenous Fatty Acid Ligand. *JBC* **41**: 37973-37976. **2002.**

CHAPTER 4

INVESTIGATION OF SELECT MALE-ENRICHED METABOLITES

Contributions and Acknowledgments

The research presented in this chapter will be part of the submission of a manuscript described in Chapter 1, prepared by Russell N. Burkhardt (RNB) and Dr. Frank C. Schroeder (FCS). This research was performed with input and assistance from others in the Schroeder Lab (Cornell University, Ithaca, NY) and the Lee Lab (Cornell University, Ithaca, NY). Experiments were designed by RNB with input from FCS, Dr. Bennett Fox (BF), and Dr. Amaresh Chaturbedi (AC). Cultures of *C. elegans* for metabolomic analysis were grown by RNB and AC. Metabolomic analysis was performed by RNB. Synthesis for compound confirmation was performed by RNB and Brian Curtis (BC).

Abstract

In addition to the β-methyl lipids described in Chapter 3 we discovered a large number of other metabolites of diverse biosynthetic origins that are enriched in the male metabolome. This includes the several families of gluconucleosides (named panglu# and uglas#) as well as ascarosides and a unique dipeptide. Similar to the bemeth#-family of compounds discussed in Chapter 3, upregulation of the panglu#s is dependent on the male germline, and correspondingly their production is also upregulated in masculinized *fem-3* (OE) cultures. Related to the panglu#s, we also observe a set of gluconucleosidyl ascarosides that are enriched in males, but, unlike the panglu#s, their increased production does not depend on the male germline. Whereas previous work reported that ascr#10 is the predominant "male ascaroside," our analysis revealed a much more complex blend of male-enriched ascarosides, including a large number of ascr#1 derivatives. For example, ascr#1 and uglas#14, a conjugate of ascr#1 and a uric acid glucoside, are 8- and 86-fold increased, respectively, in *him-5* cultures compared to hermaphrodites. In addition, we identified a novel nucleoside derivative found in *fem-3* (OE) animals and a dipeptide of dimethyltryptophan and isoleucine, which is elevated in a male germline-dependent manner. Lastly, we report stark upregulation of a class of polyunsaturated fatty acids enriched in *him-5* cultures.

4.1 Introduction

Given that males and hermaphrodites have different body plans, behaviors, and transcriptomes, it follows that they may exhibit differences in small molecule-mediated signaling pathways, in addition to differences in primary metabolism. Our comparative metabolomic analysis of wildtype and male-enriched *him*-5 cultures revealed over 200 compounds that are unique to or upregulated in males. Although the biological roles of the metabolites discussed in

this chapter are not yet known, we anticipate that many of the newly identified compounds may serve as signaling molecules or are otherwise reflective of change in primary and/or secondary metabolism. In Chapter 3, we described the bemeth#s as an example for a new class of compounds discovered in males that were then shown to serve as signaling molecules regulating lipid metabolism via the nuclear hormone receptor NHR-49.

Among the >200 male-enriched compounds, we discovered a novel family of nucleoside derivatives, in which the nucleobase is linked to glucose instead of ribose or deoxyribose. These unusual gluconucleosides, named panglu#s, complement the large number of modular glucosides (MOGLs), incorporating a wide variety of different substituents, recently reported in *C. elegans*[1]. In the following paragraphs, we will first describe identification of the panglu#s and another family of gluconucleosides, the uglas#s, followed by sections on male-enriched ascaroside derivatives, a unique dipeptide incorporating dimethyltryptophan (DMW), as well as polyunsaturated fatty acids.

4.2 Novel gluconucleosides are enriched in male worms

Among metabolites increased in the endo-metabolomes of *him-5* worms we observed three compounds with very similar fragmentation patterns suggesting that they represent gluconucleoside derivatives incorporating a phenylacetic acid moiety. The first-eluting compound (*m/z* 508.1239, $C_{20}H_{23}N_5PO_9^-$, 7.32 min) produced characteristic phosphate peaks (*m/z* 78.9595 and 96.9702) as well as a phosphohexose-like fragment (*m/z* 241.0141, Fig. 4.1a, b). Neutral loss of $C_6H_7N_5^-$ (*m/z* 149.0680) suggested the presence of a methyladenine moiety, and a fragment at *m/z* 390.0844 ($C_{12}H_{17}N_5PO_8^-$) appeared to represent loss of a phenylacetyl group. Based on the fragmentation pattern, we proposed that this compound is a phenylacetylated phosphohexose with a methyladenine headgroup, which we named panglu#1. In analogy with other phosphorylated glucosides recently identified from *C. elegans*, we proposed that panglu#1 is based on a 3-

phosphorylated glucose; however, the attachment site of the phenylacetyl moiety and the methylation side could not be inferred. Subsequent syntheses by Brian Curtis (Schroeder lab) confirmed the presence of a 3-phosphorylated glucose and established the positions of the phenylacetyl and methyl groups (Fig. 4.1c).

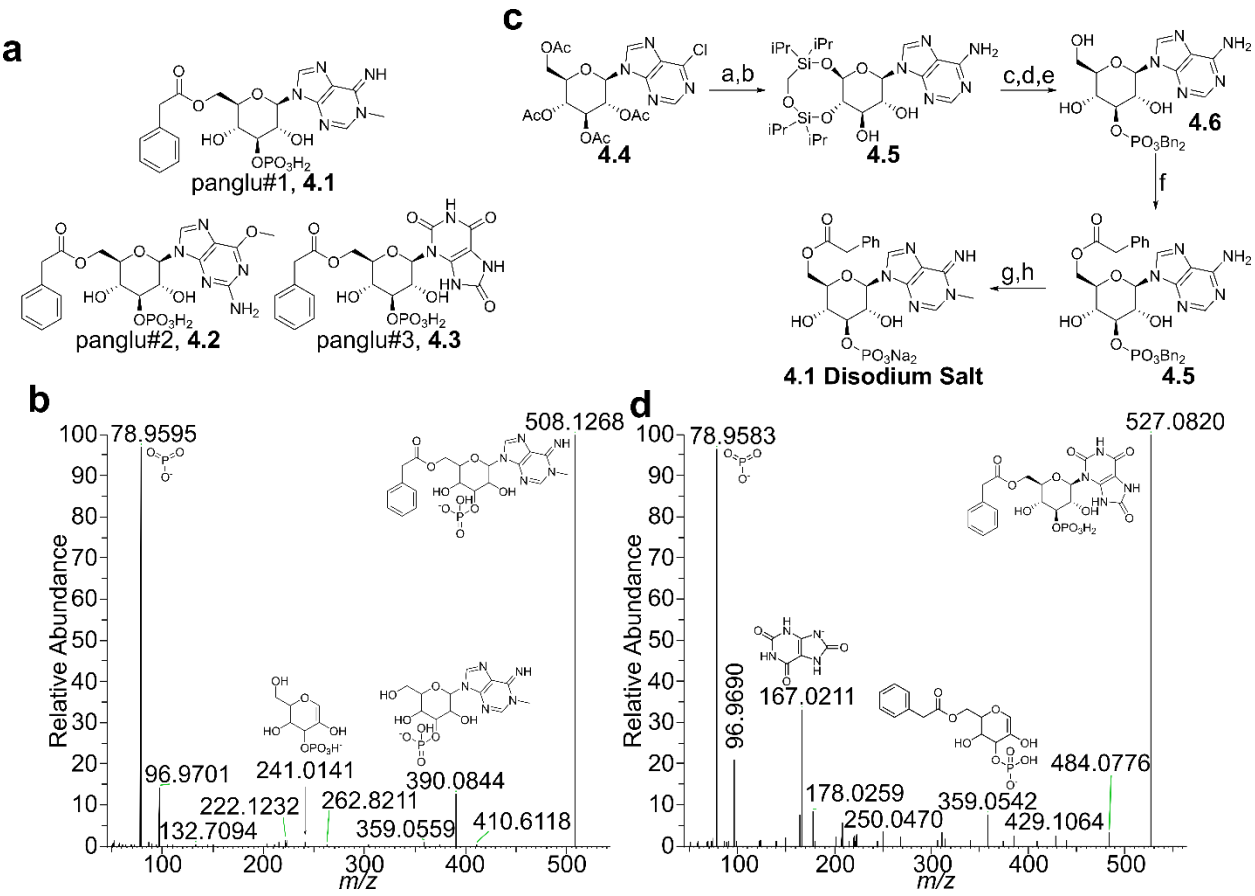

Fig. 4.1 | Identification of gluconucleosides of the panglu# family. **a.** Three panglu#s have been identified, representing phenylacetylated gluconucleosides incorporating methyladenine, (panglu#1), methylguanine (panglu#2), and uric acid (panglu#3). **b.** MS2 fragmentation of natural panglu#1 (**4.1**). **c.** Synthetic panglu#1 was synthesized by Brian Curtis to verify the exact structure. **d.** MS2 fragmentation of panglu#3 (**4.2**).

The second putative nucleoside derivative, named panglu#2 (*m/z* 524.1188, $C_{20}H_{24}N_5PO_{10}$, 7.63 min), showed a fragmentation that was similar to that of panglu#1, with the difference of a fragment representing methylguanine (*m/z* 164.0592) instead of methyladenine, a slightly different phosphoglucose-derived fragment ($C_6H_8PO_7^-$ rather than $C_6H_{10}PO_8^-$), and the cleavage of the

phenylacetyl group resulting in a $C_{12}H_{17}N_5PO_9^-$ (*m/z* 406.0797) fragment. Therefore, the structure of panglu#2 was proposed in analogy to that panglu#1, with the substitution of a methylguanine for a methyladenine (Fig. 4.1a).

The MS2 spectrum of the third member of this family of male-enriched gluconucleosides (*m/*z 527.0819, $C_{19}H_{21}N_4PO_{12}$, 7.5 min, named panglu#3), shows the same classical phosphate fragments, a uric acid fragment (*m/z* 167.0220), phosphoglucose-derived fragment ($C_6H_8PO_7^-$), and a fragment representing the loss of uric acid (*m/z* 359.0561). Based on the MS2 fragmentation data, panglu#3 appears to represent a phenylacetylated derivative of the known uric acid glucoside, gluric#2 (Fig. 4.1d)[4].

The panglu# family of glucosides are all significantly enriched in males, ranging from a 6-fold increase in panglu#2 to a 9-fold increase in panglu#1 (Fig. 4.2a). As a result of the low abundance of the panglu#s even in large *him*-5 cultures, we were unable to detect their presence in our small sample of hand-picked males or in our plated cultures of N2 hermaphrodites or male-enriched N2. Suggesting that panglu#s accumulate in the soma, rather than getting excreted, the levels detected in the endo-metabolome of old worms (6 days of adulthood) were 3- to 9-fold higher than in the pellets of young adults (Fig. 4.2b). We also observe that panglu#s are germline dependent, as they range from 5- to 9-fold enriched in germline-masculinized *fem-3* (OE) cultures relative to N2, and even more enriched relative to germline-feminized *fem-2* (KO) and germline-null *glp-4* (KO) (Fig. 4.2c).

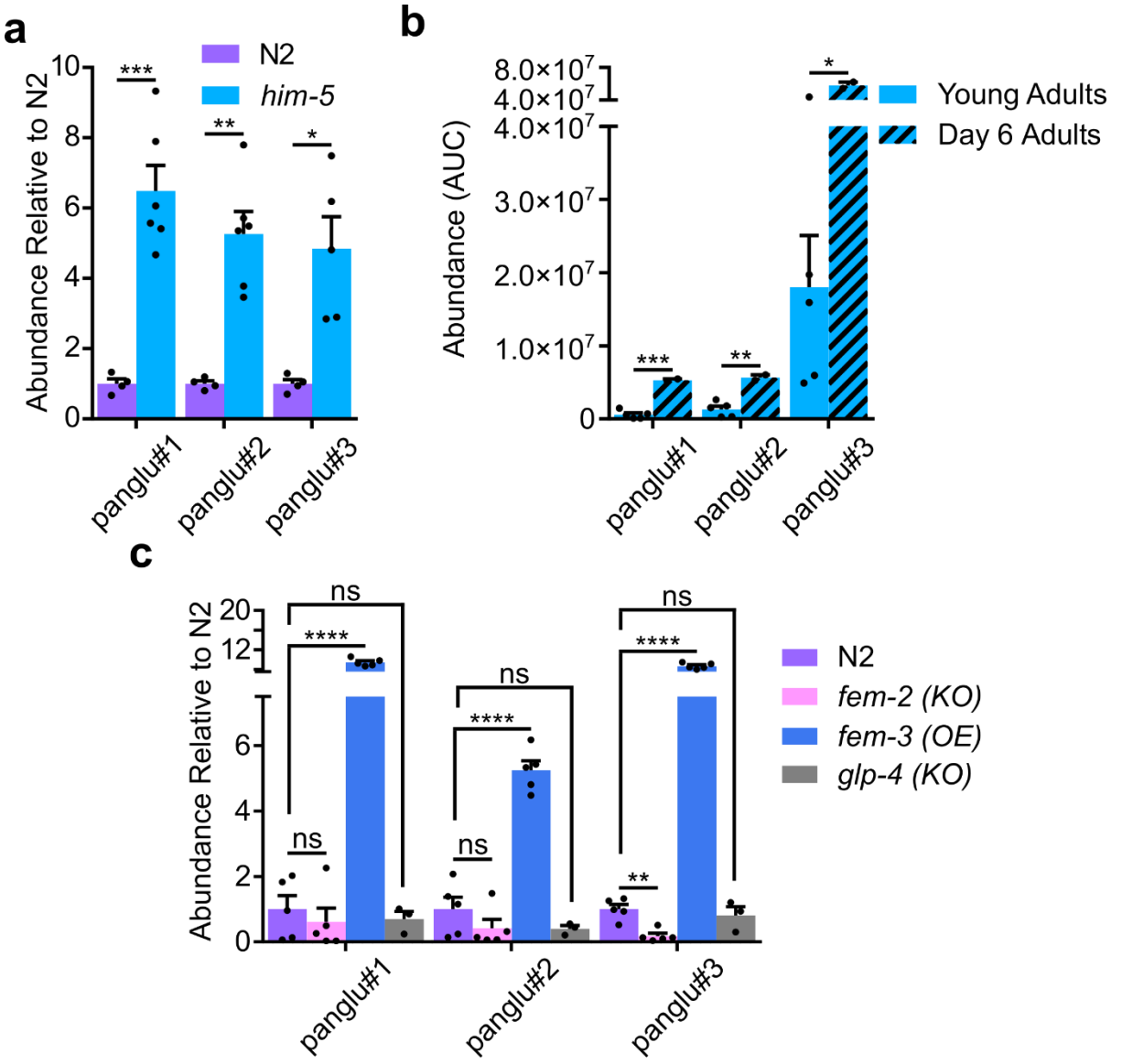

Fig. 4.2 | Abundance of panglu# family metabolites in different genetic backgrounds. a. In the endo-metabolome of *him-5* animals, panglu#s are 6-9 times more abundant than in the endo-metabolome of N2 animals. **b.** Older *him-5* contain more panglu#s in their endo-metabolome. **c.** panglu#s are enriched in *fem-3* (OE) cultures over N2 but are not completely absent in *fem-2* (KO) or *glp-4* (KO) cultures. Data are presented as mean ± s.e.m. *, p≤0.05; **, p≤0.005; ***, p≤0.0005; ns, not statistically significant.

4.3 Ascaroside-containing gluconucleosides

In addition to panglu#1-3, we detected four metabolites increased in the *him-5* endo-metabolome, whose MS2 spectra suggest that they also represent nucleoside derivatives, featuring an ascaroside as part of their structures, rather than phenylacetic acid as in panglu#1-3. The most

drastically increased (75-fold in the endo-metabolome) member of this family (*m/*z 667.1880, $C_{24}H_{37}N_4PO_{16}$, 7.08 min) fragments to yield diagnostic phosphate fragments (*m/z* 78.9595 and 96.9690), as well as uric acid (*m/z* 167.0208, $C_5H_3N_4O_3^-$), and a fragment consistent with the ascaroside ascr#1 (*m/z* 275.1500, $C_{13}H_{23}O_6^-$) and a loss of uric acid (*m/z* 499.1578, $C_{19}H_{32}PO_{13}^-$), suggesting that this compound representsed a conjugate of ascr#1 and gluric#2 (Fig. 4.3a). Recently, the Schroeder lab described identification of an isomer of this compound, named uglas#11, from WT hermaphrodites[4]. However, uglas#11, which bears an ascr#1 moiety in the 2'-position of the glucose, has a significantly earlier retention time (6.36 min) than the male-enriched isomer and is virtually absent in male-enriched cultures. Fortuitously, during the initial an identification of uglas#1, the corresponding 6'-substituted isomer of uglas#1, named uglas#14 (*m/z* 587.2211, $C_{24}H_{36}N_4O_{13}$, 7.16 min), was also synthesized[4]. This compound, which is the unphosphorylated version of uglas#15, is also upregulated in *him-5* (23-fold) and comparison of retention time and MS2 spectra then established that the male-enriched isomer is identical to uglas#14, suggesting that the male-enriched isomer of uglas#11represents uglas#15 (Supp. Fig. 4.6 and 4.21).

In addition to uglas#14 and uglas#15, we detected two compounds with analogous fragmentation patterns, which appeared to incorporate the 9-carbon sidechain ascaroside, ascr#10, instead of the 7-carbon sidechain ascr#1. These compounds, uglas#104 (*m/z* 615.2531, $C_{26}H_{40}N_4O_{13}$, 8.24 min) and uglas#105 (*m/z* 695.2189, $C_{26}H_{41}N_4PO_{16}$, 8.14 min), were found to be upregulated also up 3- and 4-fold respectively, in the *him-5* endo-metabolome (Fig. 4.3b).

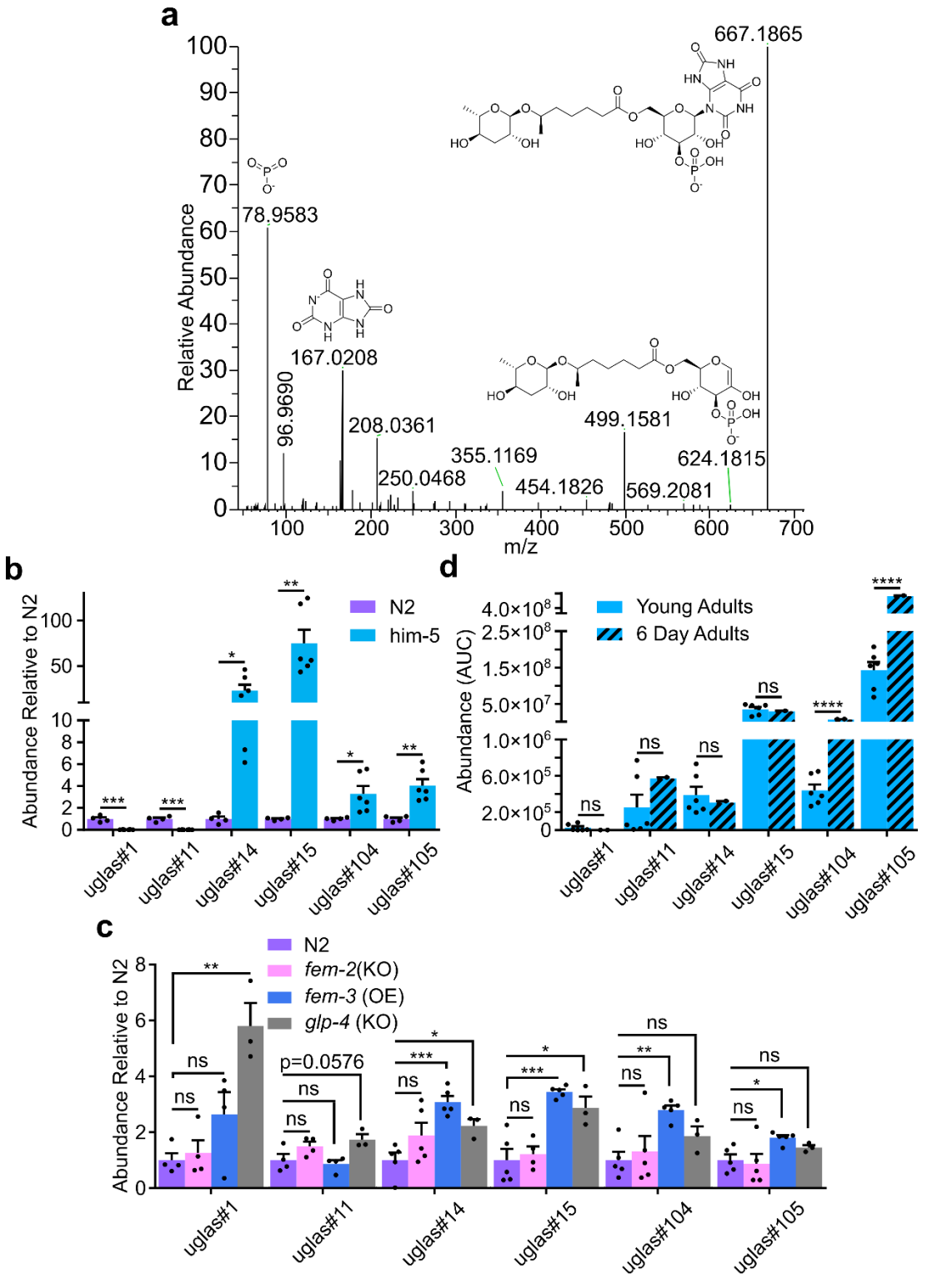

Fig. 4.3 | ascarosides conjugated to gluconucleosides are enriched in males. a. MS2 fragmentation of uglas#15 produces classical phosphate fragments, uric acid, and a phospo-glas#1 fragment. **b.** HPLC-MS quantification of uglas# compounds in the supernatants of N2 and *him-5* cultures normalized to the abundance levels in N2. **c.** HPLC-MS quantification of uglas# compounds in N2, *fem-2* (KO), *fem-3* (OE), and *glp-4* (KO) cultures normalized to N2. **d.** HPLC-MS quantification of uglas# compounds in young and 6 day old adults. Data are presented as mean ± s.e.m. *, p≤0.05; **, p≤0.005; ***, p≤0.0005; ****, p≤0.0001; ns, not statistically significant.

Unlike the panglu#s, all four uglas#s enriched in the endo-metabolome of large *him-5* cultures were also detected, and enriched, in small hand-picked samples of N2 and *him-5* males although only two samples of each limit the ability to assign statistical significance (Fig. 4.4a). As is the case with the larger *him*-5 cultures, uglas#11 is significantly decreased or even absent in hand-picked samples of males relative to N2 hermaphrodites. Similarly, in cultures of 50:50 mixtures of hermaphrodites:males uglas#1 and uglas#11 are significantly less abundant than in normal hermaphrodite samples (Fig. 4.4b). While uglas#14 and uglas#15 appear increased in male-enriched cultures relative to hermaphrodites, this difference is not independently significant. The ascr#10 derivatives, uglas#104 and uglas#105, however are highly and significantly enriched at 40- and 37-fold, respectively.

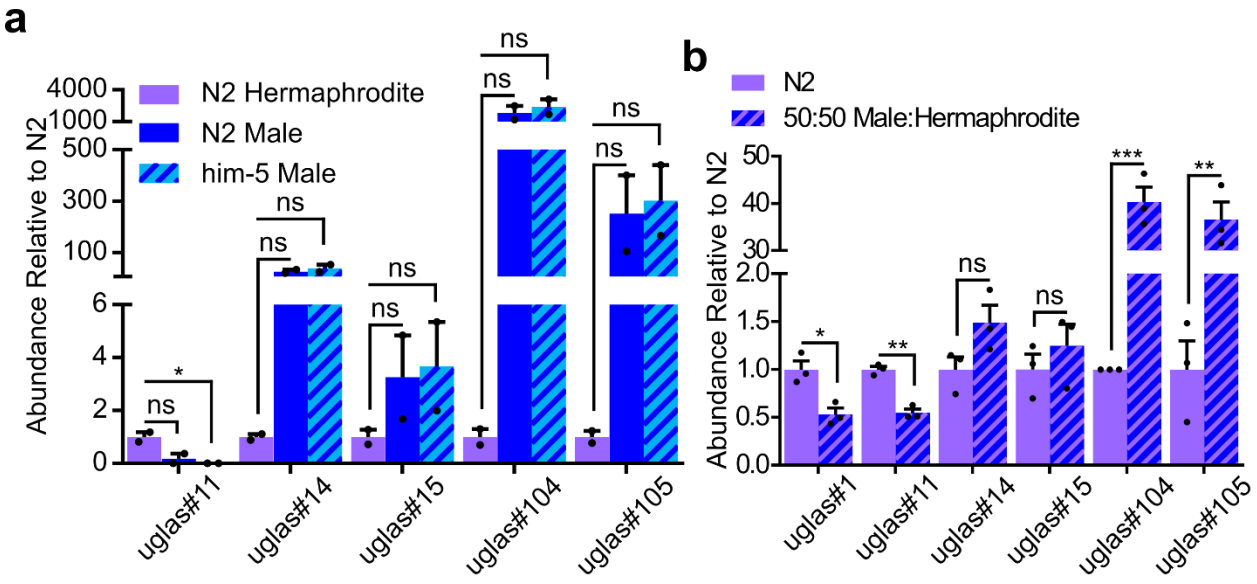

Fig. 4.4 | Abundance of uglas# family metabolites in male cultures. a. In small samples of pure, hand-picked hermaphrodites and males, all *him*-5-enriched uglas# family metabolites are also enriched in N2 and *him-5* males. **b.** In 50:50 cultures of N2 males and hermaphrodites grown on plates, abundances of uglas#1 and uglas#11 are significantly reduced, there is a modest increase in the abundances of uglas#14 and uglas#15 which, however, does not reach significance, and uglas#104 and uglas#105 are 40- and 37-fold enriched, respectively. Data are presented as mean ± s.e.m. *, p≤0.05; **, p≤0.005; ***, p≤0.0005; ns, not statistically significant.

As is the case with the panglu# family of metabolites, the uglas#s are almost exclusively retained within the worm body, and thus our experimental set-up for determining changes of abundances during the adult lifespan (see Chapter 1) allows only for comparison of abundances in young adults and 6 day-old adults. In this case uglas#14 and uglas#15 are not differential between young and old worms, but uglas#104 and uglas#105 are 2- and 5-fold increased in old worms (Fig. 4.3d). Although the uglas# family metabolites share the gluric#1 moiety with panglu#3, abundances of uglas#-family metabolites are not strongly germline dependent, in contrast to panglu#3 (Fig. 4.3c). Whereas levels in *fem-3* (OE) are increased over N2 in all cases, uglas#14 and uglas#15 are also significantly increased in germline-null *glp-4* (KO) animals. Levels of uglas#104 and uglas#105 are also increased, but not to the level of significance.

4.4 Male-enriched ascaroside derivatives

Previous work reported that the saturated 9-carbon sidechain saturated ascaroside, ascr#10, is increased in males[1]. Our data show that the 7-carbon sidechain saturated ascaroside, ascr#1, is also increased, about eight times in the endo-metabolome of *him-5* cultures relative to WT (N2) cultures (Fig. 4.4a), and in the previous section, we showed that a subset of ascr#1 derived gluconucleosides, uglas#14 and uglas#15, are increased in males.

Comparative metabolomic analysis of *him-5* and WT cultures revealed several additional metabolites whose MS2 spectra suggested that they represent modular metabolites incorporating an ascr#1 moiety. One of the most highly enriched metabolites ascr#1 derivatives in the *him-5* endo-metabolome actually occurs as a pair of isomers, both of which are male-enriched (*m/z* 517.1699, $C_{19}H_{35}PO_{14}$, 6.70 min and 6.91 min). The earlier-eluting compound fragments to produce phosphate fragments (*m/z* 76.9584 and 96.9690), a phosphoglucose fragment (*m/z* 241.0117, $C_6H_{10}PO_8^-$), and a neutral loss of ascarylose (*m/z* 355.1161, $C_{13}H_{24}PO_9^-$), indicating the

compound is likely the phosphoglucosylated ascaroide, glas#11 (Fig. 4.4). The later-eluting isomer, although more enriched than the earlier-eluting isomer, is of lower abundance and produces the same phosphate and phosphoglucose fragments. Since ascarosides incorporating a sidechain attached via the ω-1 position are often accompanied by their ω-attached isomers, which generally have slightly higher retention times on revers-phase columns, we proposed that the later-eluting isomer represents the the phosphoglucosylated ω-attached isomer of glas#11, gl**o**s#11.

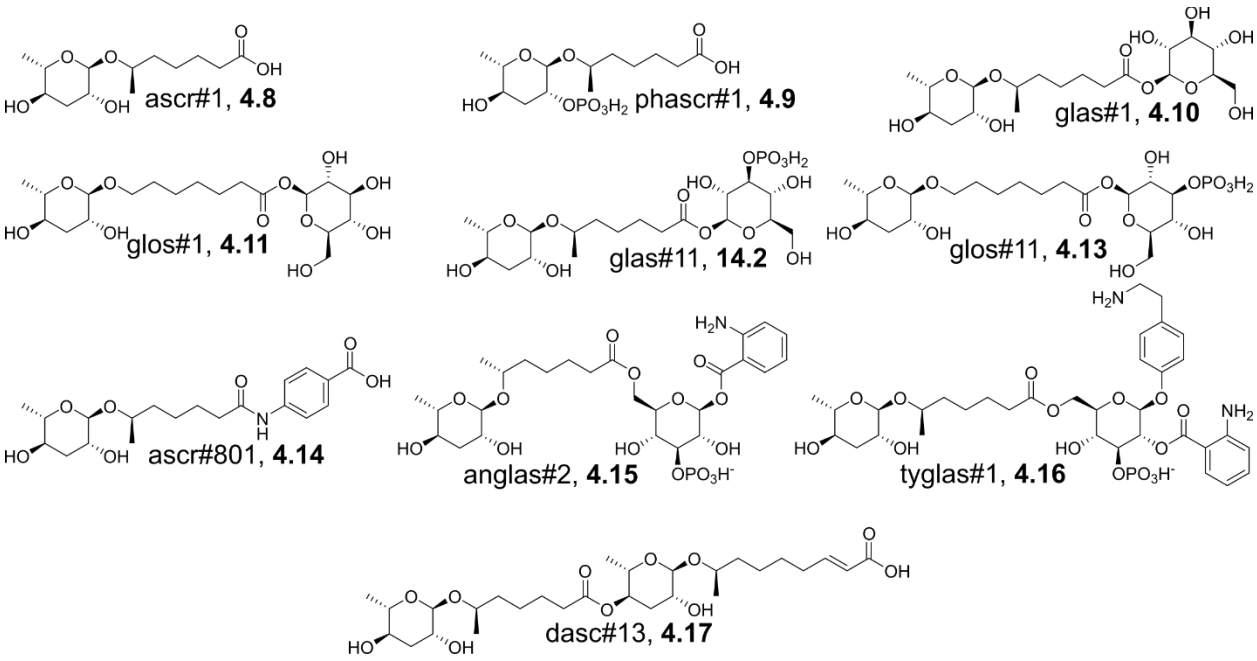

Fig. 4.5 | Male-enriched ascr#1 derivatives

In addition to the phosphorylated glas#11 and glos#11 we also observed the non-phosphorylated glas#1 (*m/z* 461.1995(w/ Na^+ adduct), $C_{19}H_{34}O_{11}Na^+$, 6.86 min) and glos#1 (7.00 min). Another glucosylated compound (*m/z* 636.2070, $C_{26}H_{40}NPO_{15}$, 9.15 min) fragmented to produce phosphate fragments, phosphoglucose fragments (*m/z* 207.9903, $C_6H_6PO_6^-$ and *m/z* 223.0012, $C_6H_8PO_7^-$), ascr#1 (*m/z* 275.1500, $C_{13}H_{26}O_6^-$), and fragments corresponding to a loss of anthranilic acid (*m/z* 481.1506, $C_{19}H_{30}PO_{12}^-$ and *m/z* $C_{19}H_{32}PO_{13}^-$), indicating it is likely the known ascaroside anglas#2[5]. We additionally observed a compound that appears to be the previously

described tyglas#1 (*m/z* 755.2807, $C_{34}H_{48}N_2PO_{15}^-$, 8.05 min) as it fragments to produce classical phosphate fragments, anthranilic acid (*m/z* 136.0403, $C_7H_6NO_2^-$), ascr#1, a phosphoglucose-tyramine fragment ($C_{14}H_{19}NPO_8^-$), and a loss of anthranilic acid (*m/z* 618.2316, $C_{27}H_{41}NPO_{13}^-$)[1].

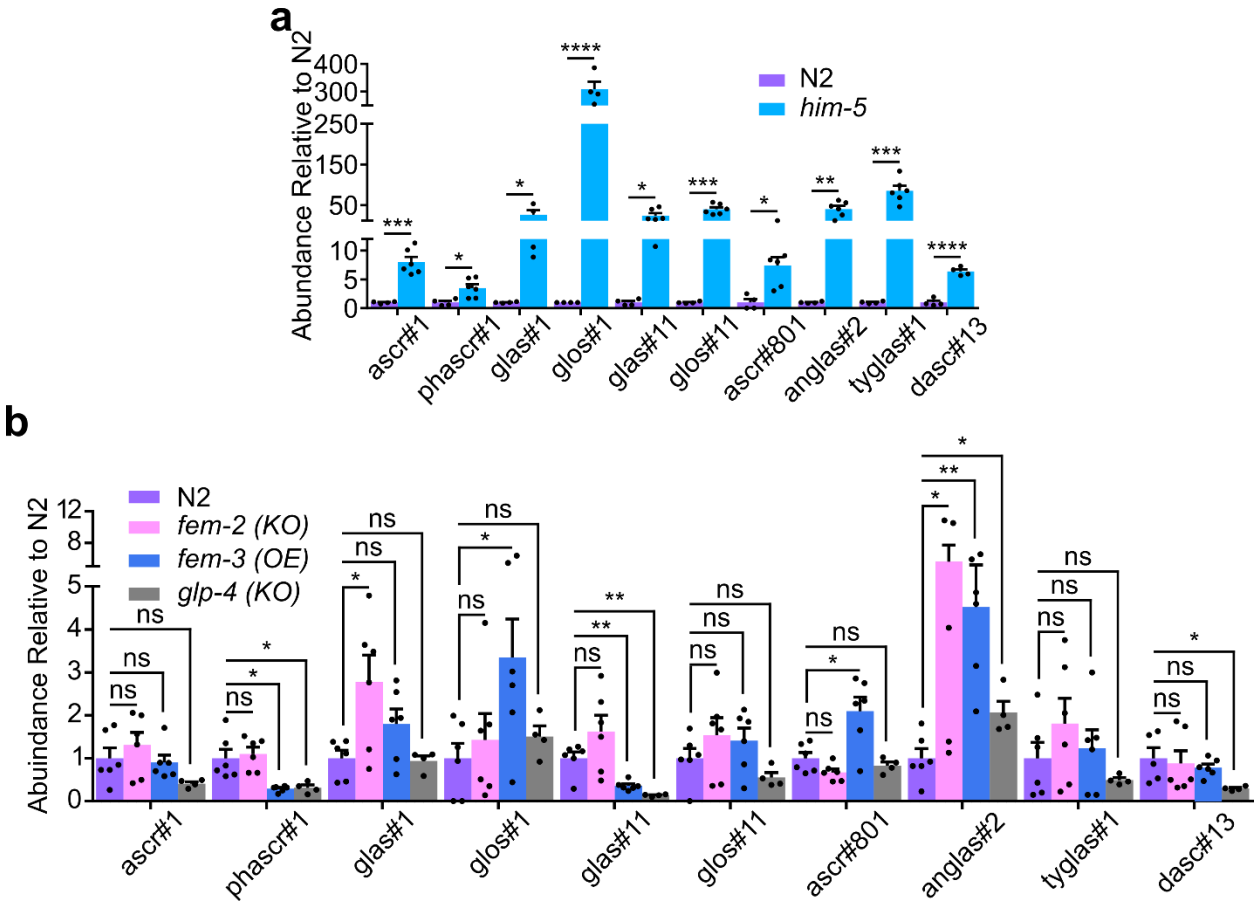

Fig. 4.6 | ascr#1 and its derivatives are enriched in males. Derivatives of ascr#1 are highly enriched in *him-5* cultures. Most glucosylated asc#1 derivatives are ~50-fold enriched., glos#1 is virtually absent in N2 cultures, leading to a an over 300-fold increase in *him-5*. Data are presented as mean ± s.e.m. *, p≤0.05; **, p≤0.005, ***, p≤0.0005; ****, p≤0.0001.

In addition to glucosylated derivatives we identified several other male-enriched ascr#1 derivatives. One such compound, named ascr#801 (*m/z* 394.1875, $C_{16}H_{29}O_6^-$, 8.78 min), appears to represent a dihydro variant of the dauer pheromone component, ascr#8, as it fragments to yield the characteristic ascaroside fragment (*m/z* 73.0288, $C_3H_5O_2^-$), an aniline-like ion (*m/z* 92.0499, $C_6H_6N^-$), an ion corresponding to *p*-amino benzoic acid (*m/z* 136.0402, $C_7H_6NO_2$), fragments

matching the ascr#1 sidechain conjugated to aniline (*m/z* 202.1236, $C_{13}H_{16}NO^-$, *m/z* 220.1348, $C_{13}H_{18}NO_2^-$, and *m/z* 246.1143, $C_{14}H_{16}NO_3^-$), and the decarboxylation ion (*m/z* 350.1968, $C_{19}H_{28}NO_5^-$)[6]. Another ascr#1 derivative enriched in males appears to be a dimeric ascaroside, named dasc#13 (*m/z* 559.3129, $C_{28}H47O_{11}^-$, 11.37 min), consisting of ascr#1 and ascr#3 linked by an ester bond, which fragments to produce ascr#1 (*m/z* 275.1497, $C_{13}H_{24}O_6^-$) and ascr#3 (*m/z* 301.1652, $C_{15}H_{25}O_6^-$)[7]. Lastly, we detected a phosphorylated derivative of ascr#1, named phascr#1 (*m/z* 355.1168, $C_{13}H_{24}PO_9^-$, 6.76 min), that was previously reported by Dr. Jason Hoki as ascr#1(P) and which yields phosphate fragments and a phospho-ascarylose fragment (*m/z* 209.0217, $C_6H_{10}PO_6^-$)[8].

Although the described ascr#1 derivatives are robustly enriched in *him-5* cultures, many could not be detected in other male-enriched cultures. In small, hand-picked samples of males and hermaphrodites, ascr#1 itself is the only ascr#1-related compound that could be detected, and, notably, it is present at lower levels in both N2 and *him-5* males than in N2 hermaphrodites. Small plated cultures of 50:50 male:hermaphrodite and N2 hermaphrodites, likewise, show only ascr#1 and phascr#1. While there is no difference in the levels of phascr#1, ascr#1 is 2.5-fold increased in the 50:50 cultures.

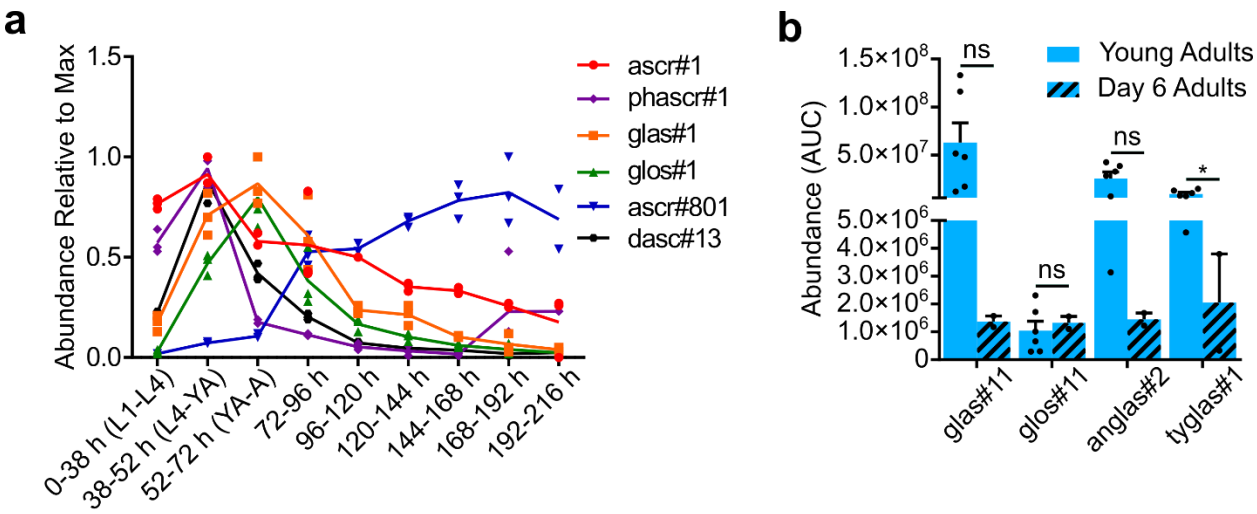

Fig. 4.7 | ascr#1 derivatives in males do not age uniformly. a. For most ascr#1 derivatives that can be detected in the supernatant, peak production occurs early in life, though ascr#801 does not become produced in large quantities until later in life. **b.** Like most ascr#1 derivatives, those that are solely retained in the body are mostly produced early in life and their levels decline with age. Data are presented as mean ± s.e.m. *, $p \leq 0.05$; ns, not statistically significant.

Excretion of most *him-5* upregulated ascarosides, including ascr#1 itself, peaks early in life, either during the L4-young adult molt or the first day of adulthood, and then drops off. An interesting exception to this is ascr#801 which is barely produced early in life and peaks in older animals (~5 days of adulthood). Some of the male-upregulated ascr#1 derivatives were detected primarily or almost exclusively in the endo-metabolome samples, and thus appear to be mostly retained within the worm body, such as glas#11. Therefore, a detailed time course for the production of these compounds was not possible using our experimental design; this would require analysis of worm bodies of different developmental stages and different ages of adulthood. However, it appears that most of the ascr#1 derivatives that are retained in the body are produced early in life and metabolized through adulthood (Fig. 4.5b). As for the nucleoside ascarosides, there is no real pattern to production of ascr#1 derivatives in the sex mutants (Fig. 4.6). The only ascr#1 derivative that is significantly increased in *fem-3* (OE) is anglas#2, which is also significantly increased in *fem-2* (KO), which produce virtually no sperm, indicating that anglas#2, like the other ascr#1 derivatives, is not germline dependent.

4.5 An *S*-adenosylmethionine-derivative is enriched in *fem-3* (OE) worms

The two male enriched compounds discussed in this section were not detected in our initial comparison of N2 and *him-5* mutant animals, but were instead observed as 30-fold enriched in the endo-metabolome of germline-masculinized *fem-3* (OE) cultures (Fig. 4.6a). The two compounds (*m/z* 340.1074, $C_{13}H_{18}N_5SO_4^+$, 6.69 and 7.30 min) represent two isomers that fragment in a near identical manner, with the later-eluting compound being the predominant isomer. Their MS2 spectra revealed peaks consistent with dimethylsulfide (*m/z* 61.0104, $C_2H_5S^+$), pentose (*m*/z 97.027, $C_5H_5O_2^+$), adenine (*m/z* 136.0608, $C_5H_6N_5^+$), a fragment of *m/z* 145.0307 ($C_6H_9SO_2^+$), and a loss of adenine (*m/z* 205.0513, $C_8H_{13}SO_4^+$). From this fragmentation pattern we hypothesized that the two compounds (named amta#1 and amta#2) are acetylation products of *S*-methylthioadenosine (MTA)[9]. To verify these structures, acetylation of commercially available MTA yielded a mixture of two isomers of the same retention time as the natural compounds (Supp. Fig. 4.23).

While these compounds were not initially detected as significantly differential between N2 and *him-5* cultures, amta#1 and amta#2 were found to be about 2-fold enriched in the small hand-picked samples (Fig. 4.8b,c). The compounds appear even further enriched in hand-picked *him-5* males, though this difference did not reach statistical significance (Fig. 4.8c). Like many of the other nucleoside-derived compounds in *C. elegans*, amta#1 and amta#2 are retained within the worm body, so production throughout adulthood could not be studied in detail. In older adults (6 days), however, we observed that amta#2 is 5-fold enriched over young adults (Fig. 4.8d).

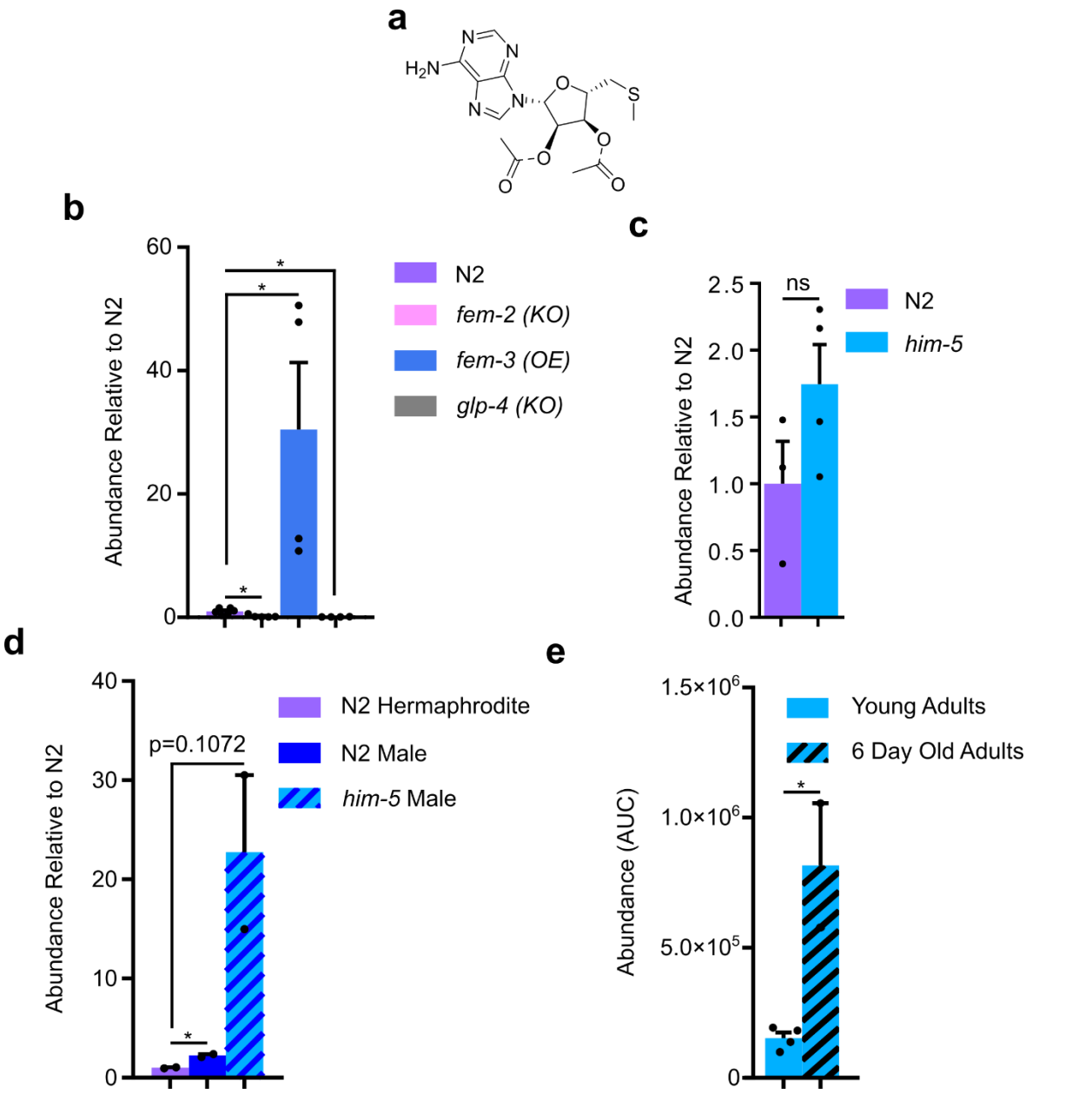

Fig. 4.8 | Abundance of amta#2. a. The acetyl group of amta#1 and amta#2 can be on the 2'- and 3'-position of the ribose sugar. **b.** amta#1 is 30-fold enriched over N2 in *fem-3* (OE) and 5- and 10-fold down in *fem-2* (KO) and *glp-4* (KO) respectively. **c.** In large cultures of N2 and *him-5* there is no significant difference between levels of amta#1. **d.** amta#1 is 2-fold enriched in N2 males over N2 hermaphrodites and 22-fold enriched in *him-5* males (though not significantly). **e.** In cultures of *him-5* that are grown for 6 days of adulthood, amta#2 is 5-fold increased over young adults. Data are presented as mean ± s.e.m. *, p≤0.05; ns, not statistically significant.

4.6 A unique dipeptide is upregulated in males

This section reports the identification of a unique male-enriched dipeptide incorporating an amino acid not previously reported in *C. elegans*. Comparative metabolomic analysis of the exo-metabolomes of *him-5* and WT animals revealed a compound (*m/z* 344.1978, $C_{19}H_{27}N_3O_3$, 7.94 min) whose MS2 spectra showed an indole fragment (*m/z* 116.0512, $C_8H_6N^-$), (iso)leucine (*m/z* 130.0872, $C_6H_{12}NO_2^-$), loss of methylindole (*m/z* 215.1413, $C_{10}H_{19}N_2O_3^-$), loss of indole (*m/z* 227.1415, $C_{11}H_{19}N_2O_4^-$), loss of CO_2 and dimethylamine (*m/z* 255.1516, $C_{16}H_{19}N_2O^-$), and loss of CO_2 (*m/z* 300.2102, $C_{18}H_{26}N_3O^-$) (Fig. 4.7a). This fragmentation pattern indicated that the compound likely represents a dipeptide of (iso)leucine and dimethyltryptophan. To confirm these assignments and to differentiate between incorporation of leucine or isoleucine, we developed a short synthesis (Fig. 4.7b). Dimethylation of tryptophan with formaldehyde and sodium cyanoborohydride yielded dimethyltryptophan, which was then conjugated to either *O*-tBu-leucine or *O*-tBu-isoleucine via DDC coupling[10]. Deprotection with trifluoroacetic acid yielded the dipeptides for analysis. Injection of the leucine and isoleucine compounds revealed that the natural compound is dimethyltryptophan-isoleucine (dmwi#1) (Fig. 4.7c).

While dmwi#1 was only 2-fold increased over WT in the *him-5* endo-metabolome, it was 13-fold increased in 50:50 male:hermaphrodite cultures, nearly 500-fold increased in *fem-3* (OE) over N2, and undetectable in *fem-2* (KO) and *glp-4* (KO) indicating it is strongly dependent on the male germline (Fig. 4.10a, b). This dipeptide is also a good example of the interactions between males and hermaphrodites, as in the small samples of pure males and pure hermaphrodites the compound is undetectable in the hermaphrodites but still present, up to an e5 peak, in male samples. This indicates that dmwi#1 is either produced by males at increased levels in the absence of hermaphrodites or is actively degraded by hermaphrodites. This compound, although only 2-

fold increased at young adulthood, is made by males for a few days after adulthood before dropping off whereas hermaphrodites cease production almost immediately after maturing as adults (Fig. 4.10c).

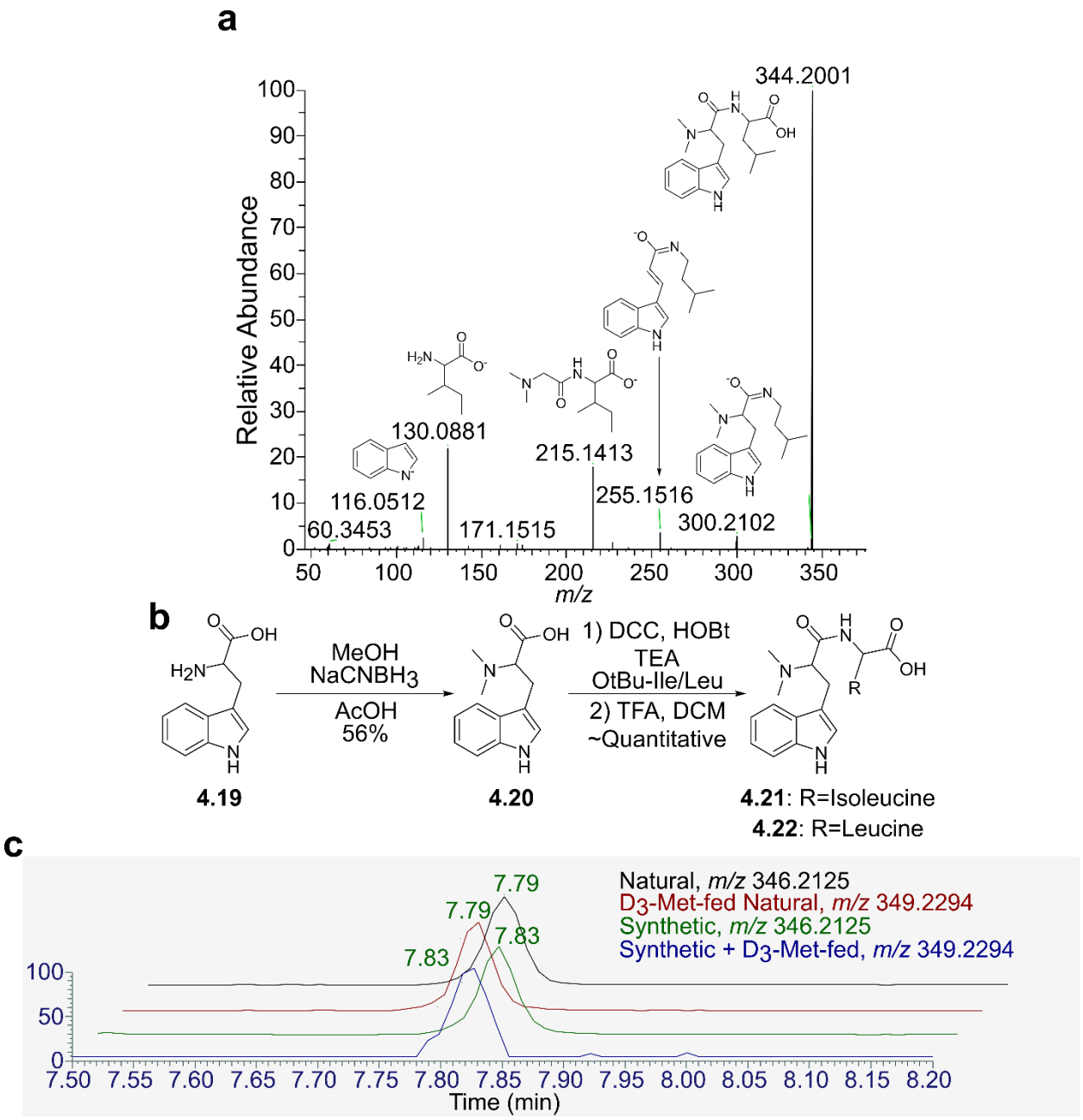

Fig. 4.9 | Dimethyltryptophan-isoleucine is a unique male-enriched dipeptide. a. Identification of the compound by MS2 fragmentation based on the (iso)leucine fragment and indole-containing fragments. **b.** Synthesis of the dipeptides accomplished by methylating tryptophan followed by DCC coupling with protected isoleucine or leucine and deprotection with TFA. **c.** EIC traces of the synthetic and natural samples, and mixtures thereof, show that the natural compound is the isoleucine conjugate **4.21**.

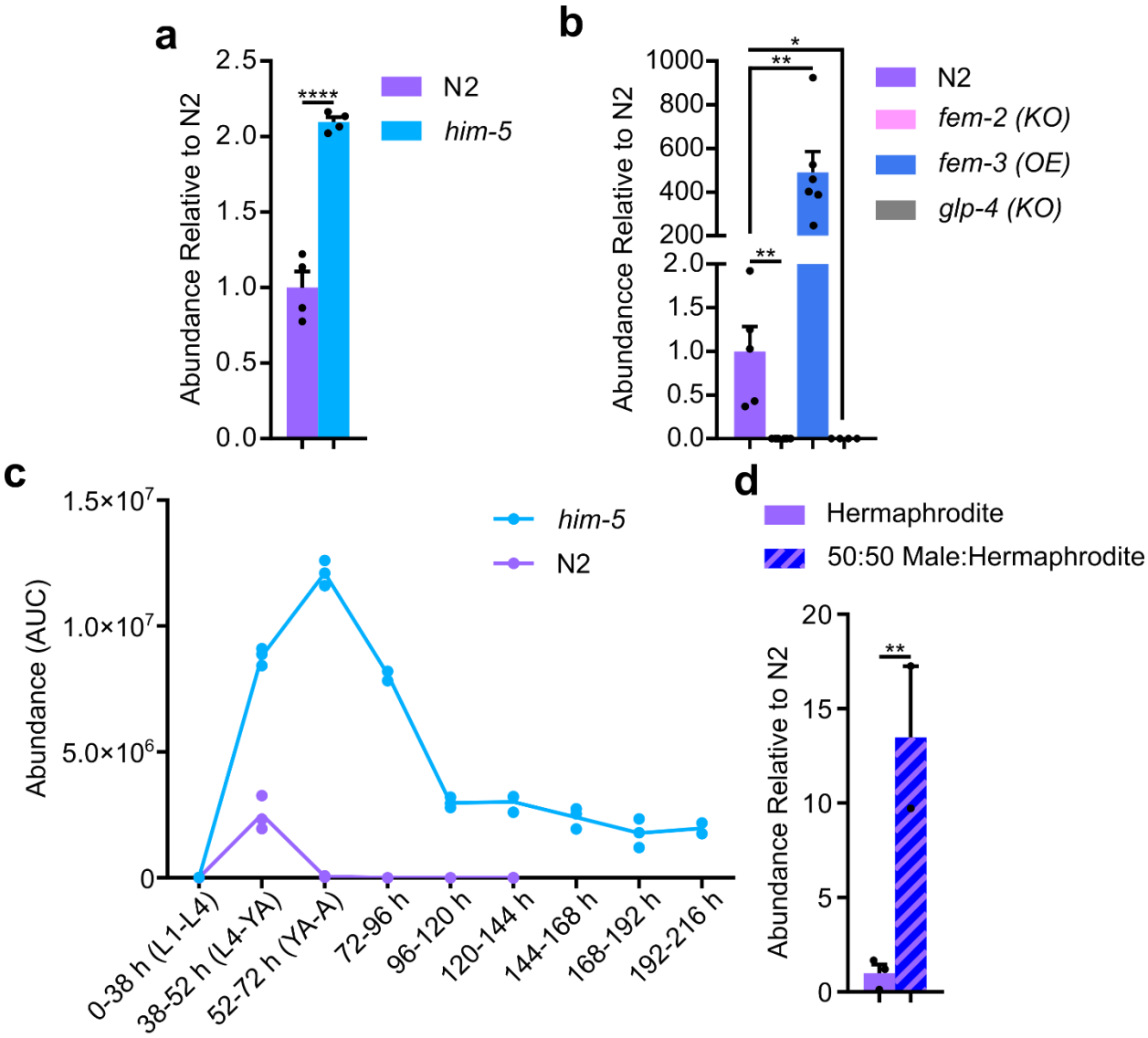

Fig. 4.10 | dmwi#1 is enriched in males in a germline-dependent manner. a. dmwi#1 is 2-fold enriched in *him-5* cultures relative to N2 cultures. **b.** dmw#1 is over 500-fold enriched in *fem-3* (OE) relative to N2 and undetectable in *fem-2* (KO) and *glp-4* (KO). **c.** When harvested as young adults, DMW-I is only ~2-fold increased in *him-5*, but production stops in N2 afterwards while *him-5* males continue production. **d.** dmwi#1 is 13-fold enriched in plated N2 cultures of 50:50 males:hermaphrodites over pure hermaphrodites. Data are presented as mean ± s.e.m. *, p≤0.05, **; p≤0.005; ****, p≤0.0001.

Dimethyltryptophan (DMW), a plausible precursor of dmwi#1, is a potential precursor to the psychedelic drug dimethyltryptamine that has not previously been reported from *C. elegans* or other animals, we decided to investigate its biosynthetic origin. Feeding of D_3-methionine to *C. elegans* resulted in robust D_3- and D_6-labeling of dmwi#1 (Supp. Fig. 4.18), indicating that methylation of the tryptophan-isoleucine dipeptide occurs in an *S*-adenosyl methionine- (SAM-)

dependent manner. In the HPLC-MS data from this labeling experiment, we also looked for compounds related to dmwi#1, including the free amino acid dimethyltryptophan, as well as mono- and trimethyltryptophan, and the non-methylated dipeptide. While a feature corresponding to the dimethyltryptophan (233.1308, 6.22 min) is found to elute at the same retention time as a synthetic standard, it is not D_3-labeled (Supp. Fig. 4.19). Interestingly, none of the alternately methylated tryptophan derivatives, or their corresponding dipeptides, were observed. In addition, we looked for dimethyltryptamine (DMT); however, although we observe a compound of the appropriate mass of DMT (*m/z* 189.1380, 6.95 min), it, like DMW, is not D_3-labeled.

Assuming that the biosynthesis of dmwi#1 involves an N-methyltransferase, we looked for methyltransferases homologous to the human methyltransferase indolethylamine-*N*-methyltransferase (INMT)[3]. A BLAST search for homologs in *C. elegans* revealed two homologous genes, *anmt-1* (amine n-methyltransferase 1) and *anmt-2*[11]. As anmt-1 is upregulated in males, it became our first target, however animals lacking *anmt-1* still produced DMW-I (Supp. Fig. 4.22). Similarly, *anmt-2* deficient worms also retained production of DMW-I. With over 20 annotated *N*-methyltransferases expressed more highly in males, further study will be necessary to reveal the enzyme responsible[11].

4.7 Very long chain polyunsaturated fatty acids are enriched in males

The final class of compounds detected as enriched in males was, like amta#1 and amta#2, not initially discovered in our comparison of N2 and *him-5*. During a parallel lipidomics investigation using sex mutants, in this case using germline-null *glp-1(e2141)* (KO), germline-feminized *fem-3(e2006)* (KO), and germline-masculinized *mog-3(q74)* (KO) mutants, we observed a series of oxygenated hydrocarbon derivatives in the worm body that were strongly

enriched in *mog-3* (KO) over all other strains. This series of metabolites began with a compound of formula $C_{24}H_{37}O_2^-$ (*m/z* 357.2798) and appeared in regularly spaced increments of C_2H_4 up to $C_{34}H_{57}O_2^-$ and ranged from 9- to 14-fold increases in *mog-3* (KO) over N2 (Fig. 4.11b). From the molecular formulae, and the repeating addition of C_2H_4 units, we deduced that the compounds were very long chain polyunsaturated fatty acids (VLCPUFAs) like eicosapentaenoic acid (EPA) and docosapentaenoic acid as demonstrated by co-elution of synthetic samples with the first two peaks in the series (Supp. Fig. 4.24).

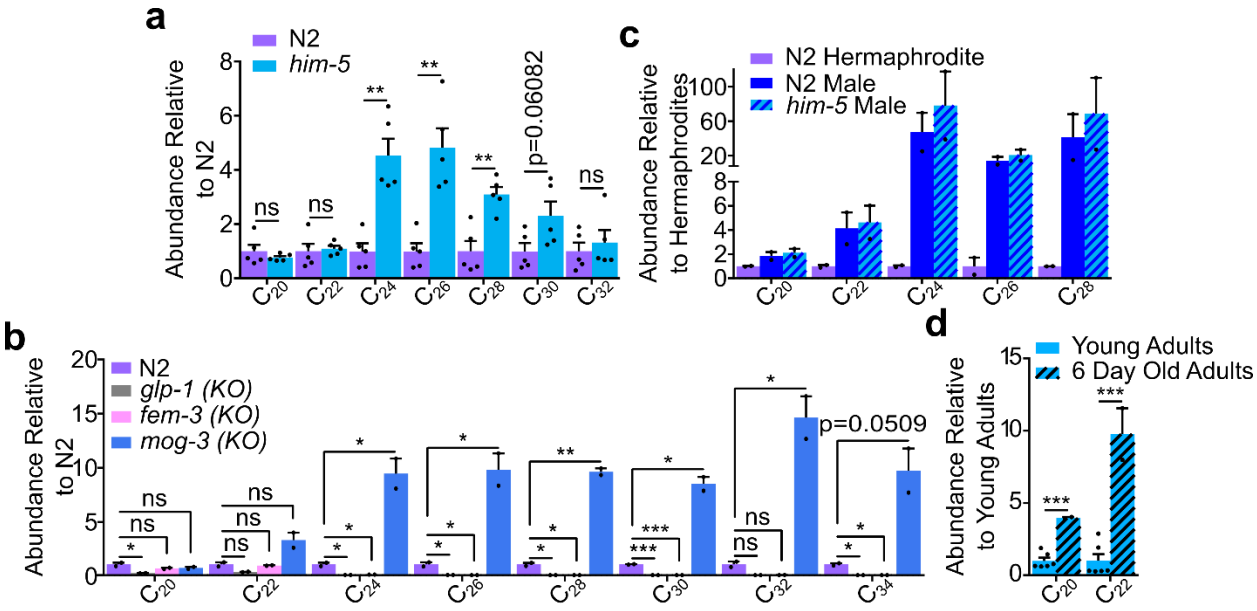

Fig. 4.11 | Enrichment of VLCPUFAs. a. In *him-5* and N2 endo-metabolomes extracted for lipids, penta-unsaturated VLCPUFAs 24-28 carbons long are significantly enriched in *him-5* cultures. **b.** VLCPUFAs 24-32 carbons in length are enriched in germline masculinized *mog-3* over N2. **c.** Although only two VLCPUFAs are detected in worm bodies extracted with methanol, EPA and DPA are 4- and 10-fold enriched in old worms over young worms. Data are presented as mean ± s.e.m. *, p≤0.05; **, p≤0.005; ***, p≤0.0005; ns, not statistically significant.

The increase in VLCPUFAs we observed in these earlier sex mutants was also evident in *him-5* cultures that were extracted specifically for lipids. In the case of *him-5* animals the increase was not as extreme, ranging from 2- to 5-fold enrichment and the enrichment was only statistically significant for $C_{24}H_{37}O_2^-$ through $C_{28}H_{45}O_2^-$ (Fig. 4.11a). The small samples of

males and hermaphrodites followed a similar trend with an increase in all VLCPUFAs detected though only two replicates of each were available and thus the increases were not statistically significant (Fig 4.11c). Unfortunately, the 50:50 male:hermaphrodite samples were extracted using methanol, and thus do not contain any detectable amounts of VLCPUFAs beyond EPA and docosapentaenoic acid, which were not enriched. Similarly, the six-day old adults were not extracted in a manner that would allow for large non-polar molecules to be observed, though EPA and DPA are both significantly enriched in six-day old adults over young adults (Fig. 4.11d).

Enrichment of VLCPUFAs in germline masculinized *mog-3* (KO) mutants and *him-5* cultures indicated that VLCPUFAs might be associated with sperm production. The increased abundance in older *him-5* cultures tentatively agrees with this, as sperm production in males reaches a maximum between two and three days of adulthood, with day six production approximately matching day two of adulthood[12]. This increase also aligns with a marked increase in the expression of a homolog of mammalian proteins ELOVL4, which is involved in the elongation of very long fatty acids[13,14]. Specifically, ELO-7 which is expressed 26-fold higher in males over feminized worms (A. Chaturbedi, personal communication, July 7, 2020).

4.8 Discussion

In our examination of the metabolomic differences between *him-5* and N2 cultures, we previously described nacq#1, which causes animals to develop faster and is partially responsible for male-induced demise, and the bemeth#s, a family of C_{11} fatty acids of varying degrees of oxidation that originate from a ligand for NHR-49[15]. In this Chapter, we discussed six additional compounds and/or classes of compounds that are enriched in male and masculinized animals with biosynthetic origins from all major branches of primary metabolism. Production of the first

class of compounds, the panglu#s, is dependent on the male germline and draws on aspects of carbohydrate and nucleoside metabolism, most likely RNA metabolism. panglu#1 and panglu#2 both contain methylated nucleobases, likely derived from 1-methyladenosine (m^1A) in the case of panglu#1 and 7-methylguanosine (m^7G), as both are common RNA modifications although the structure of panglu#2 has yet to be verified[16,17]. The uric acid in panglu#3 may be the product of general purine metabolism, though it could also be derived from a dedicated catabolic pathway of RNA-derived purines given that panglu#1 and panglu#2 both likely originate from RNA degradation[18].

The second class we discussed in this chapter, the uglas#-family of metabolites, additionally connects to lipid metabolism. In addition to the ascarylose sugar core and a lipid sidechain, the uglas#s all contain the gluric#1 moiety observed in panglu#3. It is also of interest to note that only uric acid-derived gluconucleosides were found among the male-enriched ascarosides, whereas ascaroside conjugates of the 1-methyladenine and methylguanine glucosides were not observed or not upregulated in males. This suggests that the biosynthesis of the uglas#s and panglu#s is highly specific, in turn suggesting that they serve distinct functions.

Another unique aspect of the uglas#-family metabolites, in particular the ascr#1 derivatives, is that different enzymes are responsible for conjugating gluric#1 and/or gluric#2 to ascr#1 in males and hermaphrodites. While hermaphrodites produce large amounts of the uglas#1 and uglas#11, which are acylated at the 2' position of the glucose moiety, uglas#1 and uglas#11 are virtually absent in males. Instead, males produce large amounts of uglas#14 and uglas#15, which are acylated at the 6' position of the glucose moiety[1]. While there is no significant difference in the expression of *cest-1.1*, which encodes the enzyme responsible for the biosynthesis of uglas#1 and uglas#11, between males and hermaphrodites, *cest-5.1*, which has no

activity assigned to it, is expressed over 300-fold higher in males than hermaphrodites[13,19]. *cest-5.1* is also not differential between *mog-3* (KO) masculinized worms and N2 hermaphrodites, making it an excellent candidate for the 6' acylation that results in uglas#14 and uglas#15, and likely uglas#104 and uglas#105, as none of the uglas#s are upregulated in a male germline-dependent manner (A. Chaturbedi, personal communication, July 7, 2020).

In addition to the gluric#1-conjugated ascarosides, we observed derivatives of ascr#1 that are also enriched in *him-5* and male cultures, six of which are proposed to also be glucose conjugates. In addition to conjugation of an undecorated glucose in the case of glas#1 and glos#1, we observed their phosphorylated versions, glas#11 and glos#11. Further decorated glucose moieties can be observed in anglas#2 and tyglas#1, however glucosides are not the only groups attached to ascr#1. Phosphorylation of ascarylose was observed in the case of phascr#1 and "ascarosylation" to ascr#3 resulted in the dimeric ascaroside dasc#13. Lastly, the saturated form of ascr#8, ascr#801, was found to be significantly enriched in *him-5*, males, and *fem-3* (OE) germline-masculinized animals. This compound is not absent in *fem-2* (KO) germline-feminized animals or *glp-4* (KO) germline-null animals, suggesting that ascr#801, like ascr#8 itself, is a product of CEST-2.2, which is expressed 9-fold higher in males than in hermaphrodites and 2.3-fold higher in *mog-3* (KO)[1,13].

We also observed two compounds almost straight out of primary metabolism, amta#1 and amta#2, which are likely the product of *S*-adenosylmethionine (SAM) metabolism[10]. These two compounds, although originally observed in *fem-3* (OE) animals, were also found to be enriched in both *him-5* cultures and pure males to varying degrees. Similarly, dmwi#1, which is the first reported case of dimethyltryptophan in *C. elegans*, was highly enriched in the *fem-3* (OE) exo-

metabolome, over 500-fold, but is only 2-fold enriched in *him-5* cultures and 13-fold enriched in 50:50 male:hermaphrodite cultures.

The last class of male-enriched compounds that we discussed in this chapter were the VLCPUFAs, fatty acids over 22-carbons in length with 5 double bonds. These, like amta#1/2 and dmwi#1, were originally found enriched in germline-masculinized animals, in this case in *mog-3* (KO) animals originally used for a separate experiment. While we found that these lipids are 9- to 14-fold enriched in *mog-3* mutants, they were only 2- to 5-fold enriched in *him-5* cultures. One explanation for this can be found in Chapter 3 – the bemeth#s, which are most profoundly enriched in males in the absence of hermaphrodites, are ligands for NHR-49, which has been implicated in fatty acid metabolism and regulation[14,20,21]. Specifically, NHR-49 regulates the expression of FAT-6 and FAT-7, which are responsible for the first desaturation step in the PUFA metabolic pathway, indicating VLCPUFA production may be the result of bemeth# signaling[22]. The alteration of lipid metabolism in hermaphrodites upon detection of male bemeth#s would only be the third example of a male-enriched metabolite actively altering hermaphrodite biology reported in *C. elegans*. This absence of information on the chemical interactions between males and hermaphrodites makes clear the need for further study.

References

(1) Wrobel, C. J. J., Yu, Jingfang, Rodrigues, P. R., Ludewig, A. H., Curtis, B. J., Cohen, S. M., Fox, B. W., O'Donnell, M. P., Sternberg, P. W., Schroeder, F. C. Combinatorial Assembly of Modular Glucosides via Carboxylesterases Regulates *C. elegans* Starvation Survival. *JACS* **143**: 14676-14683. **2021**.

(2) Izrayelit, Y., *et al.* Targeted metabolomics reveals a male pheromone and sex-specific ascaroside biosynthesis in *Caenorhabditis elegans. ACS Chem. Biol.* **7**: 1321-1325. **2012**.

(3) Dean, J. G., Liu, T., Huff, S., Sheler, B., Barker, S. A., Strassman, R. J., Wang, M. M., Borjigin, J. Biosynthesis and Extracellular Concentrations of N,N-dimethyltryptamine (DMT) in Mammalian Brain. *Sci. Rep.* **9**: 9333. **2019**.

(4) Curtis, B. J., Kim, L. J., Wrobel, C. J. J., Eagan, J. M., Smith, R. A., Burch, J. E., Le, H. H., Artyukhin, A. B., Nelson, H. M., Schroeder, F. C. Identification of uric acid gluconucleoside-ascaroside conjugates in *Caenorhabditis elegans* by combining synthesis and MicroED. *Org. Lett.* **22**: 6724-6728. **2020**.

(5) Artyukhin, A. B., Zhang, Y. K., Akagi, A. E., Panda, O., Sternberg, P. W., Schroeder, F. C. Metabolomic "dark matter" dependent on peroxisomal β-oxidation in *Caenorhabditis elegans. JACS* **140**: 2841-2852. **2018**..

(6) Von Reuss, S. H. *et al.* Comparative metabolomics reveals biogenesis of ascarosides, a modular library of small molecule signals in *C. elegans. JACS* **134**: 1817-1824. **2012**.

(7) Tarr, G. E., Schnoes, H. K. Structures of Ascaroside Aglycones. *Arch. Biochem. Biophys.* **158**: 288-296. **1973**.

(8) Hoki, J. Development of Click-Chemistry Based Enrichment Strategies to Characterize Ligand Binding and Metabolism. *Doctoral Dissertation. Cornell University*. **2020**.

(9) Avila, M. Z., García-Trevijano, E. R., Lu, S. C., Corrales, F. J., Mato, J. M. Molecules in focus Methylthioadenosine. *Int. J. Biochem. Cell Bio.* **36**: 2125-2130. **2003**.

(10) Brandt, S. D., Moore, S. A., Freeman, S., Kanu, A. B. Characterization of the synthesis of *N,N*-dimethyltryptamine by reductive amination using gas chromatography ion trap mass spectrometry. *Drug Test. Anal*. **2**: 330-338. **2010**.

(11) Shaye, D. D., Greenwald, I. OrthoList: A Compendium of *C. elegans* Genes with Human Orthologs. *PLoS One* **6**: e20085. **2011**.

(12) Chou, W., Lin, Y., Lee, Y. Short-term starvation stress at young adult stages enhances meiotic activity of germ cells to maintain spermatogenesis in aged male *Caenorhabditis elegans*. *Aging Cell* **18**: e12960. **2019.**

(13) Albritton, S. E., Kranz, A., Rao, P., Kramer, M., Dieterich, C., Ercan, S. Sex-Based Gene Expression and Evolution of the X Chromosome in Nematodes. *Genetics* **197**: 865-883. **2014.**

(14) Yu, M., Benham, A., Logan, S., Brush, R. S., Mandal, M. N. A., Anderson, R. E. ELOVL4 protein preferentially elongates 20:5n3 to very long chain PUFAs ove3r 20:4n6 and 22:6n3. *J. Lipid Res.* **53**: 494-504. **2012**.

(15) Fox, B. W., *et al. In preparation.*

(16) van Delft, P., Akay, A., Huber, S. M., Bueschl, C., Rudolph, K. L. M., Domenico, T. D., Schuhmacher, R., Miska, E. A. Balasubramanian, S. The Profile and Dynamics of RNA Modifications in Animals. *Chembiochem*. **18**: 979-984. **2017**.

(17) Shima, H., Igarashi, K. N^1-methyladenosine (m^1A) RNA modification: the key to ribosome control. *J. Biochem.* **167**: 535-539. **2020.**

(18) Johnson, R. J., Lanaspa, M. A., Gaucher, E. A. Uric acid: A Danger Signal from the RNA World that may have a role in the Epidemic of Obesity, Metabolic Syndrome and Cardiorenal Disease: Evolutionary Considerations. *Sem. in Nephrol.* **31**: 394-399. **2011**.

(19) Le, H. H., Wrobel, C. J. J., Cohen, S. M., Yu, J., Park, H., Helf, M. J., Curtis, B. J., Kruempel, J. C., Rodrigues, P. R., Hu, P. J., Sternberg, P. W., Schroeder, F. C. Modular metabolite assembly in *Caenorhabditis elegans* depends on carboxylesterases and formation of lysosome-related organelles. *eLife* e61886. **2020**.

(20) Ratnappan, R., Amrit, F. R. G., Chen, S., Gill, H., Holden, K., Ward, J., Yamamoto, K. R., Olsen, C. P., Ghazi, A. Germline Signals Deploy NHR-49 to Modulate Fatty-Acid β-Oxidation and Desaturation in Somatic Tissues of *C. elegans. PLoS Genet.* **10**: e1004829. **2014.**

(21) Van Gilst, M. R., Hadjivassilou, H., Jolly, A., Yamamoto, K. R. Nuclear Hormone Receptor NHR-49 Controls Fat Consumption and Fatty Acid Composition in *C. elegans. PLoS Biol.* **3**: e53. **2005**.

(22) Watts, J. L., Browse, J. Genetic dissection of polyunsaturated fatty acid synthesis in *Caenorhabditis elegans. PNAS* **99**: 5854-5859. **2002.**

CHAPTER 5

INVESTIGATION OF DAFACHRONIC ACID METABOLISM

Contributions and Acknowledgments

The research described herein branches off of work performed by Dr. Joshua Judkins (JJ). The initial synthetic pathway was developed by JJ and modified by Russell N. Burkhardt (RNB). Isotopically labeled dafachronic acids were synthesized by RNB. Feeding experiments were performed by PG and data analyzed by PG, Dr. Frank C. Schroeder (FCS), and RNB. Assays were performed by PG and RNB.

Abstract

The dafachronic acids are steroidal ligands of the nuclear hormone receptor (NHR) DAF-12, which plays a central role in the signaling cascade controlling growth and reproductive maturation. While these compounds play an essential role in the lifecycle of nematodes, it remains unknown if the presently identified ligands are the most active species. Feeding of isotopically labeled dafachronic acids revealed additional molecules that originate from dafachronic acids, though whether they are active ligands has yet to be determined. To investigate the origin of these, we attempted to identify protein interaction partners through affinity-based protein purification, however, we found that even seemingly minor modifications to their structure greatly reduced the dafachronic acids' activity.

5.1 Introduction

C. elegans has two alternate developmental trajectories (Fig. 5.1a). If growth conditions are satisfactory, animals will develop through four larval stages (L1-L4) and reproductive adulthood after about three days[1]. If, however, the population density is very high, there is insufficient food, or the temperature is unfavorable, animals will proceed from the L1 larval stage into an alternate larval stage named "dauer" (from the German word for "enduring")[2]. Dauer larvae are non-feeding, highly stress resistant, and can survive for months until conditions become favorable again, at which point they will resume development and proceed to the L4 stage and continue to adulthood as normal (Fig. 5.1a)[2].

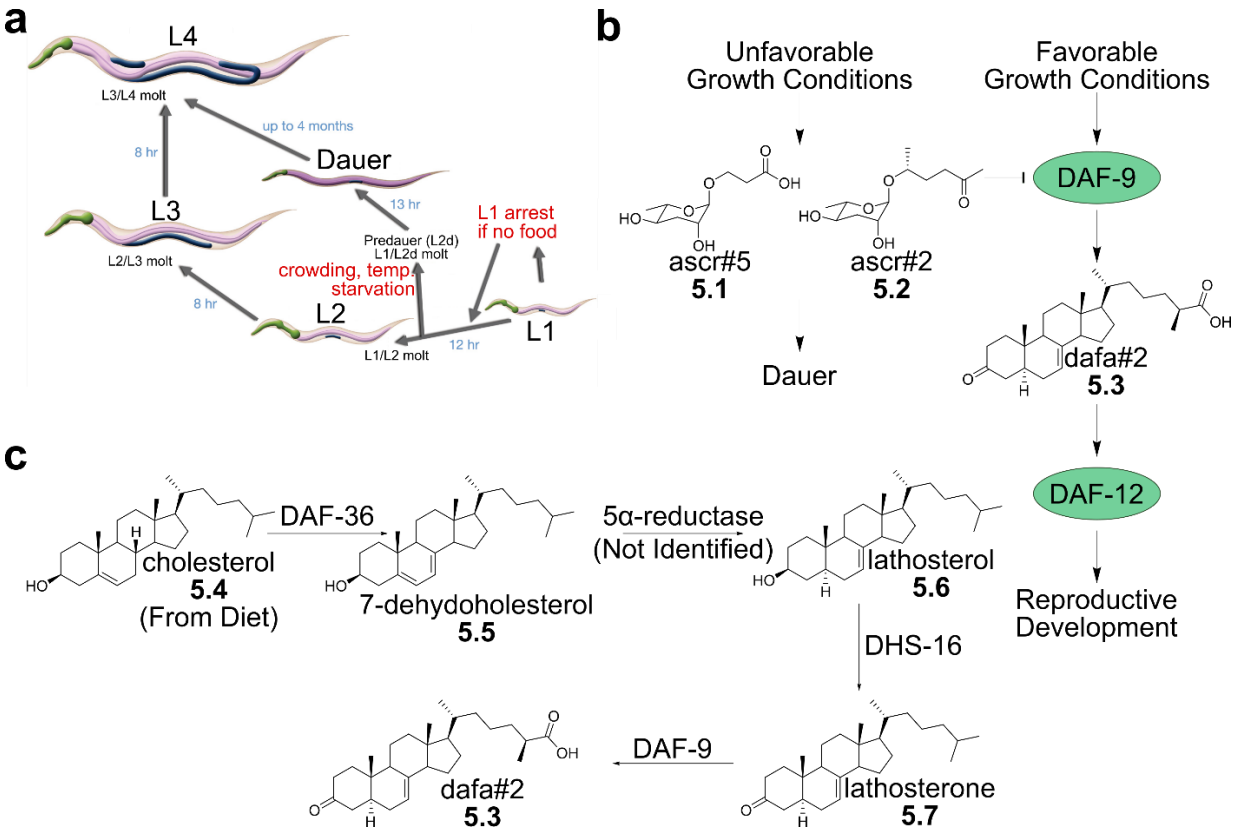

Fig. 5.1 | Regulation of Development in *C. elegans*. **a.** *C. elegans* may arrest at the L1 larval stage if no food is present or proceed through development to the L2 larval stage or, alternately, the dauer life stage where they can persist for months before proceeding with development. Adapted from WormAtlas[3]. **b.** Under detection of favorable growth conditions DAF-9 will perform the presumably final (known) step of dafachronic acid biosynthesis and the produced dafa#s will bind DAF-12, recruiting transcriptional coactivators that promote development. **c.** The dafachronic acids e.g. dafa#2 are derived from dietary cholesterol.

The decision which developmental pathway to take is determined by two sets of molecules; the dauer inducing ascarosides (e.g. ascr#5 (**5.1**) and ascr#2 (**5.2**)), pheromones that accumulate in the growth media and serve as a measure for population density, and the dafachronic acids, which are steroid hormones that signal to bypass or exit dauer and promote reproductive development (Fig. 5.1b)[4-6]. The dafachronic acids are ligands of the vitamin D-receptor homolog DAF-12, an NHR that, when unliganded, represses transcriptional programs for development, thereby triggering the transition into the dauer stage[7-9]. The most well-characterized natural dafachronic acid, Δ^7-dafachronic acid (dafa#2, **5.3**) has been synthesized using a number of different approaches[10-12]. The final step in the proposed biosynthetic pathway for the dafachronic acid

family is selective oxidation of one of the side chain methyl groups to a carboxylic acid by the P450 DAF-9[6] As such, *daf-9* mutant worms, which lack dafachronic acids and thus constitutively enter dauer unless supplemented with synthetic dafachronic acids, are an important model for the study of DAF-12 signaling (Fig. 5.1c)[6]. Investigations in our lab have revealed an additional putative P450 oxidoreductase, named DAF-40, that appears to be involved in dafachronic acid biosynthesis. *daf-40* (KO) mutant worms are only slightly more likely to enter dauer than wildtype worms; however, *daf-9;daf-40* double mutants are much less responsive to synthetic dafachronic acids than *daf-9* single mutants. The incomplete rescue by supplemental dafachronic acids distinguishes *daf-40* from all other known enzymes in dafachronic acid biosynthesis. From this, we hypothesized that DAF-40 oxidizes dafa#2 to a more active ligand, which due to the presence of additional double bonds conjugated to the carbonyl in the A-ring of the steroid core, is more labile and thus has escaped previous attempts at identification. In order to find and identify this more active ligand, we pursued a three-pronged approach, involving isotopic labeling, affinity-based protein profiling (ABPP), and tagging of activated species.

5.2 Synthesis of isotopically labeled dafa#2.

In order to track metabolic products of the known ligand dafa#2, such as the putative product(s) of DAF-40, we first developed a synthesis for a ^{13}C-labeled version of dafa#2. This isotopically labeled dafa#2 could then be fed to *daf*-9 (KO) worms, and compounds that are putatively the result of DAF-40 activity on dafa#2 could be identified via comparative metabolomic analysis of wildtype and *daf-40* (KO) mutant worms fed the labeled compounds.

Our synthetic scheme followed the previously published synthesis developed by Dr. Joshua Judkins in the Schroeder Lab (Fig. 5.2)[12]. Beginning with chenodeoxycholic acid (**5.8**), we prepared the methyl ester (**5.9**) using TMS-diazomethane. Oxidation with Fétizon reagent

(Ag_2CO_3 on celite) resulted in the 3-keto ester (**5.10**), which was reacted with benzyl chloromethyl ester to form the protected alcohol (**5.11**). Oxidation with 2-iodoxybenzoic acid (IBX) formed the Δ^4 desaturated ester (**5.12**), which was subsequently reduced to the triol (**5.13**) via dissolved metal reduction. Re-oxidation with Fétizon reagent yielded the 3-keto aldehyde (**5.14**). Here, we substituted $^{13}C_3$-triethyl phosphonopropionate for the unlabeled version in the Horner-Wadsworth-Emmons (HWE) olefiniation, allowing us to insert three ^{13}C labels into ethyl ester (**5.16**). Burgess elimination to install the Δ^7-desaturation (**5.17**), hydrolysis (**5.18**), and chiral reduction with a ruthenium-BINAP catalyst yielded the $^{13}C_3$-dafa#2 (**^{13}C$_3$-5.3**).

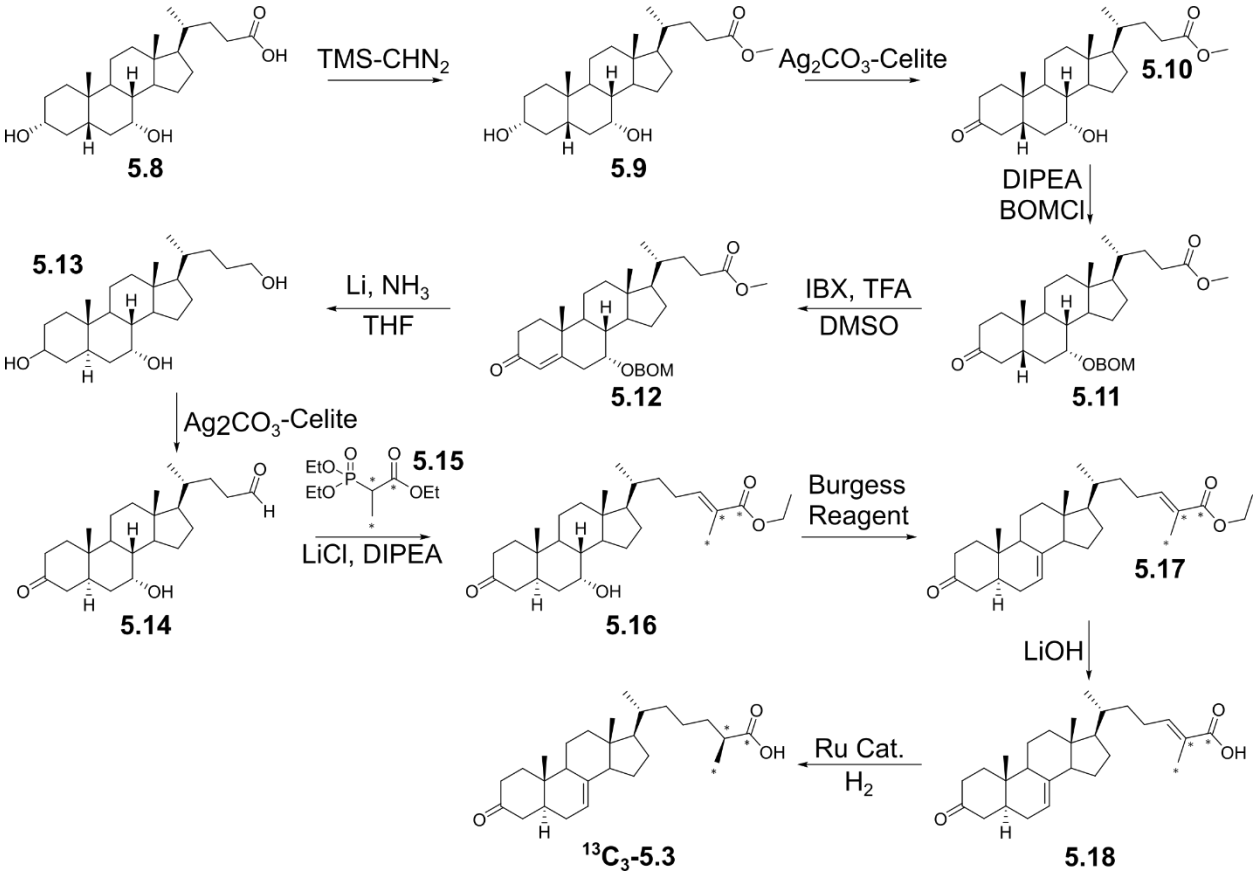

Fig. 5.2 | Synthesis of ^{13}C-labeled dafa#2. Synthesis of $^{13}C_3$-dafa#2 proceeded as previously published by Dr. Joshua Judkins with incorporation of ^{13}C achieved during the HWE chain-elongation[12].

5.3 Synthetic work towards a small molecule probe for affinity-based protein purification

As a second strategy to investigate activation and/or metabolism of dafachronic acids, we endeavored to make a dafa#2-derivative that could be crosslinked to form a covalent bond to proteins with which it interacts and further could be clicked to a solid phase support for protein enrichment and identification. Previous studies by Dr. Joshua Judkins revealed that the 25-methyl group of dafa#2 can be extended to an ethyl group with only a 5-fold loss of activity, as such it seemed the optimal position for a clickable alkyne handle[13]. As such, we exchanged the 25-methyl group for a butyl group to grant distance from the carboxylic acid terminus of dafa#2. This substitution also lent itself to our current synthetic scheme, as we were able to substitute triethyl-2-phosphonohexanoate for triethyl-2-phosphonopropionate during the HWE (Fig. 5.3a).

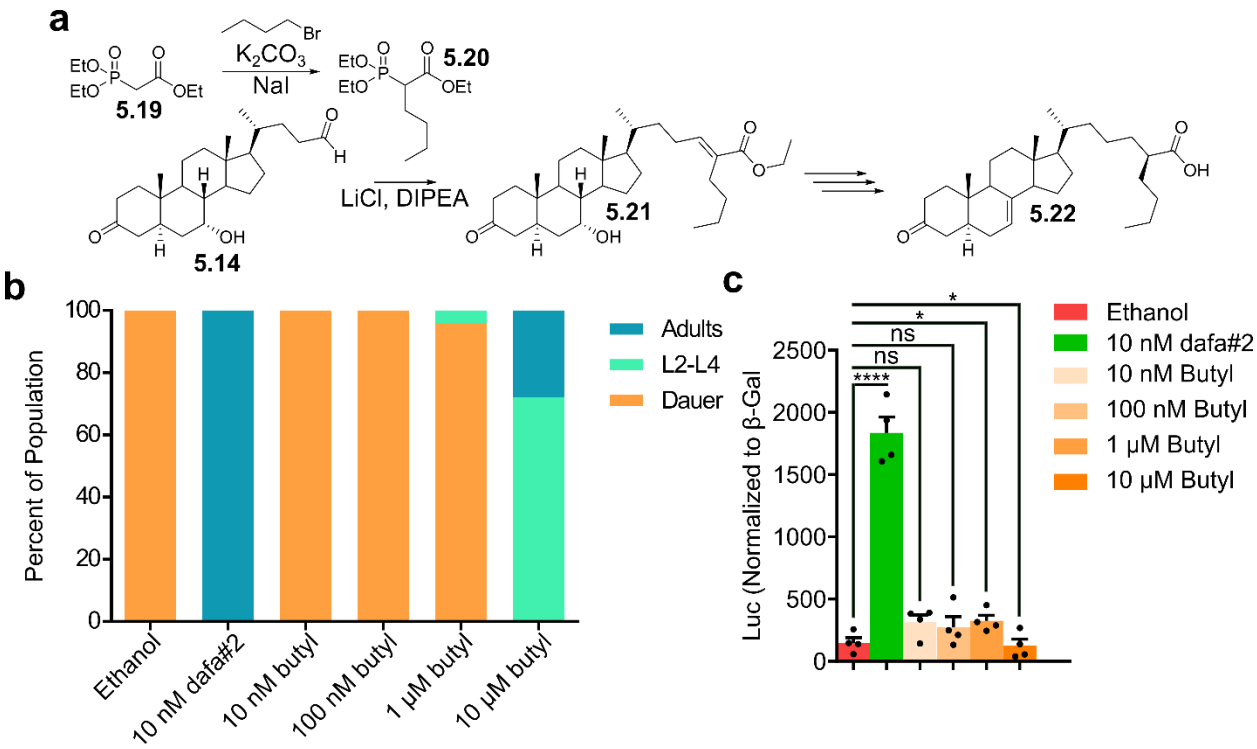

Fig. 5.3 | 25-butyl dafa#2. a. 25-butyl dafa#2 was prepared by substitution of triethyl 2-phosphonohexanoate (**5.20**) for triethyl 2-phosphonopropionate. **b.** Results of dauer rescue assays performed on *daf-9 (KO)* animals with varying concentrations of 25-butyl dafa#2 reported as percentage of the total worm population. **c.** Luciferase assay results for varying concentrations of 25-butyl dafa#2 normalized to β-galactosidase expression. Data are presented as mean ± s.e.m. *, $p \leq 0.05$; ****, $p \leq 0.0001$; ns, not statistically significant.

Next, we tested the activity of the 25-butyl-dafa#2 (**5.22**) to determine if this probe design was worth further pursuit. To examine the bioactivity of **5.22**, we used a dauer-rescue assay, in which *daf-9* (KO) worms, which do not produce their own dafachronic acids, are exposed to the compound of interest. As *daf-9* (KO) worms lack the cytochrome P450 that installs the carboxylic acid moiety in dafachronic acids, they lack any natural ligands for DAF-12, and thus constitutively enter the dauer stage[8]. Addition of an active ligand for DAF-12, e.g. dafa#2, then allows them to exit dauer and proceed to reproductive maturity. In this assay, the ratio of dauer-to-adults can be tallied to compare the activity of different ligands at different concentrations. In the case of dafa#2, we see full rescue of the dauer phenotype at 10 nM concentrations. While 25-butyl-dafa#2 is not active at such low concentrations, rescue is observed at 1 μM and full rescue can be achieved at a concentration of 10 μM, roughly in line with a 5-fold reduction in potency with each additional carbon as was observed with 25-ethyl dafa#2 relative to dafa#2 (Fig. 5.3b)[13].

A second assay available to examine the activity of dafachronic acids is an *in-vitro* luciferase assay. In this assay, DAF-12 is expressed in HEK 293T cells and, when activated by dafachronic acids, induces transcription of a luciferase construct, which includes a mir241 promoter, one of the known DAF-12 binding sites. The relative luciferase activity can then be quantified and the ligand activity assessed. Here, we observed a robust luciferase signal at 100 nM dafa#2 and only moderate signals for 25-butyl-dafa#2 at 100 nM to 10 μM concentrations, with no significant differences between the levels (Fig. 5.3c).

While the activity of 25-butyl-dafa#2 is significantly lower than actual dafa#2, the compound was still capable of rescuing *daf-9* (KO) worms, and so we continued our probe design, looking to install a covalently crosslinking moiety. Here, we chose to pursue a diazirine functionality as it was the smallest, and hopefully least disruptive, of the photo-activated

crosslinking groups. Installation of the diazirine moiety was most easily envisioned at the 3-position and would conceivably produce the least difference in the functionality of the molecule by replacing the ketone. We began by forming the diaziridine (**5.23**) with ammonia and hydroxylamine-*O*-sulfonic acid, which was oxidized to the diazirine (**5.24**) with iodine (Fig. 5.4a)[14]. Unfortunately, bioactivity assays of 3-diazo-dafa#2 demonstrated activity in neither the dauer-rescue assay nor the luciferase assay, aside from a small amount of activity at 10 µM, which was found to be the result of trace amounts of dafa#3 present in the sample that was the result of diazirine degradation (Fig. 5.4b,c). With no other readily modified position available and the negative results for the 3-diazo-dafa#2, we set aside further investigations as we focused on the research outlined in Chapters 1-4.

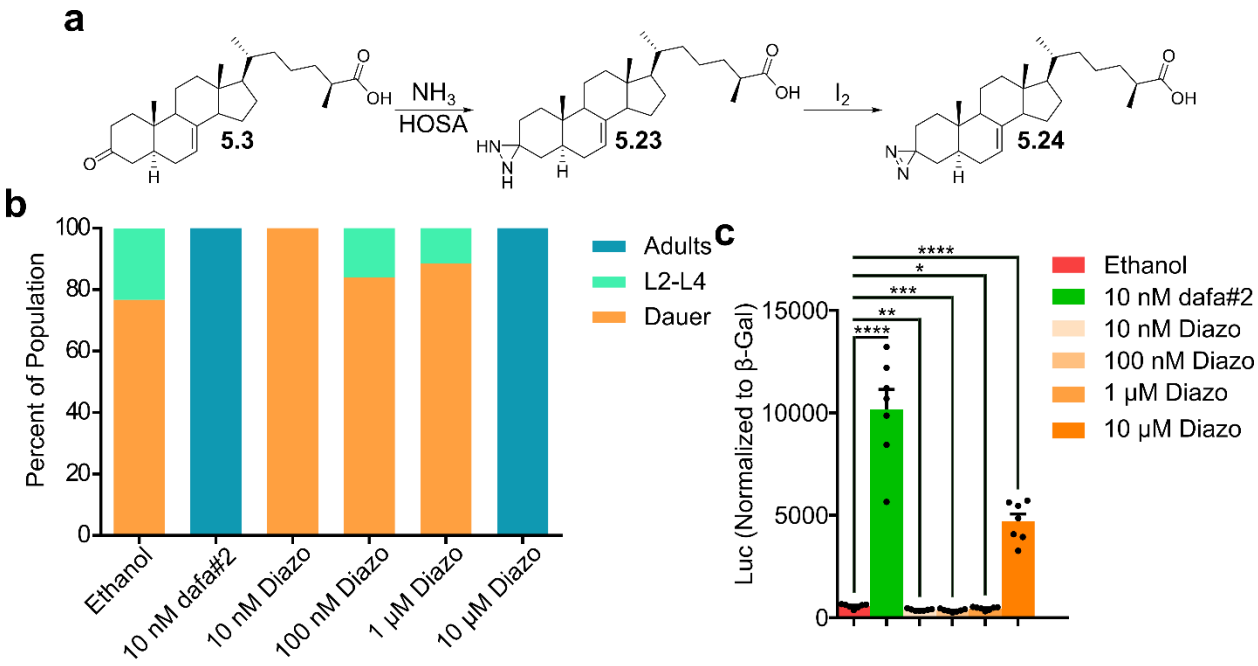

5.4 | 3-diazo dafa#2. a. 3-dizao dafa#2 was prepared from dafa#2 by forming the diaziridine and oxidation with I_2. **b.** Results of dauer rescue assays performed on *daf-9 (KO)* animals with varying concentrations of 3-diazo dafa#2 reported as percentage of the total worm population. **c.** Luciferase assay results for varying concentrations of 3-diazo dafa#2 normalized to β-galactosidase expression. Data are presented as mean ± s.e.m. *, p≤0.05; **, p≤0.005; ***, p≤0.0005; ****, p≤0.0001.

5.4 Future methodology for investigation of dafachronic acids

The Schroeder lab recently developed a strategy for the identification and characterization of activated species of small molecules[15]. As we believe that dafachronic acids like dafa#2 are likely oxidized to more active, and reactive species via DAF-40, dafachronic acids have become one of the families of molecules that we have planned to investigate. Reactive, electrophilic species can be studied by addition of light (^{14}N) and heavy (^{15}N) hydroxylamine, which will react with electrophilic species such as CoA thioesters, aldehydes, ketones, and double bonds conjugated with carbonyls[15]. Use of heavy hydroxylamine verifies that the compound observed in the light arm of the study tagging possesses a hydroxylamine tag rather than simply having a nitrogen and oxygen in their structure (Fig. 5.5a). Furthermore, use of $^{13}C_3$-dafa#2 will allow us to differentiate activated species that are derived from dafa#2 from those that are derived from other steroids or bile acids (Fig. 5.5b).

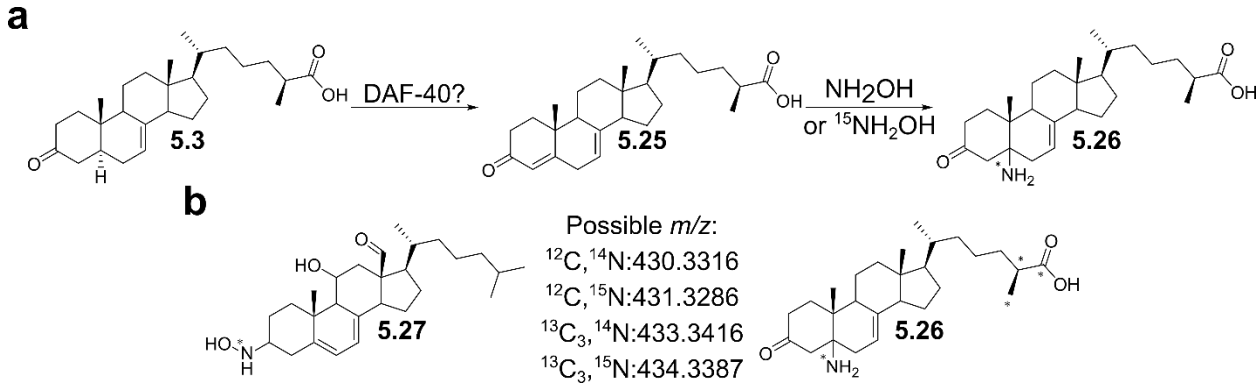

Fig. 5.5 | Hydroxylamine tagging and stable isotope labeling. a. Activation of dafa#2, perhaps through oxidation via DAF-40, would result in a more reactive species which can be tagged with ^{14}N and ^{15}N hydroxylamine. **b.** Compounds derived from dafa#2, such as 5-amino dafa#2, could be differentiated from other steroid-derived compounds, such as the oxidized cholesterol derivative shown, by the $^{13}C_3$ labeling incorporated in dafa#2.

In addition to such tracking of isotopes with tagging, a functionalized dafachronic acid may still be an option. While our research has demonstrated how finely-tuned the dafachronic acid-DAF-12 interactions are, modification at sites outside of the AB ring system may prove more amenable. Although originally demonstrated on testosterone, the human cytochrome P450 3A4

has been shown to hydroxylate the 18- and 19- methyl groups of the steroid core[16]. If such enzymatic activity could be applied to dafa#2 or a synthetic intermediate a diazirine or alkyne could then be incorporated into the final structure for use as a probe. Although extension of the 25-methyl of dafa#2 to a 25-butyl chain reduced activity approximately 1000-fold, a propargyl chain, which would be significantly shorter, may yield a reasonable activity.

References

(1) Byerly, L., Cassada, R. C., Russell, R. L. The life cycle of the nematode *Caenorhabditis elegans. Dev. Biol.* **51**: 23-33. **1976.**

(2) Cassada, R. C., Russell, R. L. The dauerlarva, a post-embryonic developmental variant of the nematode *Caenorhabditis elegans. Dev. Biol.* **46**: 326-342. **1975.**

(3) Altun, Z. F., Hall, D. H. Introduction. *In WormAtlas*. **2009.** doi:10.3908/wormatlas.1.1

(4) Butcher, R. A., Fujita, M., Schroeder, F. C., Clardy, J. Small-molecule pheromones that control dauer development in *Caenorhabditis elegans. Nat. Chem. Biol.* **3**: 420-422. **2007.**

(5) Butcher, R. A., Ragains, J. R., Kim, E., Clardy, J. A potent dauer pheromone component in *Caenorhabditis elegans* that acts synergistically with other components. *PNAS* **105**: 14288-14292. **2008**.

(6) Antebi, A. Yeh, WH, Tait, D., Hedgecock, E. M., Riddle, D. L. daf-12 encodes a nuclear receptor that regulates the dauer diapause and developmental age in C. elegans. *Genes Dev.* **14**: 1512-1527. **2000**.

(7) Motola, D. L, Cummins, C. L., Rottiers, V. Sharma, K. K., Li, T., Li, Yong, Suino-Powell, K., Xu, H. E., Auchus, R. J., Antebi, A., Mangelsdorf, D. J. Identification of ligands for DAF-12 that govern dauer formation and reproduction in C. elegans. *Cell* **124**: 1209-1223. **2006**.

(8) Gerisch, B., Antebi, A. Hormonal signals produced by DAF-9/cytochrome P450 regulate C. elegans dauer diapause in response to environmental cues. *Development* **131**: 1765-1776. **2004**.

(9) Gerisch, B., Rottiers, V., Li, D., Motola, D. D., Cummins, C. L., Lehrach, H., Mangelsdorf, D. J., Antebi, A. A bile acid-like steroid modulates Caenorhabditis elegans lifespan through nuclear receptor signaling. *PNAS* **104**: 5014-5019. **2007**.

(10) Giroux, S., Corey, E. J. Stereocontrolled Synthesis of Dafachronic Acid A, the Ligand for DAF-12 Nuclear Receptor of *Caenorhabditis elegans*. *JACS* **129**: 9866-9867. **2007**.

(11) Sharma, K. K., Wang, Z., Motola, D. L., Cummins, C. L., Mangelsdorf, D. J., Auchus, R. J. Synthesis and activity of dafachronic acid ligands for the C. elegans DAF-12 nuclear hormone receptor. *Mol. Endocrinol.* **23**: 640-648. **2009**.

(12) Judkins, J. C., Mahanti, P., Hoffman, J. B., Yim, I. Antebi, A., Schroeder, F. C. A Photocleabable Masked Nuclear-Receptor Ligand Enables Temporal Control of *C. elegans* Development. *Angew. Chemie.* **53**: 2110-2113. **2014**.

(13) Judkins, J. Synthesis, Biosynthesis, and Function of Small Molecules Regulating Behavior and Development in C. elegans. *Doctoral dissertation, Cornell University.* **2014.**

(14) Zhang, Y. K. Synthesis of Nematode Signaling Molecules. *Doctoral dissertation, Cornell University.* **2019.**

(15) Yu, Y., Le, H. H., Curtis, B. J., Wrobel, C. J. J. Zhang, B., Maxwell, D. N., Pan, J. Y., Schroeder, F. C. An Untargeted Approach for Revealing Electrophilic Metabolites. *ACS Chem. Biol.* **15**: 3030-3037. **2020**.

(16) Cheng, Q., Sohl, C. D., Yoshimoto, F. K., Guengerich, F. P. Oxidation of Dihydrotestosterone by Human Cytochromes P450 19A1 and 3A4. *J. Biol. Chem.* **287**: 29554-29567. **2012**.

CHAPTER 6

CONCLUDING REMARKS

Conclusions

Caenorhabditis elegans has been studied for over 50 years and has become one of the most studied and best understood organisms on earth[1]. Despite all this knowledge, many aspects of their biology remain poorly understood. Lack of understanding of the small molecules that regulate the underlying signaling networks may be one primary reason holding back progress. Furthermore, the differences that arise due to the sexual dimorphism are often overlooked since males make up only a fraction of a percent of the population in most laboratory cultures[2]. Here we presented evidence for major differences in the biosynthetic and signaling networks of different sexes, identifying several classes of small molecules that are enriched in males by comparing a variety of male, male-enriched, and masculinized animals to hermaphrodites, females, and germline-null animals.

Chapter 2 described the identification, synthesis, and bioactivity of the first male-enriched compound that we identified, nacq#1, which served as a catalyst for our identification of other male compounds. nacq#1 was initially identified through activity-guided fractionation during a search for compounds responsible for acceleration of development. Isolation of nacq#1 allowed structural determination via NMR and synthesis of nacq#1 further verified the assignment and provided material for biological studies. It was found that nacq#1 not only accelerates development in isolated animals, particularly during the L4 larval stage, but also reduces the lifespan of animals, indicating that nacq#1 is partially responsible for both population density-dependent acceleration (PDDA) and male-induced demise (MID)[3].

In Chapter 3 we discussed a class of β-methyl fatty acids, the bemeth#s, for which initial examples had previously been identified during a study of the methyltransferase F13D12.9[4]. This class of compounds also appeared in studies of peroxisomal α-oxidation, where it was found that they are enriched in animals deficient in B0334.3, the *C. elegans* homolog of human HACL1. We observed not only increased levels of members of the bemeth# family in males but an increase in masculinized animals indicating that their production is tied to sperm production. In addition to several of the previously identified hydroxylated-bemeth#-family metabolites we observed novel amino acid conjugates. Further, we developed an enantioselective synthesis of bemeth#1, bemeth#23, and bemeth#71, and through biological studies we found that (*R*)-bemeth#1 is an active endogenous ligand for NHR-49[5].

The class of β-methyl fatty acids and nacq#1 were not the only compounds that were enriched in males, and we discussed several additional classes and compounds in Chapter 4. A group of gluconucleosides, the panglu#s, was found to be derived from the male soma. In addition to the panglu#-family of compounds, novel male-enriched nucleosides included a new class of ascarosides, in which ascr#1 and ascr#10 were conjugated to the uric acid glucosides gluric#1 and gluric#2. Additional derivatives of ascr#1 were found to be enriched in males in a germline-independent way, including diverse glucosides. Furthermore, three other compounds, the SAM-derived amta#1, amta#2, and the highly unusual dimethyltryptophan dipeptide dmwi#1 were also found to be enriched in males in a germline-dependent manner. The final class, the VLCPUFAs, was also enriched in males and appeared to be related to sperm production. Further, we postulated that the increase in VLCPUFAs present in males is the result of NHR-49-dependent response to the increased levels of bemeth#s observed in Chapter 3.

Finally, in Chapter 5, we discussed our work on investigation of dafachronic acids and their metabolism. Using the biosynthetic scheme previously developed by Dr. Joshua Judkins we prepared ^{13}C-labeled dafa#2 which can be used to track the metabolism of dafachronic acids. We also endeavored to make a small molecule probe for proteins that interact with dafachronic acids which, although unsuccessful, demonstrated the specificity with which DAF-12 and other interacting proteins bind to dafachronic acids. Furthermore, we discussed a method developed in our lab which may allow us to find activated, and potentially more active, species of dafachronic acids.

Proposed future research

Throughout this work we focused on compounds that are enriched in the male metabolome; however, additional compounds remain to be identified. Of the over 200 male-enriched compounds discovered in our analysis, we have discussed just over 30, incorporating building blocks from diverse biochemical pathways, including from nucleic acid, amino acid, lipid, and carbohydrate metabolism. Further examination and structural elucidation will no doubt reveal additional metabolites of equal or even greater biosynthetic diversity.

Examination of the biosynthetic origins of these metabolites would likewise be an area of interest. Research from in the Schroeder Lab has partially elucidated the biosynthetic pathways of the nacq#1 and the bemeth#s, but the enzymes for amino acid conjugation remain unknown for both compounds. While CEST-5.1 is a putative enzyme for performing the conjugation of gluric#1 (or gluric#2) to ascr#1 and ascr#10, this remains unproven. Observation of a loss of production of the uglas#s in a masculinized *cest-5.1* (KO), such as a *fem-3* (OE):*cest-5.1* (KO) double mutant, would be appropriate for confirmation. Similarly, examination of

methyltransferase mutants, particularly those that are expressed at higher levels in males, would be of use for the biosynthesis of panglu#1, panglu#2, and dmwi#1.

While bioactivity of the compounds identified would be of great interest, synthesis of all such compounds will remain an ambitious goal due to the structural diversity observed. Further examination of the bioactivity of bemeth#1 and bemeth#23 is ongoing in the Schroeder lab, and synthesis of other bemeth#-family metabolites will be straightforward given the developed synthesis. Ongoing experiments with dmwi#1 by our collaborator Ilya Ruvinsky (Northwestern) have the potential to reveal new and exciting aspects of male small molecule signaling, given its novelty and the bioactivity of dimethyltryptamine (DMT). While synthesis of panglu#1 was achieved, feeding experiments using such polar molecules may prove difficult as demonstrated by prior feeding experiments with gluric#1.

With the ^{13}C-dafa#2 synthesized, it may be of interest to examine male metabolism of dafachronic acids by feeding the compound to *daf-9* (KO) animals in a *him-5* background. The ^{13}C-labeled-dafa#2 can also be combined with hydroxylamine tagging for verification that tagged species are truly derived from dafa#2 and not other steroids or bile acids.

In addition, the data we have collected have other compounds that may prove of interest. The metabolites we have discussed in the preceding chapters are those enriched in multiple comparisons, but an additional 125 compounds were enriched only in *him-5*. Although some of these compounds would undoubtedly be detected at increased levels in larger samples of true males, some of these compounds may help to shed light on the nature of the *him-5* mutation and any previously unobserved phenotypes that differ from true males. We have also not examined compounds that are enriched in hermaphrodites or females. In Chapter 1 we mentioned that over 22,000 features are at least 2-fold enriched in hermaphrodites over *him-5*. A similar comparison

between feminized *fem*-2 (KO) and germline-null *glp-4* (KO) animals should reveal all the compounds produced by females that are related to the female germline. In particular, it would be of interest to find endo-metabolites produced by females and hermaphrodites in the absence of males, as they could represent potential male attractants. Cumulatively, investigation of male-enriched compounds and hermaphrodite/female-enriched compounds presents an opportunity to examine what truly defines sex at a molecular level.

References

(1) Brenner, S. The Genetics of Caenorhabditis Elegans. *Genetics* **77**: 71-94. **1974**.

(2) Hodgkin, J. Sex Determination in the Nematode *C. elegans*: Analysis of TRA-3 Suppressors and Characterization of FEM Genes. *Genetics* **114**: 15-52. **1986.**

(3) Ludewig, A. H., Artyukhin, A. B., Aprison, E. Z., Rodrigues, P. R., Pulido, D. C., Burkhardt, R. N., Panda, O., Zhang, Y. K., Gudibanda, P., Ruvinsky, I., Schroeder, F. C. An excreted small molecule promotes *C. elegans* reproductive development and aging. *Nature Chem. Biol.* **15**: 838-845. **2019.**

(4) Helf, M. J., Fox, B. W., Artyukhin, A. B., Zhang, Y. K., Schroeder, F. C. Comparative metabolomics with Metaboseek reveals functinos of a conserved fat metabolism pathway in *C. elegans. Submitted August 2021.*

(5) Fox, B. W., *et al. In preparation.*

APPENDIX A

Supplemental information for Chapter 1

EXPERIMENTAL PROCEDURES

Nematodes and Bacterial Strains

Unless otherwise described, worms were maintained on 10 cm plates of nematode growth media (NGM) seeded with *E. coli* OP50. The following strains were used: wildtype Bristol N2, CB4088 *him-5(e1490)*, DH245 *fem-2(b245)*, JK816 *fem-3(q20)*,SS104 *glp-4(bn2)*, JK569 *mog-3(q74)*, CB3844 *fem-3(e2006)*, CB4037 *glp-1(e2141)*, VC3126 *anmt-2(gk3185)*.

Growth Conditions for Liquid Cultures

Animals were maintained at 15 °C on 10 cm plates until they reached the L4 larval stage then rinsed off the plate with M9 buffer and washed three times with M9 to remove OP50, and incubated overnight in M9 at 25 °C. The cultures were then settled to remove adults and unhatched eggs, yielding L1 larvae. The L1 worms were rinsed three times with M9 and incubated overnight in M9 at 25 °C. The worms were settled a second time to yield synchronized L1 animals which were grown at 25 °C in S-Complete media supplemented with OP50 at a final concentration of 3 L1/µL. When all animals had reached adulthood, cultures were settled to separate adults from any L1 offspring. The adult animals were rinsed three times with M9 and once with water to remove OP50 and salts. The supernatant containing L1 larvae was centrifuged to remove L1 larvae and OP50. All worm pellets and supernatant samples were then frozen and stored at -20 °C until extraction.

Heat-Shock Generation of 50:50 Male:Hermaphrodite Samples

Four N2 animals were placed on 3.5 cm plates seeded with OP50 and grown at 20 °C to the L4 stage. The worms were then transitioned to 30 °C for 5 hours, after which point they were transitioned back to 20 °C and allowed to reproduce. Males resulting from this were then mated with N2 hermaphrodites to yield plates with approximately 50% males.

Growth Conditions for 50:50 Samples and N2 Control Plates

Animals were grown on 10 cm plates at 20 °C for 12 hours at which point adults were rinsed off the plate with M9. L1 worms were washed off of the plates with M9, rinsed with M9, and transferred to new 10 cm plates seeded with OP50. Worms were grown at 20 °C for 72 hours, at which point Day 1-adults were collected by washing the plate with M9. The animals were centrifuged and the supernatant frozen and stored at -80 °C. The worms were rinsed twice with M9 and once with water then frozen and stored at -80 °C.

Growth Conditions for Hand-Picked Males and Hermaphrodites

N2 and *him-5* animals were grown on 10 cm plates seeded with OP50 as described above for 50:50 and N2 plates. After 72 hours 2000 N2 hermaphrodites, 2000 N2 males, and 2000 *him-5* males were picked with a platinum-tipped worm pick, rinsed twice with M9 and once with water, pelleted, frozen, and stored at -80 °C.

Procedure for exo-Metabolome Collection During Adult Aging

N2 and *him-5* animals were grown on 10 cm plates at 20 °C until gravid and rinsed off the plates with M9. The worms were rinsed three times with M9 and incubated in M9 overnight at 20 °C. The cultures were settled to pellet adults and unhatched eggs and the supernatant

containing L1 animals was centrifuged, and the resulting pelleted L1 larvae were rinsed three times with M9 and incubated overnight in M9 at 20 °C. The L1 larvae were then settled to remove breakthrough animals, centrifuged to collect pure L1s larvae, rinsed three times with M9, and then 100,000 larvae were grown at a concentration of 3 L1/µL in S-Complete with OP50 at 20 °C. After 38 hours, animals at the L4 larval stage were settled and 25 mL of culture medium frozen. The worms were then rinsed two times with M9, once with S-Complete, and growth was resumed in S-Complete medium supplemented with concentrated OP50. This process was repeated, and medium was collected after 52 hours (at which time the worms were young adults), 72 hours, 96 hours, 120 hours, and 144 hours, at which point the N2 adults were pelleted, rinsed three times with M9 and once with water, and frozen. The *him-5* cultures were continued for an additional 48 hours with medium collected at 168 hours and 192 hours before the pellet frozen as above.

Procedure for Liquid Growth

N2 and *him-5* L1 animals were synchronized and 100,000 animals grown in S-Complete at 25 °C as described above. After 56 hours the culture was settled, the pellet rinsed three times with M9 and once with water, the supernatant was centrifuged to remove L1s and OP50, and both pellet and supernatant were frozen at -80 °C.

Procedure for ^{13}C-Methionine Feeding

Synchronized *him-5* L1 larvae were prepared as above, and 70,000 animals were grown in S-Complete with one of the following treatments. 1) Animals were grown with no additions. 2) Animals were grown to the L4 stage (38 hours) and supplemented with ^{12}C-methionine at a final concentration of 10 mM. 3) Animals were grown as in (2) but supplemented with ^{13}C-

methionine at a final concentration of 10 mM. 4) Animals were supplemented with ^{12}C-methionine at a final concentration of 10 mM at the start. 5) Animals were grown as in (4) but supplemented with ^{13}C-methionine at a final concentration of 10 mM.

Extraction Procedure

Frozen pellets and culture media were lyophilized, and pellets homogenized with a tissue grinder. Media and pellets were extracted in 30 mL and 13 mL pure methanol, respectively, for 16 hours with shaking. The methanol extracts were separated from insoluble material by centrifugation, dried *in vacuo*, and resuspended in 50 µL of methanol for plated cultures and 150 µL of methanol for liquid cultures.

Lipid Extraction Procedure

Frozen pellets were lyophilized and homogenized as above, then extracted with 12 mL 9:1 ethyl acetate:ethanol for 16 hours with stirring. The organic extracts were treated as the methanol extracts above and resuspended in 150 µL of ethanol.

UHPLC-HRMS

Liquid chromatography was performed on a Thermo Vanquish Horizon UHPLC coupled with a Thermo Q-Exactive HF high-resolution mass spectrometer, a Dionex 3000 UHPLC coupled with a Thermo Q-Exactive high-resolution mass spectrometer, or a Dionex 3000 UHPLC coupled with a Thermo Exploris high-resolution mass spectrometer. UHPLC separation was achieved using a Thermo Hypersil GOLD C18 column (2.1×150 mm 1.9 µm particle size) maintained at 40 °C. Normal chromatographic conditions started with an isocratic gradient of 99% water with 0.1% formic acid and 1% acetonitrile with 0.1% formic acid until 3 minutes followed by a linear ramp to 98% acetonitrile and 2% water at 20 minutes which was held for 5

minutes. Chromatography for lipid extracts started with an isocratic gradient of 95% water with 0.1% ammonium formate and 5% acetonitrile until 3 minutes, followed by a linear ramp to 2% water and 98% acetonitrile, which was held for 5 minutes. Analysis of lipid extracts was performed as above with the addition of a 15 µL/min addition of 800 mM ammonia in methanol.

Metaboseek Analysis

UHPLC-HRMS data were analyzed using Metaboseek software after file conversion to the mzXML format via MSConvert (version 3.0, ProteoWizard)[1,2]. The feature filtration criteria used were a minimum 2-fold increase in strain of interest over control (i.e. *him-5* over N2), a minimum average intensity of 100,000 for the feature in the strain of interest, and a p-value less than 0.05 for samples with three or more replicates and 0.2 for samples with two replicates.

Manual Integration and Normalization

For compounds discussed, the area under the curve (AUC) of the compound of interest was manually obtained through integration in Thermo FreeStyle. Normalization to N2 was achieved by dividing the AUC of the compound of interest by the AUC of ascr#3, as detected in the exo-metabolome in ESI- ionization, which was then multiplied by the average ascr#3 level for corresponding N2 trials, also as detected in the exo-metabolome in ESI- ionization. Below is an example for the normalization of ascr#10 in a *him-5* sample.

AUC of ascr#10 in *him-5* sample: 1.30×10^{8}

AUC of ascr#3 in *him-5* sample: 2.29×10^{8}

AUC of ascr#3 in N2 paired-replicate #1: 3.24×10^{8}

AUC of ascr#3 in N2 paired-replicate #2: 4.11×10^{8}

$$\text{Normalized AUC} = \frac{1.30 \times 10^8}{2.29 \times 10^8} \times \frac{3.24 \times 10^8 + 4.11 \times 10^8}{2} = 0.5677 \times 3.675 \times 10^8 = 1.76 \times 10^8$$

Statistical Analysis

All p-values were calculated by GraphPad Prism via paired *t*-tests with correction using the Holm-Sidak method. All error bars are presented as standard errors of the mean (SEM).

Supplemental Table 1.1. *him-5*-enriched compounds.

If a molecular formula was not able to be determined from the *m/z* and isotope pattern, the *m/z* for the feature is included in the "Molecular Formula" column. If the compound was initially detected as enriched in the endo- or exo-metabolome of *him-5* samples it is denoted as a "P" for the pellet/endo-metabolome and/or "S" for the supernatant/exo-metabolome. If a metabolite was not detected in a sample it is denoted "ND". Fold-change values are derived from Metaboseek analysis and those provided for *fem-3* (OE) are relative to N2 samples.

Molecular Formula	Pellet/ Super-natant	RT (min)	Fold Change	Identity	Up in *fem-3* (OE)?	Up in Small Males	Up in 50:50?
C7H11NO3	S	2.59	3.46		No	ND	ND
C10H13NO3	P	4.52	3.04		No	10.33	No
C9H16N2SO	S	5.27	2.14		3.3	No	ND
C9H19NO3	S	5.34	4.11		No	ND	ND
C20H25N2PO11	P	5.39	2.07	tyglu#501	No	ND	No
C16H23NO7	P	5.66	16.5	No MS2	No	No	ND
C17H25NO9	P	5.66	32.1	No MS2	No	No	No
C11H12N2O2	S	5.7	2.4		No	No	ND
C11H11NO4	S	5.78	2.55		No	ND	ND
C9H11N2PO4	P	5.8	2.05		No	No	No
C18H21N6PO10	P	5.8	2.76		No	ND	ND
C17H21N4PO10	P	5.94	2.16		No	ND	No
C13H12N2O3	P	5.98	2.19		No	ND	No
C12H11N2SO5	S	6.05	2.99		No	No	ND
C23H30N2PO15	P	6.08	2.28		No	ND	ND
639.1559 [-]	P	6.23	6.31		1.86	ND	ND

C11H20O5	S	6.23	3.8		No	ND	ND
C10H17NO6	S	6.25	2.8		No	ND	ND
C13H12N2O3	P	6.26	2.35		No	ND	No
628.1308 [-]	P	6.27	60.6	No MS2	No	ND	ND
C21H27N2PO10	P	6.32	2.22	tyglu#2	No	No	1.21
C26H35N2PO12	P	6.33	289.33	No MS2	No	ND	ND
619.1799 [+]	P	6.43	7.17		No	ND	1.13
C19H27N3PO11	P	6.52	2.16		No	ND	ND
C27H44NPO14	P	6.58	3.81		No	ND	ND
C23H35N4PO16	P	6.58	20.52	No MS2	No	ND	ND
C10H7NO2	P	6.59	4.87		No	No	1.26
C9H14N2O4	S	6.59	2.27		No	ND	ND
C15H32NPO8	S	6.59	4.03		No	ND	ND
C20H36N4O6	S	6.65	2.41		No	ND	ND
C16H24N2O3	S	6.66	20.59		2.59	No	ND
C13H16N2O4	P	6.7	3.07		4.61	3.74	No
C26H53N10PO5	S	6.7	2.05		No	ND	ND
C13H25PO11	P	6.71	25.18	No MS2	No	ND	ND
C19H35PO14	P	6.72	21.94	glas#11	No	ND	ND
C26H28N3PO11	P	6.73	2.31		No	ND	ND
C21H26NPO11	P	6.75	12.33	oglu derivative?	No	8.03	ND
C6H11O6P	S	6.76	3.79		No	ND	ND
C13H25PO9	S	6.76	3.84	phascr#1?	No	No	ND
C14H28N4O13	P	6.8	3.03		No	ND	ND
C18H25N4PO13	P	6.83	6.86	gluric#2-derivative?	No	ND	ND
C27H37N2PO13	P	6.84	29.05	anglas#?	No	ND	ND
C19H34O11	P	6.86	17.11	glas#1	No	No	ND
C20H36O13	P	6.86	19.39	ascr#1-heptulose?	No	No	ND
C18H35N5O7	S	6.87	2.39		No	No	ND
C24H28N3PO11	P	6.89	2.39	tyglu#24	No	ND	No
C11H14N3P	S	6.89	2.24		No	No	ND

C28H30N3PO12	P	6.9	2.24		No	ND	ND
C13H25PO11	P	6.9	39.02	No MS2	No	2.47	ND
C19H35PO14	P	6.91	55.36	glos#11	No	ND	ND
C27H35PO13	P	6.95	2.12		No	ND	ND
C18H25N4PO13	P	7	5.44	gluric#2-derivative?	No	ND	ND
C19H34O11	S	7	3.52	glos#1	No	ND	ND
C12H22N2O2	S	7.02	3.59		No	No	ND
C9H10N2O	S	7.04	2.3		No	ND	ND
C18H27N4PO13	P	7.07	77.82	gluric#2-derivative?	No	No	1.31
C20H28NPO11	P	7.08	54.3	No MS2	No	1.82	ND
C24H37N4PO16	P	7.08	75.18	uglas#15	No	38.87	1.25
C29H37N2PO13	P	7.09	46.07	oglu?	No	ND	ND
C24H36N4O13	P	7.16	23.01	uglas#14	No	6.39	1.48
C21H27N2PO10	P	7.22	46.07	tyglu#2?	No	No	ND
C14H22NPO9	P	7.22	66.04	No MS2	No	ND	ND
C19H28NPO11	P	7.24	8.36		No	ND	No
C24H25N2PO9	P	7.25	2.21		No	ND	ND
C10H19PO7	S	7.28	2.11		No	ND	ND
C28H30N3PO12	P	7.29	2.74	tyglu#6?	No	No	No
C27H44NPO14	P	7.29	146.6	anglas#-derivative?	No	ND	ND
C17H20N2PO11	P	7.3	3.28		No	ND	ND
C19H28NPO10	P	7.31	2.8	Glucoside - tyramine tiglic acid	No	2.11	ND
C20H24N5PO9	P	7.32	23.01	panglu#1	No	ND	ND
613.2157 [+]	P	7.37	33.85	No MS2	No	No	No
C32H46N2PO15	P	7.44	2.34		No	ND	ND
C17H26N2O3	S	7.45	13.07		No	ND	ND
C15H27NO5?	S	7.47	2.75		No	No	ND
C19H21N4PO12	P	7.5	11.1	panglu#3	No	ND	ND
663.4187 [M+H]	P	7.53	43.84	No MS2	No	ND	ND
C28H54N6O7?	S	7.54	2.24		No	ND	ND

C17H29N3O5	S	7.54	2.57		3.61	1.89	ND
C19H30NPO10?	P	7.55	3.78	tyglu#9	2.12	ND	ND
C19H28NPO14	P	7.58	5.67		1.75	ND	ND
743.2785 [+]	P	7.6	12.55	No MS2	No	ND	ND
C19H27N4PO13	P	7.6	15.11		No	ND	ND
C13H24O6	P	7.63	8.31	ascr#1	No	No	2.52
C20H24N5PO10	P	7.63	8.57	panglu#2	No	ND	ND
C31H51N10PO6	S	7.63	3.37		No	ND	ND
C9H17N3O13	P	7.64	5.26		No	No	1.77
C10H19N3O15	P	7.64	6.58		No	No	3.86
C14H13N5O3	P	7.64	7.33		No	No	1.89
C13H17NO4	P+S	7.66	6.06	angl#1	No	ND	ND
C6H8O7	S	7.67	2.36		No	ND	ND
C20H28NPO11	P	7.7	10.57		No	1.22	ND
C26H37N5PO12	P	7.75	40.23	No MS2	No	ND	ND
636.3602 [+]	P	7.81	27.85	No MS2	No	ND	ND
C22H28NPO10	P	7.84	32.83	No MS2	1.61	ND	ND
C25H31N2PO11	P	7.85	2.95		No	ND	ND
C25H38NPO15	P	7.85	22.88	nicotinic glucoside	No	ND	ND
C19H27N3O3	S	7.94	2.01	dmwi#1	490.9	ND	13.71
C23H33NO10	S	7.94	4.19	osas#9	No	ND	ND
755.2768 [+]	P	7.97	7.18		No	ND	ND
C10H19NSO3	S	7.97	2.53		No	No	ND
C28H45N5O7	P	8	44.52	Peptide – LGLVT/VALVT?	No	No	ND
C30H34N4O11	P	8.03	62.53	No MS2	No	ND	ND
C10H19NO3	P	8.04	2.51		No	No	No
C34H49N2PO15	P	8.05	46.64	tyglas#1	No	ND	ND
C13H27N6PO6	P	8.06	2.68		No	ND	ND
C20H32N4PO13	P	8.14	2.91		No	No	1.13
C26H41N4PO16	P	8.14	3.22	uglas#105	No	2396	21.605

C25H38NPO15	P	8.21	5.77		No	ND	ND
C28H32N3PO11	P	8.23	2.6	tyglu#4?	No	No	5.13
C26H40N4O13	P	8.24	2.21	uglas#104	No	302.3	5.15
C26H33N2PO11	P	8.24	2.6	tyglu#8	No	No	45.3
C29H48NPO14	P	8.24	1560.59	No MS2	No	No	ND
C27H33N2PO12	P	8.25	2.22	angl#34?	No	ND	ND
C13H23NO3	S	8.37	2.31		No	ND	ND
C20H31N3O8	S	8.42	2.8		No	ND	ND
C18H29N3O6	S	8.44	2.03		No	ND	ND
482.1238 [-]	S	8.44	2.14		No	ND	ND
C11H18O4	S	8.52	4.85	bemeth#5.1	3.05	ND	ND
C11H18O3	S	8.54	3.22		1.72	No	ND
C11H20O4	S	8.54	5.28	bemeth#3.1	2.39	No	1.76
C11H18O5	S	8.54	7.44	bemeth#6	1.55	No	ND
C22H33N4PO13	P	8.64	2.08		1.45	ND	ND
C11H20O4	S	8.7	2.72	bemeth#3.2	2.37	No	1.47
C28H31N6PO7	P	8.71	6.05		1.2	ND	1.3
C14H19NO4	S	8.78	2.2		No	ND	ND
C20H29NO7	S	8.78	2.5	ascr#801	No	ND	ND
C30H43N2PO12	P	8.8	15.79	No MS2	No	ND	ND
C25H46NPO13	S	8.92	2.62		No	ND	ND
C20H30NPO12	P	9.15	30.48	No MS2	No	No	ND
C26H40NPO15	P	9.15	40.98	anglas#2	No	ND	ND
C21H33N3O8	S	9.16	2.24		No	ND	ND
679.2625 [+]	P	9.18	11.51		No	ND	No
C14H21NO3	S	9.21	2.06		No	ND	ND
679.2625 [+]	P	9.26	13.86		No	ND	ND
C14H21NO4	S	9.27	2.72		1.4	1.32	ND
C11H18N2SO3	S	9.37	2.09		No	No	ND
743.2422 [+]	P	9.65	16.3		No	No	ND
C19H26NPO11	P	9.66	10.62	No MS2	No	No	ND

C27H48NPO13	S	9.76	2.3		No	ND	ND
C11H23NO2	S	9.81	2.857		2.74	No	ND
C11H16O4	S	10.05	3.44		No	No	ND
C25H44O10	S	10.23	2.75		No	ND	ND
C18H29NO3	S	10.27	2.02		No	ND	ND
C25H44O10	S	10.36	2.06		No	ND	ND
681.2781 [+]	P	10.55	3.93		1.31	ND	ND
C11H13PO5	P	10.57	2.18		No	No	No
C13H16PO5	P	10.57	2.64		No	No	1.74
C15H30NPO8	P	10.74	10.39		No	ND	ND
779.3510 [+]	P	10.77	22.12	No MS2	No	ND	ND
C16H30O6	P	10.78	2.47	ascr#16?	No	ND	14.06
C15H30NPO8	P	10.85	11.83	No MS2	No	ND	ND
649.2480 [+]	P	10.88	4.45		No	ND	ND
C43H52N2O10	P	10.89	13.92		No	ND	ND
C17H33NO4	S	10.9	3.1	ω-OH C11 – crotonobetaine?	2.01	ND	ND
C31H54NPO13	P	10.91	5.25		No	ND	ND
741.3670 [2+]	P	10.92	85.95	No MS2	No	ND	ND
C25H40NPO10	P	10.99	24.66	tyglu#54/55	No	ND	ND
C27H44NPO10	P	11.13	16.17		No	ND	ND
C16H20O6	S	11.19	2.13		No	ND	ND
C13H20O5	S	11.21	2.07		No	ND	ND
C36H59N2PO13	P	11.22	17.18	No MS2	No	ND	ND
C28H48O11	S	11.24	2.86		No	ND	ND
C16H20O6	S	11.27	2.24		No	ND	ND
C11H19NO3	P	11.33	8.75		5.49	4.48	ND
C36H59N29O13	P	11.34	10.13		No	ND	ND
C28H48O11	S	11.37	2.94	dasc#13	No	ND	ND
C30H47N2PO12	P	11.46	6.97		No	ND	ND
C38H44N2O8	P	11.49	6.59		No	ND	ND

C17H29PO10	P	11.52	7.24		3.02	ND	ND
C27H43N4PO13	P	11.55	16.92	No MS2	No	ND	ND
C19H32O6	P	11.98	2.28		No	ND	ND
C34H49N2PO11	P	12.01	22.24	Glucoside?	No	ND	ND
C32H50NPO11	P	12.01	15.53	Glucoside?	No	ND	ND
299.1031 [+]	S	12.09	2.17		No	ND	ND
C28H45N4PO13	P	12.10	15.49		No	ND	ND
687.2657 [-]	P	12.13	25.48	No MS2	No	ND	ND
577.1922 [-]	P	12.15	3.82		No	ND	ND
675.2654 [-]	P	12.25	10.20		No	ND	ND
C12H21NO3	P	12.27	5.79		8.22	ND	ND
C27H44NPO10	P	12.28	37.72	No MS2	No	ND	ND
C22H39PO12	P	12.66	2.06		No	ND	ND
C23H43PO11	P	12.67	5.99		No	ND	ND
691.2925 [+]	P	12.71	66.46	No MS2	No	ND	ND
C11H14O3	S	12.74	2.71		No	ND	ND
C18H22N2O8	P	13.13	2.26		No	No	ND
C12H16O3	S	13.42	2.01		No	ND	ND
C24H47N3O2	P	13.57	5.75		No	ND	ND
C23H31N2PO7	P	13.72	3.08		No	ND	ND
C26H37NO7	P	13.89	2.09	icas#18?	No	No	ND
C26H55NO8	P	14.72	3.69		No	ND	ND
C29H62N6O6	P	15.05	4.71		No	ND	ND
C22H26N2O5	P	15.27	2.23		No	No	ND
C25H47NO4	P	15.75	2.25		No	No	ND
C29H58NPO9	S	16.18	4.07		No	ND	ND
C25H49NO4	P	16.59	2.75		No	No	ND
C29H62NPO9	S	16.76	3.29		No	No	ND
C26H51NO4	P	17.05	2.19		No	2.21	ND
C28H55NO4	P	17.94	2.82		No	No	ND
C29H57NO4	P	18.32	2.18		No	No	ND

746.4602	P+S	18.60	4.39	PE/PC	No	ND	ND
C28H54N2O5	S	20.21	2.21		No	ND	ND
544.4351	S	20.54	2.26		No	ND	ND
C24H30O3	P	21.12	2.86		No	ND	ND
C35H61N3O6	S	21.19	2.67		No	ND	ND
C37H67NO4	S	22.72	2.31		No	ND	ND
C36H67NO4	S	22.89	2.00		No	ND	ND
C33H66N2O9	P	23.60	2.03		No	ND	ND
763.5134 [+]	P	23.68	674.84	No MS2	No	No	ND
C37H72O6	S	24.66	2.13		No	No	ND
779.6343 [+]	S	25.31	2.11		No	No	ND

Supplemental Table 1.2. *fem-3* (OE)-enriched compounds.

If a molecular formula was not able to be determined from the *m/z* and isotope pattern, the *m/z* for the feature is included in the "Molecular Formula" column. If the compound was initially detected as enriched in the endo- or exo-metabolome of *fem-3* (OE) samples it is denoted as a "P" for the pellet/endo-metabolome and/or "S" for the supernatant/exo-metabolome. If a metabolite was not detected in a sample, it is denoted "ND". Metabolites not enriched the metabolome of young *him-5* cultures that are enriched in the metabolome of older *him-5* cultures are denoted with a "*".

Molecular Formula	Pellet /SN	RT (min)	Identity	Fold over N2	Fold over *fem-2* (KO)	Fold over *glp-4* (KO)	Up in *him-5*	Up in Small Males	Up in 50:50
C10H12N5PO7	P	2.55		2.64	3.18	2.07	No	ND	ND
C11H22N2O4	P	4.68		15.18	42.6	46.22	ND	ND	ND
C15H26O11	P	4.79		2.34	8558	421	5.41*	26.29	ND
C15H26O11	P	5.19		2.75	19746	2022	52.82*	61.64	ND

479.1735 [+]	P	5.24		1.1	5250	2578	2.93*	12.47	ND
C10H18N2O4	S	5.79		3.21	46.37	124.4	1.64	ND	No
C24H38O9	P	5.81		9.02	15.44	21.67	7.32*	ND	No
469.0656 [-]	P	5.97		0.79	3.53	2.1	13.82*	ND	ND
C15H24NO4	S	6.61		3.26	39.7	48.49	13.11*	No	ND
C13H16N2O4	P+S	6.72		5.07	51.96	75.31	2.97	52.88	No
C13H17N5SO4	P	6.77	amta#1	19.22	132.9	211.2	1.75	2.37	ND
C8H15NO3	S	6.91		2.4	3.9	18.9	No	No	No
C16H30N6O6	S	7.18		4.58	2058	4684	2.1	ND	4.89
C21H36NPO17	P	7.30		5.94	38.02	51	9.01*	ND	ND
C20H24N5PO9	P	7.34	panglu#1	3.75	5.22	2.95	5.56	ND	ND
C13H17N5SO4	P	7.39	amta#2	16.31	95.33	182	1.75	2.37	ND
C19H21N4PO12	P	7.47	panglu#3	6.1	22.89	3.59	3.44	ND	ND
C14H27N5O6	S	7.49		2.44	92.57	4.38	7.18*	ND	ND
C14H28N6O5	P	7.56		8.85	252.3	571.9	No	1.79	ND
C24H21N3PO12	S	7.57		1.13	2.09	2.74	6.22*	ND	ND
C19H28NPO14	P	7.58	tyglu#9	2.12	4.89	2.71	3.62	No	ND
C20H24N5PO10	P	7.61	panglu#2	2.33	5.41	4.85	5.67	No	ND
C16H30N6O7	S	7.65		4.53	1260	370	139.6*	20.99	1.74
C19H23N3O4	S	7.78		5.41	5415	4772	1.59	39.55	3.31
C13H29PO12	P	7.79		2.58	4.6	4.49	No	ND	No
C14H27N5O6	S	7.82		1.87	92.57	39.49	2.05	ND	ND
C19H27N3O3	S	7.87	dmwi#1	3.74	4526	380	1.33	1.97	15.25
C15H29N5O5	S	8.07		3.85	6.45	48.57	ND	ND	No
C8H16N8O2	S	8.09		2.48	19.59	19.41	ND	ND	ND
C16H22NO17	P	8.16		2.5	4.67	8.74	34.91*	ND	ND
C12H20N2O4	S	8.20		2.09	182.53	2797	38.49*	ND	No
C11H20O4	S	8.29		9.02	12.93	48.59	2.91	ND	ND
C11H20O4	S	8.35		1.57	12.18	59.97	ND	ND	ND
C14H27N5O6	S	8.39		7.15	248.3	48.57	17.03*	1.82	1.72
C10H18NO4	S	8.45		17.87	680.9	3388	50.27*	ND	No

C14H25NO5	S	8.50	alanine bemeth	15.45	134.99	870	2.53	ND	No
C17H20N2O3	S	8.53		13.39	1129	818.2	42.91*	ND	ND
C11H18O4	S	8.54	bemeth#5.1	2.62	9.19	42.15	7.53	ND	ND
C11H18O3	S	8.55		1.96	8.25	10.25	3.25	ND	ND
304.0169 [-]	S	8.56		5.41	578.3	2208	8.3	ND	ND
C11H20O4	S	8.57	bemeth#3.1	2.39	174.5	513.1	7.53	2.01	1.76
C14H25NO5	S	8.69	alanine bemeth	15.45	161.7	566.9	1.84	6.48	1.9
C11H20O4	S	8.72	bemeth#3.2	2.37	11.83	131.5	5.45	4.01	1.47
498.1528 [+]	P	8.72		1.35	2.21	2.12	32.83	14.76	No
C28H31N6PO7	P	8.72		0.68	2.24	2.12	6.05	ND	No
484.1005 [+]	P	8.91		2.08	3.46	5.36	13.56*	ND	ND
482.0848 [+]	P	8.96		1.22	2.14	2.37	56.78*	ND	ND
C11H20O4	S	8.99		4.09	37.08	42.78	4.1	ND	ND
C11H20O4	S	9.06		4.94	10.28	34.38	4.28	ND	ND
C14H25NO4	S	9.13		4.72	12.59	92.82	3.48	ND	1.39
C7H17N7	S	9.33		0.83	35.41	44.09	1.91	No	3.89
C11H21NO4	S	9.48		19.68	48.17	5792	16.34*	ND	No
C10H24N2O3	S	9.52		6.3	45.14	22.59	2.11	ND	ND
C11H23NO2	S	9.74		4.39	16.73	11.12	3.18	No	No
574.2268 [+]	P	9.89		2.04	11258	331.2	16.18	ND	ND
C21H36NPO17	P	9.98		508.3	10788	5299	229.2*	ND	ND
C31H41N2PO12	P	10.02		4.69	55.86	44.83	52.84*	ND	ND
501.1267 [+]	P	10.02		3.44	20.67	22.762	No	ND	ND
C22H33N4PO13	P	10.06		3.81	23668	11630	4.68	ND	ND
656.2957 [+]	P	10.10		3.95	2.64	2.69	No	ND	ND
C22H27N9O11	P	10.14		2.25	2085	486.42	651.8*	ND	ND
C15H22NO4	P	10.28	nacq#1	4.17	500	260.5	1.37	11.18	3.02
C10H17NO3	S	10.29		9.69	693.1	4008	13.60	3.42	No
466.0899 [+]	P	10.39		2.19	3.98	5.9	23.16*	ND	No

C11H26N2O3	S	10.40		11.66	193.7	120.22	ND	No	ND
498.1159 [+]	P	10.43		1.26	3.07	3.7	173.9*	No	ND
C11H20O4	S	10.66	bemeth#33	1.74	1891	11.2	No	No	No
C11H20O4	S	10.75	bemeth#34	3.09	5.22	4.39	No	No	No
466.0892 [+]	P	10.92		1	2.57	5.9	5.69*	ND	ND
C16H27NP8O15	P	10.92		1	2.69	9.27	14.79*	ND	ND
C20H17NO6	P	10.92		1.11	2.21	6.67	20.07*	ND	ND
C15H25N2O4	P	11.03		4.31	8347	91.56	311.4*	ND	No
514.1470 [+]	P	11.20		4.3	9028	289.9	15.21*	ND	ND
C11H19NO3	P	11.23	glycine lipid conjugate	21.47	34.88	43.37	8.07*	4.48	No
C14H25NO5	S	11.24	bemeth#71	6.61	3162	1089	2.5	208.0	2.83
C11H19NO3	P	11.34		9.47	11.23	7.59	8.75	ND	No
C14H25NO5	S	11.46	bemeth#72	1.82	16.26	28.23	1421*	1.53	ND
447.1386 [+]	P	11.53		5939	6672	2697	ND	ND	ND
C13H23NO4	S	11.68		4.45	87503	683.3	2.39	ND	ND
C17H29PO10	P	11.77	phosphoglucose conjugate	37.35	335.9	312.6	6.48	ND	4.31
516.1622 [+]	P	11.90		18.19	6945	3417	No	ND	ND
530.1785 [+]	P	12.06		10.29	58.81	15.79	67.71*	ND	ND
C14H23NO4	S	12.08	bemeth#81	20.34	9052	7344	2.72	1.44	1.77
C11H18O3	S	12.26	bemeth	2.62	24.32	65.54	15.76*	ND	ND
C12H21NO3	P	12.35		12.61	14.89	12.73	5.79	ND	ND
C14H25NO4	S	12.37	bemeth#61	4	9413	1941	2.67*	7.01	1.54
530.1781 [+]	P	12.52		143.4	1368	881.5	24.88*	ND	ND
C14H25NO4	S	12.57	bemeth	1.32	1075	322.3	92.76*	ND	No
C11H20O3	S	12.62	bemeth#22	1.26	4.05	42.38	ND	ND	ND
C11H20O3	S	12.77	bemeth#23	1.3	27.16	30.17	13.99*	No	No
C14H23NO3	S	13.15		3.11	11.52	11.22	27.07*	ND	ND
C11H22O3	S	13.26		1.91	2.15	2.3	ND	ND	ND

C11H20O3	S	13.83	bemeth#24	3.2	22.32	27.83	ND	ND	ND
C18H41N9O9	P	15.20		2.67	5.18	2.1	No	No	No
570.3547 [+]	P	15.32		1	2.18	6.07	No	No	No
570.3547 [+]	P	15.53		2.73	2.55	3.96	No	No	No
C18H43N9O9	P	15.82		2.45	8.9	3.03	ND	ND	No
556.3394 [+]	P	16.31		3.66	12.2	3.17	No	No	No
650.4020 [+]	P	16.72		4.39	4.71	3.29	ND	No	ND
706.4642 [+]	P	17.86		2.83	2.47	3.21	No	ND	ND
674.4380 [+]	P	17.87		2.54	2.01	1.57	No	ND	ND

Supplemental Table 1.3. Hand-picked males over hand-picked hermaphrodites.

If a molecular formula was not able to be determined from the *m/z* and isotope pattern, the *m/z* for the feature is included in the "Molecular Formula" column. If a metabolite was not detected in a sample, it is denoted "ND". Fold-change values are derived from Metaboseek analysis and those provided for *fem-3* (OE) are relative to N2 samples.

Molecular Formula	RT (min)	Fold Increase	Identity	Up in him-5?	Up in *fem-3* (OE)?	Up in 50:50?
C8H13NO4	5.77	2.04		ND	No	ND
C7H13NO	6.5	48.8		No	No	ND
C14H18NPO8	6.73	5.59	iglu#2?	ND	ND	ND
C14H17NO5	7.29	3.84	iglu#1	No	No	No
C8H14N5	7.62	9.89		No	No	No
C25H42NPO7	13.63	2.35	LPE 20:5?	No	No	No
C15H29NO2	14.04	5.29	C14 lipid-ethanolamine?	No	No	1.95
C23H44NPO7	14.54	2.27	LPE 18:2?	No	No	No
399.0445 [+]	14.63	3.8		ND	No	ND
C23H46NPO7	16.87	3.57	LPE 18:1?	No	ND	ND
C18H38N2O2	17.67	28.68		No	No	No
784.5828 [+]	25.97	6.71		ND	No	No

Supplemental References

(1) Chambers, M. C. *et al.* A cross-platform toolkit for mass spectrometry and proteomics. *Nat. Biotech.* **30**: 918-920. **2012**.

(2) Helf, M. J., Fox, B. W., Artyukhin, A. B., Zhang, Y. K., Schroeder, F. C. Comparative metabolomics with Metaboseek reveals functions of a conserved fat metabolism pathway in *C. elegans. Submitted August 2021*.

APPENDIX B

Supplemental Information for Chapter 2

Experimental

General Procedures

Unless stated otherwise, all reactions were performed under argon in flame-dried glassware. All commercially available reagents were used as is unless otherwise stated. All solvents were dried over activated 3Å sieves for a minimum of 24 hours unless used in reactions where aqueous reagents were involved. Thin-layer chromatography (TLC) was performed with J.T. Baker Silica Gell IB2-F plastic-backed plates. Reverse-phase column chromatography was performed using Teledyne ISCO CombiFlash Rf and Rf+ systems with Teledyne ISCO RediSep Rf and Rf Gold silica columns. Nuclear Magnetic Resonance (NMR) spectra were recorded on a Varian INOVA 600 (600 MHz) or Bruker AV 500 (500 MHz) in the Cornell University NMR Facility and a Bruker AVANCE III HD 800 (800 MHz) in the State University of New York College of Environmental Science and Forestry (SUNY ESF). ^{1}H NMR chemical shifts are reported in ppm (δ) relative to the residual solvent peaks (7.26 ppm for $CDCl_3$ and 3.31 ppm for CD_3OD) and ^{13}C NMR shifts relative to their respective residual solvent peaks (77.16 for $CDCl_3$ and 49.00 for CD_3OD).

Synthetic Procedures

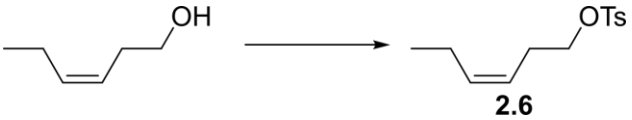

2.6

(*Z*)-Hex-3-en-1-yl *p*-toluene sulfonate (2.6). Following previously reported syntheses[1,2], pyridine (1.8 equiv, 1.23 mL) was added to a stirring solution of *cis*-3-hexen-1-ol (**7**) (1 equiv., 1 mL) in DCM (30mL) under an argon atmosphere at 0 °C. 4-Toluenesulfonyl chloride (1.2 equiv., 1.94 g) was added in three portions and the reaction stirred to 40°C. After 80 min the solution was concentrated under reduced pressure. The resulting residue was purified by flash chromatography on silica gel. Elution with DCM gave the resulting tosylate **2.6** (1.88 g, 87%) as a colorless liquid.

^{1}H NMR (C_6D_6, 600 MHz) δ (ppm) 7.74 (d, *J* = 8.3 Hz, 2H), 6.75 (d, *J* =8.3 Hz, 2H), 5.33 (m, 1H), 5.03 (m, 1H), 3.81 (t, *J* = 6.8 Hz, 2H), 2.08 (qd, *J* = 7.0, 1.6 Hz, 2H), 1.88 (s, 3H), 1.76 (td, *J* = 7.5, 1.6 Hz, 2H), 0.77 (t, *J* = 7.5 Hz, 3H).

^{13}C NMR (C_6D_6, 125 MHz) δ (ppm) 144.5, 135.2, 134.1, 129.9, 128.1, 122.8, 69.8, 27.1, 21.2, 20.7, 14.2.

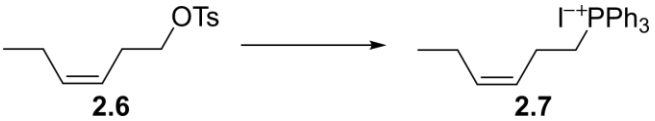

2.6 **2.7**

(*Z*)-Hex-3-en-1-yl triphenylphosphonium iodide (2.7). Adapting previously reported syntheses[1,2], sodium iodide (1.2 equiv., 1.53 g) and triphenylphosphine (1.2 equiv., 2.68 g) were added to a stirring solution of (*Z*)-hex-3-en-1-y/l *p*-toluene sulfonate (**2.6**) (1 equiv., 2.15 g) in MeCN (40 mL). The resulting suspension was stirred to reflux under ambient atmosphere. After 17 hours the reaction was cooled to RT, filtered through a pad of celite, and rinsed with DCM (150 mL) and the filtrate concentrated under reduced pressure. The resulting pale residue was purified by flash chromatography on silica gel. Elution with a gradient of 0-40% DCM/MeOH gave the resulting phosphonium iodide **2.7** (3.23 g, 81%) as a white solid**.**

^{1}H NMR (CD_3OD, 600 MHz) δ (ppm) 7.90 (td, *J* = 7.4, 1.8 Hz, 3H), 7.83 (m, 6H), 7.77 (m, 6H), 5.51 – 5.46 (m, 1H), 5.45 – 5.39 (m, 1H), 3.51 – 3.40 (m, 2H), 2.49 – 2.35 (m, 2H), 1.91 (pd, *J* = 7.5, 1.4 Hz, 2H), 0.91 (t, *J* = 7.6 Hz, 3H).

^{13}C NMR (CD_3OD, 125 MHz) δ (ppm) 136.3 (d, *J* = 2 Hz), 135.5 (d, *J* = 1.5 Hz), 134.9 (d, *J* = 10 Hz), 131.6 (d, *J* = 12 Hz), 126.5 (d, *J* = 16 Hz), 119.8 (d, *J* = 86 Hz), 22.9 (d, *J* = 49 Hz), 21.5, 21.2 (d, *J* = 3.4 Hz), 14.3.

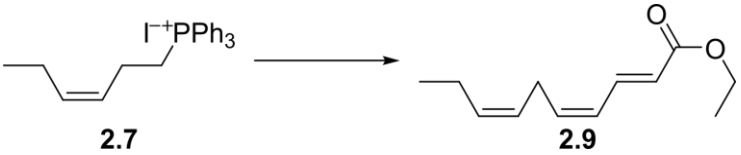

2.7 **2.9**

Ethyl (2*E,4Z,7Z)*-deca-2,4,7-trienoate (2.9). *n*-Butyl lithium (1.6 equiv., 0.59 mL) was added dropwise to a stirring solution of (*Z)*-hex-3-en-1-yl triphenylphosphonium iodide (**2.7**) (2 equiv., 0.87 g) in freshly distilled THF (50mL) at -78 °C and stirred 10 min under an argon atmosphere. Ethyl-4-oxo-*trans*-2-butenoate (**2.8**) (1 equiv., 0.11 mL) was added dropwise to the stirring reaction and consequently warmed to ambient temperature. After 25 minutes the reaction was quenched with saturated aqueous NH_4Cl (100mL) and extracted with DCM (3×50 mL). The resulting organics were combined, dried over $MgSO_4$, filtered, and concentrated under reduced pressure. The resulting liquid was purified by flash chromatography on silica gel. Elution with DCM gave the resulting unsaturated ester **2.9** (476 mg, 72%) as an orange liquid.

^{1}H NMR (C_6D_6, 600 MHz) δ (ppm) 7.74 (ddd, *J* = 15.2, 11.7, 1.2 Hz, 1H), 5.93-5.88 (m, 1H), 5.86 (d, *J* = 15.2 Hz, 1H), 5.56 – 5.51 (m, 1H), 5.34 – 5.27 (m, 1H), 5.18-5.13 (m, 1H), 4.03 (q, *J* = 7.1 Hz, 2H), 2.76 (t, *J* = 7.7 Hz, 2H), 1.92 – 1.83 (m, 2H), 1.02 (t, 7.3 Hz, 3H), 0.83 (td, *J* = 7.5 Hz, 3H).

^{13}C NMR (C_6D_6, 125 MHz) δ (ppm) 166.5, 139.0, 138.8, 133.1, 126.8, 125.8, 122.4, 60.1, 26.5, 20.8, 14.3, 14.2.

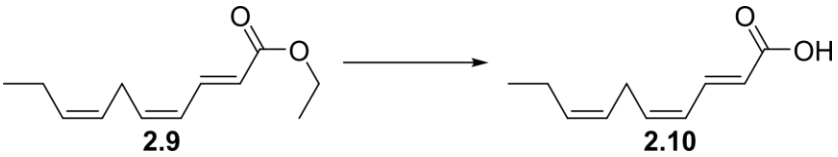

2.9 **2.10**

/(2*E,4Z,7Z)*-Deca-2,4,7-trienoic acid (2.10). Ethyl (2*E*,4*Z*,7*Z*)-deca-2,4,7-trienoate (**2.9**) (192 mg) was dissolved in 1,4-dioxane (2 mL) under an argon atmosphere. Concentrated aqueous HCl (1 mL) was added to the solution and the resulting solution was stirred and heated to 50 °C. After 8 hours the reaction was poured into a saturated NaCl solution (10 mL) and extracted with DCM (3×0 mL). The combined organics were dried over $MgSO_4$, filtered, and concentrated under reduced pressure. The resulting oil was purified by flash chromatography on silica gel.

Elution with a gradient of 0-40% DCM/MeOH returned unreacted ester (117 mg, 61% recovery) and a mixture of double bond isomers of deca-2,4,7-trienoic acid (58 mg, 35%) with the desired (2*E*,*4Z*,*7Z)*-isomer (**2.10**) representing more than 70%. This mixture of isomers was used in the next step.

^{1}H NMR (500 MHz, C_6D_6) δ (ppm) 7.87 (ddd, *J* = 15.2, 11.7, 1.1 Hz, 1H), 5.87 (d, *J* = 15.1 Hz, 1H), 5.84 – 5.77 (m, 1H), 5.54 – 5.45 (m, 1H), 5.36 – 5.29 (m, 1H), 5.18-5.12 (m, 1H), 2.75 – 2.66 (m, 2H), 1.91 – 1.77 (m, 2H), 0.83 (t, *J* = 7.5 Hz, 3H).

^{13}C NMR (C_6D_6, 125 MHz) δ (ppm) 171.4, 140.9, 139.8, 133.1, 126.6, 125.6, 121.6, 26.5, 20.7, 14.2.

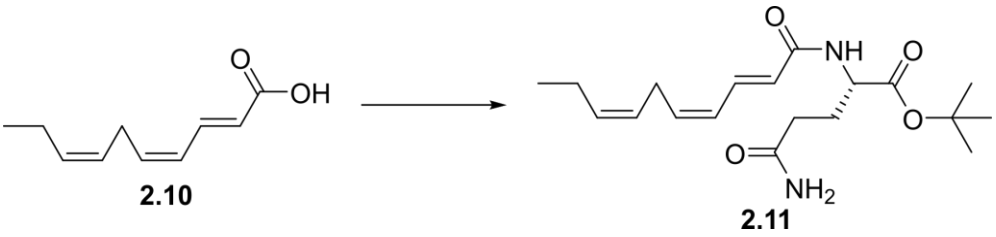

nacq#1-*tert*-butyl ester (2.11). (2*E*,*4Z*,*7Z)*-deca-2,4,7-trienoic acid (**2.10**) (containing ~30% of double bond isomers, 40 mg) was dissolved in dry DCM (2 mL) and stirred under argon atmosphere. 1-Hydroxybenzatriazole hydrate (1.2 equiv., 50 mg) was added to the stirring solution, followed by L-glutamine-*tert*-butyl ester hydrochloride (1.1 equiv., 66 mg), *N*,*N*'-dicyclohexylcarbodiimide (1.1 equiv., 56 mg), and triethylamine (1 equiv., 0.034 mL). The reaction was stirred at ambient temperature for one and a half hours and concentrated under reduced pressure. The resulting white solid was purified by flash chromatography on silica gel. Elution with a gradient of 0-40% DCM/MeOH gave a mixture of nacq#1-*tert*-butyl ester (**2.11**) and double bond isomers (43 mg, 50%), with the desired product predominating. The mixture of isomers was used without further purification.

^{1}H NMR (CD_3OD, 500 MHz) δ (ppm) 7.58 (ddd, *J* = 1.52, 11.6, 1.0 Hz, 1H), 6.16 (t, *J* = 11.5 Hz, 1H), 6.08 (d, *J* = 15.2 Hz, 1H), 5.81-5.74 (m, 1H), 5.48-5.42 (m, 1H), 5.36-5.29 (m, 1H), 4.37 (dd, J = 9.0, 5.2 Hz, 1H), 3.07 (t, *J* = 7.5 Hz, 1H), 2.34-2.28 (m, 2H), 2.19-2.05 (m, 3H), 1.99-1.90 (m, 1H), 1.48 (s, 9H), 0.98 (t, *J* = 7.6 Hz, 3H).

^{13}C NMR (C_6D_6, 125 MHz) δ (ppm) 177.5, 172.5, 168.9, 139.2, 137.0, 133.9, 127.5, 126.8, 124.8, 83.0, 54.3, 34.8, 32.6, 28.2, 26.7, 21.5, 14.6.

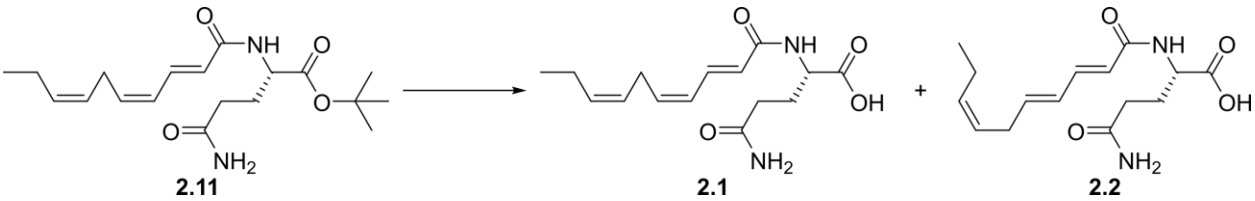

nacq#1 (2.1) and nacq#2 (2.2). Trifluoroacetic acid (80 equiv., 0.61 mL) was added to a solution of nacq#1-*tert*-butyl ester (**2.11**) (1 equiv., 15 mg) in DCM (0.6 mL) at ambient temperature. After 40 min the reaction was quenched with 1 M phosphate buffer (pH 6) and brought up to a pH of 5. The solution was frozen, lyophilized, resuspended in DCM/MeOH (1:1, 10 mL), filtered, and concentrated under reduced pressure. The resulting white solid was purified by flash chromatography on silica gel. Elution with a gradient of 0-100% DCM/MeOH yielded a mixture of nacq#1 (**2.1**) and nacq#2 (**2.2**) (12 mg, 80%) which was further purified by preparative HPLC on a C8 column with a gradient of 0-100% H_2O/MeCN (0.1% acetic acid) to yield pure nacq#1 (3.1 mg, 21%).

NMR Spectroscopic data for nacq#1 (2.1). ^{1}H (800 MHz), HSQC, and HMBC NMR spectroscopic data were acquired in methanol-d_4. Chemical shifts were referenced to ($CD_2\underline{H}OD$) = 3.31 ppm and ($\underline{C}D_2HOD$) = 49.00 ppm.

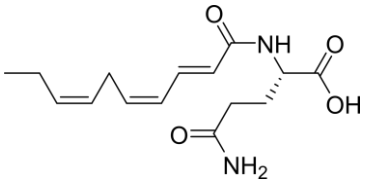

Position	^{13}C [ppm]	^{1}H [ppm]	J_{HH} couplings [Hz]	HMBC correlations
1	167.9	---		
2	125.6	6.10	$J_{2,3}$ = 15.3	C-1, C-4
3	136.0	7.54	$J_{3,4}$ = 11.3	C-1, C-2, C-4, C-5
4	127.4	6.15	$J_{4.5}$ = 11.3	C-2, C-3, C-6
5	138.3	5.74	$J_{5,6}$ = 7.3	C-3, C-6, C-7
6	26.9	3.06	$J_{6,7}$ = 7.3	C-4, C-5, C-7, C-8
7	126.6	5.33	$J_{7,8}$ = 11.4 $J_{7,9}$ = 2.5	C-9
8	133.6	5.44	$J_{8,9}$ = 7.5	C-6
9	21.2	2.12	$J_{9,10}$ = 7.8	C-7, C-8, C-10
10	14.3	0.98		C-8, C-9
1’	177.7	---		

2’	55.6	4.39	$J_{2',3'a}$ = 8.0 $J_{2',3'b}$ = 4.9	C-1, C-1’, C-3’, C-4’
3’	30.3	1.99 (a) 2.17 (b)		C-1’, C-2’, C-4’, C-5’
4’	33.0	2.24 (a) 2.28 (b)		C-2’, C-3’, C-5’
5’	178.5	---		

NMR Spectroscopic data for nacq#2 (2.2). ^{1}H (800 MHz), HSQC, and HMBC NMR spectroscopic data were acquired in methanol-*d*$_4$. Chemical shifts were referenced to ($CD_2\underline{H}OD$) = 3.31 ppm and ($\underline{C}D_2HOD$) = 49.00 ppm.

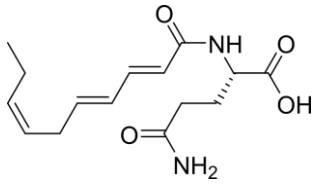

Position	^{13}C [ppm]	^{1}H [ppm]	J_{HH} couplings [Hz]	HMBC correlations
1	168.2	---		
2	123.5	6.01	$J_{2,3}$ = 15.1	C-1, C-4
3	141.6	7.12	$J_{3,4}$ = 11.0	C-1, C-4, C-5
4	129.5	6.23	$J_{4.5}$ = 15.6	C-6
5	141.4	6.07	$J_{5,6}$ = 6.3	C-3, C-6, C-7
6	31.2	2.92	$J_{6,8}$ = 3.1	C-4, C-5, C-7, C-8
7	125.9	5.37	$J_{7,8}$ = 10.8	
8	134.1	5.50	$J_{8,9}$ = 7.4	
9	21.2	2.08	$J_{9,10}$ = 7.4	C-7, C-8, C-10
10	14.3	0.98		C-8, C-9
1’	177.7	---		
2’	55.5	4.38	$J_{2',3'a}$ = 7.8 $J_{2',3'b}$ = 4.8	C-1, C-1’, C-3’, C-4’
3’	30.3	1.99 (a) 2.15 (b)	$J_{3b',4'}$ = 8.1	C-4’
4’	33.0	2.26		C-3’
5’		---		

MS and MS2 Spectra, nacq#1

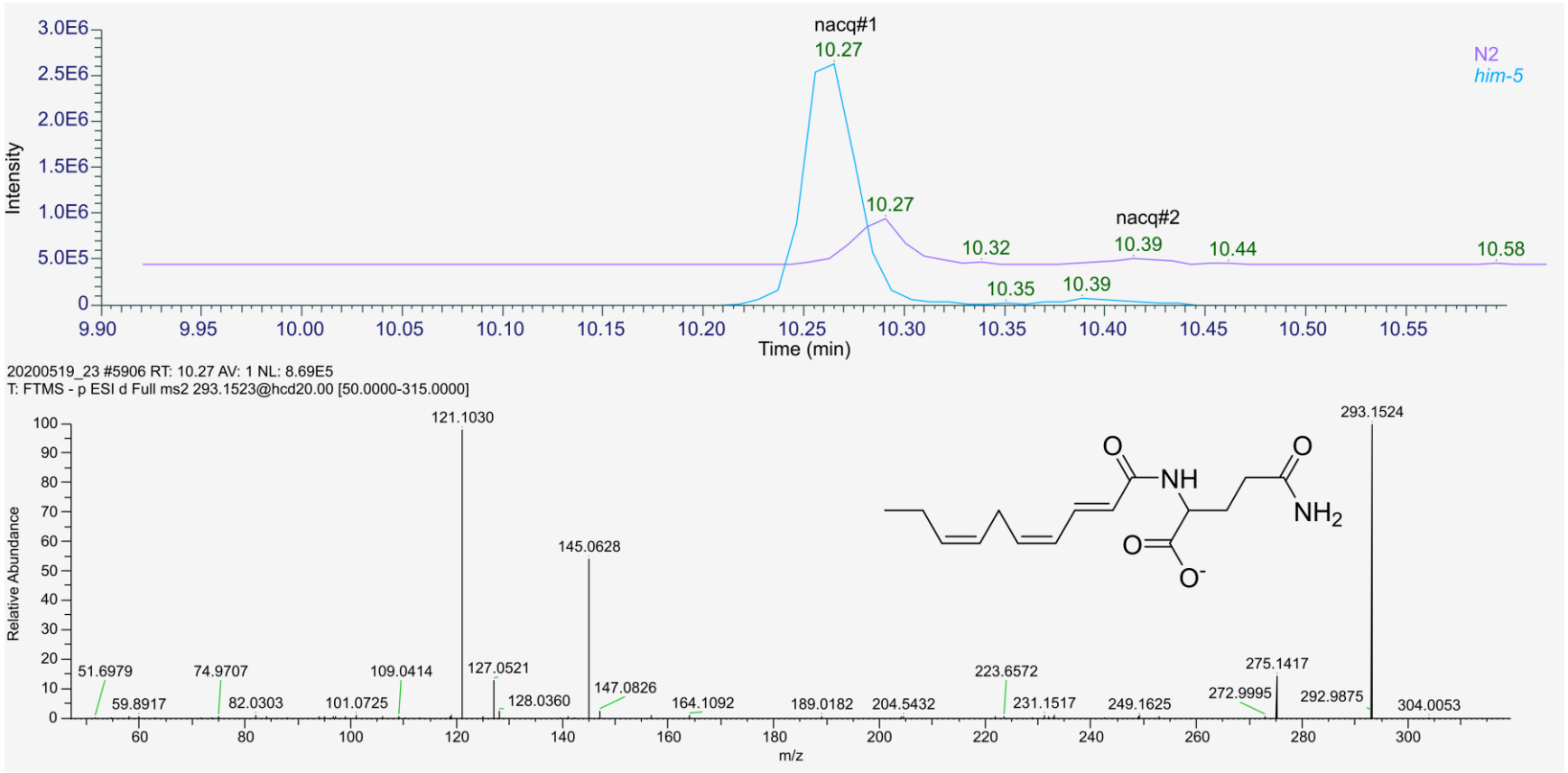

Supplemental Figure 2.1. MS and MS2 spectra for nacq#1. EIC of *m/z* 293.1507 in N2 and *him-5* exo-metabolome samples shows peaks for nacq#1 and nacq#2 and MS2 spectra for nacq#1 acquired from a *fem-3* (OE) exo-metabolome sample.

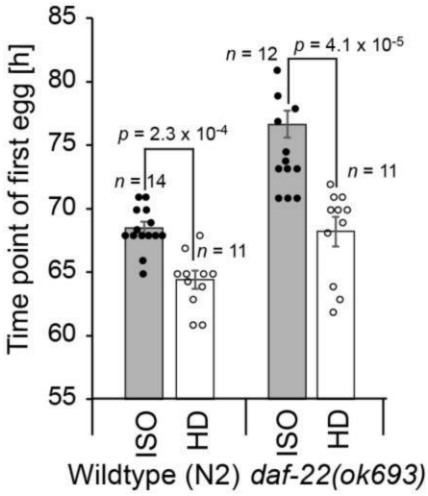

Supp Fig. 2.2. High Population density accelerates development more strongly in *daf-22(ok693)* mutants than in wildtype (N2) worms. Onset of egg laying in isolated (ISO) and high-density (HD; 50-70 animals per plate) in wildtype (N2) and *daf-22(ok693)* mutant hermaphrodites. Error bars represent mean ± s.e.m. and statistics were performed using two-tailed *t*-tests.

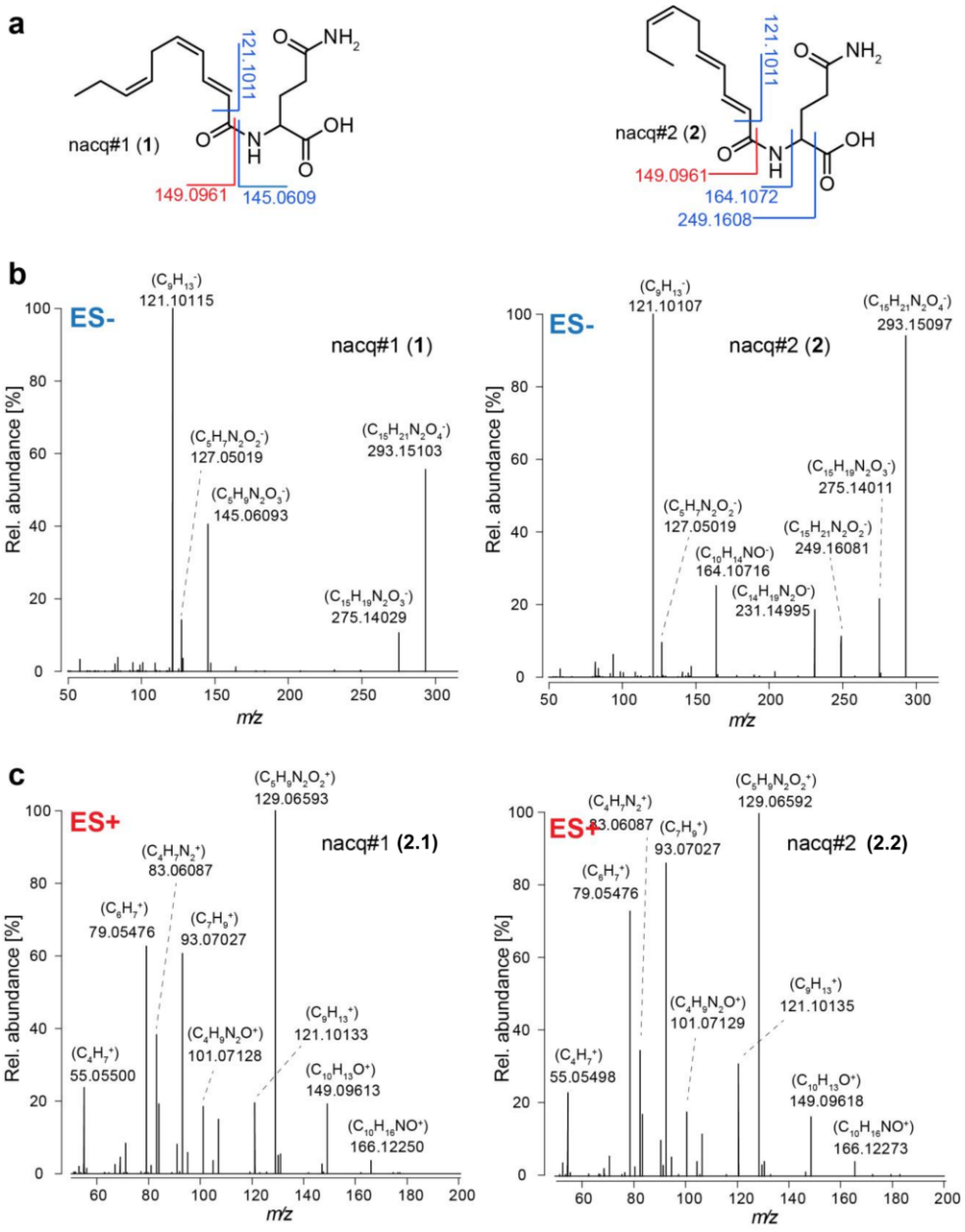

Supplemental Figure 2.3. MS fragmentation of nacq#1 and nacq#2. a. Structures and fragmentation of nacq#1 and nacq#2. **b,c.** MS/MS spectra of nacq#1 and nacq#2 in negative (ES-) and positive (ES+) electrospray ionization mode.

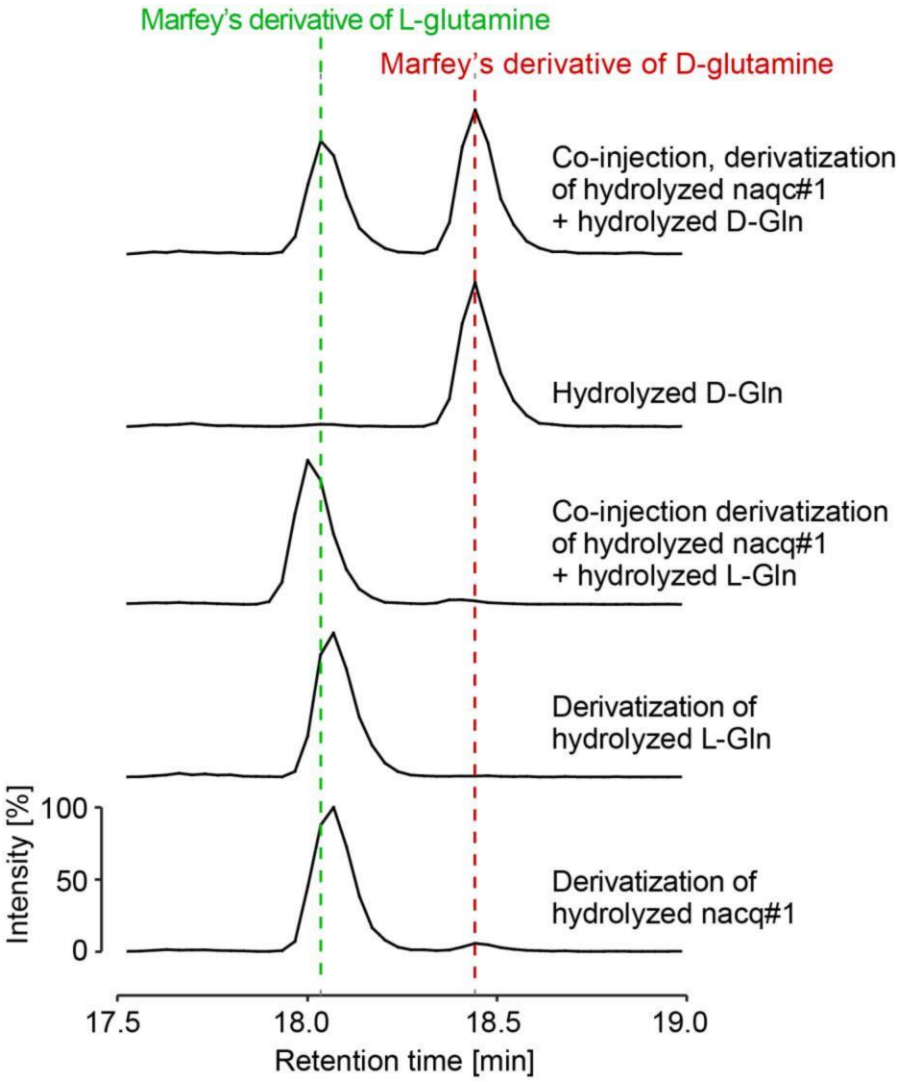

Supplemental Figure 2.4. Determination of the absolute configuration of nacq#1. The absolute configuration of the glutamine moiety in nacq#1 was determined using Marfey's reagent, followed by HPLC-MS analysis. Shown are chromatographic traces for the molecular ion of the diastereomers of the derivatized glutamine. This experiment was performed once.

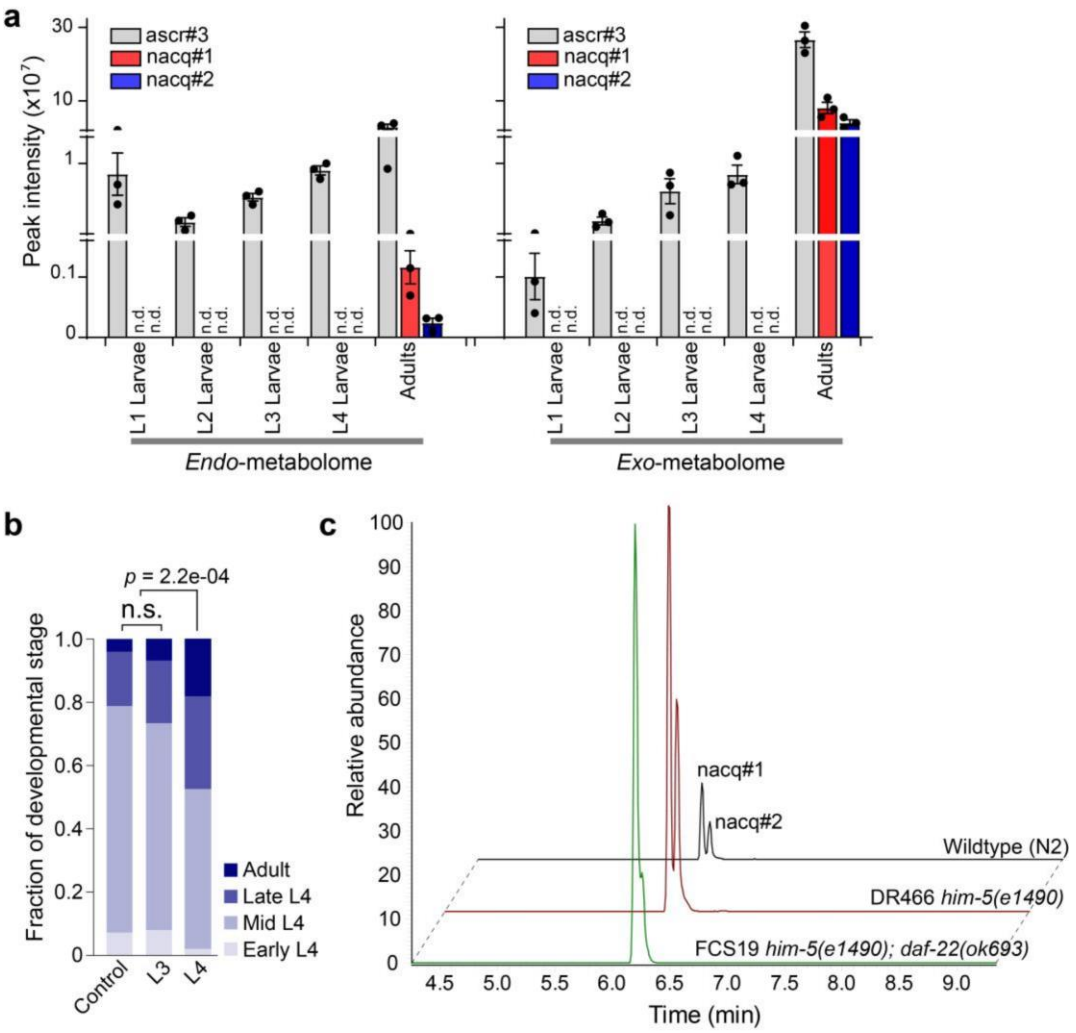

Supplemental Figure 2.5. Timing of excretion of the acceleration factor and nacq#1. a. HPLC-MS-based quantification of ascr#3, nacq#1, and nacq#2 in the exo- and endo-metabolomes of synchronized worms harvested at different developmental stages (*n*=3 biologically independent samples per life stage). Error bars represent mean ± s.e.m. **b.** Plates conditioned by L4 larvae (L4 to young adult), but not by L3 larvae (L3 to L4), accelerated development of wildtype (N2) hermaphrodites (*n*=5 biologically independent samples, where each replicate was one plate with ~25 animals). Statistics were performed using the χ^2 test. **c.** HPLC-MS ion chromatograms for nacq#1 and nacq#2 in the exo-metabolome samples of liquid cultures of wildtype (N2), *him-5(e1490)*, and *him-5(e1490); daf-22(ok693)* worms. This experiment was performed once.

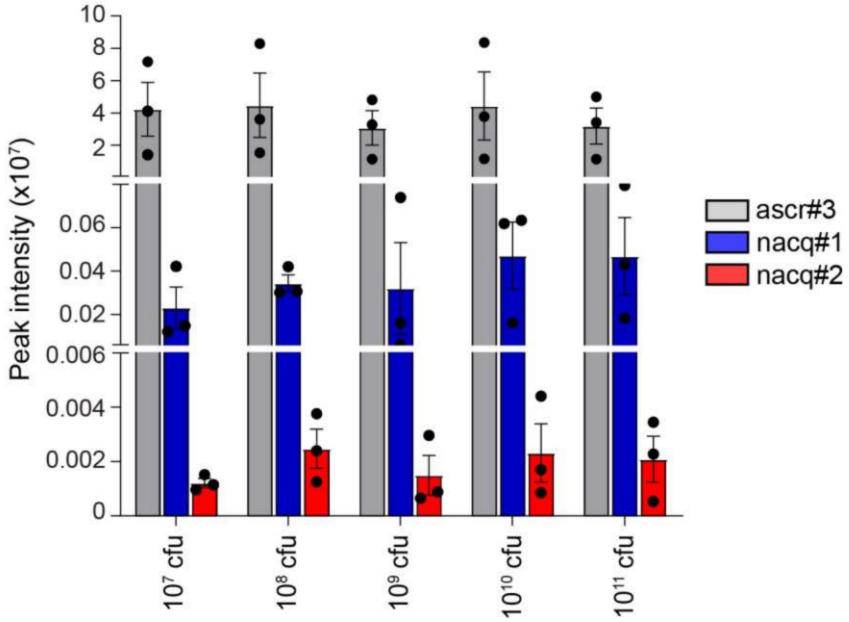

Supplemental Figure 2.6. nacq#1 (2.1) production is not strongly dependent on food availability. Relative amounts of ascr#3, nacq#1, and nacq#2 in worms raised on plates in the presence of different amounts of bacterial food (*n*=3 biologically independent samples). Error bars represent mean ± s.e.m.

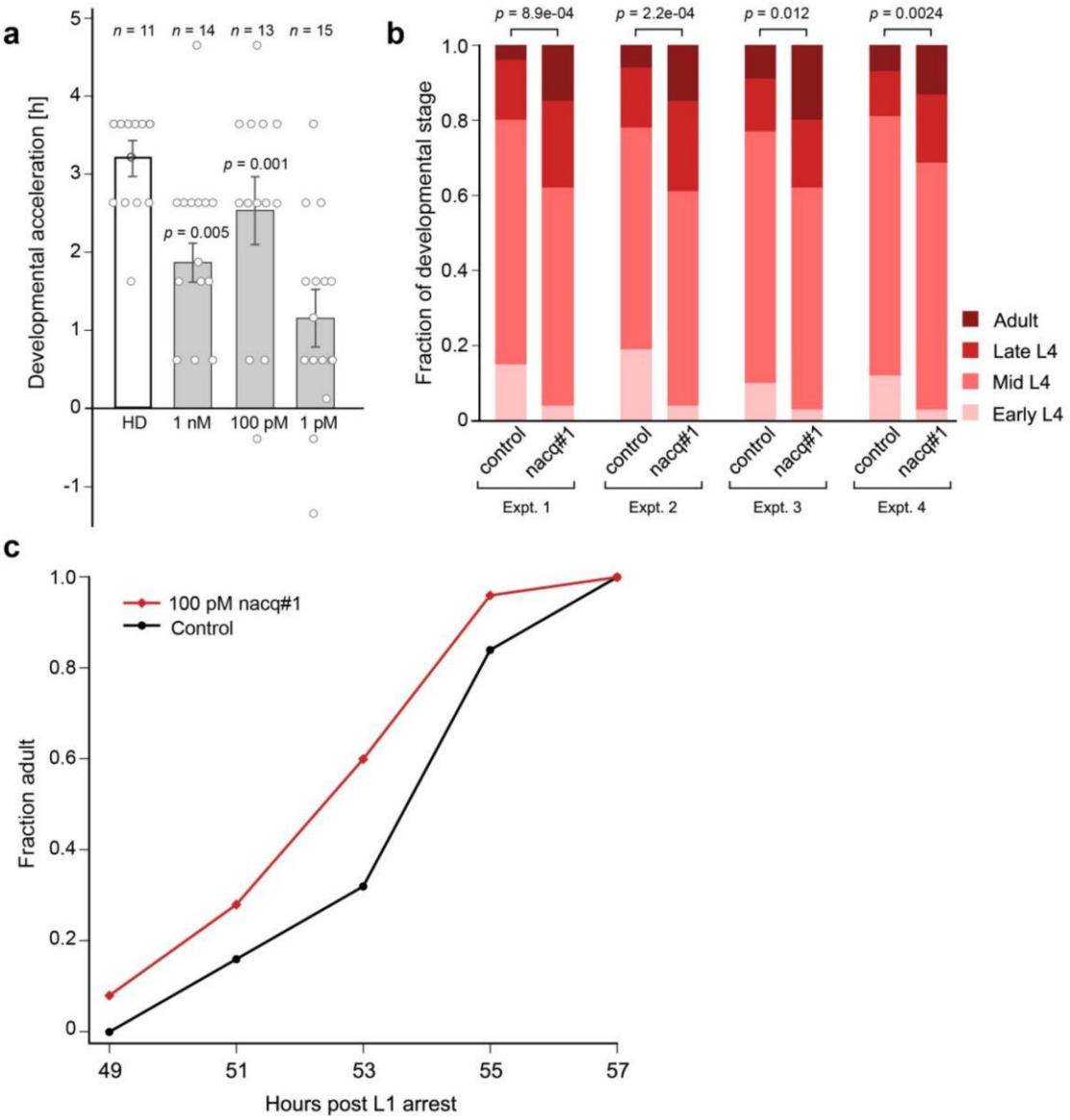

Supplemental Figure 2.7. Developmental acceleration of wildtype (N2) *C. elegans* hermaphrodites by nacq#1. a. Acceleration of development (time point of first egg laying) in singled wildtype (N2) worms treated with different concentrations of nacq#1, compared to acceleration under high density (HD) conditions. Error bars represent mean ± s.e.m. and statistics were performed using two-tailed *t*-tests. **b.** Acceleration of development (fraction of small populations reaching specified developmental stage at a fixed time point) in wildtype (N2) worms on plates conditioned with 100 pM nacq#1 compared to mock-treated control (shown are data from separate 4 experiments each using n = 5 biologically independent replicates, where each replicate was one plate with ~25 animals). Statistics were performed using the $\chi 2$ test. c, Developmental acceleration (fraction attaining morphologically-defined adulthood) of singled wildtype (N2) worms (n = 25 worms per time point).

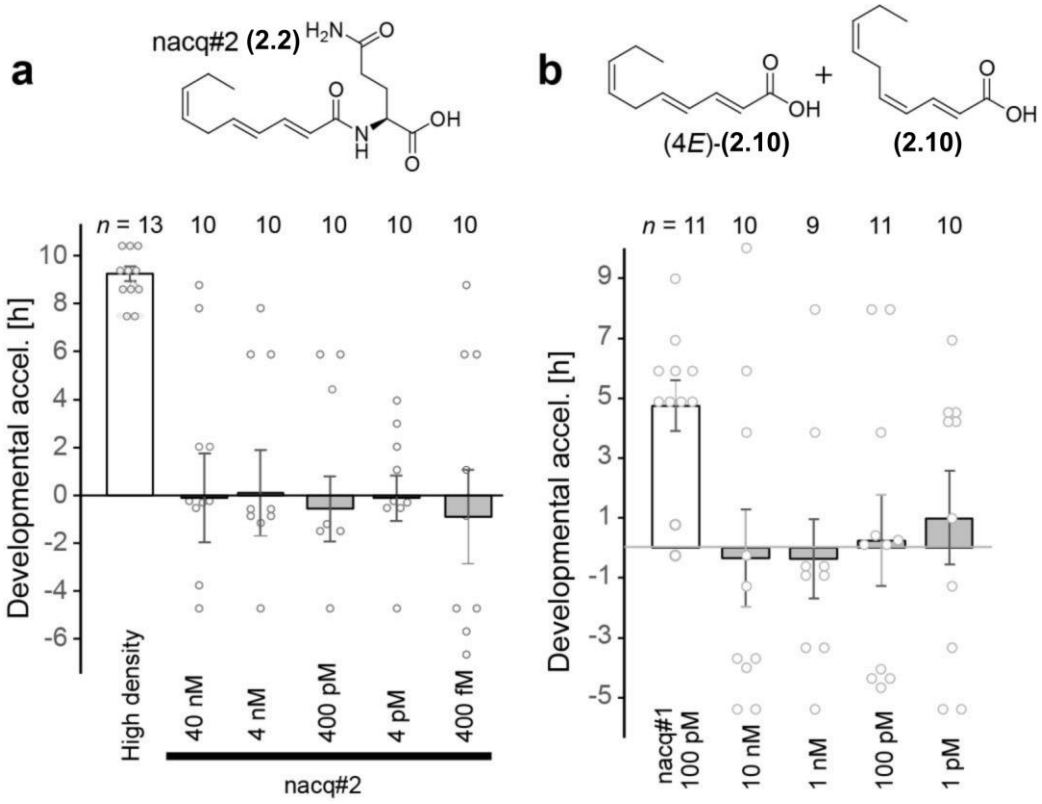

Supplemental Figure 2.8. Developmental acceleration of single worms treated with different synthetic compounds. a. Treatment with nacq#2 does not accelerate development of *daf-22(ok693)* mutants. **b.** A 1:1 mixture of *2E,4Z,7Z*-decatrienoic acid (**2.10**)) and *2E,4E,7Z*-decatrienoic acid (**(*4E*)-2.10**)) does not accelerate development of *daf-22(ok693)* mutants. Acceleration of development (time point of first egg laying in *daf-22(ok693)* mutants at 100 pM nacq#1 and at indicated concentrations of Acid-Mix. Error bars represent mean ± s.e.m. and statistics were performed using two-tailed *t*-tests.

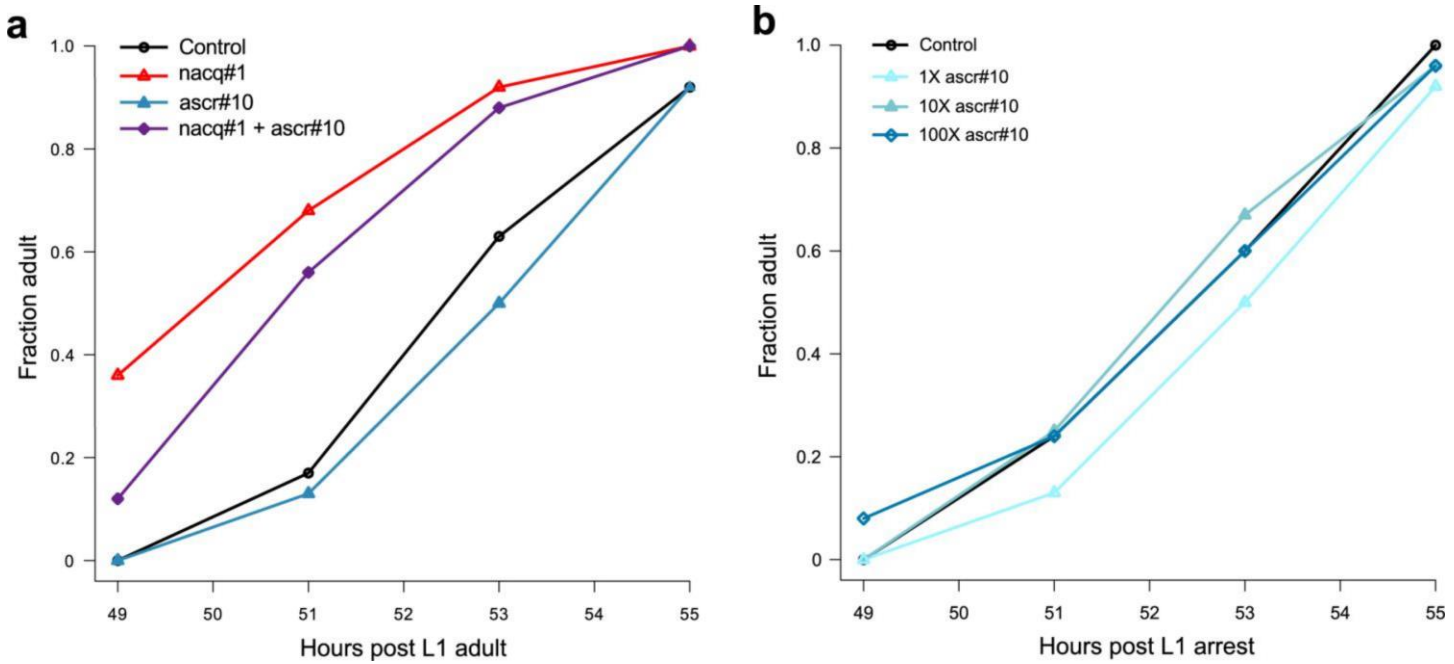

Supplemental Figure 2.9. Developmental acceleration on nacq#1 and ascr#10. a,b. Fractions of singled wildtype (N2) hermaphrodites that attained morphologically-defined adulthood at a specified time point (*n* = 24 worms per time point).

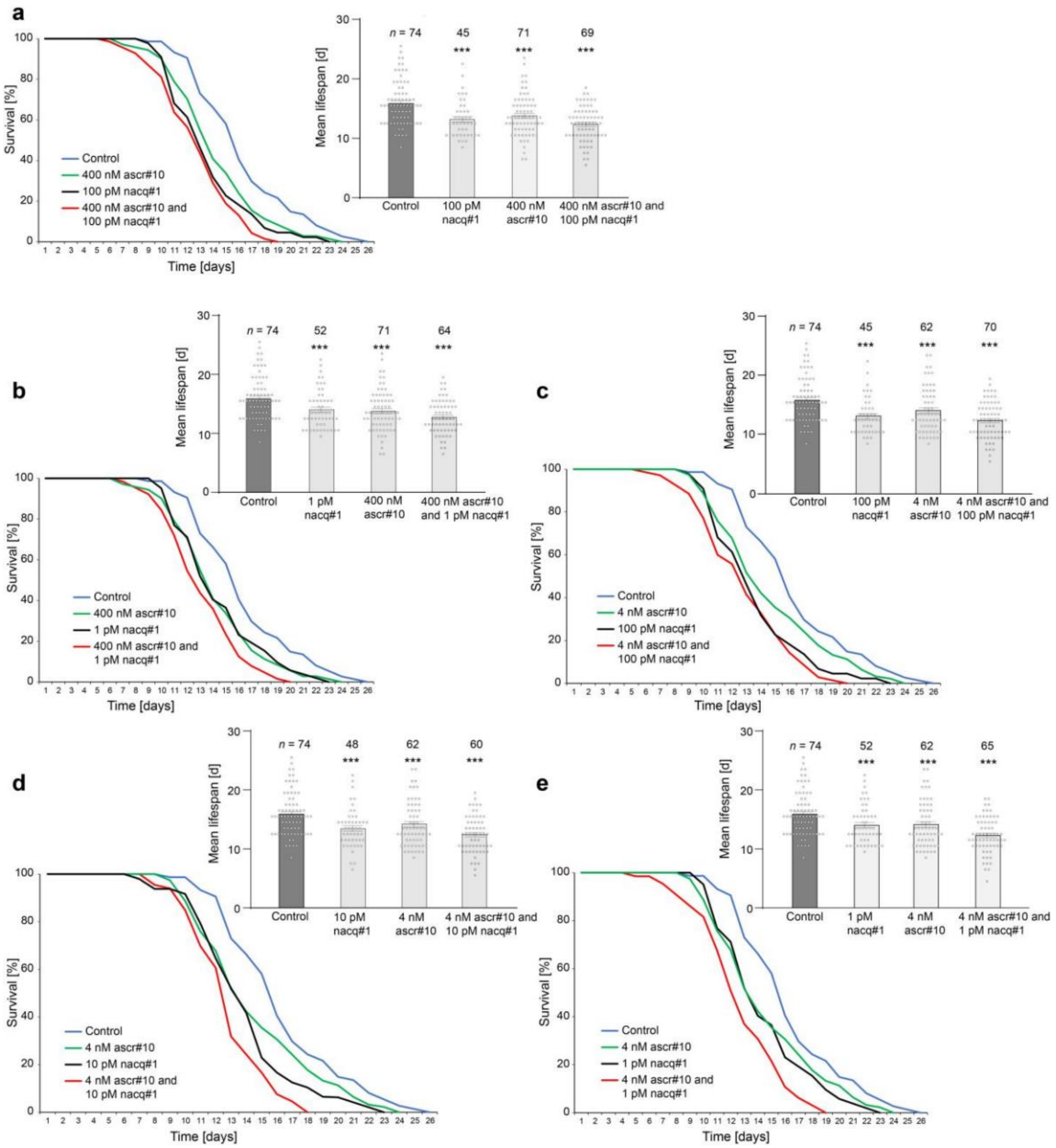

Supplemental Figure 2.10. Comparison of the effects of ascr#10 and nacq#1 on wildtype (N2) lifespan. a-e. Lifespan assays with singled worms (one worm per plate) on plates containing 100, 10, 1 pM nacq#1, or 400 and 4 nM ascr#10, or combinations. Error bars represent mean ± s.e.m.; ***, $p \leq 0.005$.

NMR Spectra of Synthetic Compounds

(*Z*)-Hex-3-en-1-yl *p*-toluene sulfonate (2.6), ^{1}H NMR spectrum (500 MHz, C_6D_6)

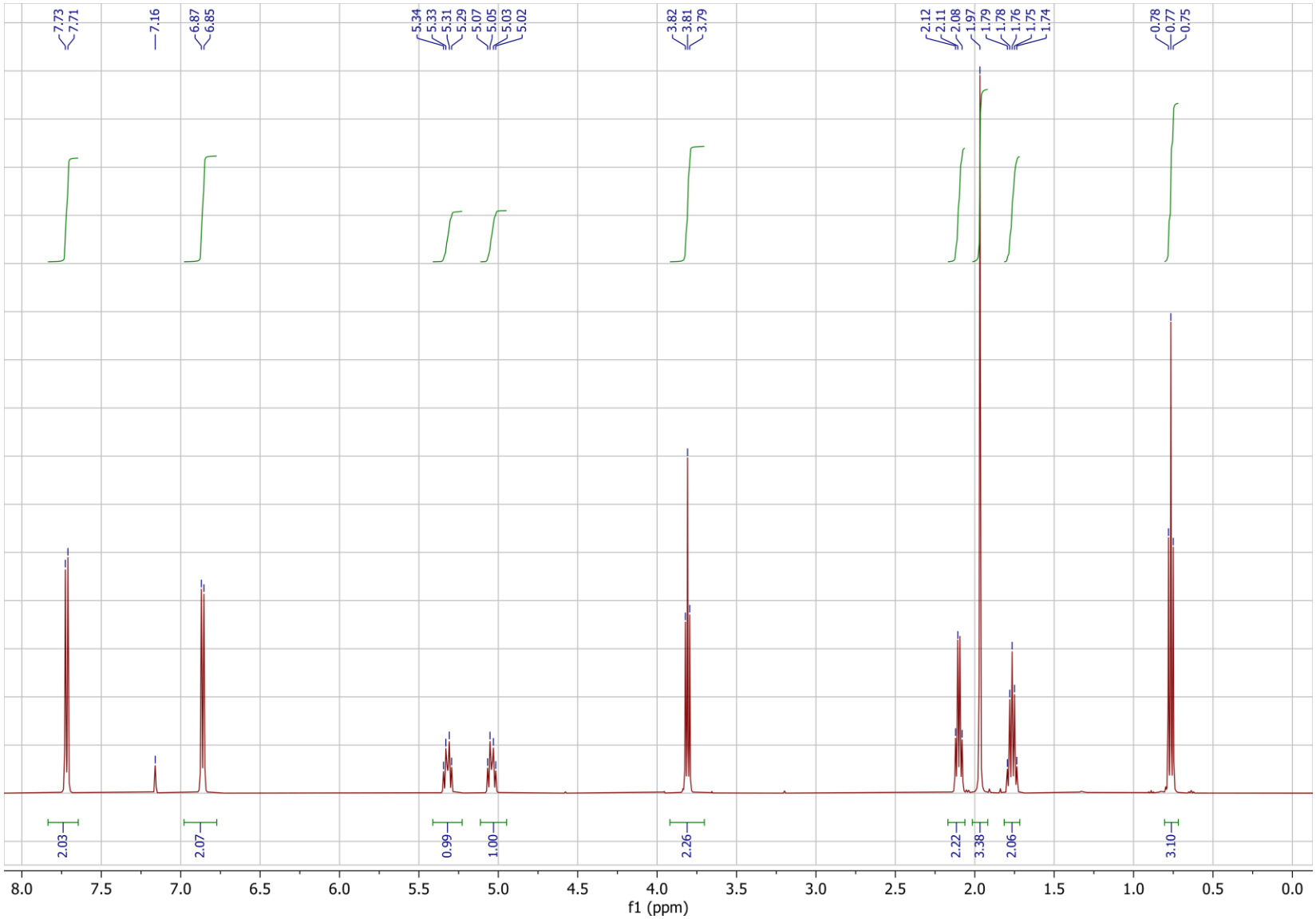

(*Z*)-Hex-3-en-1-yl *p*-toluene sulfonate, ^{13}C NMR spectrum (125 MHz, C_6D_6)

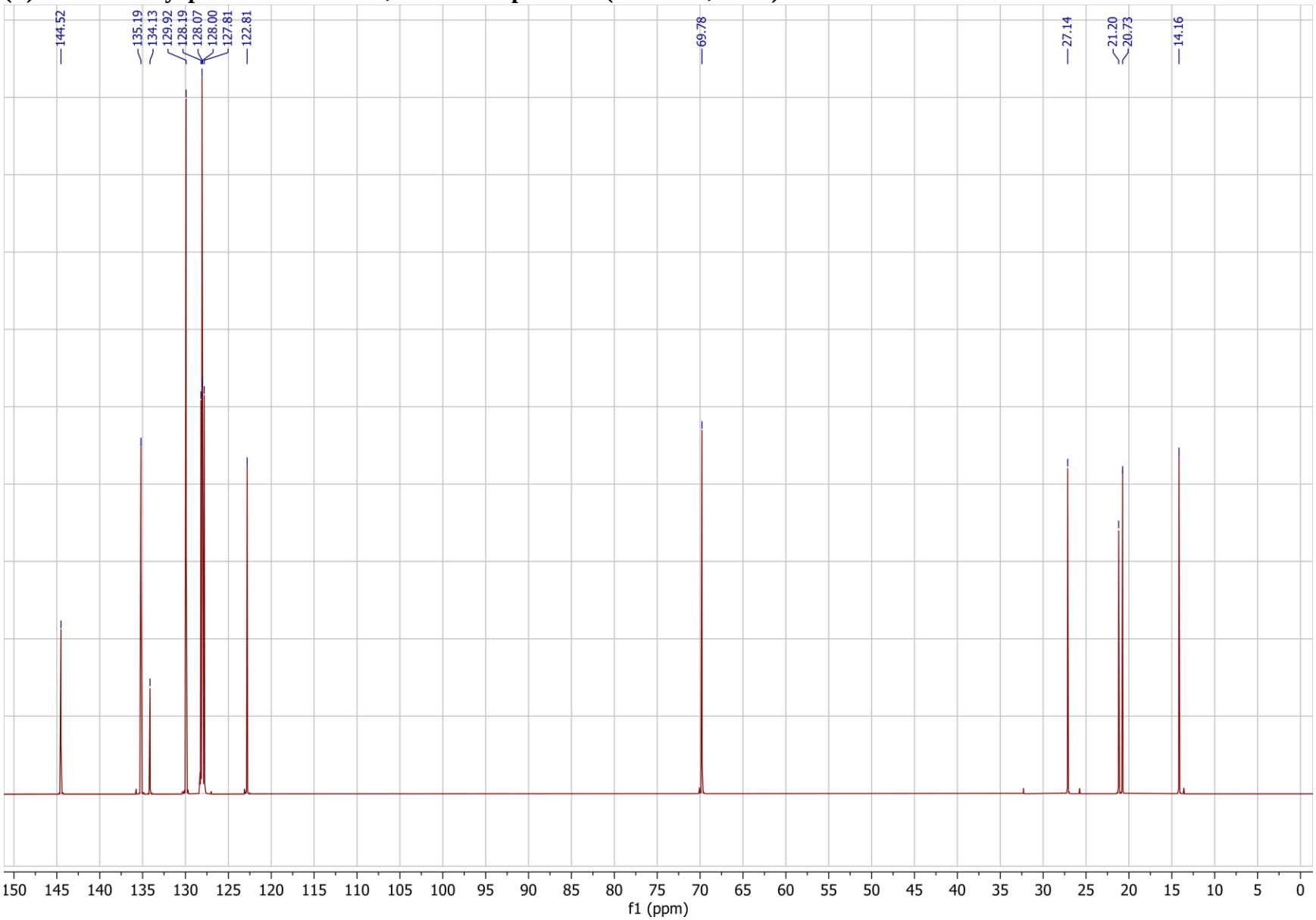

(*Z*)-Hex-3-en-1-yl triphenylphosphonium iodide (2.7), ^{1}H NMR spectrum (500 MHz, CD_3OD)

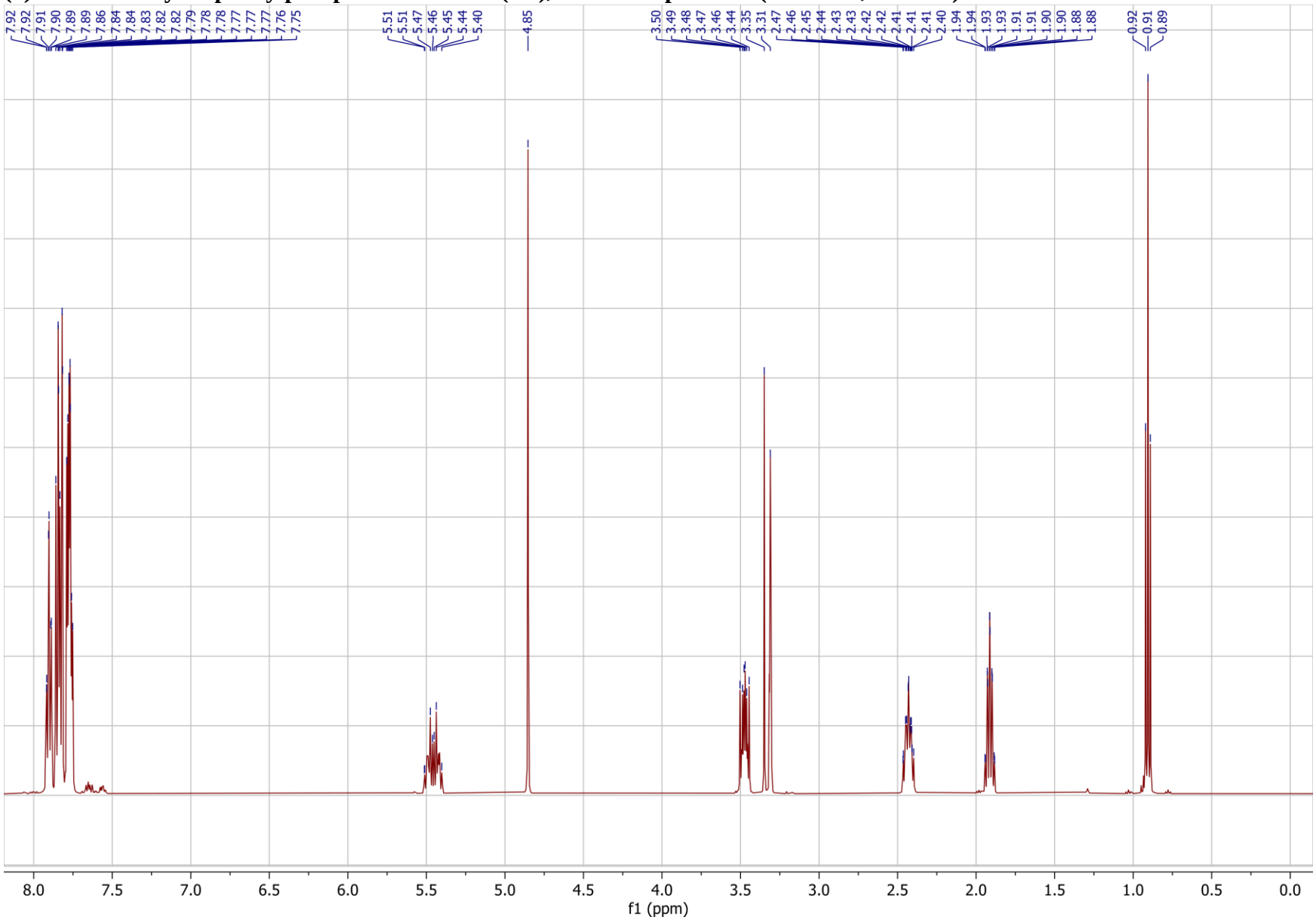

(*Z*)-Hex-3-en-1-yl triphenylphosphonium iodide (2.7), ^{13}C (125 MHz, CD_3OD)

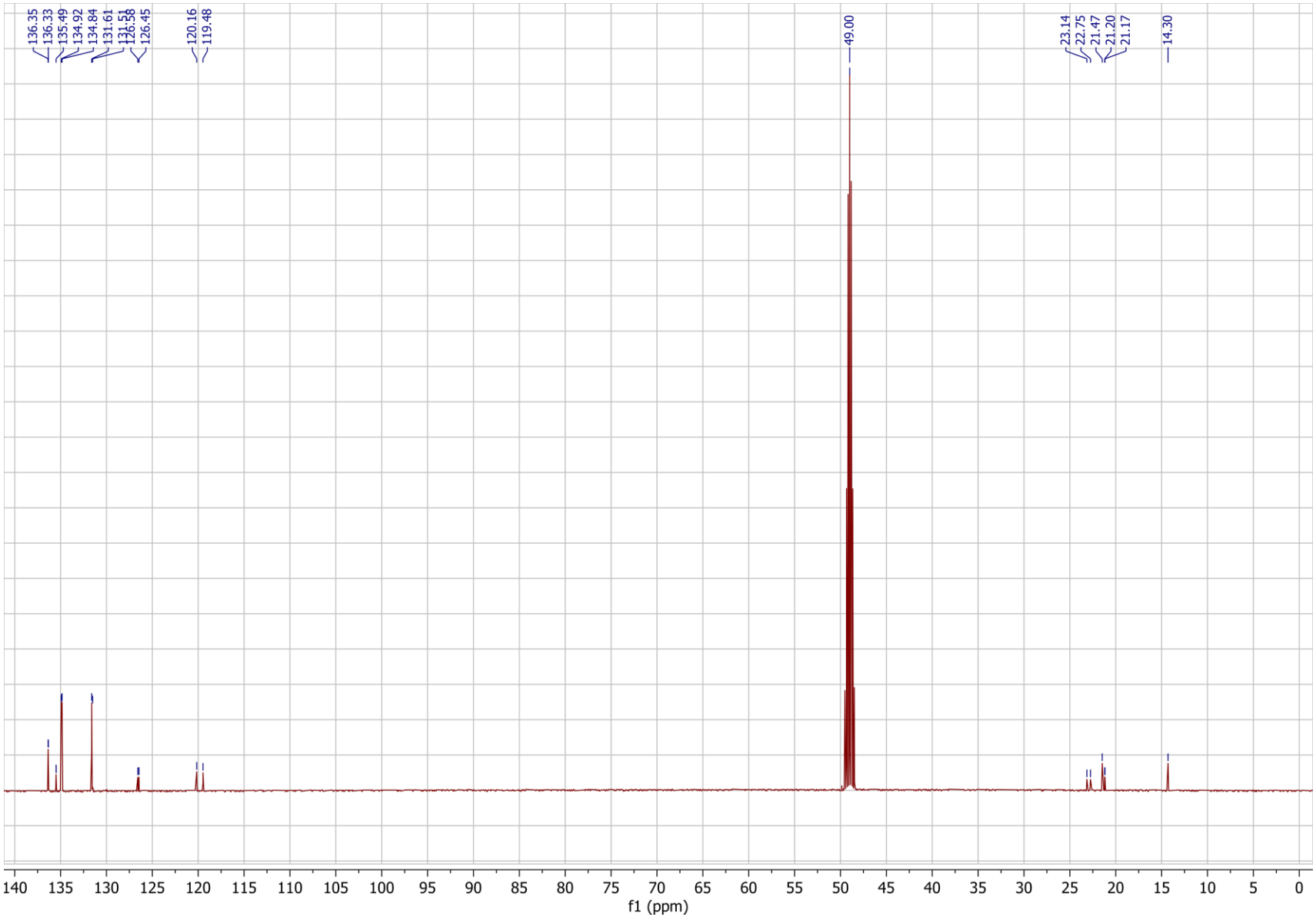

Ethyl (2*E*,4*Z*,7*Z*)-deca-2,4,7-trienoate (2.9), ^{1}H NMR spectrum (500 MHz, C_6D_6)

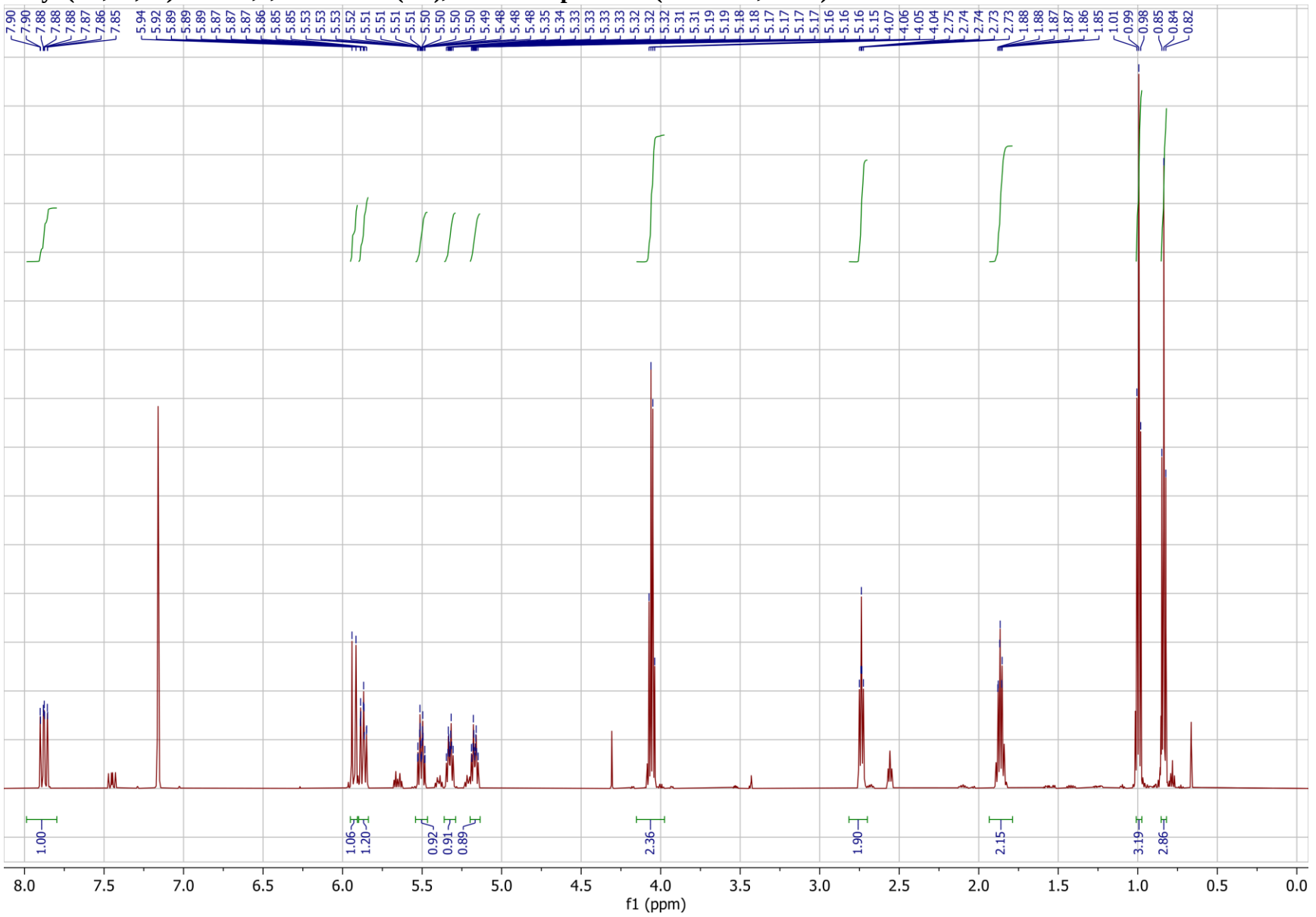

Ethyl (2*E*,*4Z*,*7Z*)-deca-2,4,7-trienoate (2.9), ^{13}C NMR spectrum (125 MHz, C_6D_6)

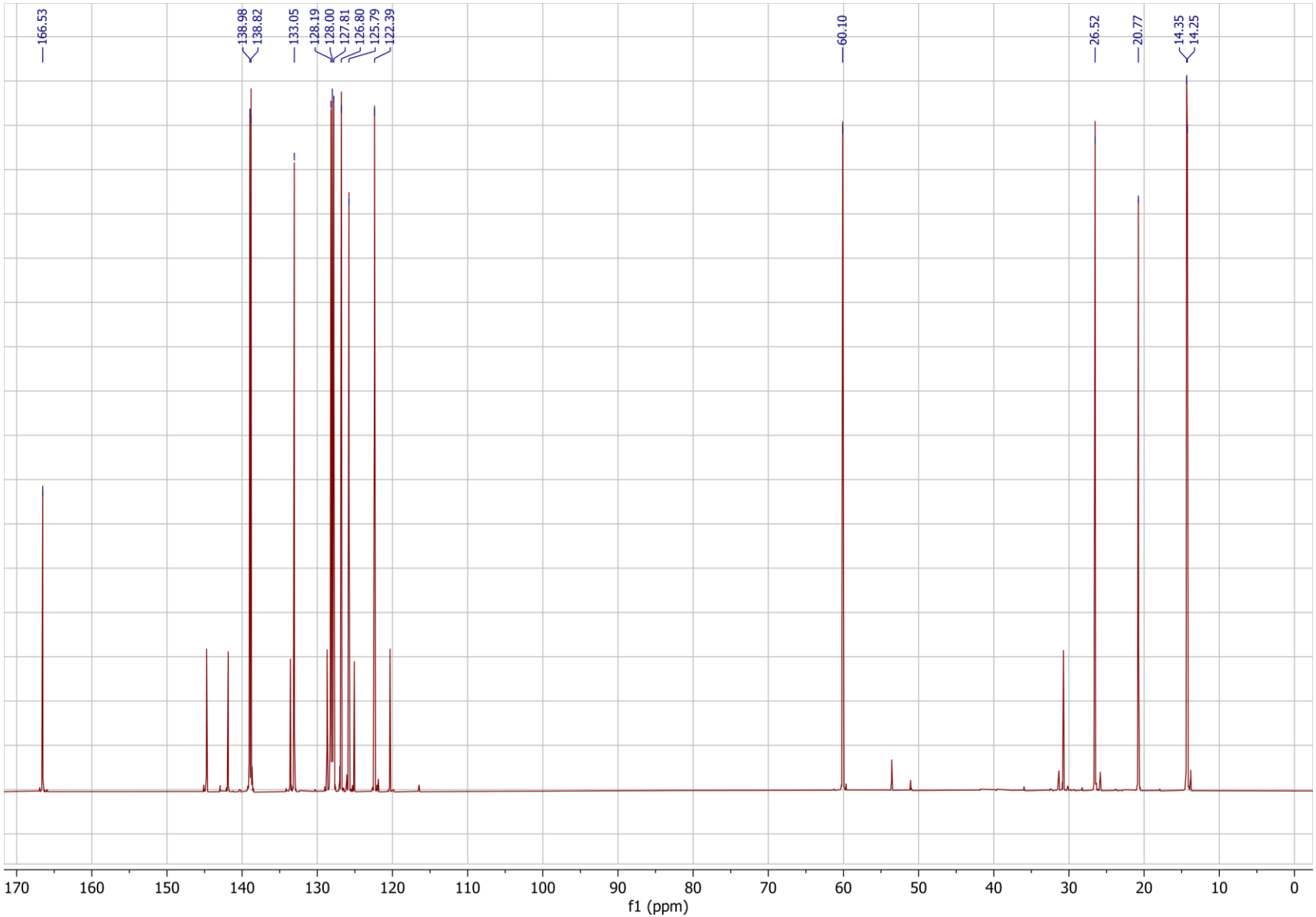

(2*E*,4*Z*,7*Z*)-Deca-2,4,7-trienoic acid (2.10), ^{1}H NMR spectrum (500 MHz, C_6D_6)

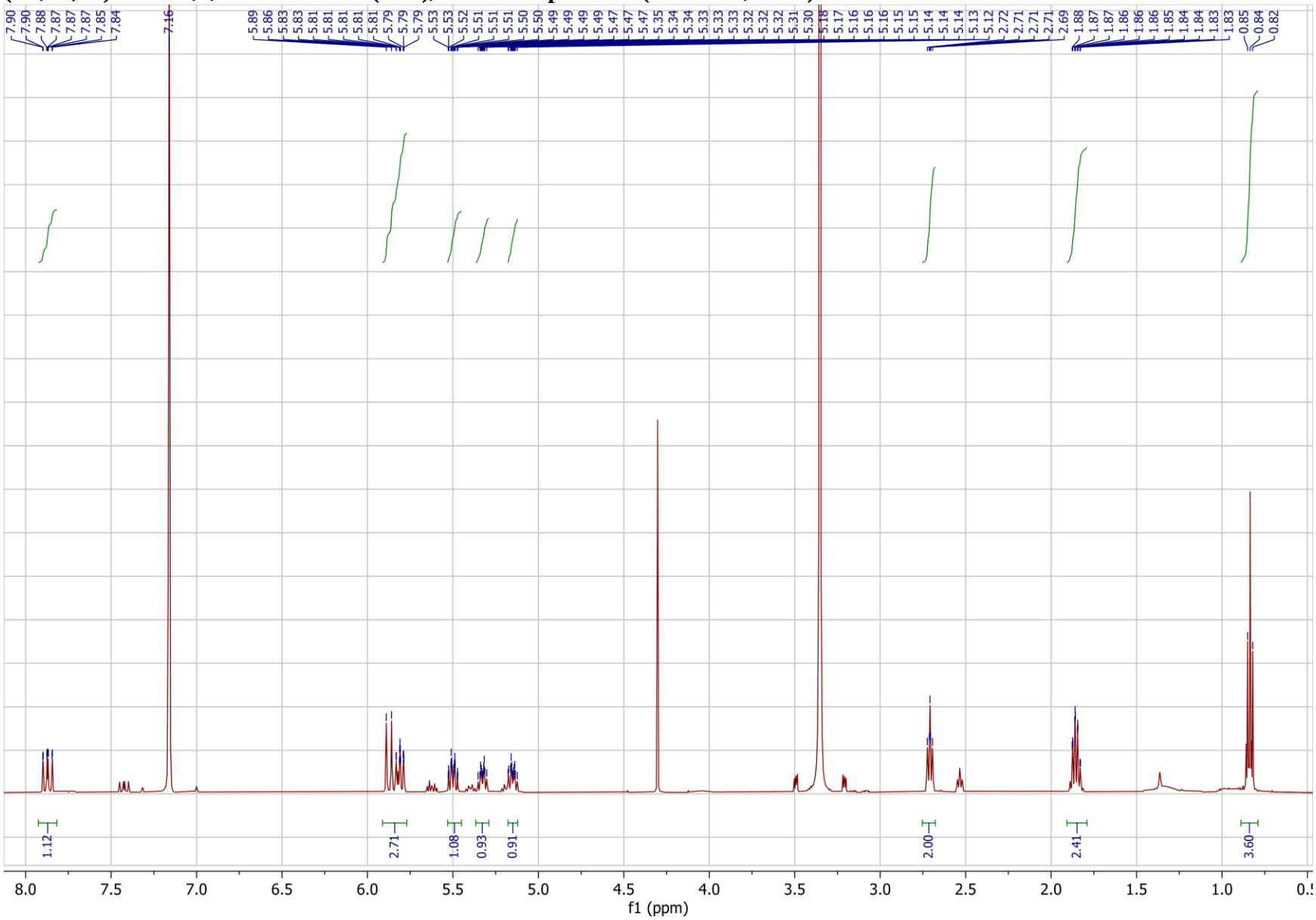

(2*E*,4*Z*,7*Z*)-Deca-2,4,7-trienoic acid (2.10), ^{13}C NMR spectrum (125 MHz, C_6D_6)

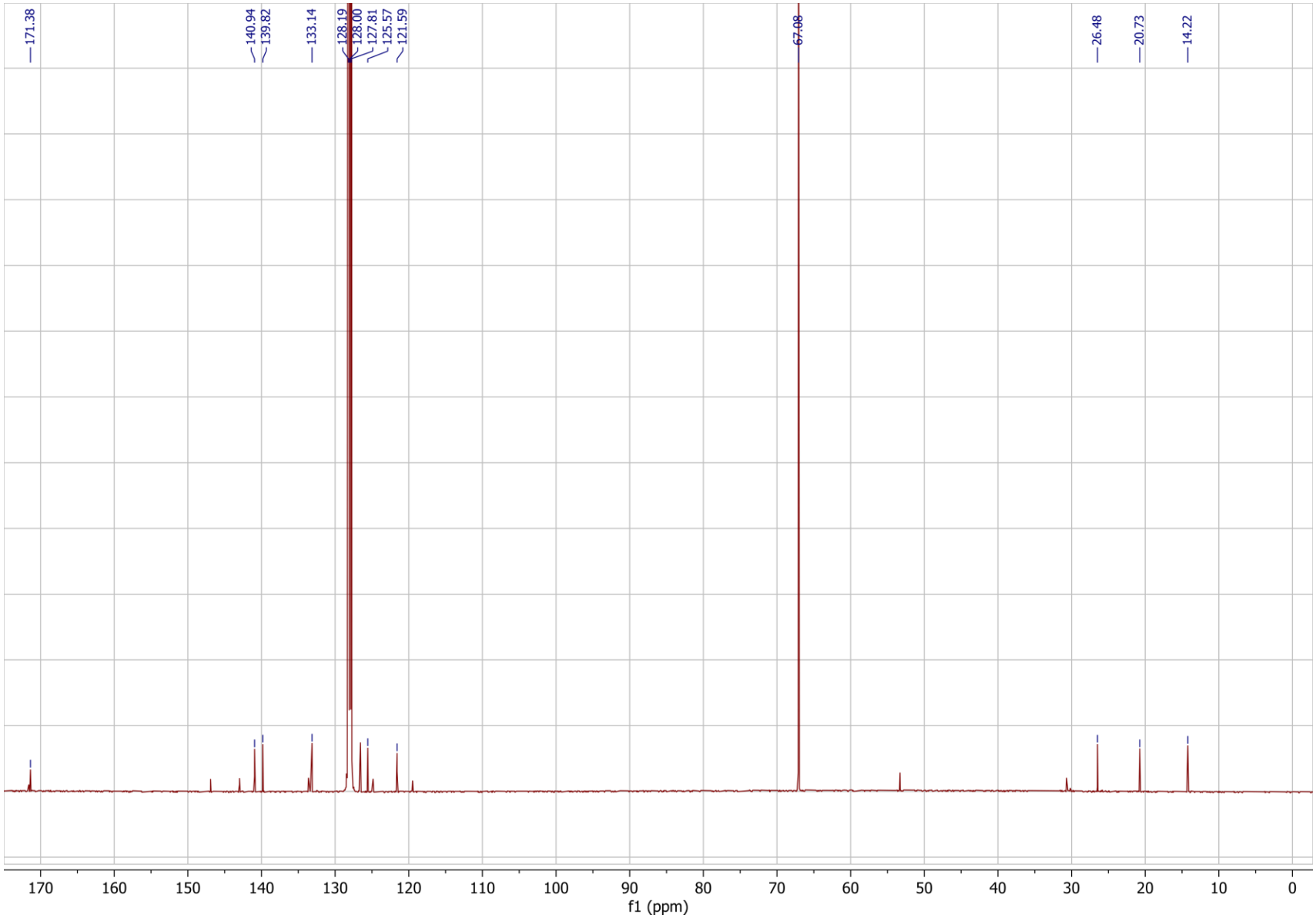

nacq#1-*tert*-butyl ester (2.11), ^{1}H NMR spectrum (500 MHz, CD_3OD)

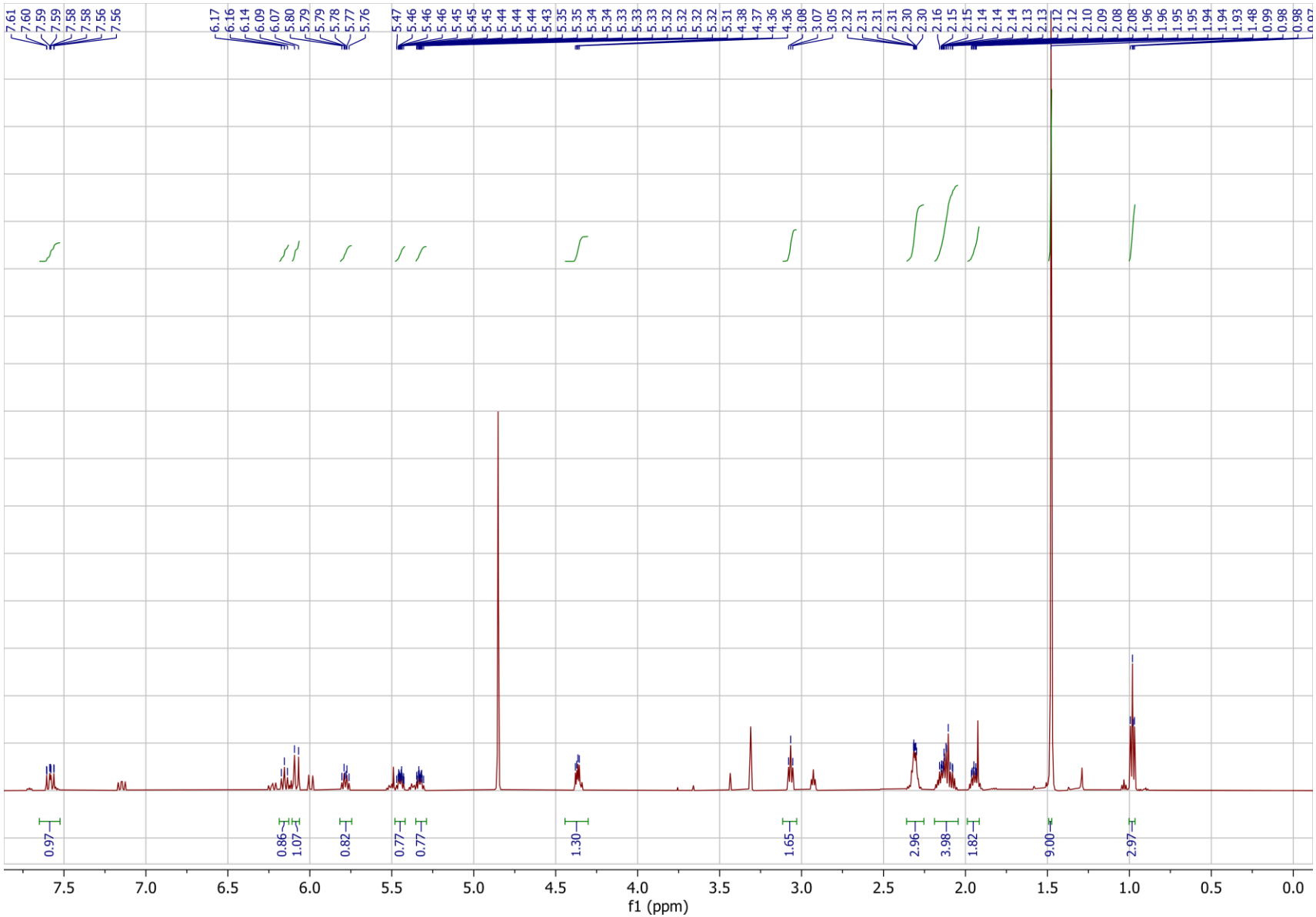

nacq#1-*tert*-butyl ester (2.11), ^{13}C NMR spectrum (125 MHz, CD_3OD)

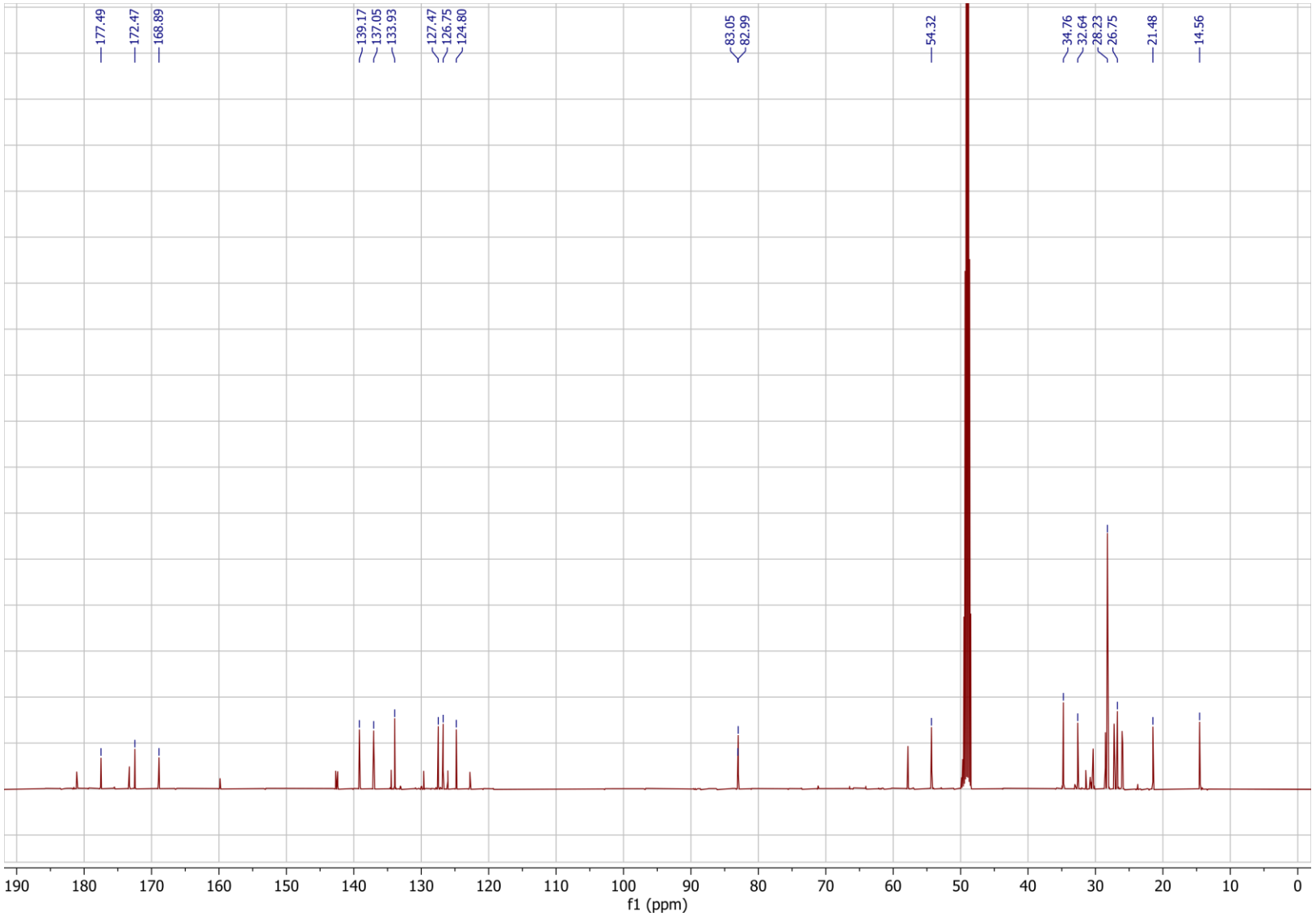

nacq#1, ^{1}H NMR spectrum(500 MHz, CD_3OD)

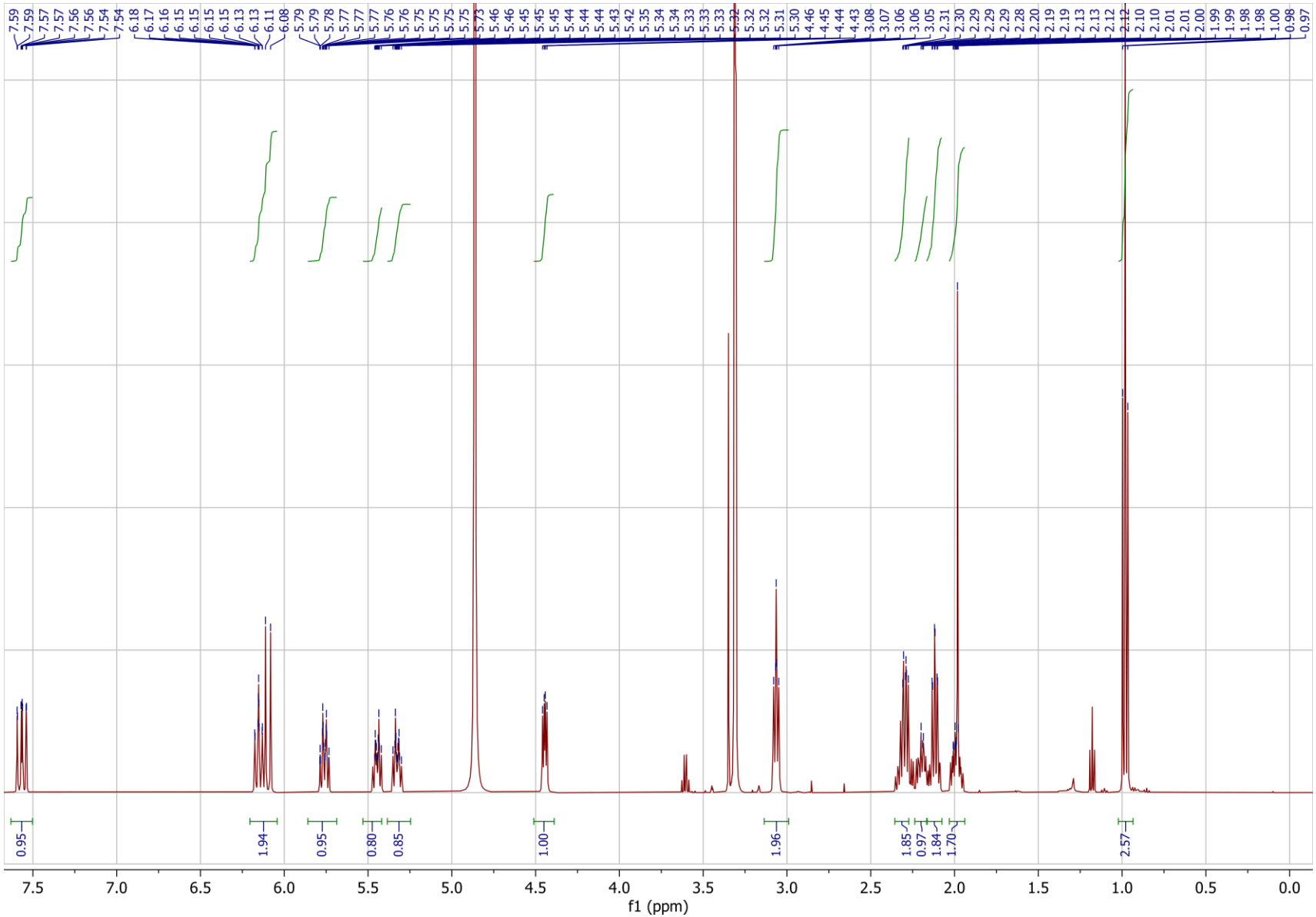

nacq#1, ^{13}C NMR spectrum (125 MHz, CD_3OD)

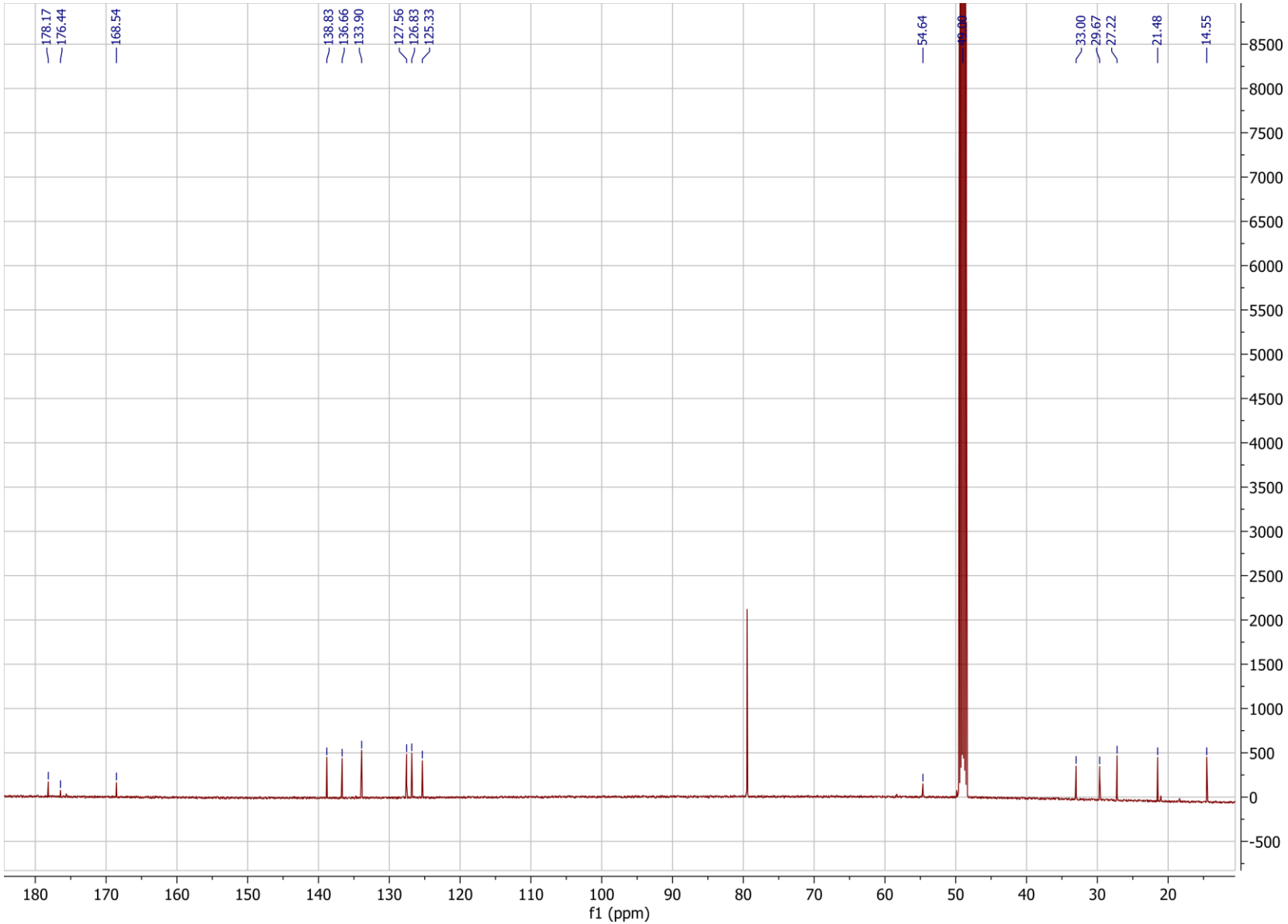

Supplemental References:

1. Kim, S., Lawson, J. A., Patricò, D., FitzGerald, G. G., Rokach, J. The first total synthesis of iPF$_{4\alpha}$-VI and its deuterated analog. *Tetrahedron Lett.* **43**: 2801-2805. **2002**.

2. Chang, C., *et al.* A new approach to the synthesis of polyunsaturated deuterated isoprostanes: Total synthesis of d$_4$-5-*epi*-8,12-*iso*-iPF$_{3\alpha}$-VI and d$_4$-8,12-*iso*-IPF$_{3\alpha}$-VI. *Bioorg. & Med. Chem. Lett.* **19**: 6755-6758. **2009**.

3. Heimberger, J., Cade, H.C., Padgett, J., Sittaramane, V., Shaikh, A., Total synthesis of Herbarin A and B, determination of their antioxidant properties and toxicity in zebrafish embryo model. *Bioorg. & Med. Chem. Lett.* **25**: 1192-1195. **2015**.

4. Subasinghe, N., *et al.* Synthesis of acyclic and dehydroaspartic acid analogs of Ac-Asp-Glu-OH and their inhibition of rat brain N-acylated α-linked acidic dipeptidase (NAALA dipeptidase). *J. Med. Chem.* **33**: 2734-2744. **1990**.

5. Breuning, A., *et al*. Michael acceptor based antiplasmodial and antitrypanosomal cysteine protease inhibitors with unusual amino acids. *J. Med. Chem.* **53**: 1951-1963. **2010**.

6. Potterat, O., Zähner, H., Metzger, J.W., Freund, S. 54. Metabolic products of icroorganisms art 269 5-henylpentadienoic-acid derivatives from *Streptomyces* sp. *Helv. Chim. Acta*. **77**: 569-574. **1994**.

APPENDIX C

Supplemental Information for Chapter 3

Experimental

General Procedures

Unless stated otherwise, all reactions were performed under argon in flame-dried glassware. All commercially available reagents were used as purchased unless otherwise stated. All solvents were dried over activated 3Å sieves for a minimum of 24 hours unless used in reactions where aqueous reagents were involved. Titanium (IV) isopropoxide was distilled under vacuum and stored under argon. Thin-layer chromatography (TLC) was performed with J.T. Baker Silica Gell IB2-F plastic-backed plates. Reverse-phase column chromatography was performed using Teledyne ISCO CombiFlash Rf and Rf+ systems with Teledyne ISCO RediSep Rf and Rf Gold silica columns. Nuclear Magnetic Resonance (NMR) spectra were recorded on a Varian INOVA 600 (600 MHz) or Bruker AV 500 (500 MHz) in the Cornell University NMR Facility. ^{1}H NMR chemical shifts are reported in ppm (δ) relative to the residual solvent peaks (7.26 ppm for $CDCl_3$ and 3.31 ppm for CD_3OD) and ^{13}C NMR shifts relative to their respective residual solvent peaks (77.16 for $CDCl_3$ and 49.00 for CD_3OD).

Synthetic Procedures

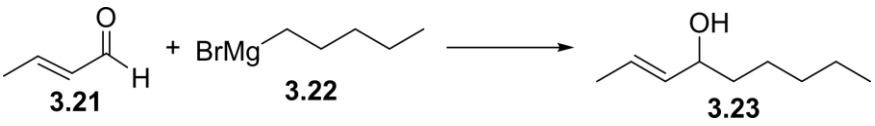

3.21 3.22 3.23

***(E)*-4-Hydroxy-non-2-ene (3.23).** *n*-Pentylmagnesium bromide (10 mL, 20 mmol in THF) was added to a diethyl ether (20mL) at 0 °C under an argon atmosphere. Crotonaldehyde (1.66 mL,

20 mmol) was added to the stirring solution over 10 minutes via addition funnel and stirred for one hour. The reaction was quenched with saturated aqueous NH_4Cl (20 mL) and extracted with EtOAc (3×20 mL). The combined organics were dried over $MgSO_4$, filtered, and concentrated under reduced pressure. The resulting liquid was purified by flash chromatography on silica gel. Elution with a gradient of 0-20% EtOAc/Hexanes gave the resulting alcohol (**3.23**) (2.61 g, 92%) as a colorless liquid.

^{1}H NMR ($CDCl_3$, 500 MHz): δ (ppm) 5.65 (dqd 15.3, 6.5, 0.8 Hz, 1H), 5.48 (ddq 15.3, 7.7, 1.5 Hz, 1H), 4.03 (q, 6.6 Hz, 1H), 1.70 (dd 6.5, 1.3 Hz, 3H), 1.25-1.58 (m, 9H), 0.89 (t, 6.8 Hz, 3H).

^{13}C NMR ($CDCl_3$, 125 MHz): δ (ppm) 134.5, 126.9, 73.4, 37.4, 31.9, 25.3, 22.8, 17.8, 14.2.

HRMS (ESI) *m/z*: Calculated: $(M+H)^+$ 143.1430. Actual: 143.1428 Δ ppm: -1.64

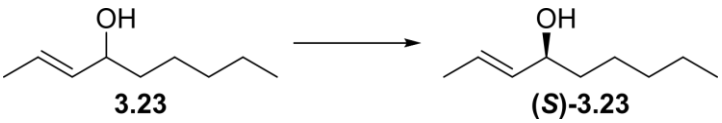

3.23 **(*S*)-3.23**

***(S,E)*-4-Hydroxy-non-2-ene (*(S)*-3.23).** *(-)*-Diisopropyl D-tartrate (183 μL, 0.88 mmol) was added to a suspension of powdered 4 Å molecular sieves (0.4 g) in DCM (21 mL) at ambient temperature under an argon atmosphere. The solution was cooled to -20 °C and titanium (IV) isopropoxide (212 μL, 0.7 mmol) was added. The solution was stirred for one hour and *tert*-butylhydroperoxide (382 μL, 2.1 mmol in decane) added. The solution was further stirred for 30 minutes and cooled to -40 °C, upon which racemic *(E)*-4-hydroxy-non-2-ene (**3.23**) (3.5 mL, 3.5 mmol in DCM) was added dropwise. After 20 hours the reaction was quenched with *(-)*-diisopropyl D-tartrate (366 μL, 1.75 mmol) in water (7 mL). The layers were separated, and the aqueous solution extracted with Et_2O (3×20 mL). The combined organics were washed with saturated aqueous $NaHCO_3$, dried over $MgSO_4$, filtered, and concentrated under reduced

pressure. The resulting liquid was purified by flash chromatography on silica gel as above, yielding chiral alcohol (**2**) (236 mg, 94%) as a colorless liquid. Enantiomeric excess was determined to be up to 88% by Mosher derivatization. All NMR spectra and mass spectrometric data are identical to alcohol (**3.23**).

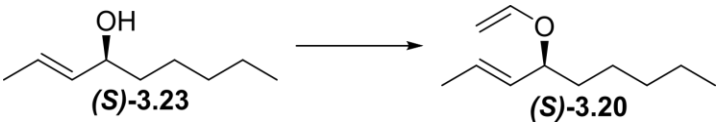

***(S)*-3.23** ***(S)*-3.20**

(S,E)*-4-(Vinyloxy)-non-2-ene (3.20).** *(S, E)*-4-Hydroxy-non-2-ene ((S)*-3.23**) (307 mg, 2.16 mmol) was added to ethyl vinyl ether (5.75 mL, 60.5 mmol) at ambient temperature under an argon atmosphere. Mercury (II) acetate (688 mg, 2.16 mmol) was added to the solution. After two hours AcOH (302 μL) was added with stirring. After 30 minutes the reaction was diluted with hexanes (45 mL) and washed with 5% aqueous KOH (4.5 mL). The organics were dried over $MgSO_4$, filtered, and concentrated under reduced pressure. The resulting liquid was purified by flash chromatography on alumina. Elution with a gradient of 0-10% EtOAc/Hexanes yielded vinyl ether (**3.20**) (178 mg, 76% BRSM) as a colorless liquid.

^{1}H NMR ($CDCl_3$, 500 MHz) δ (ppm) 6.31 (dd, 14.1, 6.6 Hz, 1H), 5.65 (dqd 15.3, 6.6, 0.8 Hz, 1H), 5.38 (ddq, 15.3, 7.6, 1.6 Hz, 1H), 4.28 (dd, 14.1, 1.4 Hz, 1H), 4.05 (q, 7 Hz, 1H), 3.96 (dd, 6.6, 1.4 Hz, 1H), 1.71 (dd, 6.5, 1.4 Hz, 3H), 1.61-1.70 (m, 1H), 1.46-1.54 (m, 1H), 1.23-1.40 (m, 6H), 0.88 (t, 6.8 Hz, 3H).

^{13}C NMR ($CDCl_3$, 125 MHz) δ (ppm) 151.0, 131.4, 128.7, 88.4, 81.2, 35.3, 31.8, 25.0, 22.7, 17.9, 14.2.

HRMS (ESI) *m/z*: Calculated: $(M+H)^+$ 169.1587 $(M+Na)^+$ 191.1406. Actual: 169.1584 Δ ppm: -1.99

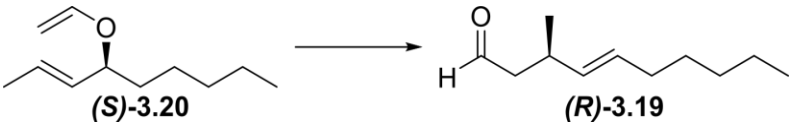

***(S)*-3.20** ***(R)*-3.19**

***(R,E)*-3-Methyl-dec-4-enal (3.19).** Vinyl ether (**3.20**) (107 mg, 0.64 mmol) was added to toluene (5 mL) and stirred with condenser at reflux under an argon atmosphere. After 23 hours the reaction was concentrated to yield aldehyde (**3.19**) (100 mg, 93%) as a colorless liquid which was used without purification.

^{1}H NMR ($CDCl_3$, 500 MHz) δ (ppm) 9.72 (t, 2.4 Hz, 1H), 5.44 (dtd, 15.4, 6.6, 1.0 Hz, 1H), 5.34 (ddt, 15.4, 7.0, 1.3 Hz, 1H), 2.72 (m, 6.9 Hz, 1H), 2.40 (ddd, 16.0, 7.3, 2.4 Hz, 1H), 2.33 (ddd16.0, 6.7, 2.4 Hz, 1H), 1.97 (q, 7.0 Hz, 2H), 1.21-1.37 (m, 6H), 1.06 (d, 6.8 Hz, 3H), 0.88 (t, 7.0 Hz, 3H).

^{13}C NMR ($CDCl_3$, 125 MHz) δ (ppm) 203.0, 133.9, 130.2, 50.7, 32.6, 31.8, 31.5, 29.3, 22.7, 20.9, 14.2.

HRMS (ESI) *m/z*: Calculated: $(M+Na)^+$ 191.1406. Actual: 191.1411 Δ ppm: 2.49.

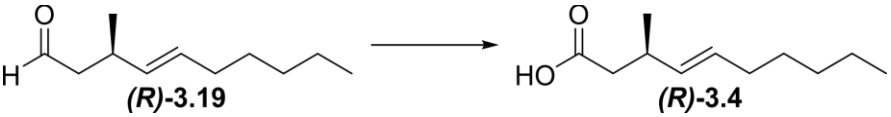

***(R)*-3.19** ***(R)*-3.4**

***(R,E)*-3-Methyl-dec-4-enoic acid, bemeth#1 (*(R)*-3.4).** Aldehyde (**3.19**) (53 mg, 0.32 mmol) was dissolved in DMSO (1.1 mL) and stirred under ambient atmosphere. Sodium chlorite (40 mg, 0.35 mmol) was dissolved in minimal water and the pH adjusted to ~4.5 with NaH_2PO_4. The aqueous solution was added to the aldehyde and the reaction stirred in an open atmosphere. After 30 minutes more sodium chlorite (20 mg, 0.18 mmol), dissolved in water and buffered as above, was added. After 45 minutes the reaction was diluted with water (2 mL) and extracted with EtOAc (3×2 mL). The combined organics were dried over $MgSO_4$, filtered, and

concentrated under reduced pressure. The resulting oil was purified by flash chromatography on silica gel. Elution with a gradient of 0-20% EtOAc(0.1% AcOH)/hexanes yielded acid (***(R)*-3.4**) (44 mg, 76%) as a colorless oil. Enantiomeric excess was determined to be 65% by 2,2,2-trifluoro-1-phenethylamine derivatization and subsequent analysis by UHPLC-MS.

^{1}H NMR ($CDCl_3$, 500 MHz) δ (ppm) 5.45 (dtd, 15.4, 6.7, 0.8 Hz, 1H), 5.33, ddt, 15.3, 7.2, 1.3, 1H), 2.63 (m, 7.0 Hz, 1H), 2.35 (dd, 14.9, 7.3 Hz, 1H), 2.28 (dd, 14.9, 7.3 Hz, 1H), 1.96 (q, 7.0, 2H), 1.21-1.36 (m, 6H), 1.05 (d, 6.7 Hz, 3H), 0.88 (t, 6.9 Hz, 3H).

^{13}C NMR ($CDCl_3$, 125 MHz) δ (ppm) 178.8, 133.7, 1.0.1, 41.8, 33.5, 32.6, 34.4, 29.3, 22.7, 20.5, 14.2.

HRMS (ESI) *m/z*: Calculated: $(M-H)^-$ 183.1391. Actual: 183.1383. Δ ppm: -4.16.

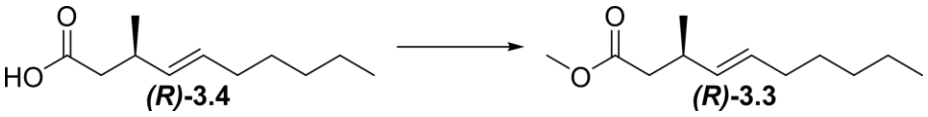

Methyl-*(R, E)*-3-methyl-dec-4-enoate (*(R)*-3.3). Trimethylsilyldiazomethane (1.2 mL, 0.72 mmol) was added dropwise to a solution of acid (***(R)*-3.4**) in DCM (3 mL) and MeOH (3 mL). After stirring for 15 minutes the reaction was concentrated under reduced pressure. The resulting oil was purified by flash chromatography on silica gel. Elution with a gradient of 0-10% EtOAc/hexanes yielded methyl ester (**3.3**) (42 mg, 89%) as a colorless oil.

^{1}H NMR ($CDCl_3$, 500 MHz) δ (ppm) 5.42 (dtd, 15.3, 6.7, 0.9 Hz, 1H), 5.31 (ddt, 15.3, 7.3, 1.2 Hz, 1H), 3.63 (s, 3H), 2.61 (m, 7.0 Hz, 1H), 2.30 (dd, 14.7, 7.3 Hz, 1H), 2.24 (dd, 14.7, 7.3 Hz, 1H), 1.95 (q, 6.9 Hz, 2H), 1.21-1.35 (m, 6H), 1.02 (d, 6.9 Hz, 3H), 0.87 (t, 6.9 Hz, 3H).

^{13}C NMR ($CDCl_3$, 125 MHz) δ (ppm) 173.3, 134.0, 129.8, 51.5, 42.0, 33.8, 32.6, 31.4, 29.3, 22.7, 20.6, 14.2.

HRMS (ESI) *m/z*: Calculated: $(M+H)^+$ 199.1693. Actual: 199.1690. Δ ppm: -1.49.

Methyl-*(2R,3S,E)*-2-hydroxy-3-methyl-dec-4-enoate (*(2R,3S)*-3.7). *n*-Butyl lithium (72 μL, 0.18 mmol) was added dropwise to a stirring solution of *N*,*N*-diisopropylamine (21 μL, 0.15 mmol) in THF (4 mL) at -15°C and stirred 10 minutes under an argon atmosphere. The solution was cooled to -78°C and methyl ester (**3.3**) was added and the reaction stirred at -15°C for 15 minutes. The reaction was cooled to -78°C and *(+)*-(8, 8-dichlorocamphorylsulfonyl)oxaziridine (90 mg, 0.3 mmol) was added in THF (2 mL) and stirred to -15°C. After stirring for one hour the reaction was quenched with aqueous saturated $NaHCO_3$ (3 mL) and the layers separated. The aqueous layer was extracted with DCM (3×5mL) and the combined organics dried over $MgSO_4$, filtered, and concentrated under reduced pressure. The resulting oil was purified by flash chromatography on silica gel. Elution with a gradient of 0-20% EtOAc/hexanes yielded alpha-hydroxy ester (***(2R,3S)*-3.8**) (9 mg, 69% BRSM).

^{1}H NMR ($CDCl_3$, 500 MHz) δ (ppm) 5.53 (dtd, 15.3, 6.7, 0.9 Hz, 1H), 5.39 (ddt, 15.3, 7.9, 1.4 Hz, 1H), 4.12 (d, 4.2, 1H), 3.78 (s, 3H), 3.76 (q, 4.3 Hz, 1H), 2.52-2.67 (m, 1H), 2.00 (qd, 7.1, 1.2 Hz, 2H), 1.21-1.38 (m, 8H), 0.99 (d, 7.0, 3H), 0.88 (t, 6.9, 3H).

^{13}C NMR ($CDCl_3$, 125 MHz) δ (ppm) 174.8, 132.4, 130.6, 74.6, 52.4, 41.3, 32.7, 31.5, 29.2, 22.7, 14.8, 14.2.

HRMS (ESI) *m/z*: Calculated: $(M+Na)^+$ 237.1461. Actual: 237.1475. Δ ppm: 5.87.

(2R,3S)-3.7 *(2R,3S)*-3.8

(2R,3S,E)*-2-hydroxy-3-methyl-dec-4-enoic acid, bemeth#23 (*(2R,3S)*-3.8).** Lithium hydroxide (40 mg, 2 mmol) was added to a stirring solution of ester (**8**) (11 mg, 0.05 mmol) in MeOH (0.4 mL), THF (0.4 mL), and water (0.2 mL). After one hour the reaction was acidified with 1 M HCl and extracted with DCM (3×5 mL). The combined organics were dried over $MgSO_4$, filtered, and concentrated under reduced pressure. The resulting oil was purified by flash chromatography on silica gel. Elution with a gradient of 0-100% DCM/MeOH(0.1% AcOH) yielded alpha-hydroxy acid ((2R,3S)*-3.8**) (8.6 mg, 86% BRSM, d.r. 67.8% as determined by Mosher analysis).

^{1}H NMR ($CDCl_3$, 500 MHz) δ (ppm) 5.58 (dt, 15.4, 6.8 Hz, 1H), 5.42 (dd, 15.4, 7.6 Hz, 1H), 4.22 (d, 3.6, 1H), 2.68 (m, 1H), 2.02 (q, 6.9 Hz, 2H), 1.22-1.40 (m, 6H), 1.05 (d, 7.0, 3H), 0.89 (t, 6.7, 3H).

^{13}C NMR ($CDCl_3$, 125 MHz) δ (ppm) 177.4, 133.1, 130.1, 74.2, 40.7, 32.7, 31.5, 29.2, 22.7, 14.3, 14.2.

HRMS (ESI) *m/z*: Calculated: $(M-H)^-$ 199.1340. Actual: 199.1339. Δ ppm: -0.28.

Typical Mosher Esterification Procedure. The alcohol of interest, e.g., bemeth#23, was dissolved in DCM with DMAP and stirred under argon at ambient temperature. (*R*)-(+)-α-Methoxy-α-(trifluoromethyl)phenylacetyl chloride (1.2 equivalents) was added and the reaction stirred for 30 minutes and quenched with MeOH. The reaction was concentrated under reduced pressure, taken up in MeOH, and analyzed by UHPLC-MS.

(*(2R,3S,E)*-2-Hydroxy-3-methyl-dec-4-enoyl) alanine, bemeth#71 (3.13). 1-Hydroxybenzotriazole hydrate (HOBt) (1.7 mg, 0.01 mmol), N-(3-dimethylaminopropyl)-N'-ethyl-ethylcarbodiimide hydrochloride (EDC) (1 mg, 0.005 mmol), and N,N-dimethylaminopyridine (DMAP) (1.8 mg, 0.015 mmol) were added to a stirring solution of bemeth#23 (***(2R,3S)*-3.8**) (1 mg, 0.005 mmol) in DCM (400 µL) and stirred for 30 min. Alanine (1 mg, 0.01 mmol) was added to the solution and the reaction was stirred overnight. After 20 h the reaction was quenched with H_2O and extracted with DCM (3×2 mL), dried over $MgSO_4$, filtered, and concentrated under reduced pressure. The resulting solid was dissolved in 50:50 EtOAc/hexanes, run through a plug of silica gel, concentrated under reduced pressure, and the mixture of alanine conjugates (**3.14**) (1.1 mg, 84.6%)was analyzed by UHPLC-MS without further purification.

HRMS (ESI) *m/z*: Calculated: $(M-H)^-$ 270.1711. Actual: 270.1698. Δ ppm: -0.62.

Natural retention time: 12.44 min.

Synthetic retention times: 11.88 min, 11.97 min, 12.21 min, 12.49 min, 12.64 min.

(*(2R,3S,E)*-2-Hydroxy-3-methyl-dec-4-enoyl) serine, bemeth#81 (3.14). 1-Hydroxybenzotriazole hydrate (HOBt) (1.7 mg, 0.01 mmol), N-(3-dimethylaminopropyl)-N'-ethyl-ethylcarbodiimide hydrochloride (EDC) (1 mg, 0.005 mmol), and N,N-dimethylaminopyridine (DMAP) (1.8 mg, 0.015 mmol) were added to a stirring solution of bemeth#23 (***(2R,3S)*-3.8**) (1 mg, 0.005mmol) in DCM (400 µL) and stirred for 30 min. Serine (1.1 mg, 0.01 mmol) was added to the solution and the reaction was stirred overnight. After 20 hr the reaction was quenched with H_2O and extracted with DCM (3×2 mL), dried over $MgSO_4$, filtered, and concentrated under reduced pressure. The resulting solid was purified by flash

chromatography on silica gel. Elution with a gradient of 0-60% Hex/EtOAc yielded a mixture of serine conjugates (**3.14**) (1.0 mg, 71.4%) which were analyzed by UHPLC-MS without further purification.

Natural retention time: 11.34 min (major), 11.53 (minor)

Synthetic retention times: 11.08 min, 11.22 min, 11.34 min, 11.43 min, 11.53 min.

HRMS (ESI) *m/z*: Calculated: $(M+H)^+$ 286.1660. Actual: 286.1661. Δ ppm: 0.39.

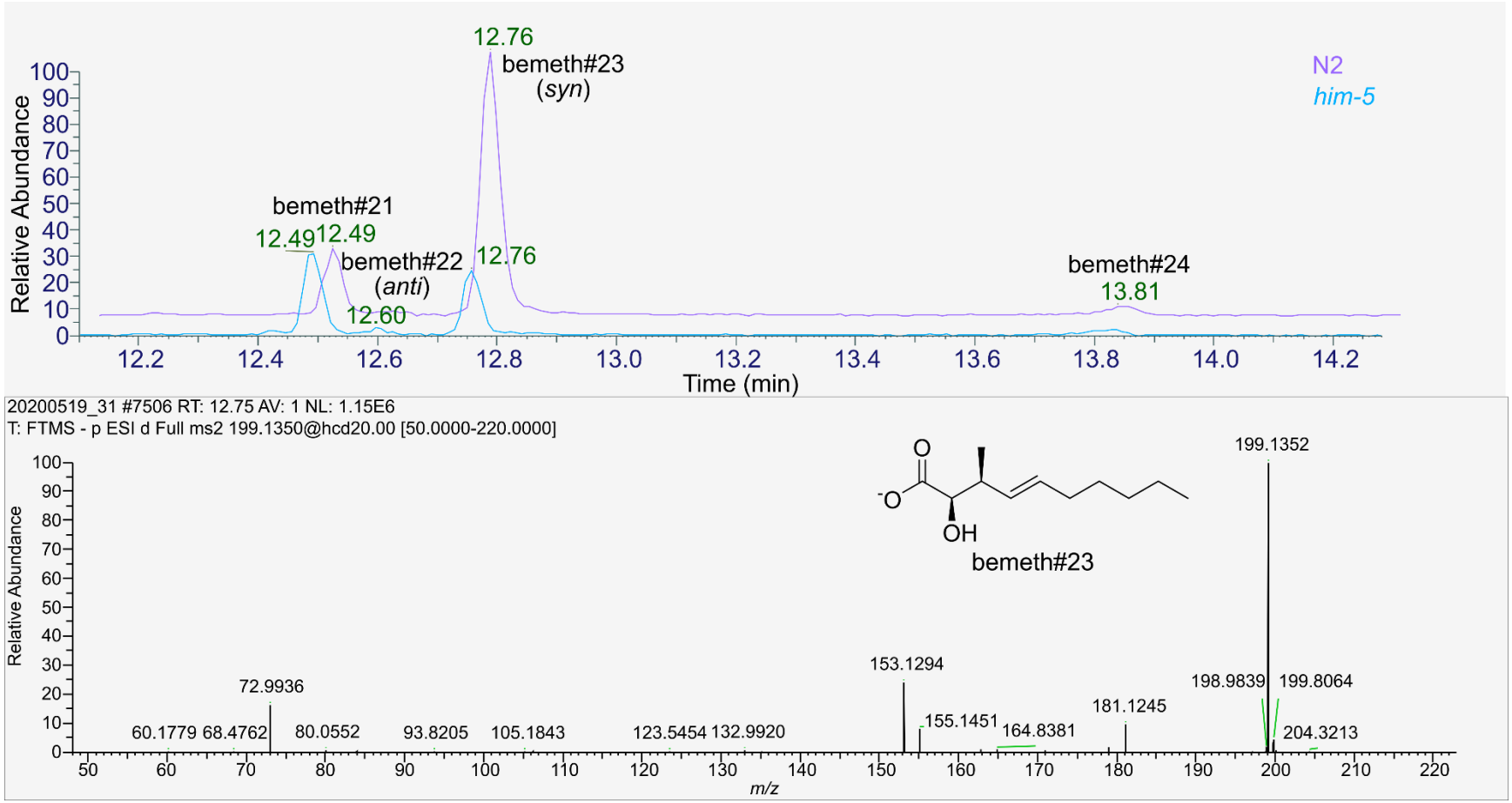

Supplemental Figure 3.1. MS and MS2 for bemeth#21-bemeth#24. EIC of *m/z* 199.1340 in N2 and *him-5* exo-metabolome samples showing peaks for bemeth#21through bemeth#24, and MS2 spectrum for bemeth#23 acquired from a *fem-3* (OE) exo-metabolome sample.

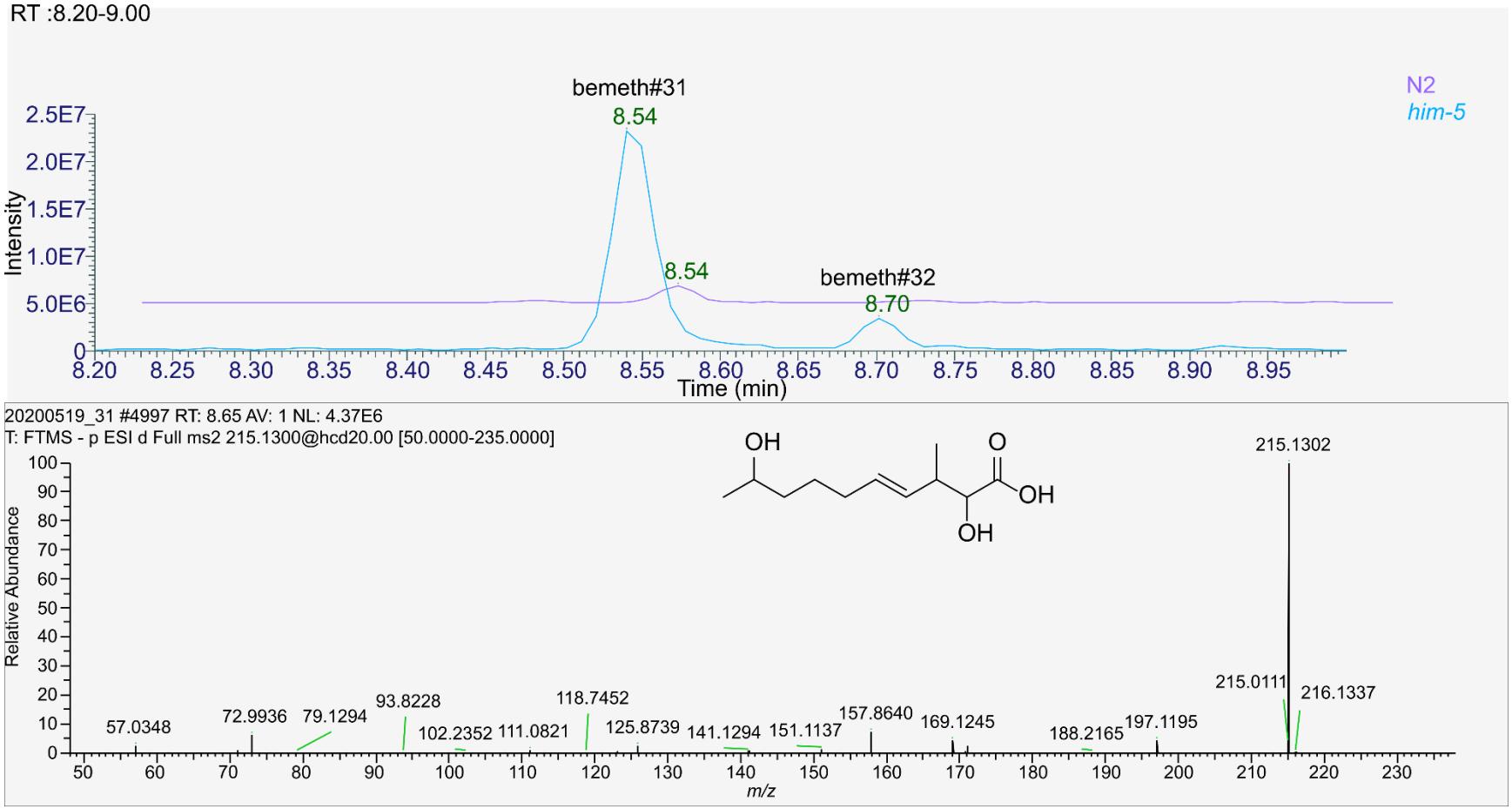

Supplemental Figure 3.2. MS and MS2 for bemeth#31 and bemeth#32. EIC of *m/z* 215.1287 in N2 and *him-5* exo-metabolome samples showing peaks for bemeth#31 and bemeth#32 and MS2 spectrum of bemeth#31 acquired from a *fem-3* (OE) exo-metabolome sample.

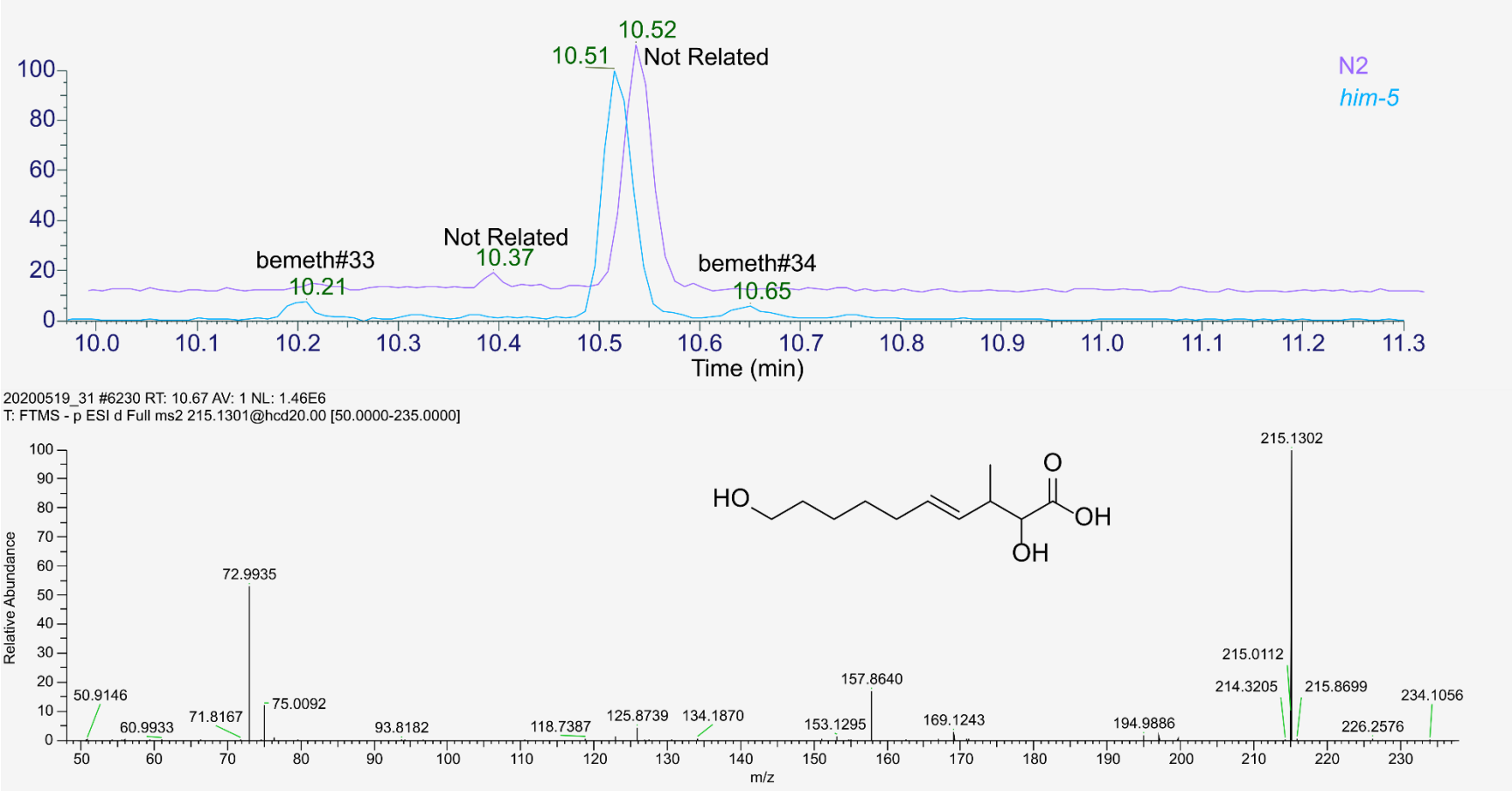

Supplemental Figure 3.3. MS and MS2 for bemeth#33 and bemeth#34. EIC of *m/z* 215.1287 in N2 and *him-5* exo-metabolome samples showing the peak for bemeth#33 and bemeth#34 and MS2 spectrum for bemeth#34 acquired from a *fem-3* (OE) exo-metabolome sample.

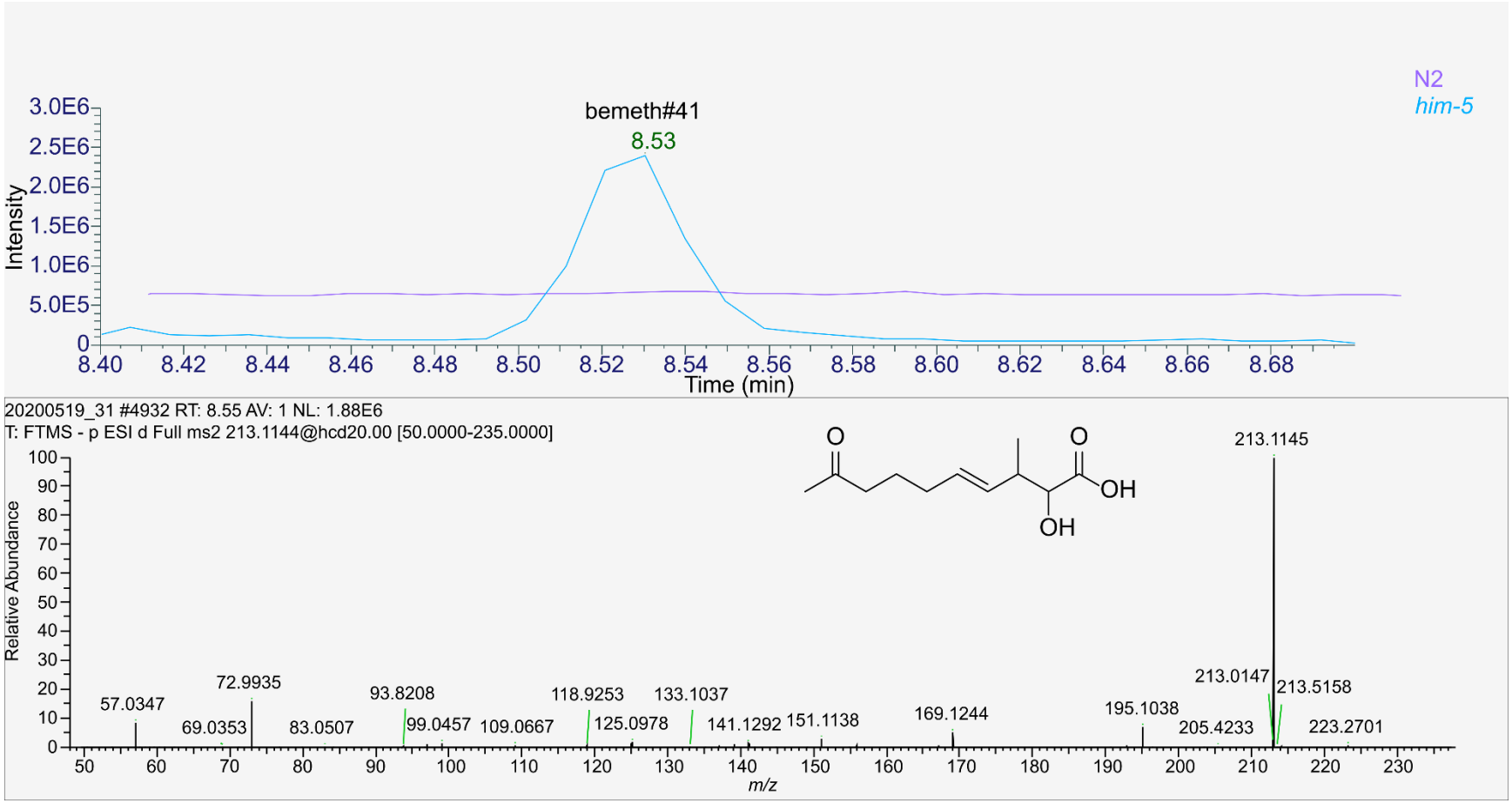

Supplemental Figure 3.4. MS and MS2 for bemeth#41. EIC of *m/z* 213.1134 in N2 and *him-5* exo-metabolome samples showing peaks for bemeth#41 and MS2 spectrum for bemeth#41 acquired from a *fem-3* (OE) exo-metabolome sample. The theorized isomer, bemeth#42, is not observed.

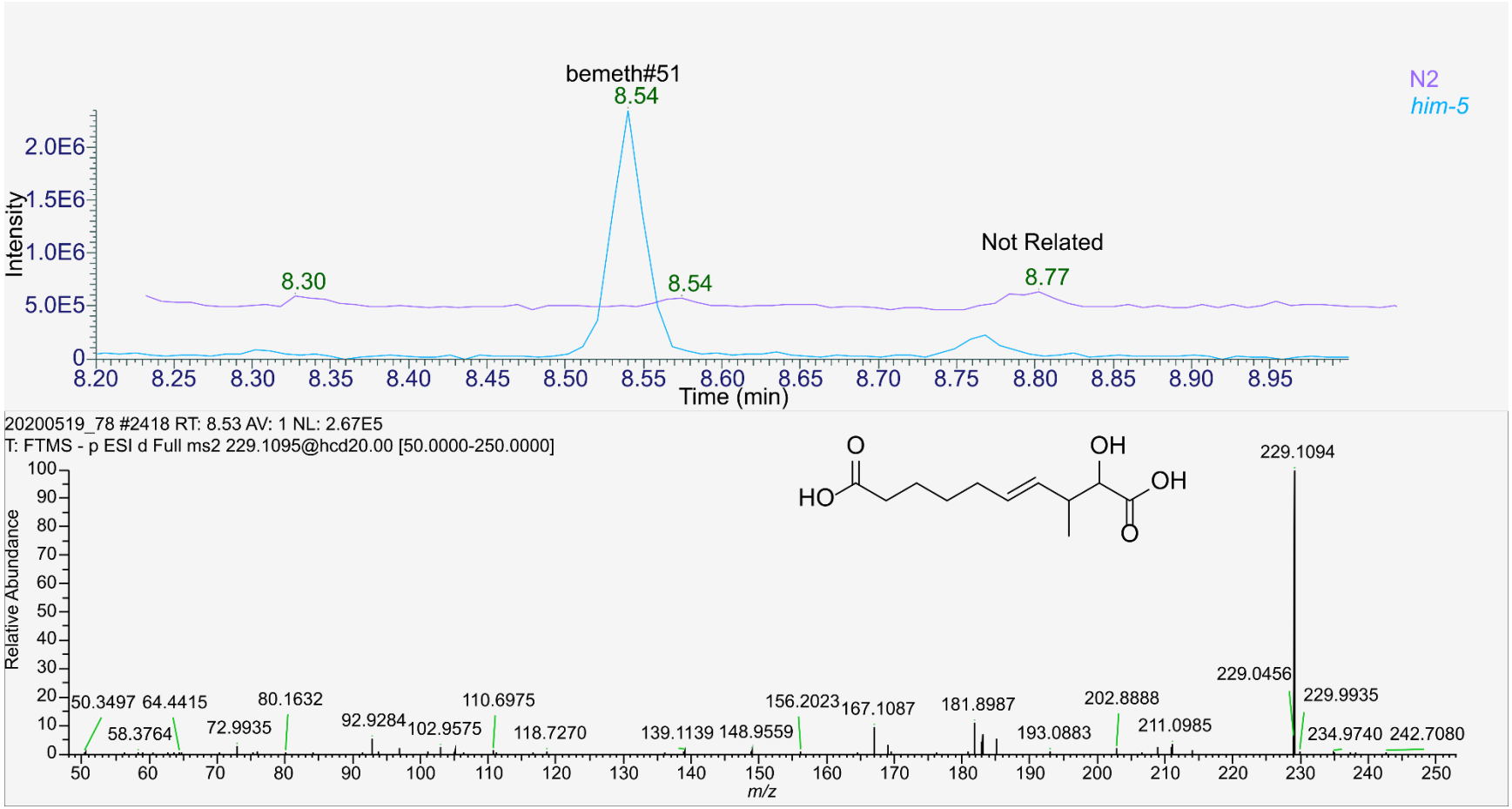

Supplemental Figure 3.5. MS and MS2 for bemeth#51. EIC of *m/z* 229.1085 in N2 and *him-5* exo-metabolome samples showing peaks for bemeth#51 and MS2 spectrum of bemeth#51 acquired from a *him-5* exo-metabolome sample. The theorized isomer, bemeth#52, is not observed.

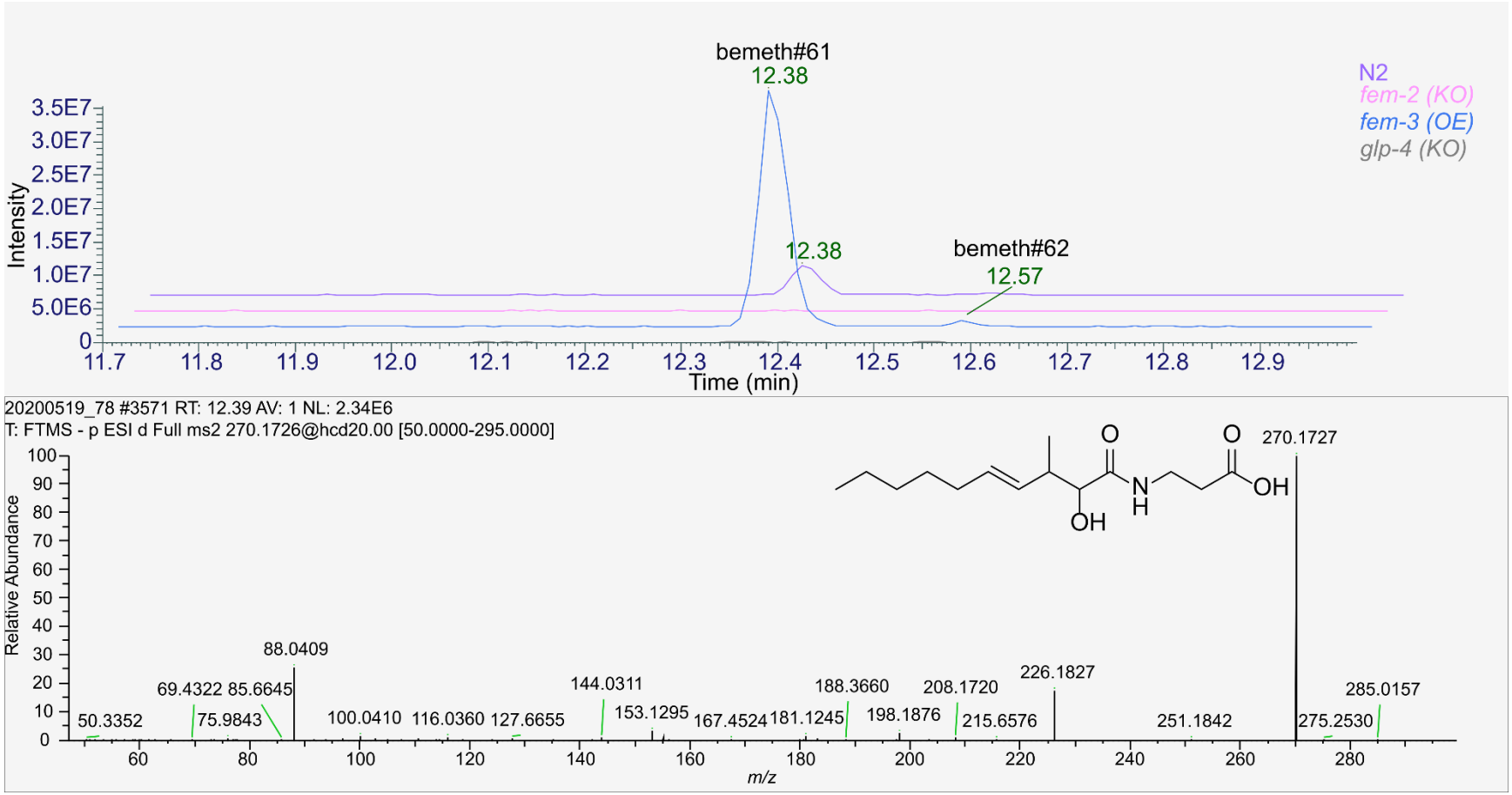

Supplemental Figure 3.6. MS and MS2 for bemeth#61 and bemeth#622. EIC of *m/z* 270.1702 in N2, *fem-2* (KO), *fem-3* (OE), and *glp-4* (KO) exo-metabolome samples showing peaks for bemeth#61 and bemeth#62 and MS2 spectrum of bemeth#61 acquired from a *fem-3* (OE) exo-metabolome sample.

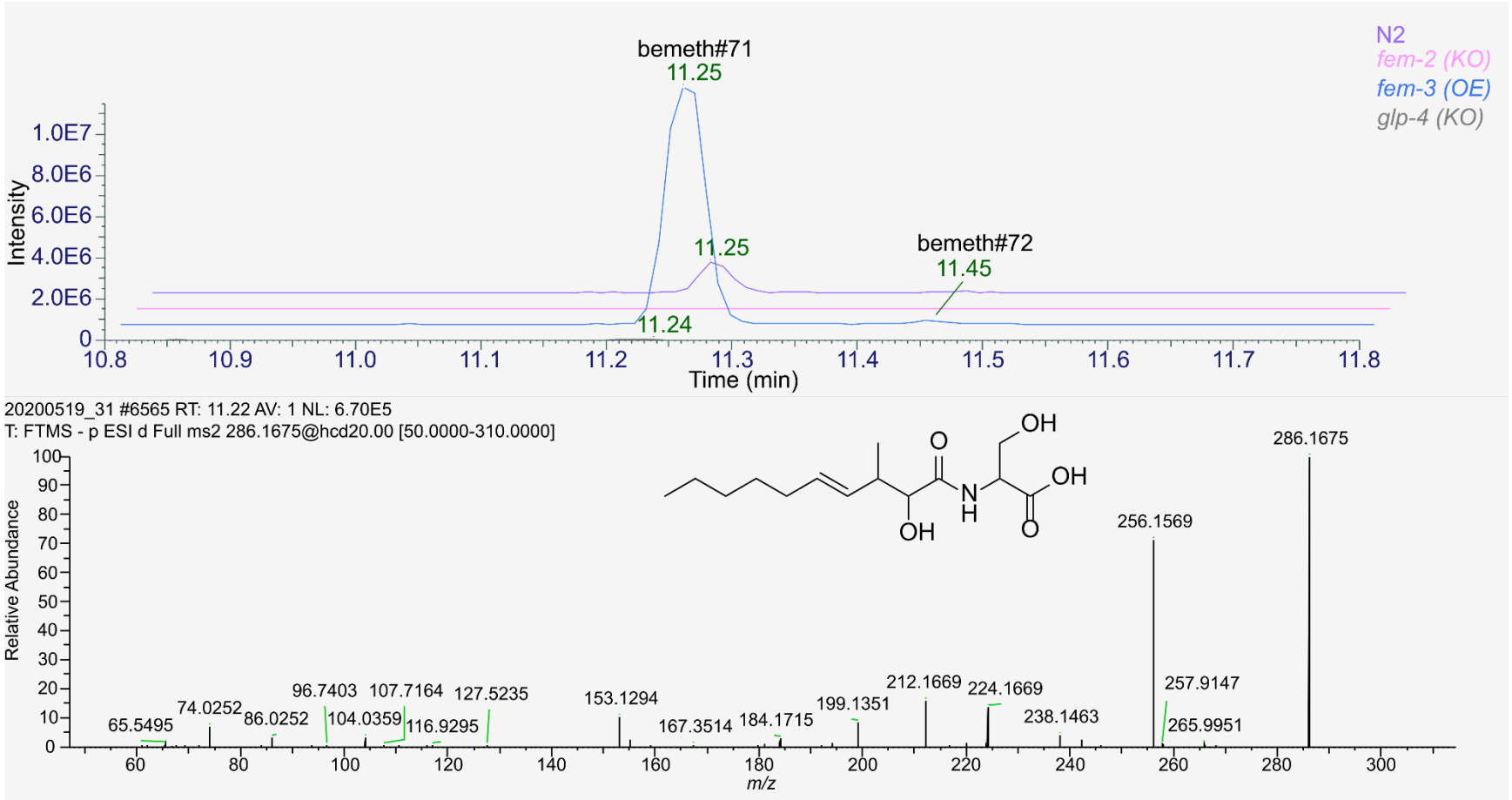

Supplemental Figure 3.7. MS and MS2 for bemeth#71 and bemeth#72. EIC of *m/z* 286.1656 in N2, *fem-2* (KO), *fem-3* (OE), and *glp-4* (KO) exo-metabolome samples showing peaks for bemeth#71 and bemeth#72 and MS2 spectrum of bemeth#71 acquired from a *fem-3* (OE) exo-metabolome sample.

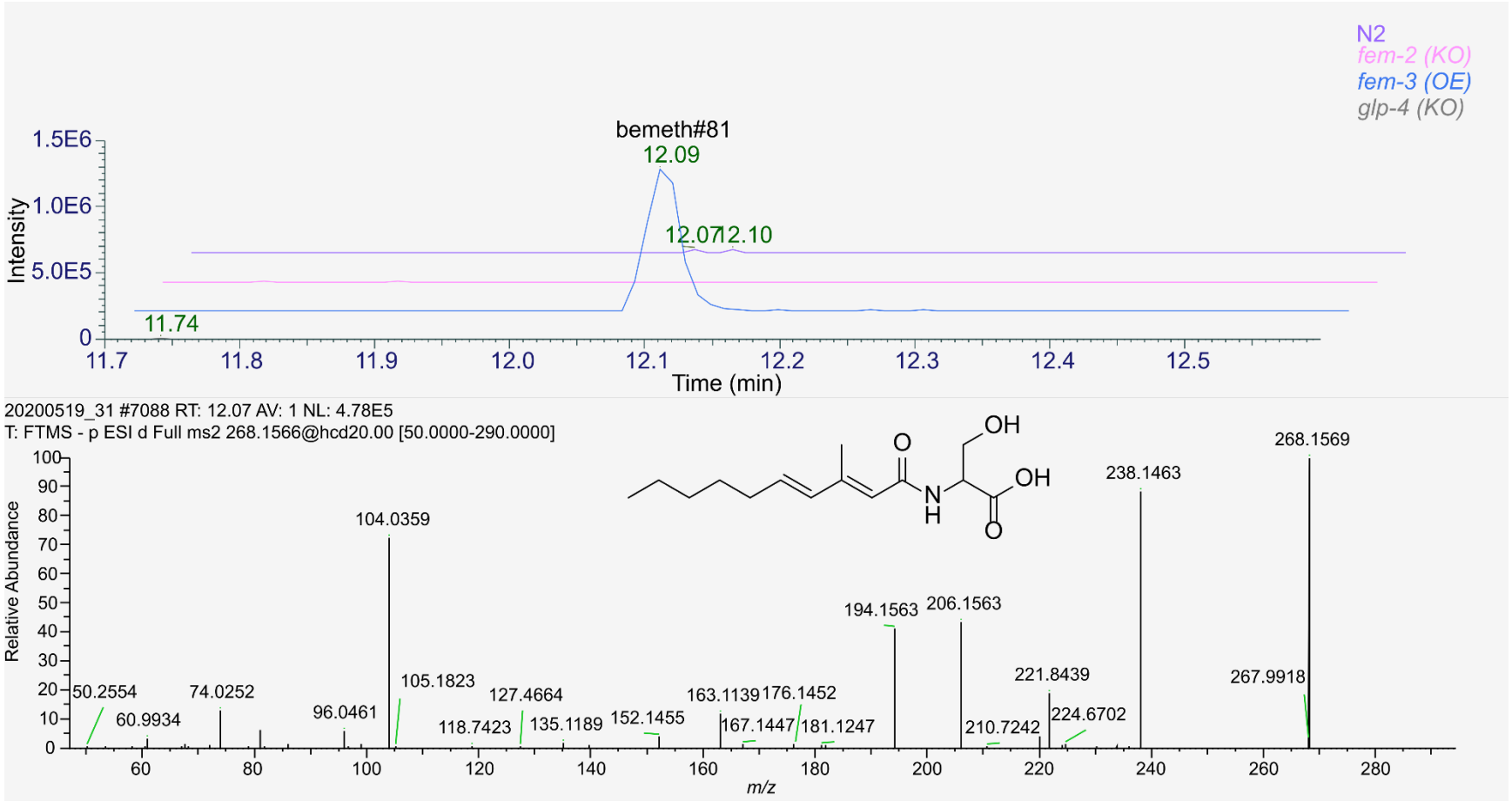

Supplemental Figure 3.8. MS and MS2 for bemeth#81. EIC of *m/z* 268.1551 in N2, *fem-2* (KO), *fem-3* (OE), and *glp-4* (KO) exo-metabolome samples showing peaks for bemeth#81 and MS2 spectrum for bemeth#81 acquired from a *fem-3* (OE) exo-metabolome sample.

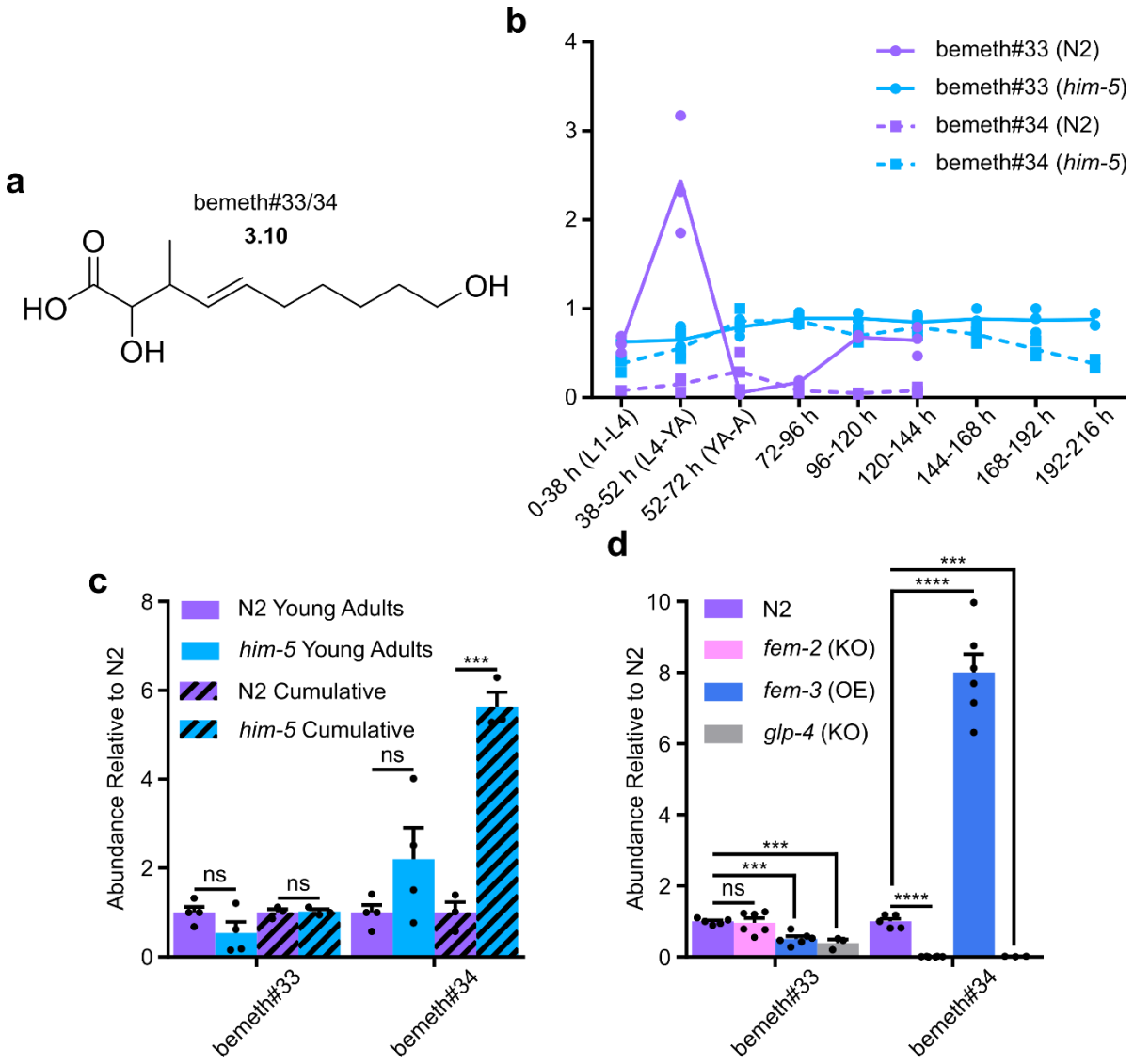

Supplemental Figure 3.9. Quantification of bemeth#33 in the endo-metabolome of N2 and *him-5*. **a.** Structure of bemeth#33. **b.** Quantification of bemeth#33 excretion through development and adulthood by UHPLC-MS in N2 and *him-5*. **c.** Quantification of bemeth#33 in N2 and *him-5* cultures harvested as young adults.

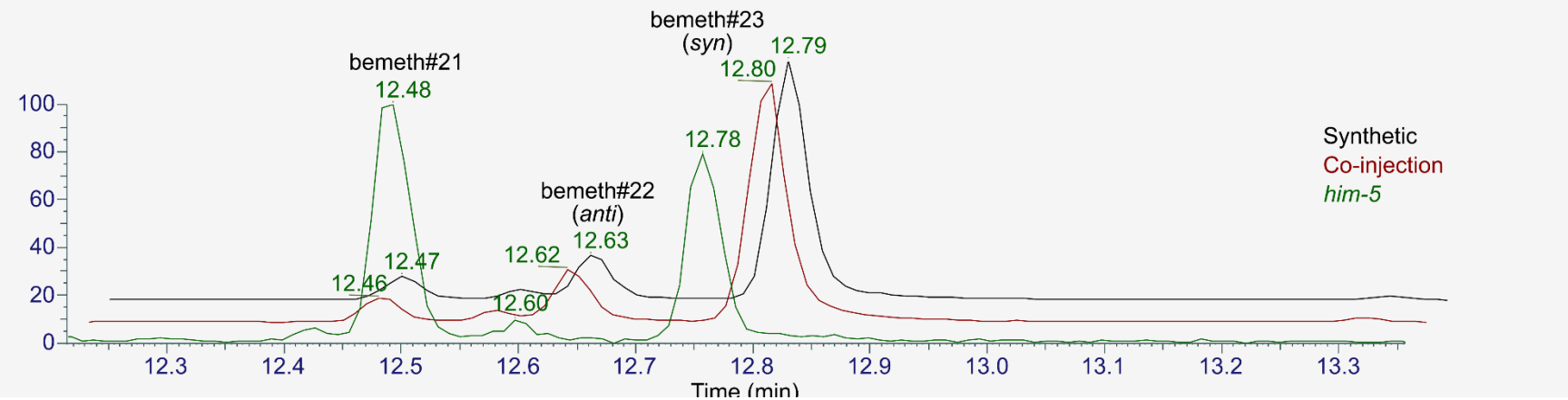

Supplemental Figure 3.10. Comparison of natural and synthetic bemeth# isomers. EIC of *m/z* 199.1340 for a synthetic sample of bemeth#21 through bemeth#23 (black), a *him-5* exo-metabolome sample (green), and co-injection (brown).

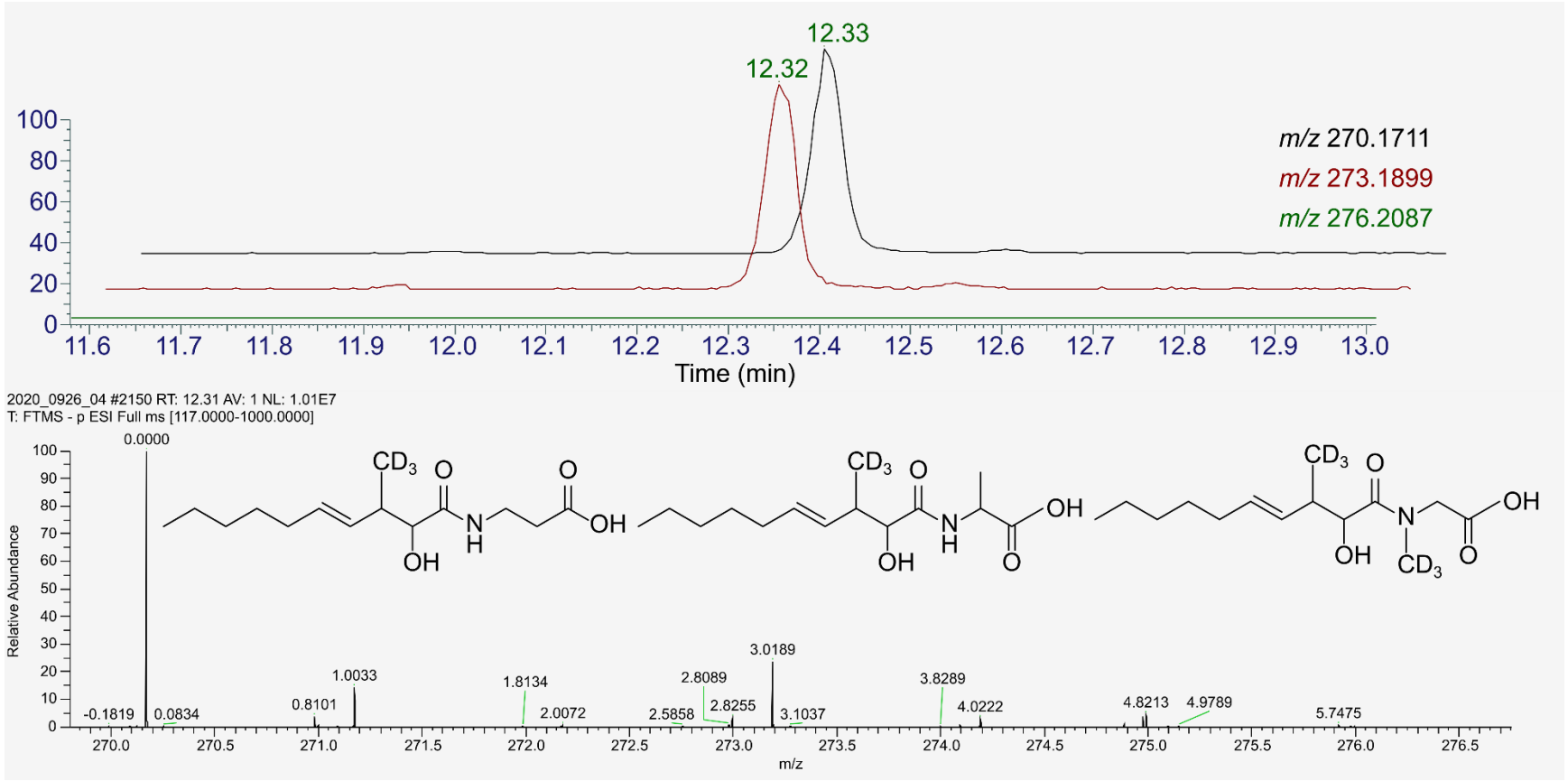

Supplemental Figure 3.11. D_3-Methionine labeling of bemeth#61 and bemeth#62. EIC of bemeth#61 and bemeth#62 in the exo-metabolome of D_3-methionine-fed *him-5* and the isotope pattern observed.

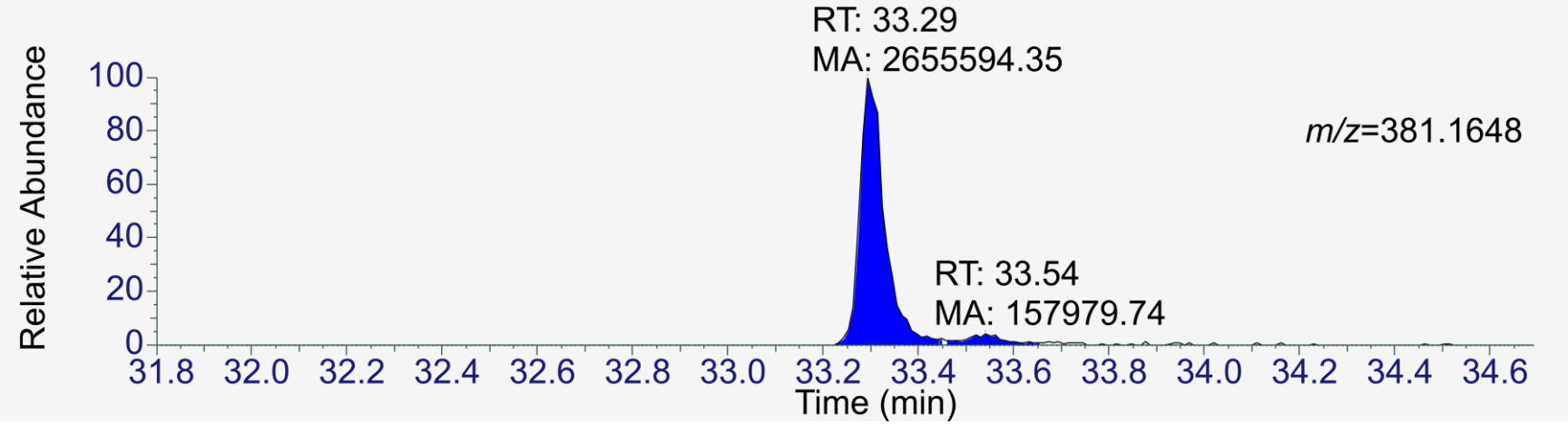

Supplemental Figure 3.12. Chromatography for e.e. calculation of alcohol (*S*)-3.23. Integration of the EIC after Mosher derivatization yielded an e.e. of 88.77% for the Sharpless epoxidation that resulted in **(*S*)-3.23**.

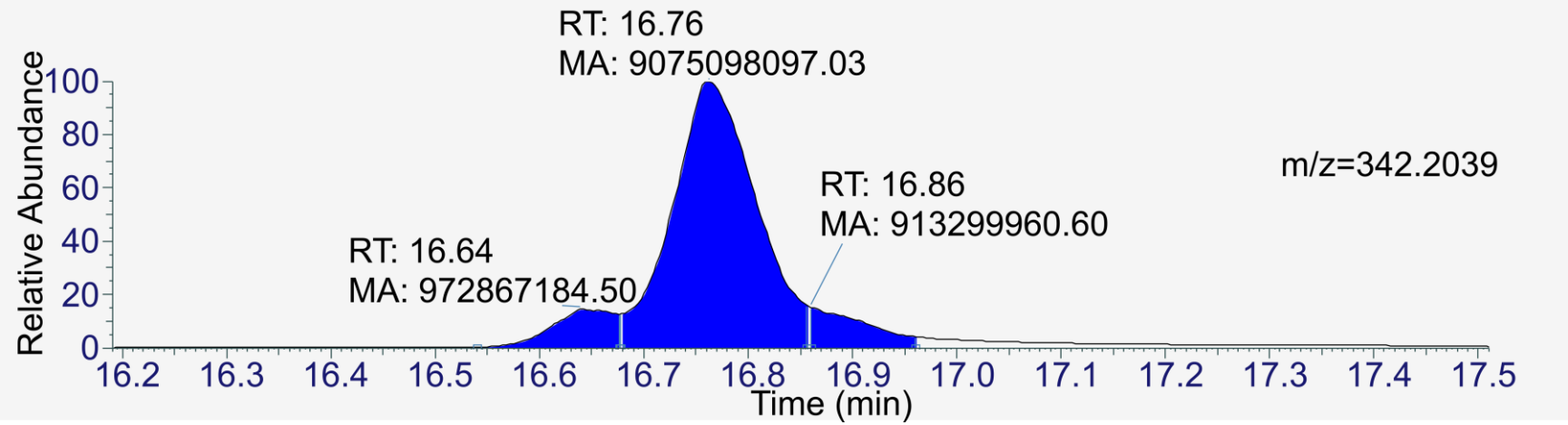

Supplemental Figure 3.13. Chromatography for e.e. caluculation of bemeth#1. Integration of the EIC after derivatization of bemeth#1 with 2,2,2-trifluoro-1-phenethylamine yielded three peaks, the earliest of which is likely the result of double bond migration. Calculation of e.e. including both non-desired isomers was found to be 65.58%.

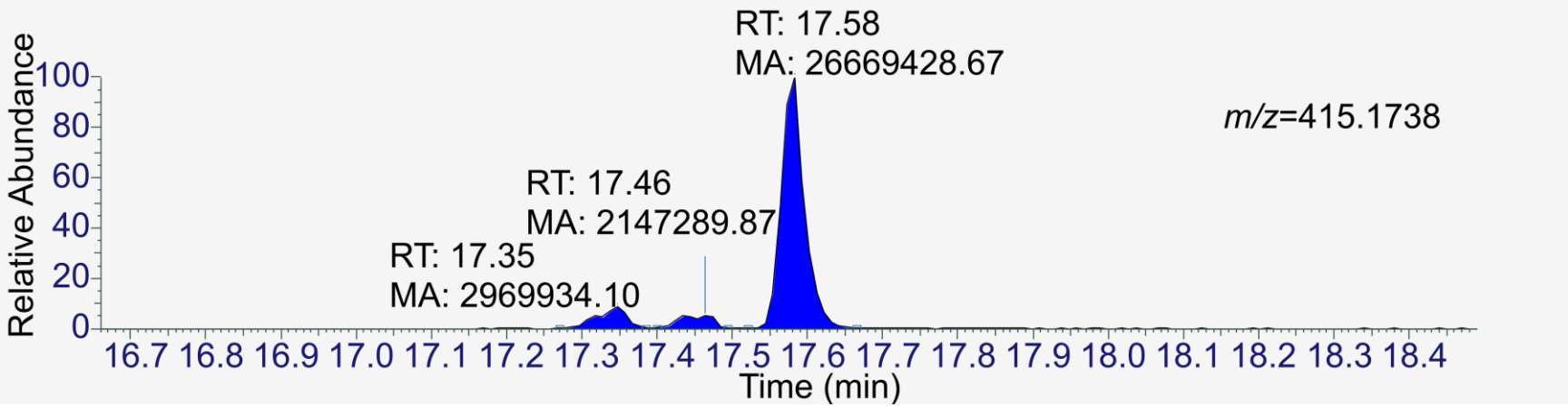

Supplemental Figure 3.14. Chromatography for e.e. calculation of synthetic bemeth#23. Integration of the EIC after Mosher derivatization of synthetic bemeth#23 yielded a d.r. of 67.80%

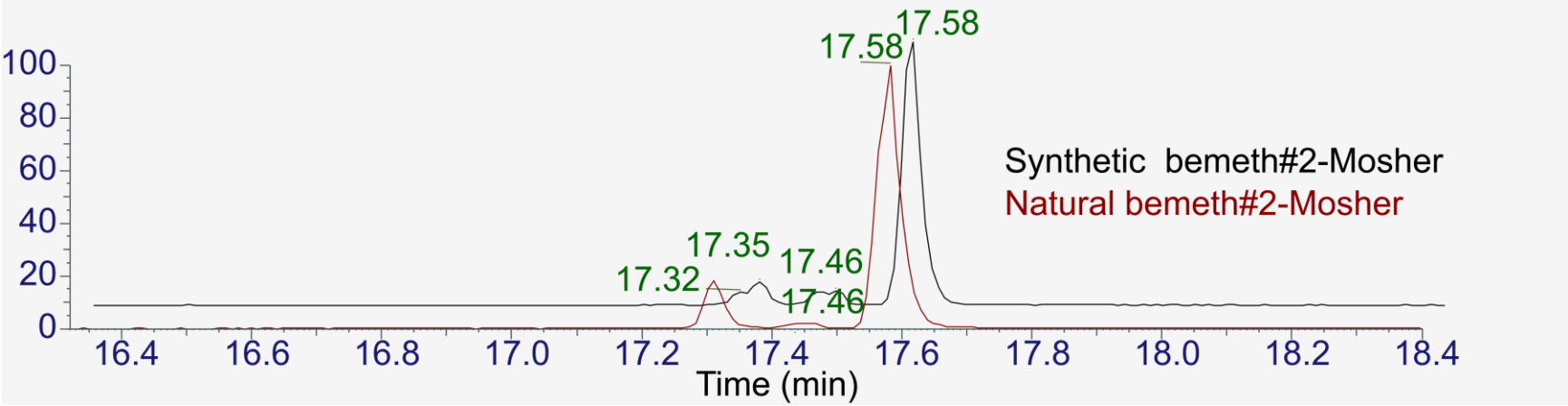

Supplemental Figure. 3.15. Chromatography of synthetic and natural bemeth#23 with (*R*)-MTPA-Cl. EIC of *m/z* 415.1738 shows that the predominant synthetic diastereomer (bemeth#23), when reacted with (*R*)-MTPA-Cl, is the same as the predominant natural diastereomer reacted with (*R*)-MTPA-Cl.

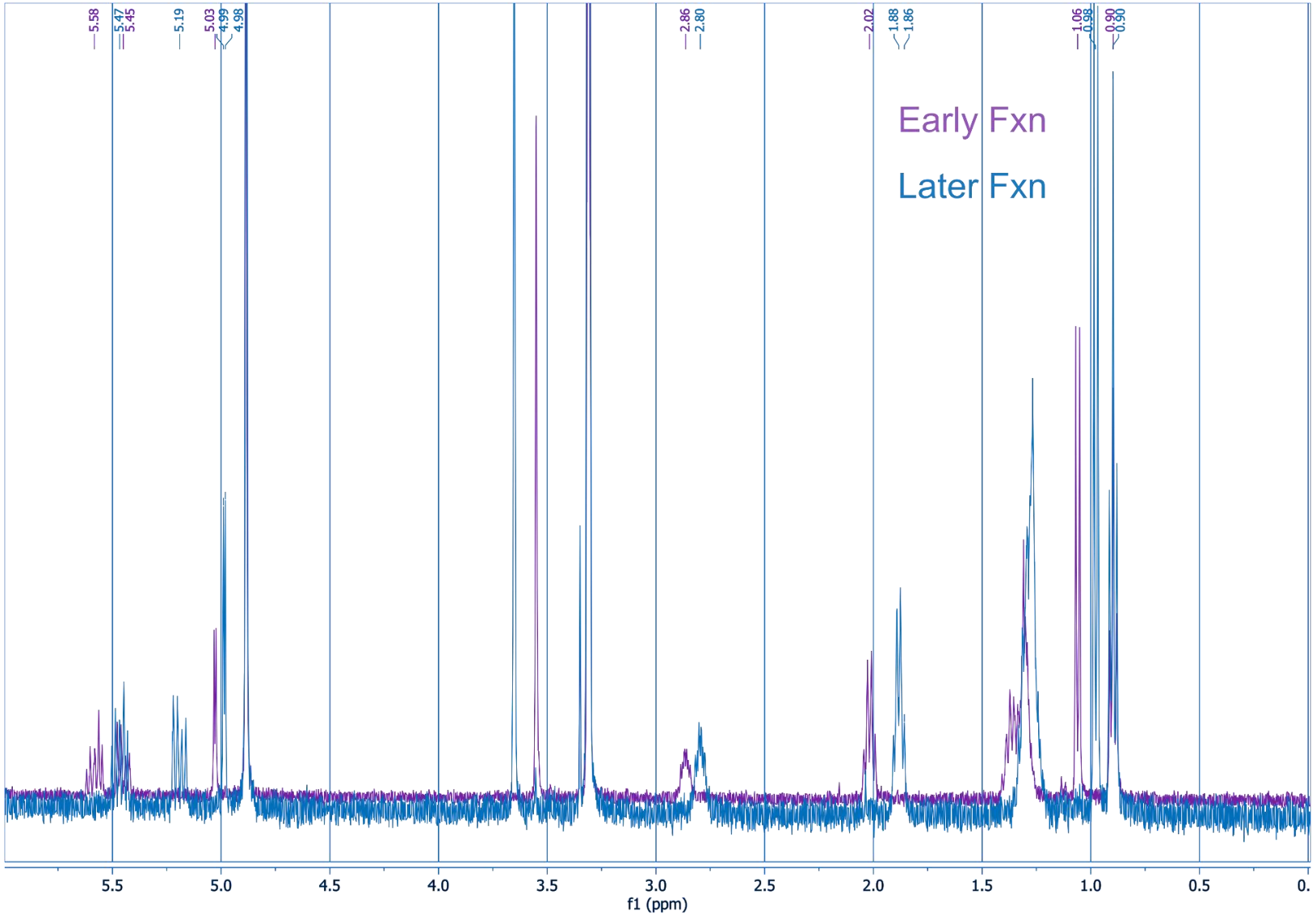

Supplemental Figure 3.16. Comparison of ^{1}H NMR spectra for Mosher analysis. Overlay of the ^{1}H NMR spectra (400 MHz, CD_3OD) for and earlier and later eluting diastereomers, (2*S*,3*R*)- (2*R*,3*S*)-bemeth#2 reacted with (*R*)-MTPA-Cl, respectively**.** NMR spectra were obtained by Dr. Ying Zhang.

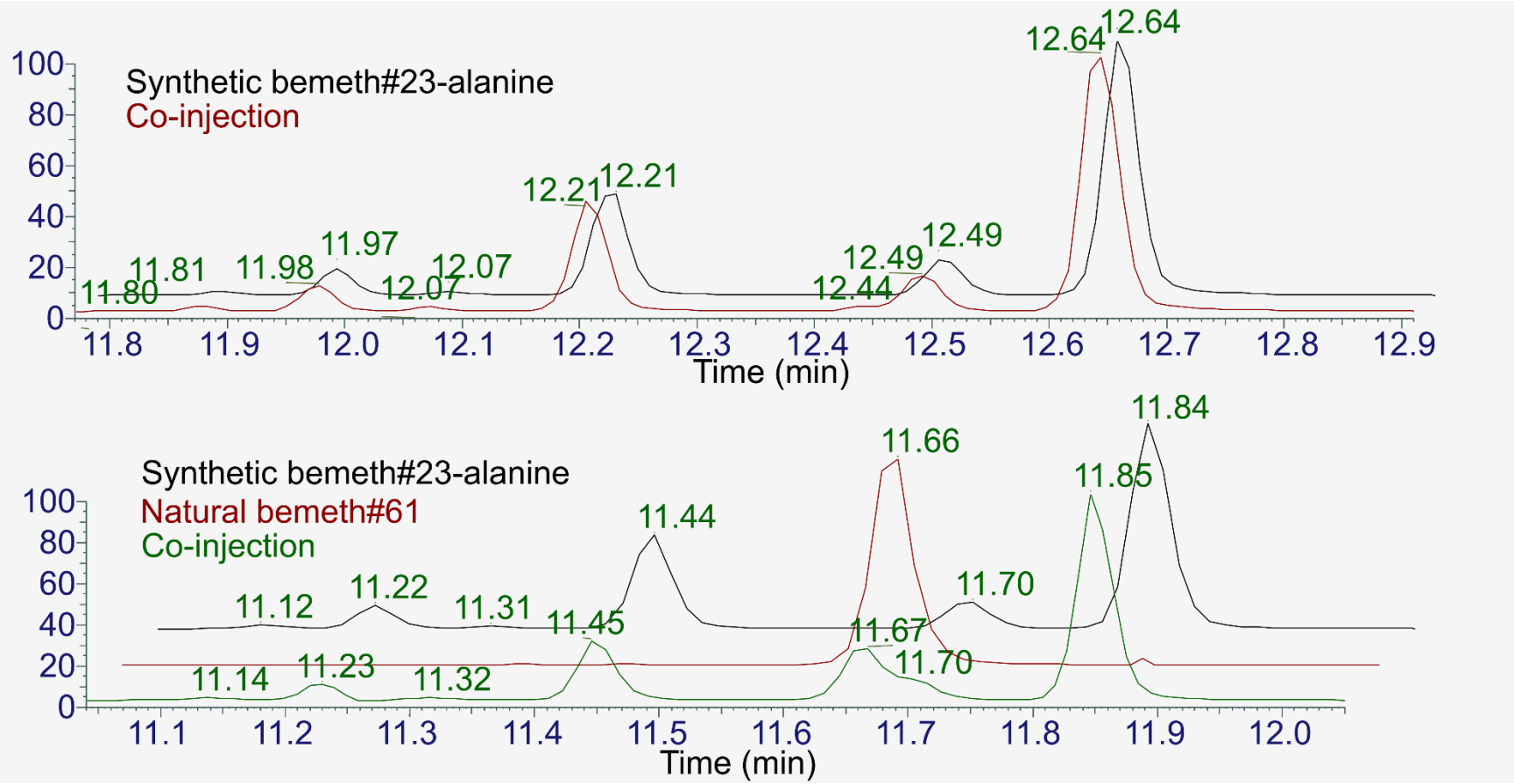

Supplemental Figure 3.17. Comparison of natural bemeth#61 with bemeth#23 conjugated to alanine. EIC of *m/z* 270.1551 in synthetic bemeth#23-alanine conjugate and *fem-3* (OE) exo-metabolome samples and co-injections show that natural bemeth#61 does not co-elute with any of the synthetic bemeth#23-alanine conjugates.

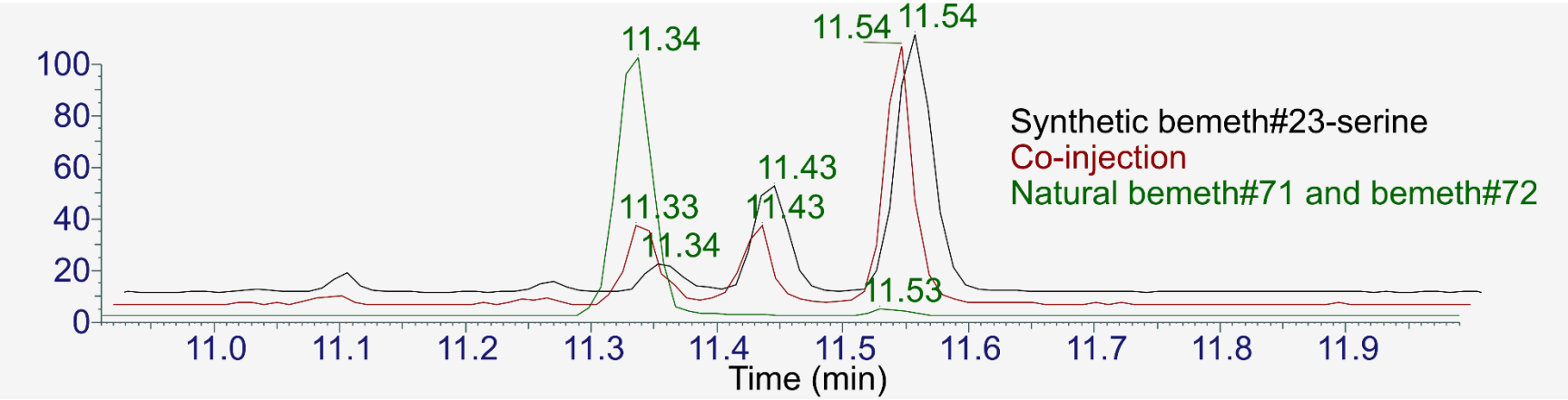

Supplemental Figure 3.18. Comparison of natural bemeth#71 and bemeth#72 with bemeth#23 conjugated to serine. EIC for *m/z* 286.1660 in synthetic bemeth#2-serine conjugate *fem-3* (OE) exo-metabolome samples and a co-injection show that natural bemeth#71 and bemeth#72 co-elute with the synthetic bemeth#23-serine conjugates at 11.34 and 11.54 min.

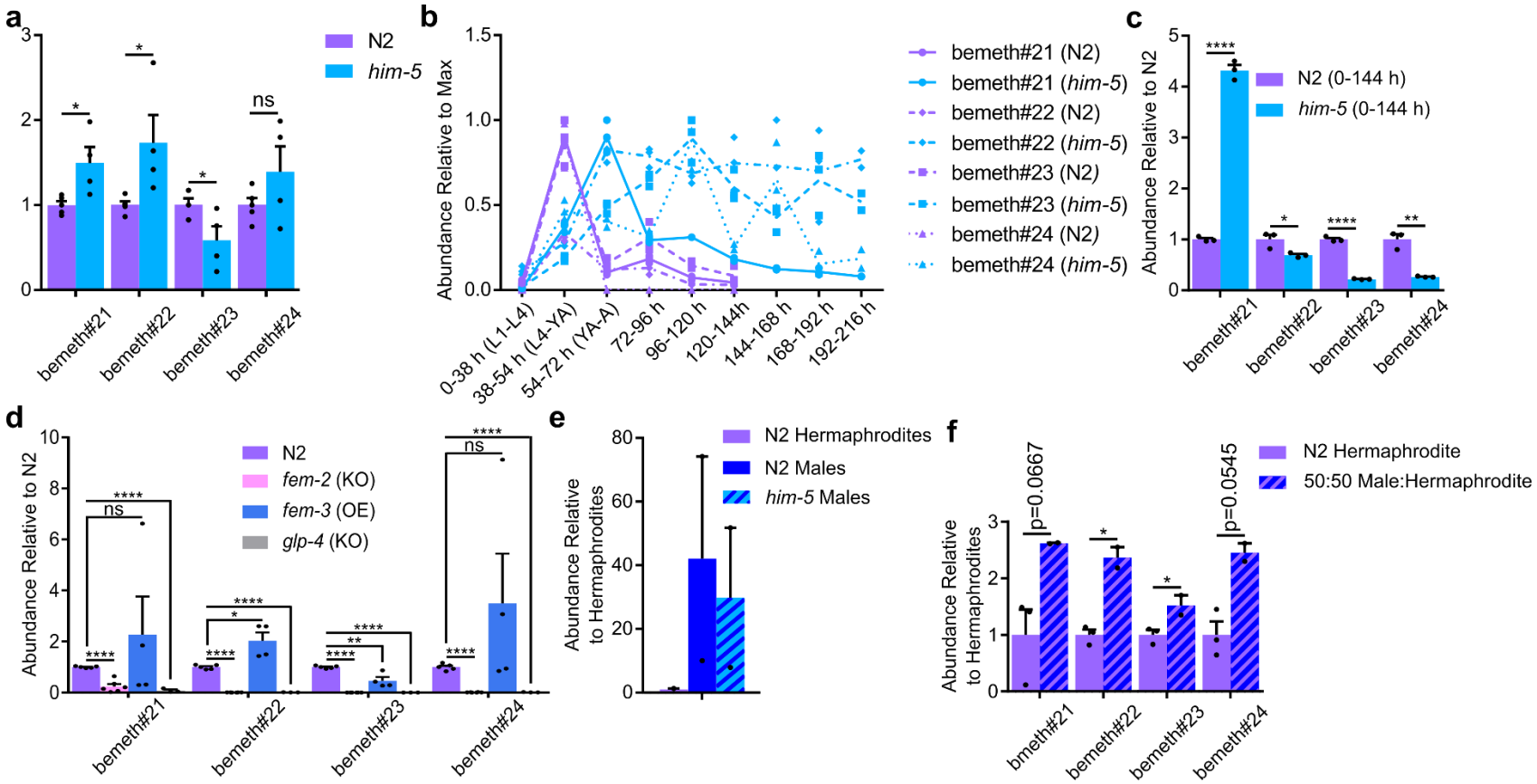

Supplemental Figure 3.19. Enrichment of bemeth#21-bemeth#24. **a.** Of the four bemeth#-family compounds with the formula $C_{11}H_{20}O_3$, two are enriched in the exo-metabolome of *him-5* cultures, one is enriched in the exo-metabolome of N2 cultures, and one is not differential. **b.** In hermaphrodites excretion of bemeth#21-bemeth#24 peaks during the L4-YA transition and decreases while in *him-5* cultures, excretion is more constant through adulthood. **c.** When cumulative levels of bemeth#21-bemeth#24 excretion are examined bemeth#21 is significantly enriched in the exo-metabolome of *him-5* cultures while the others are observed at lower levels. **d.** bemeth#21-bemeth#24 are greatly reduced or absent in *fem-2* (KO) and *glp-4* (KO) animals while their expression in *fem-3* (OE) roughly mirrors that of *him-5* though not significant in the case of bemeth#21. **e.** In small cultures only bemeth#23 is detected at elevated levels in N2 and *him-5* males. **f.** In the exo-metabolome of 50:50 male:hermaphrodite cultures bemeth#21-bemeth#24 are all enriched though not always significantly with only two replicates available. Data are presented as mean ± s.e.m. *, p≤0.05; **, p≤0.005, ***, p≤0.0005; ****, p≤0.0001; ns, not statistically significant.

NMR Spectra of Synthetic Compounds,

***(E)*-4-Hydroxy-non-2-ene (3.23), ^{1}H NMR spectrum (500 MHz, $CDCl_3$)**

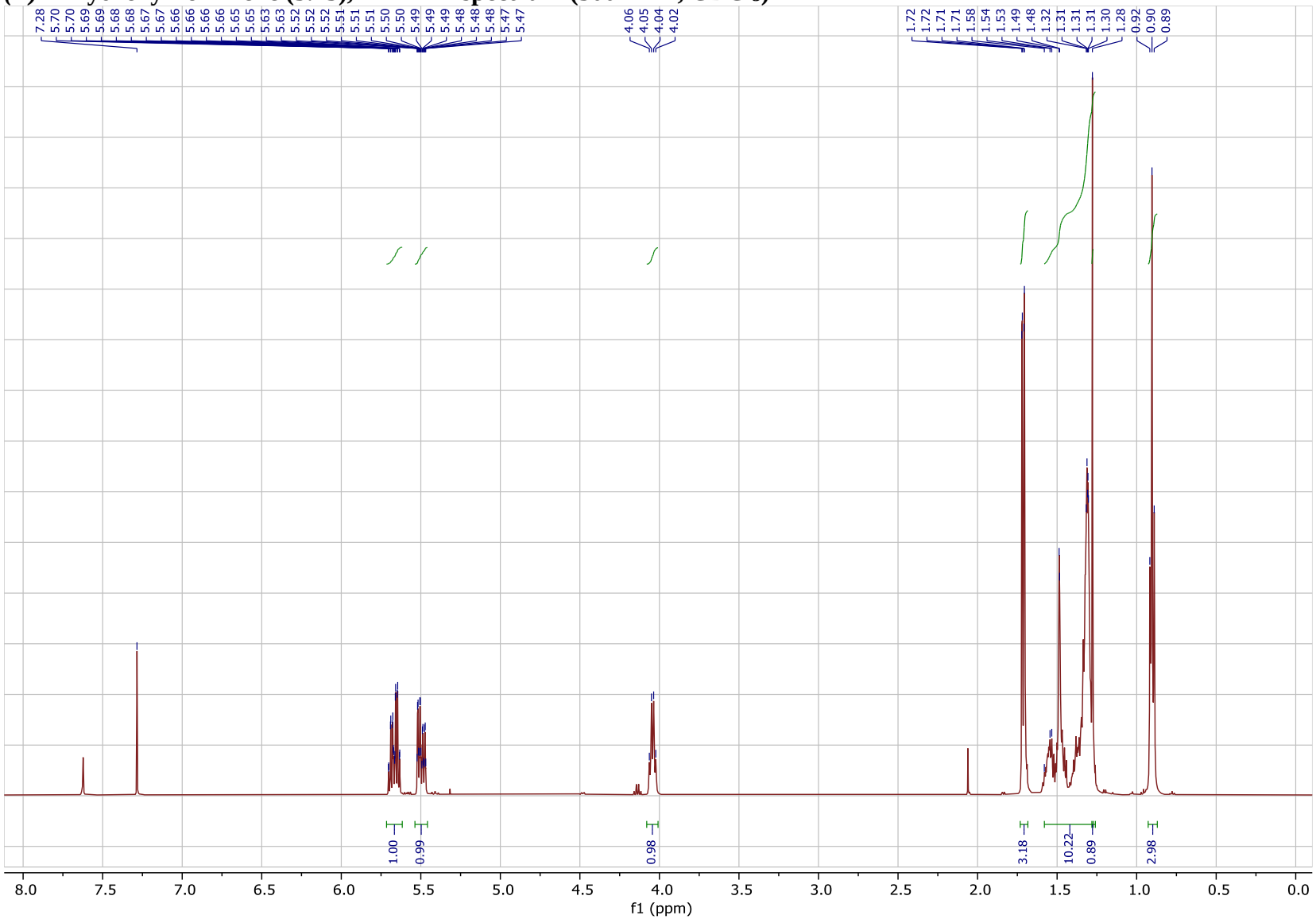

***(E)*-4-Hydroxy-non-2-ene (3.23), ^{13}C NMR spectrum (125 MHz, $CDCl_3$)**

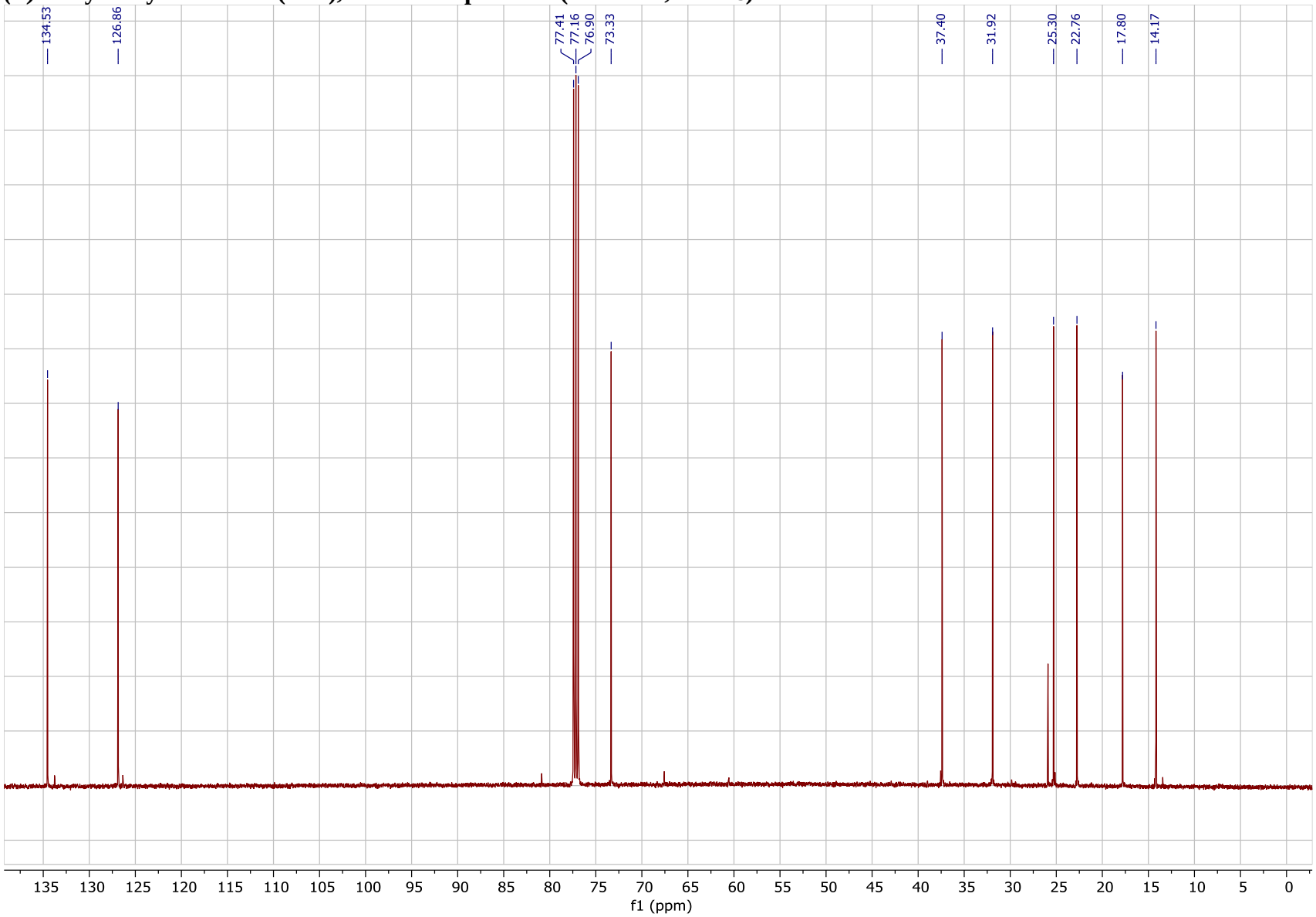

***(S,E)*-4-(Vinyloxy)-non-2-ene (3.20), ^{1}H NMR spectrum(500 MHz, $CDCl_3$)**

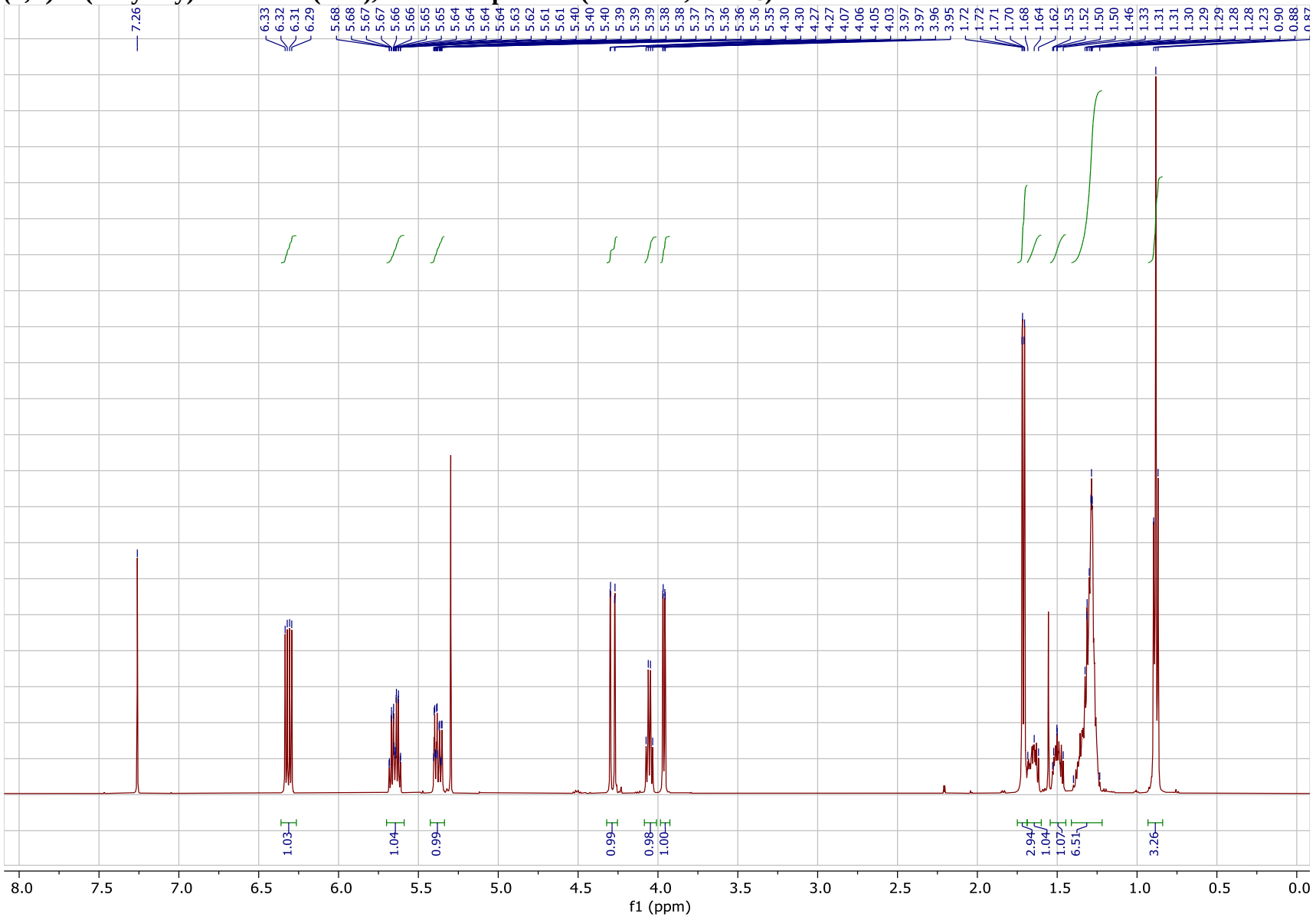

***(S,E)*-4-(Vinyloxy)-non-2-ene (3.20), ^{13}C NMR spectrum (125 MHz, $CDCl_3$)**

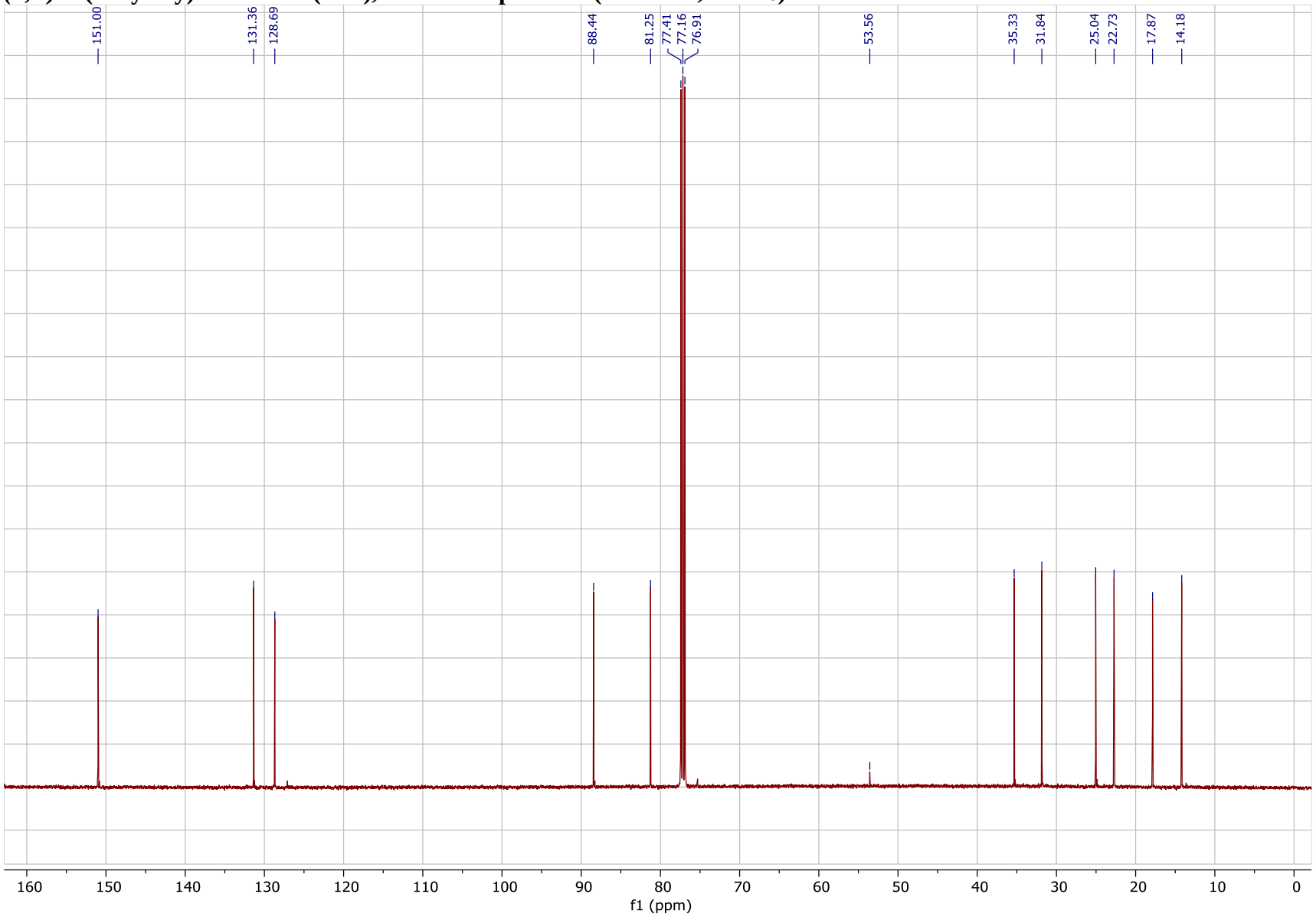

***(R,E)*-3-Methyl-dec-4-enal (3.19), ^{1}H NMR spectrum (500 MHz, $CDCl_3$)**

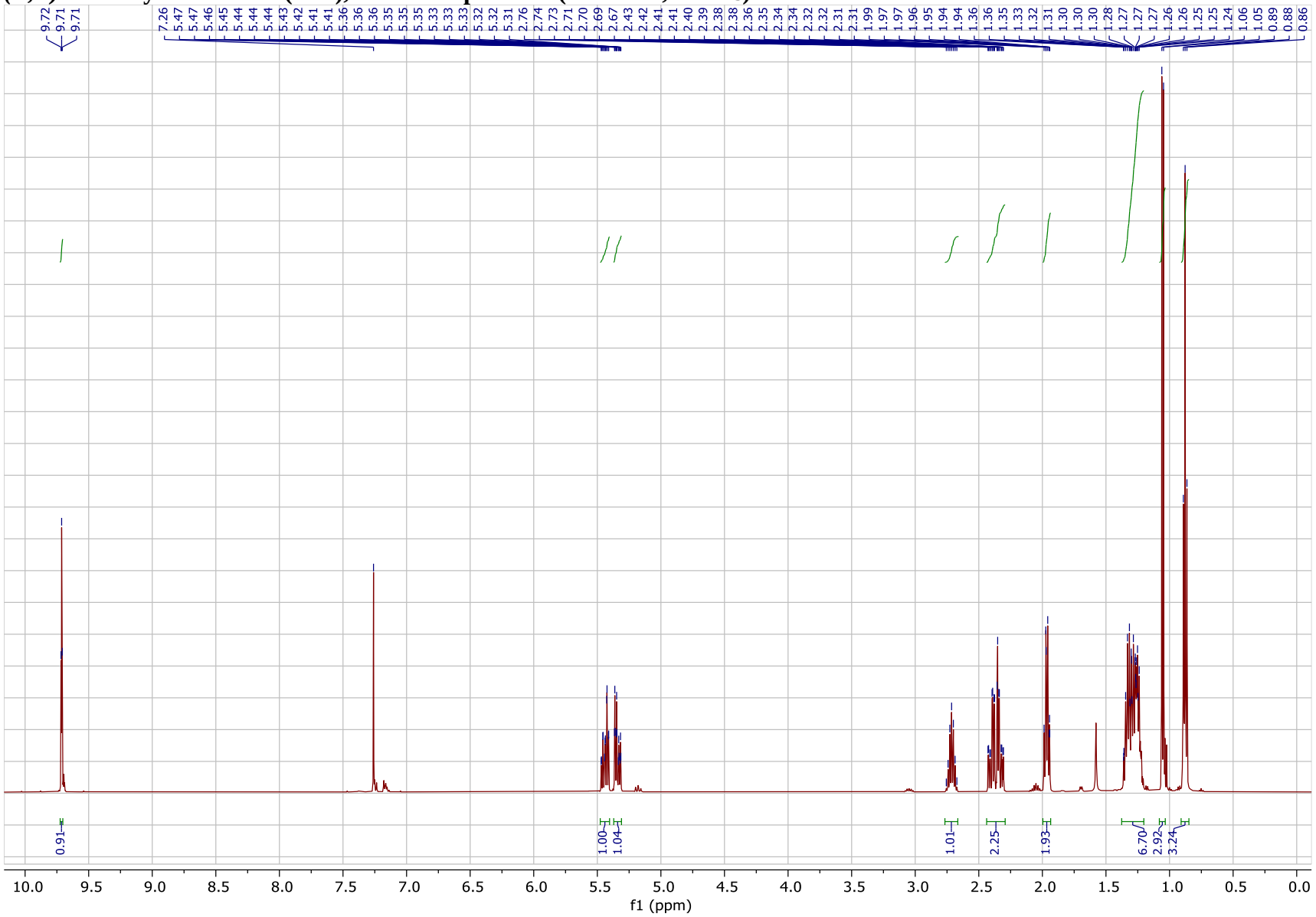

***(R,E)*-3-Methyl-dec-4-enal (3.19), ^{13}C NMR spectrum (125 MHz, $CDCl_3$)**

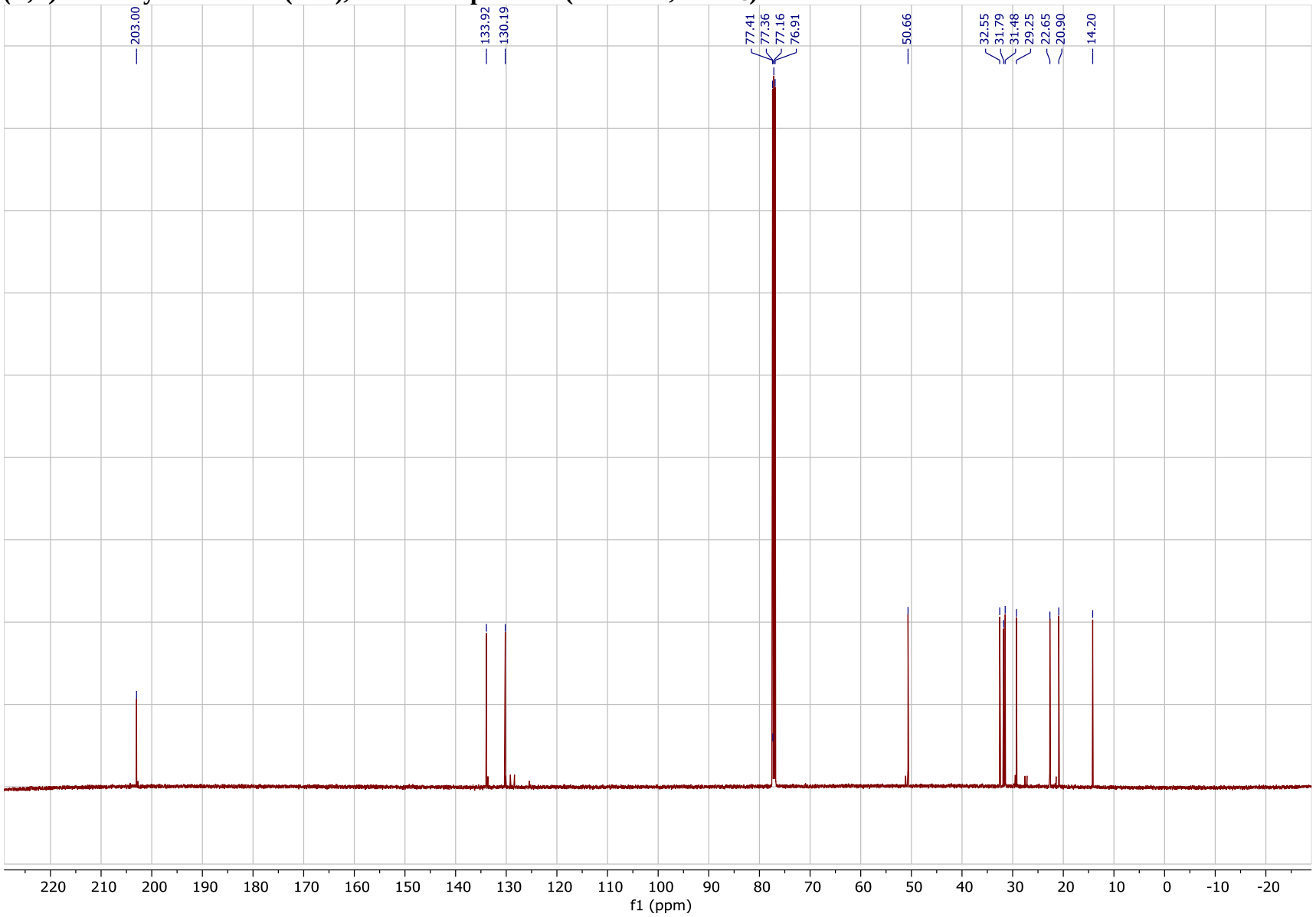

***(R,E)*-3-Methyl-dec-4-enoic acid, bemeth#1 (*(R)*-3.4), ^{1}H NMR spectrum (500 MHz, $CDCl_3$)**

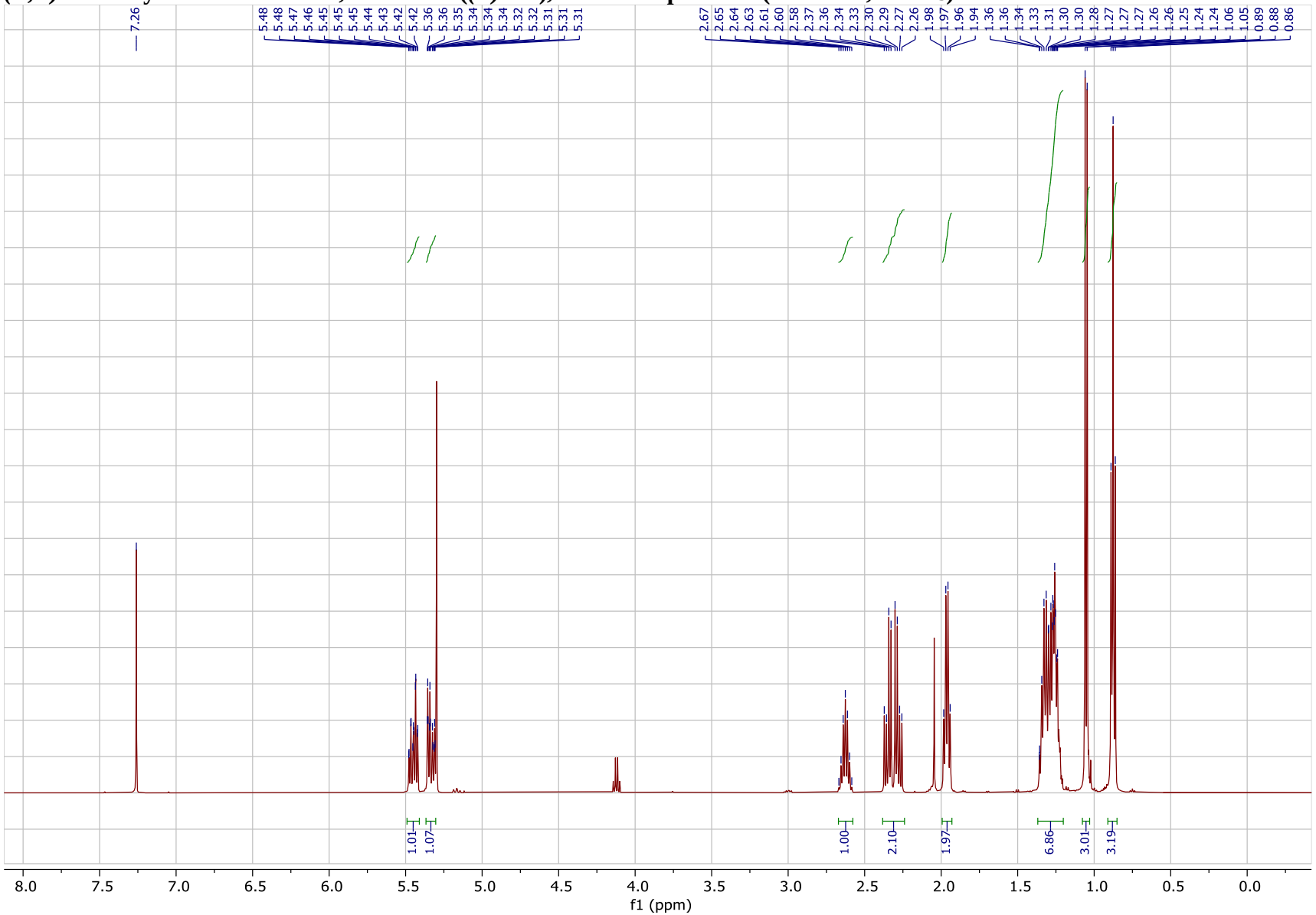

***(R,E)*-3-Methyl-dec-4-enoic acid, bemeth#1 (*(R)*-3.4), ^{13}C NMR spectrum(125 MHz, $CDCl_3$)**

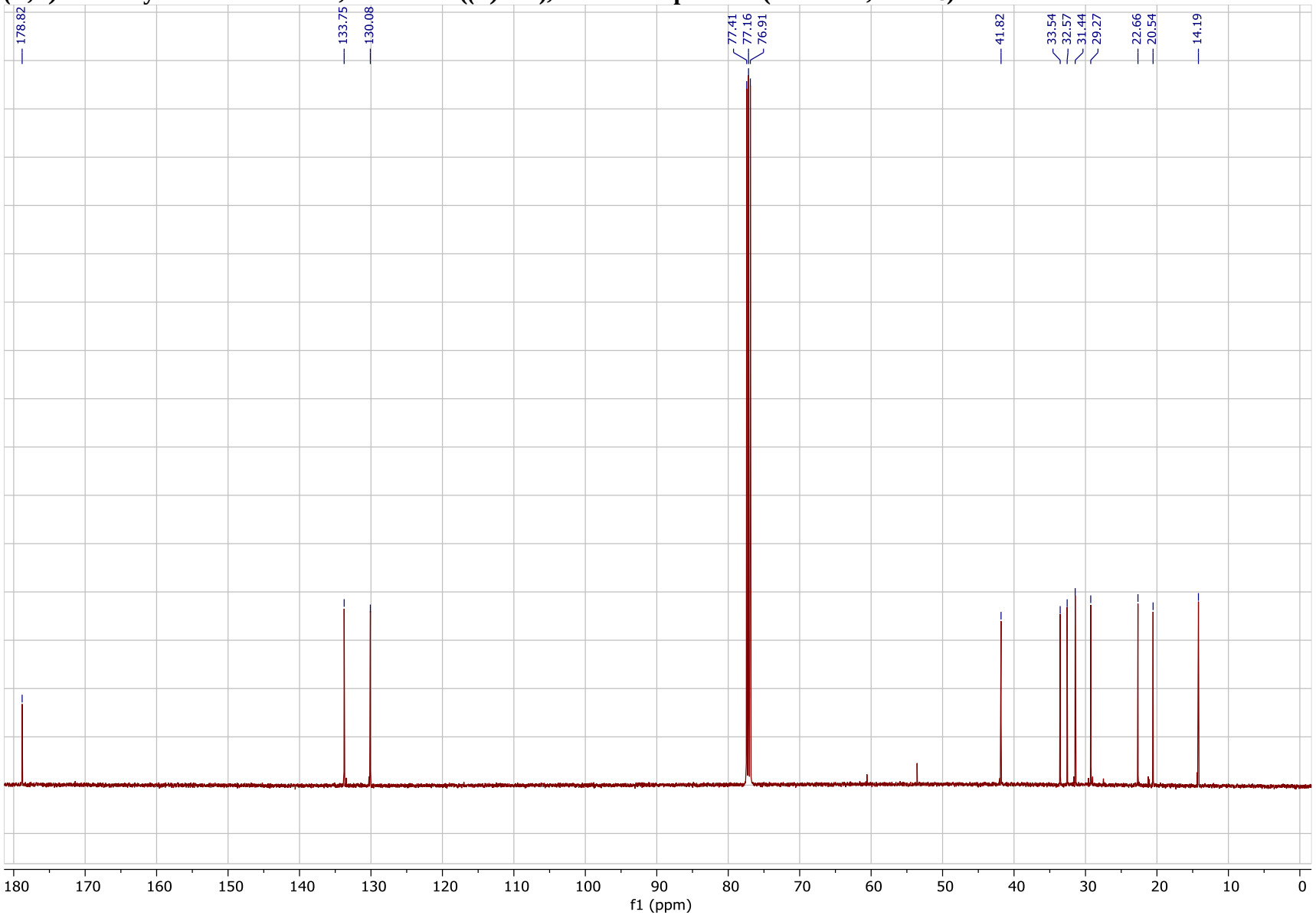

Methyl-*(R, E)*-3-methyl-dec-4-enoate (*(R)*-3.3), ^{1}H NMR spectrum (500 MHz, $CDCl_3$)

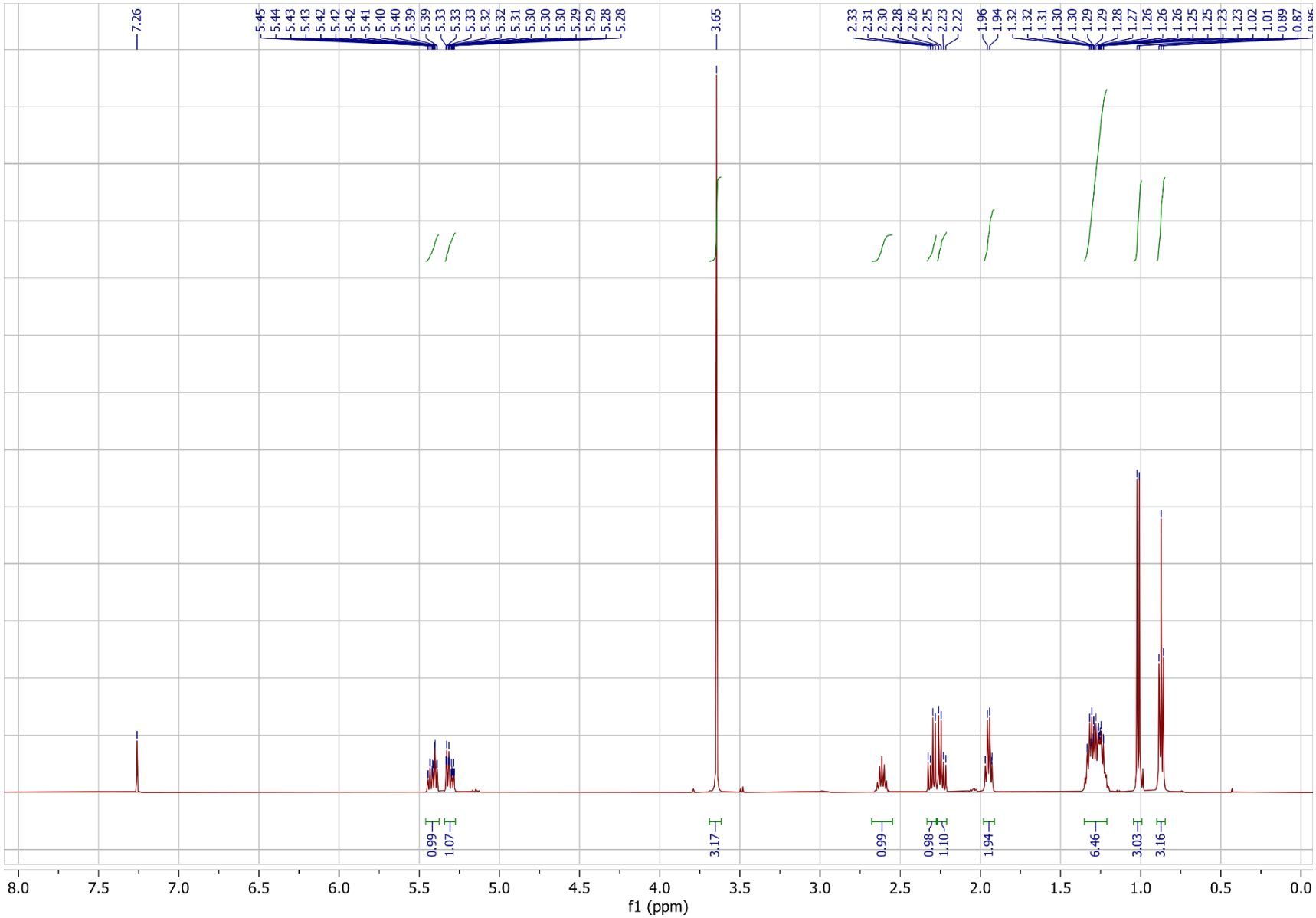

Methyl-*(R, E)*-3-methyl-dec-4-enoate (*(R)*-3.3), ^{13}C NMR spectrum (125 MHz, $CDCl_3$)

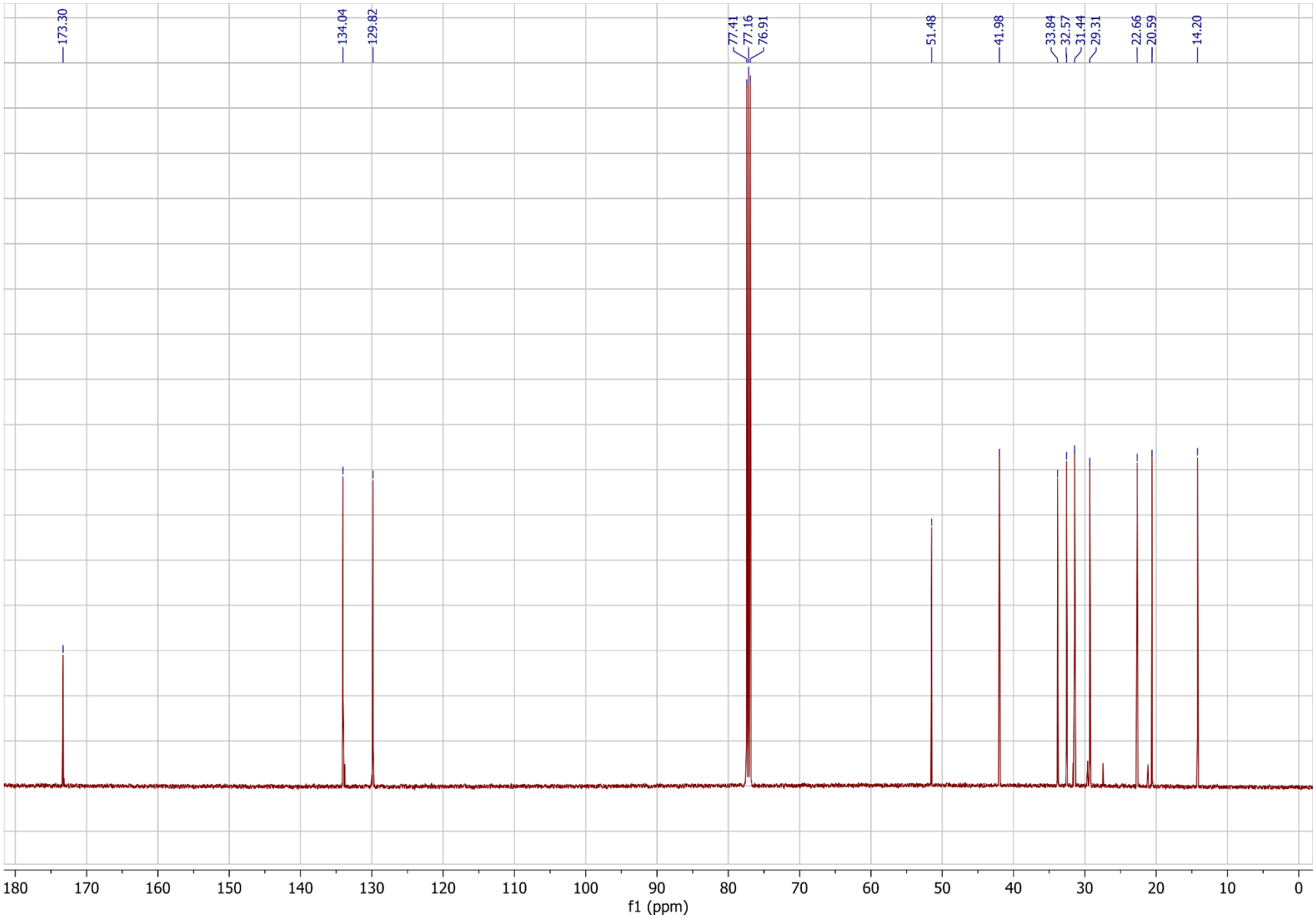

Methyl-*(2R,3S,E)*-2-hydroxy-3-methyl-dec-4-enoate (*(2R,3S)*-3.7), ^{1}H NMR spectrum (500 MHz, $CDCl_3$)

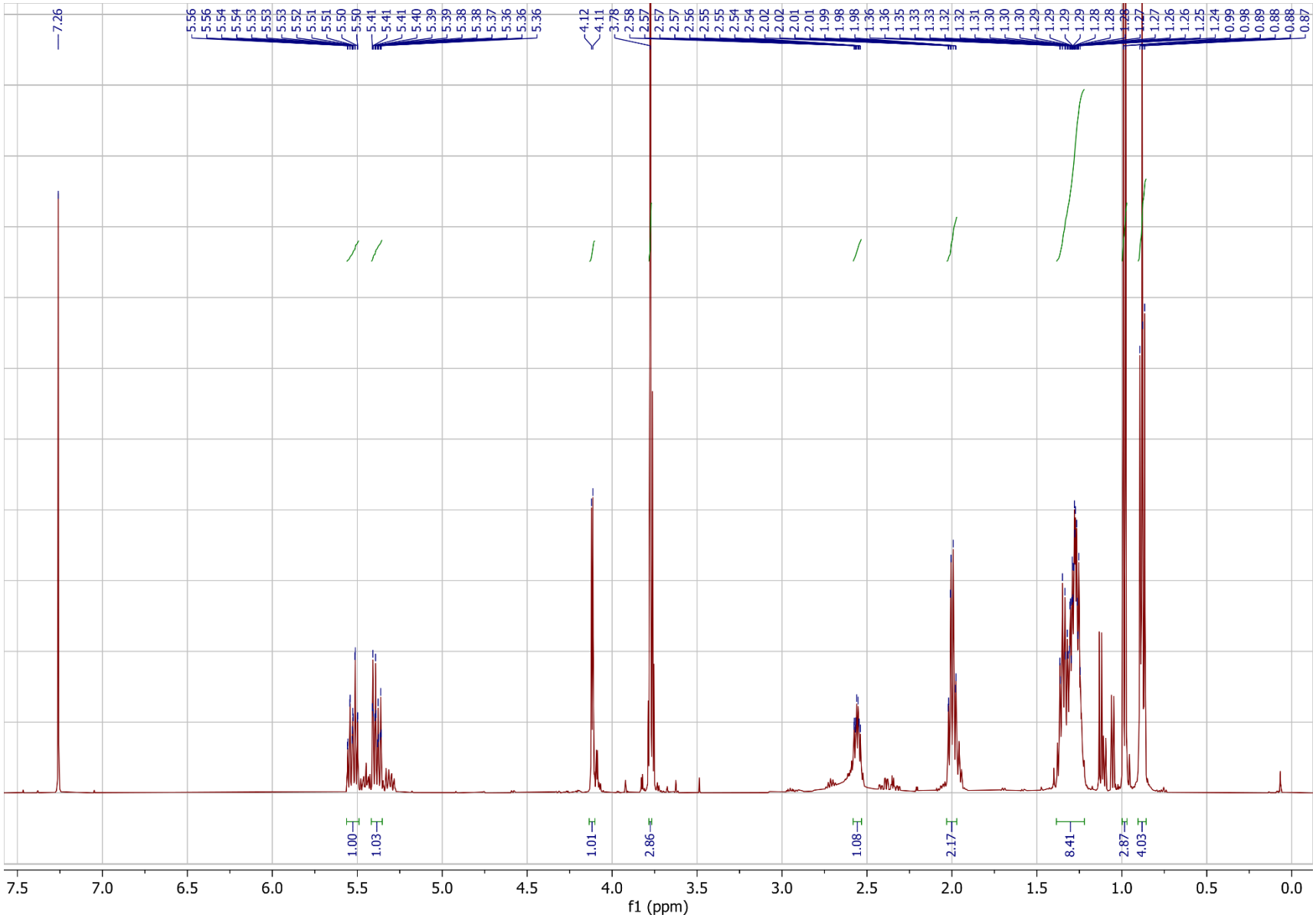

Methyl-*(2R,3S,E)*-2-hydroxy-3-methyl-dec-4-enoate (*(2R,3S)*-3.7) , ^{13}C NMR spectrum (125 MHz, $CDCl_3$)

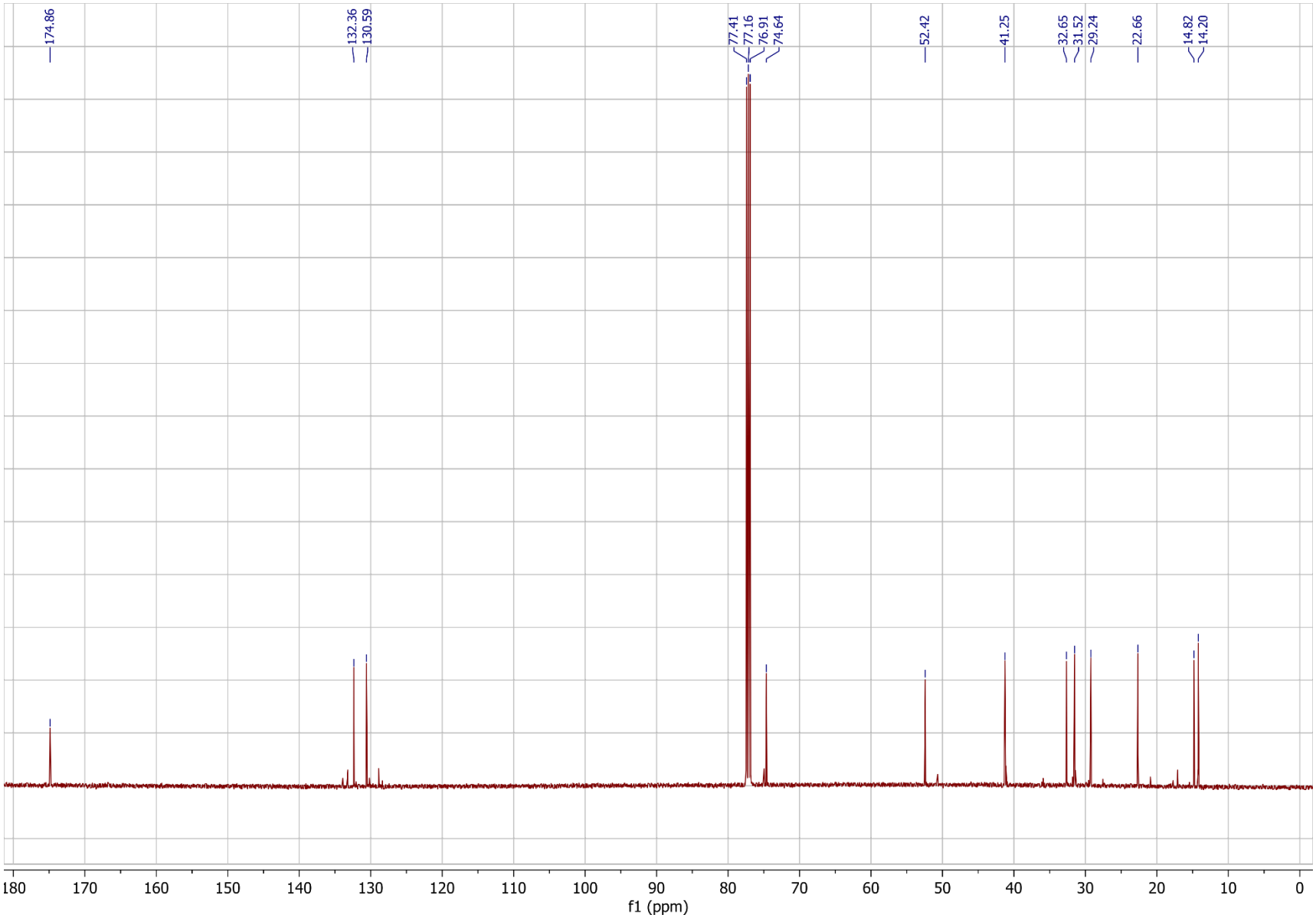

***(2R,3S,E)*-2-hydroxy-3-methyl-dec-4-enoic acid, bemeth#23 (*(2R,3S)*-3.8), ^{1}H NMR spectrum (500 MHz, $CDCl_3$)**

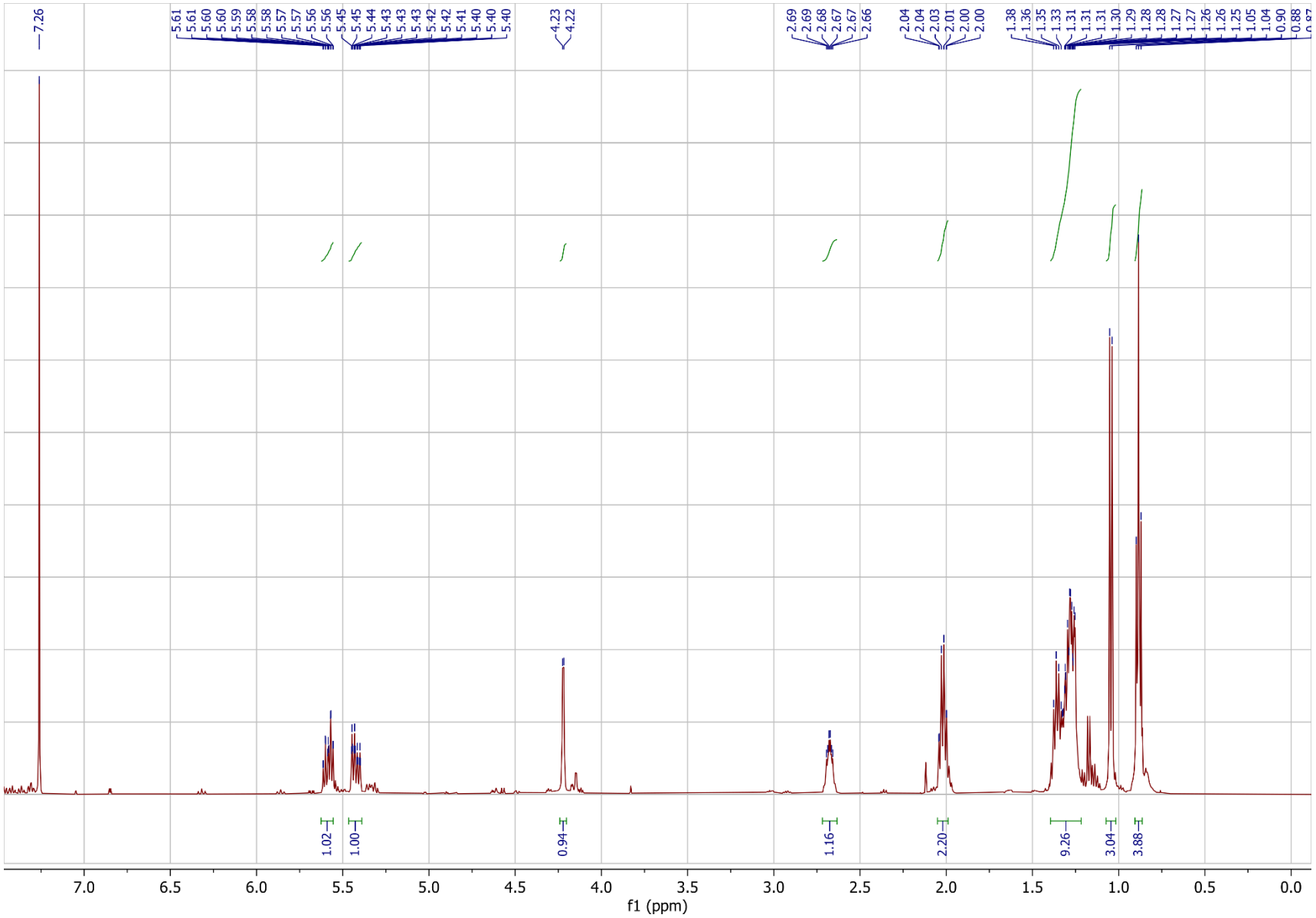

***(2R,3S,E)*-2-hydroxy-3-methyl-dec-4-enoic acid, bemeth#23 (*(2R,3S)*-3.8), ^{13}C NMR spectrum (125 MHz, $CDCl_3$)**

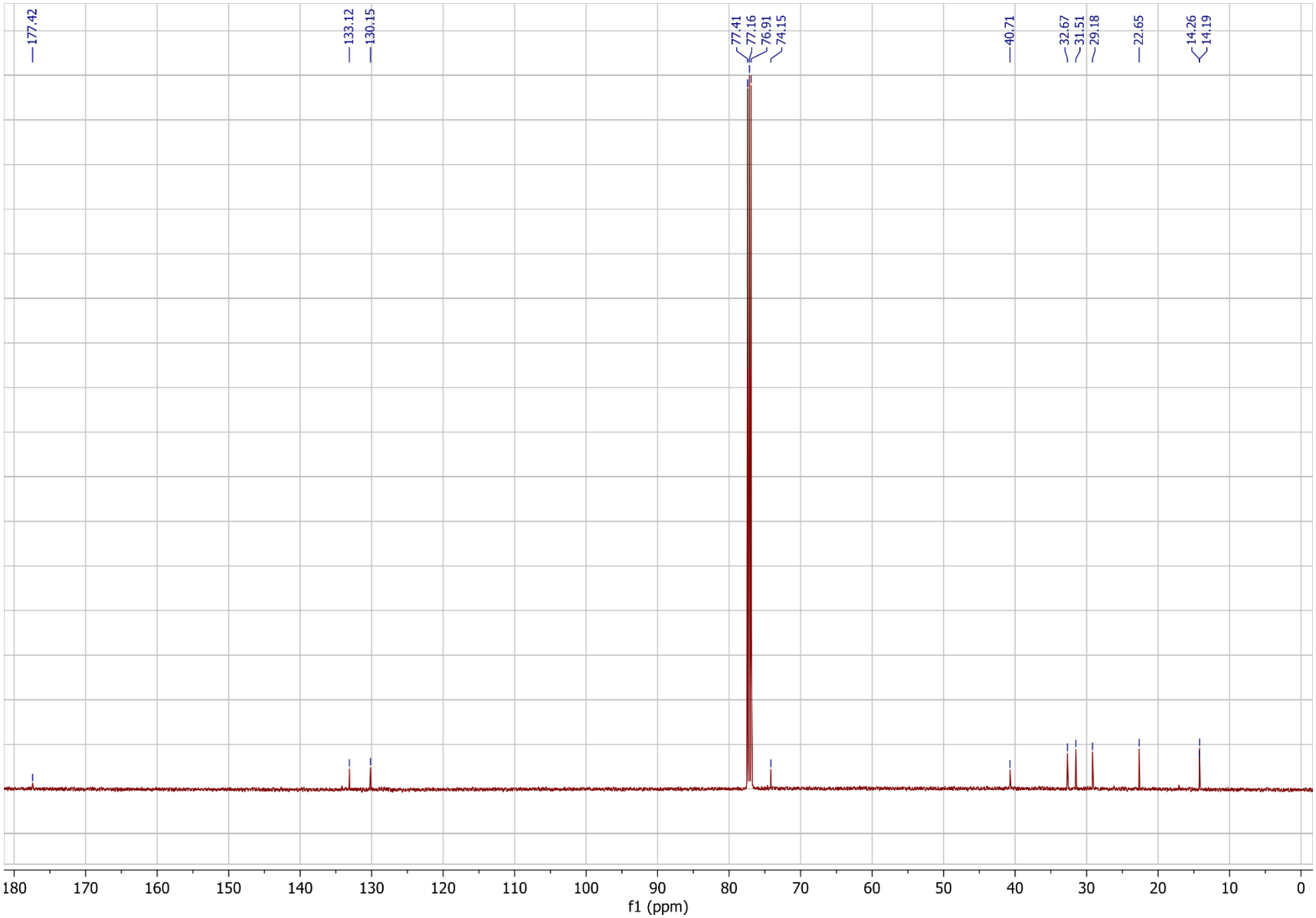

APPENDIX D

Supplemental Information for Chapter 4

Experimental

General Procedures

Unless stated otherwise, all reactions were performed under argon in flame-dried glassware. All commercially available reagents were used as purchased unless otherwise stated. All solvents were dried over activated 3Å sieves for a minimum of 24 hours unless used in reactions where aqueous reagents were involved. Thin-layer chromatography (TLC) was performed with J.T. Baker Silica Gell IB2-F plastic-backed plates. Reverse-phase column chromatography was performed using Teledyne ISCO CombiFlash Rf and Rf+ systems with Teledyne ISCO RediSep Rf and Rf Gold silica columns. Nuclear Magnetic Resonance (NMR) spectra were recorded on a Varian INOVA 600 (600 MHz) or Bruker AV 500 (500 MHz) in the Cornell University NMR Facility. ^{1}H NMR chemical shifts are reported in ppm (δ) relative to the residual solvent peaks (7.26 ppm for $CDCl_3$,3.31 ppm for CD_3OD, and 2.50 for D_6-DMSO) and ^{13}C NMR shifts relative to their respective residual solvent peaks (77.16 for $CDCl_3$ and 49.00 for CD_3OD, and 39.52 for D_6-DMSO).

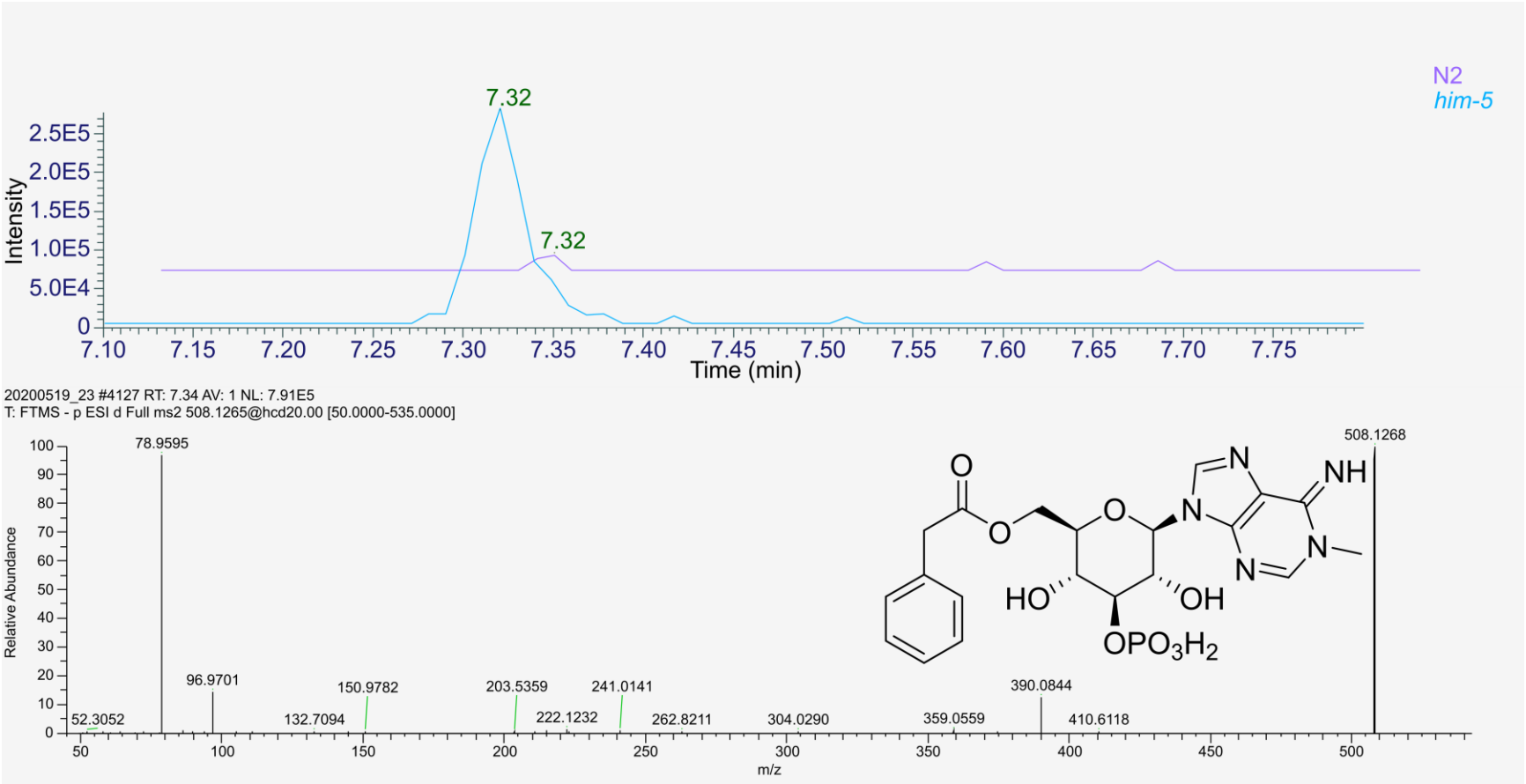

Supplemental Figure 4.1. MS and MS2 Spectra, panglu#1 (4.1) EIC of *m/z* 508.1239 in N2 and *him-5* endo-metabolome samples showing peaks for panglu#1 (**4.1**) and MS2 spectrum acquired for panglu#1 from a *fem-3* (OE) endo-metabolome sample.

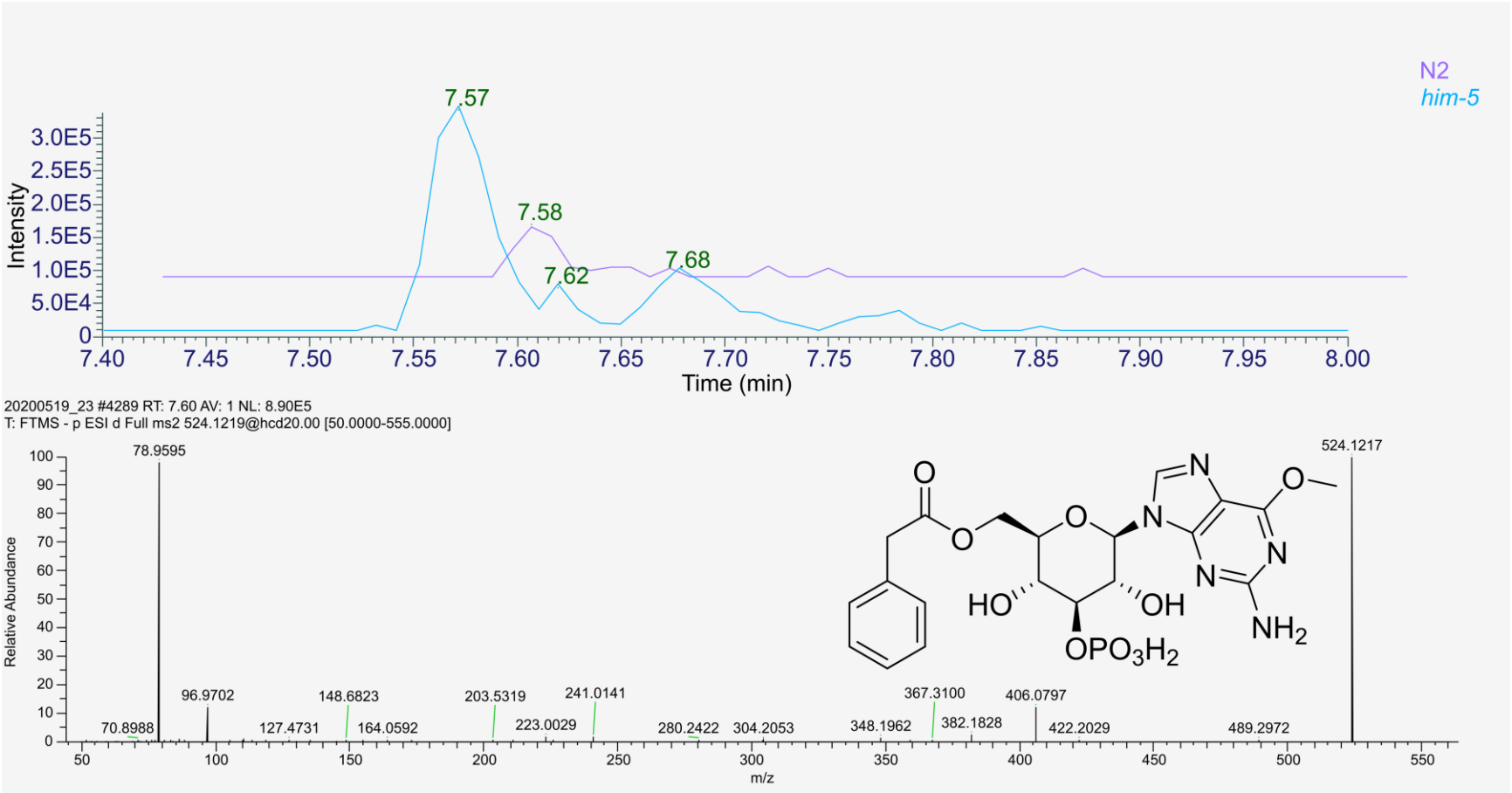

Supplemental Figure 4.2. MS and MS2 spectra of panglu#2 (4.2). EIC of *m/z* 524.1188 in N2 and *him-5* endo-metabolome samples showing peaks for panglu#2 (**4.2**) and MS2 spectrum acquired for panglu#2 from a *fem-3* (OE) endo-metabolome sample.

panglu#3 (4.3)

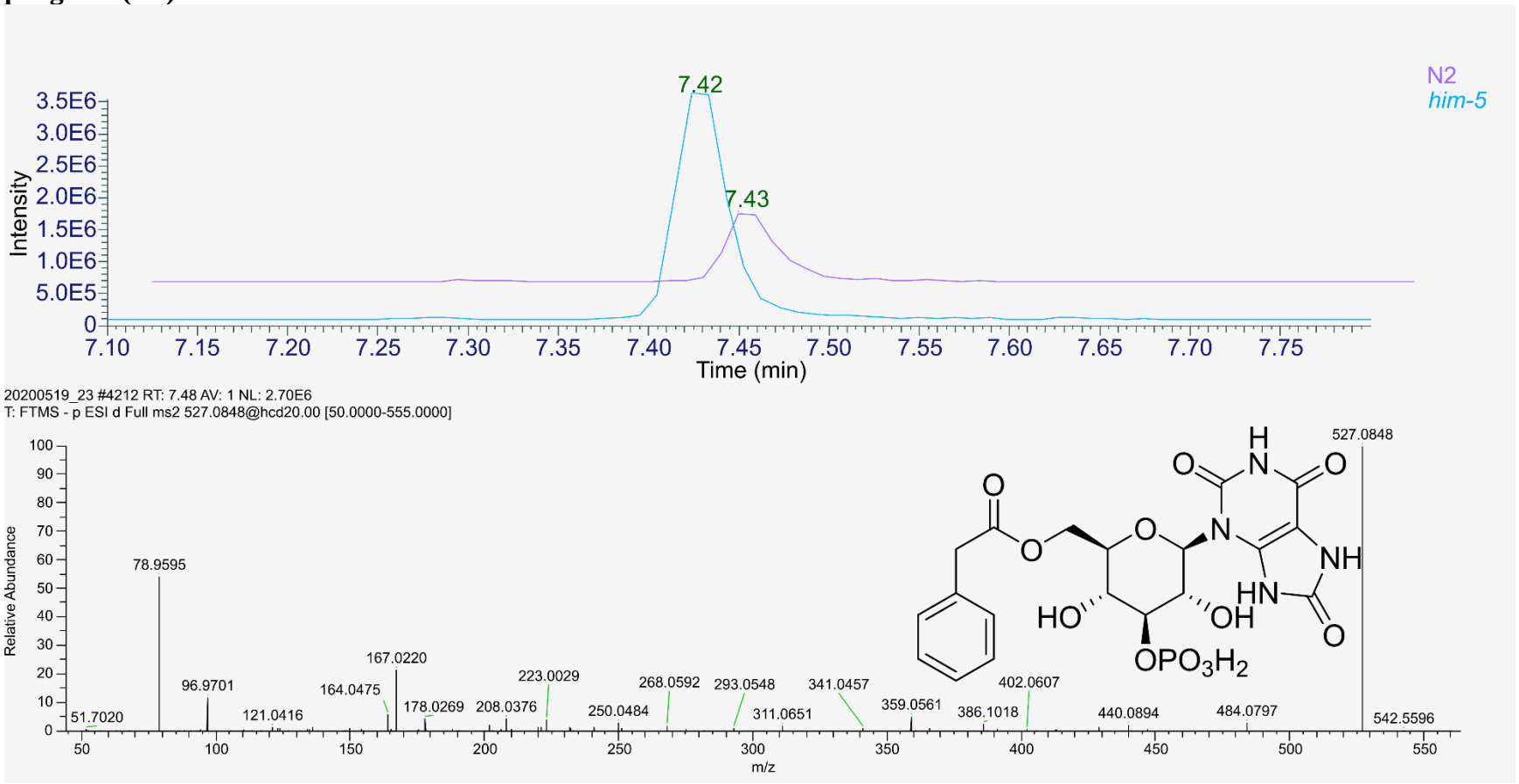

Supplemental Figure 4.3. MS and MS2 spectra of panglu#3 (4.3). EIC of *m/z* 527.0819 in N2 and *him-5* endo-metabolome samples showing peaks for panglu#3 (**4.3**) and MS2 spectrum acquired for panglu#3 from a *fem-3* (OE) endo-metabolome sample.

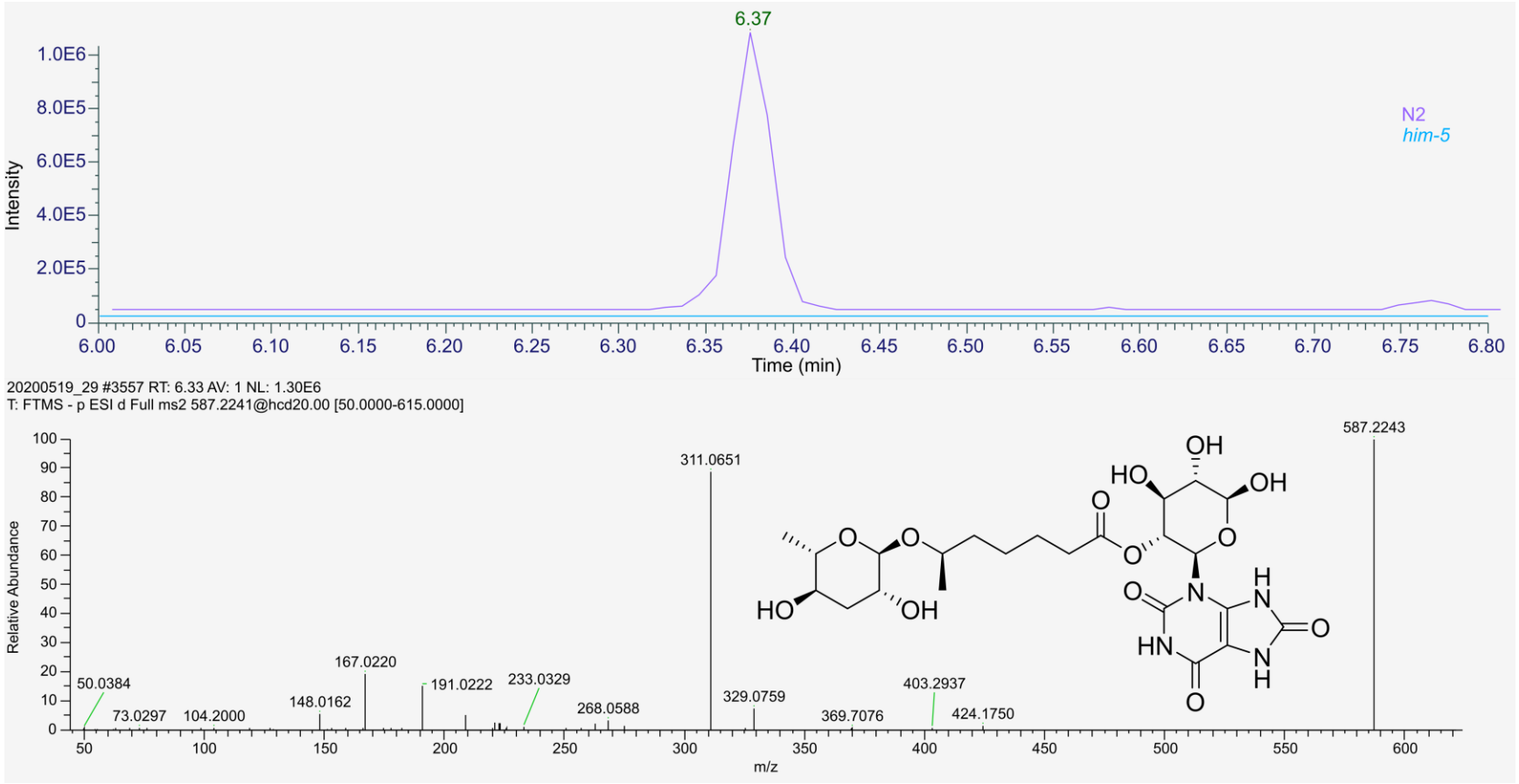

Supplemental Figure 4.4. MS and MS2 spectra of uglas#1. EIC of *m/z* 587.2211 in N2 and *him-5* endo-metabolome samples showing peaks for uglas#1 and MS2 spectrum acquired for uglas#1 from a N2 endo-metabolome sample.

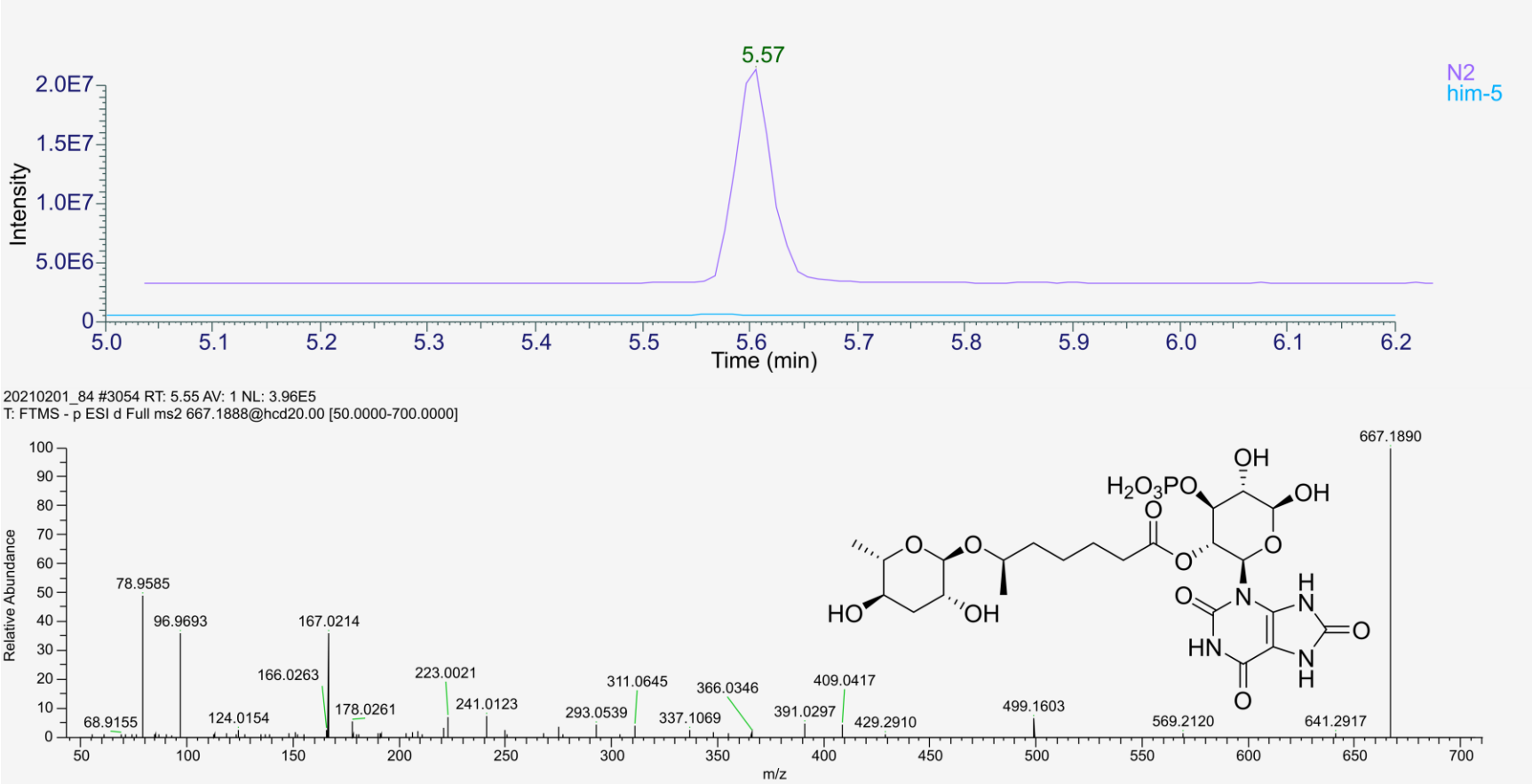

Supplemental Figure 4.5. MS and MS2 spectra of uglas#11. EIC of *m/z* 667.1880 in N2 and *him-5* endo-metabolome samples showing peaks for uglas#11 and MS2 spectrum acquired for uglas#11 from a N2 endo-metabolome sample.

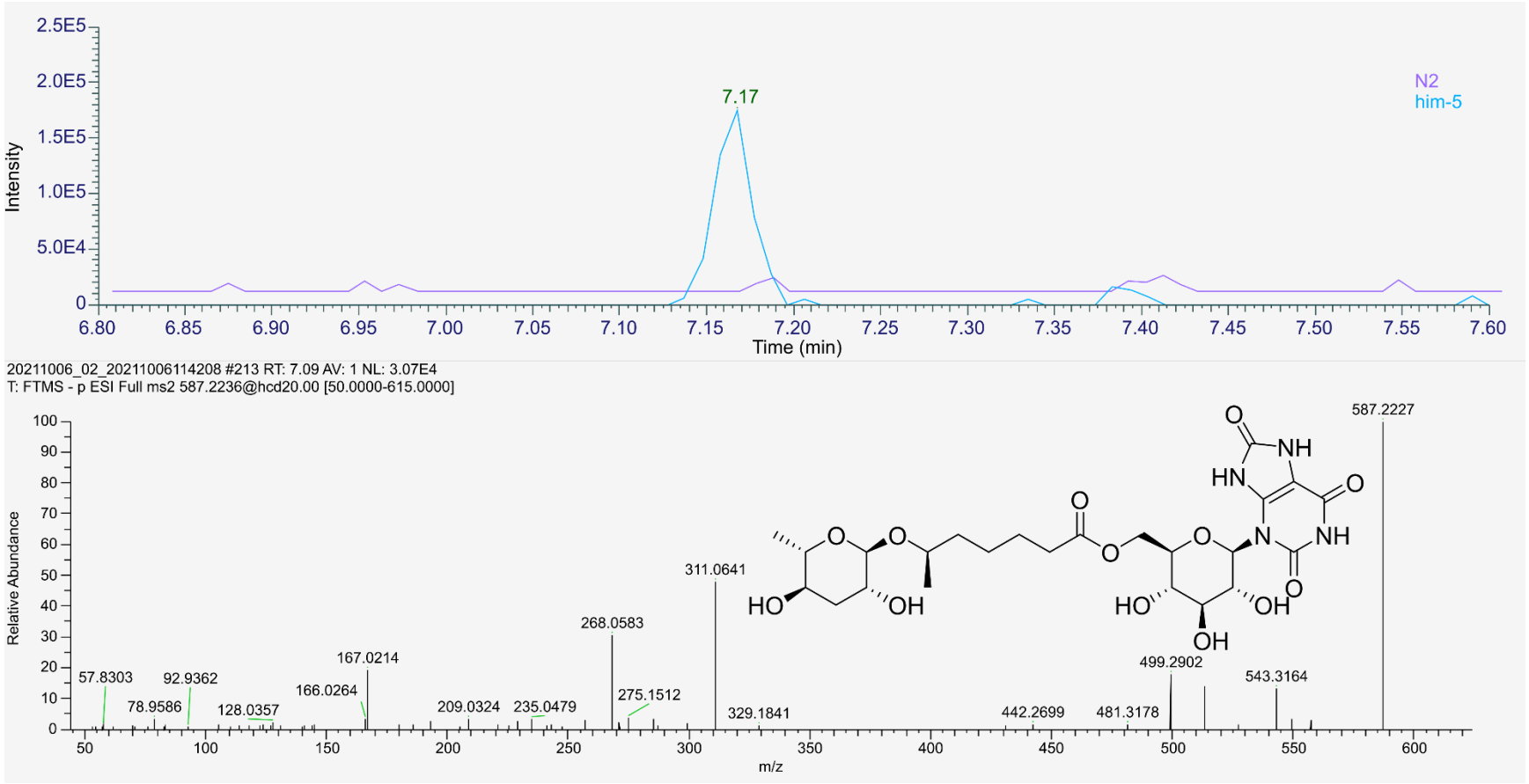

Supplemental Figure 4.6. MS and MS2 spectra of uglas#14. EIC of *m/z* 587.2211 in N2 and *him-5* endo-metabolome samples showing peaks for uglas#14 and MS2 spectrum acquired for uglas#14 from a *fem-3* (OE) endo-metabolome sample.

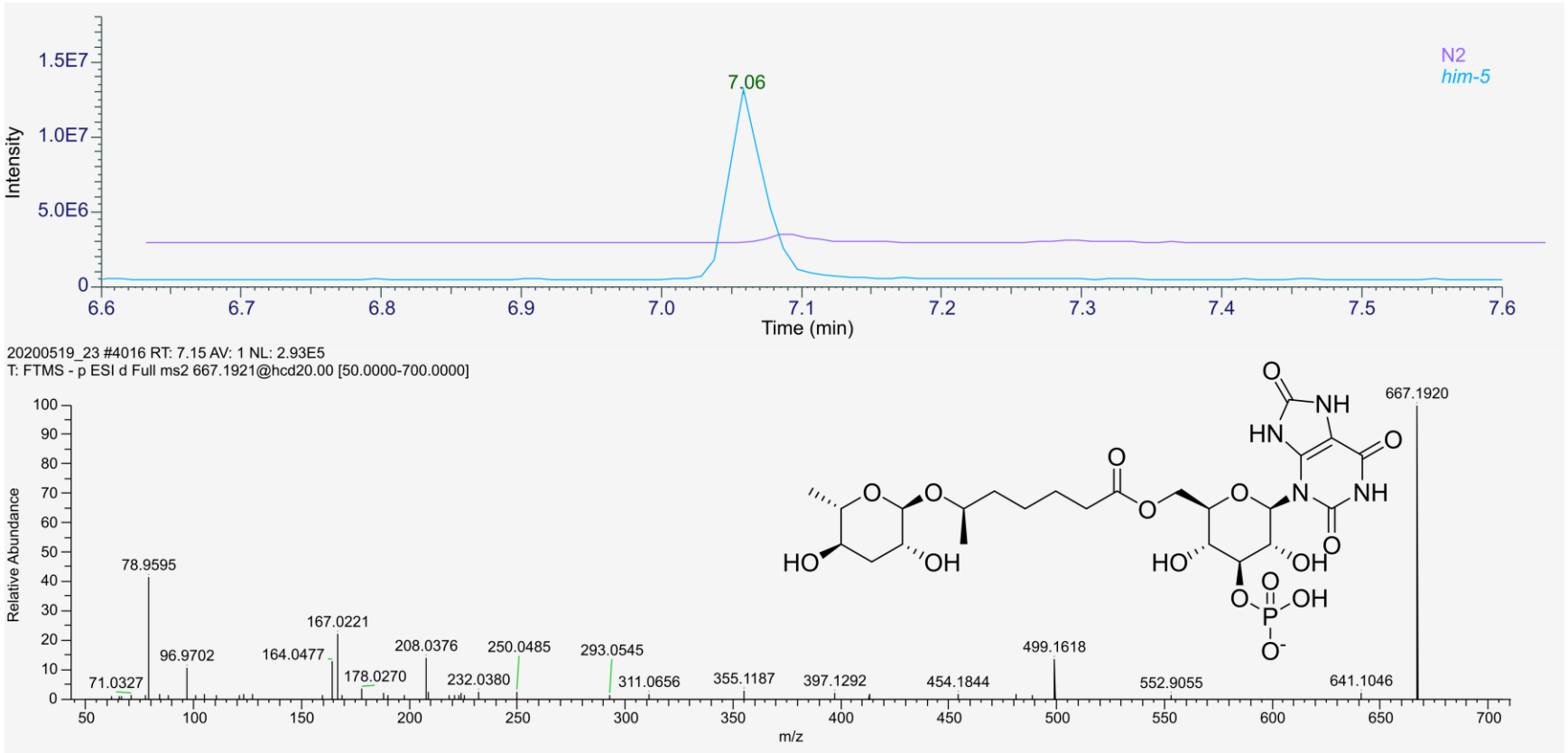

Supplemental Figure 4.5. MS and MS2 spectra of uglas#15. EIC of *m/z* 667.1880 in N2 and *him-5* endo-metabolome samples showing peaks for uglas#15 and MS2 spectrum for uglas#15 acquired from a *fem-3* (OE) endo-metabolome sample.

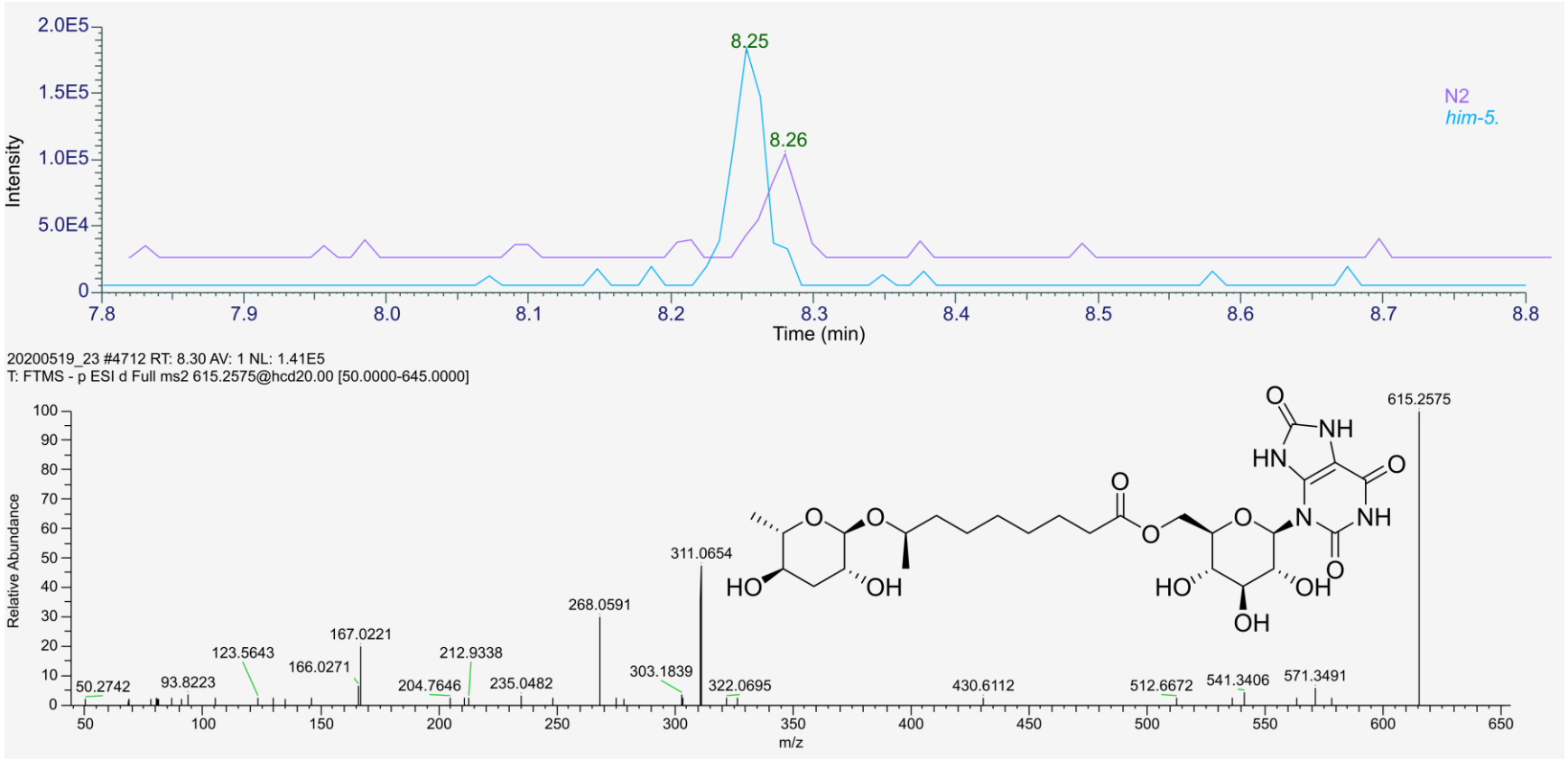

Supplemental Figure 4.6. MS and MS2 spectra of uglas#104. EIC of *m/z* 615.2531 in N2 and *him-5* endo-metabolome samples showing peaks for uglas#104 and MS2 spectrum for uglas#104 acquired from a *fem-3* (OE) endo-metabolome sample.

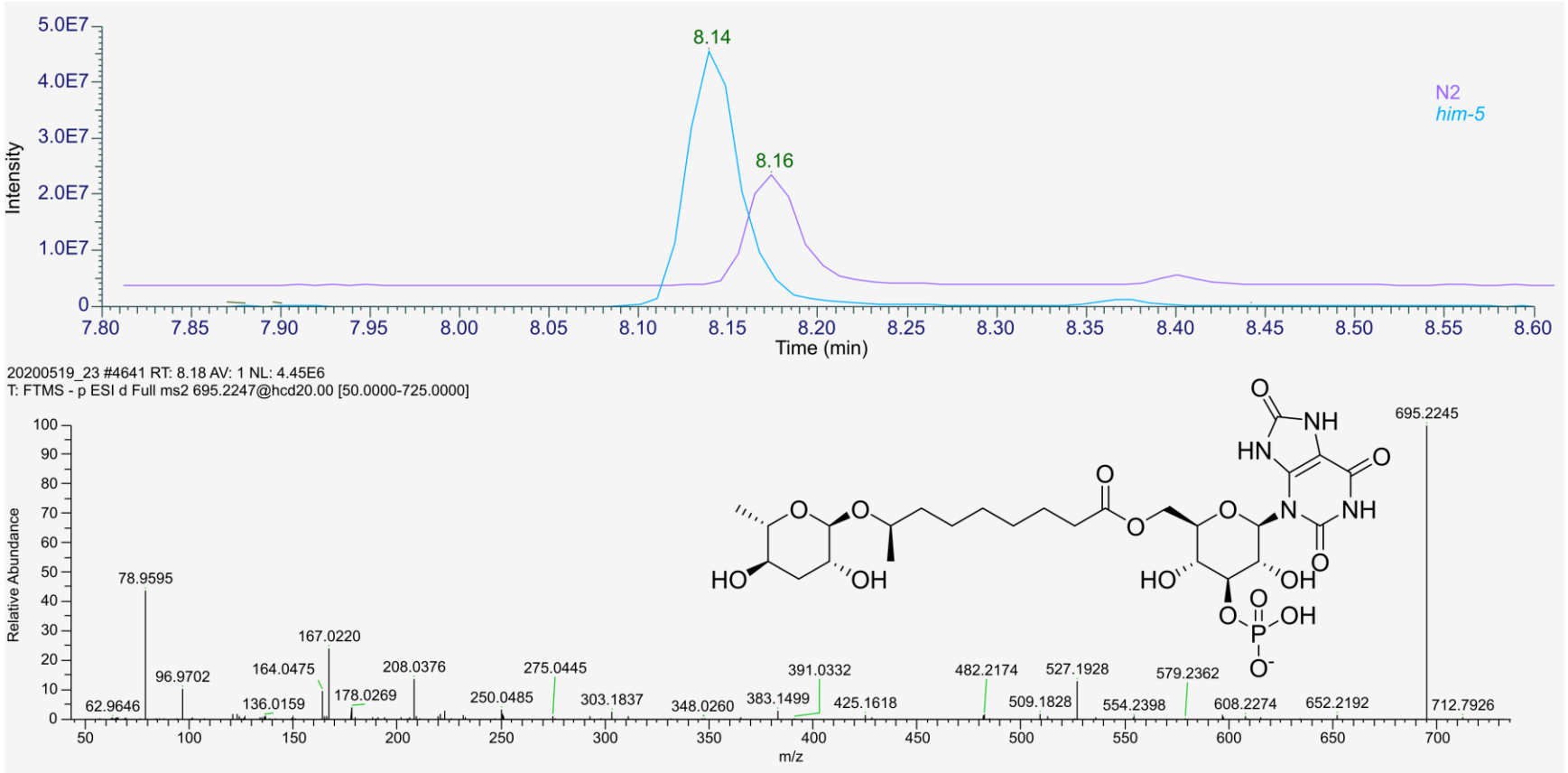

Supplemental Figure 4.7. MS and MS2 spectra of uglas#105. EIC of *m/z* 695.2189 in N2 and *him-5* endo-metabolome samples showing peaks for uglas#105 and MS2 spectrum for uglas#105 acquired from a *fem-3* (OE) endo-metabolome sample.

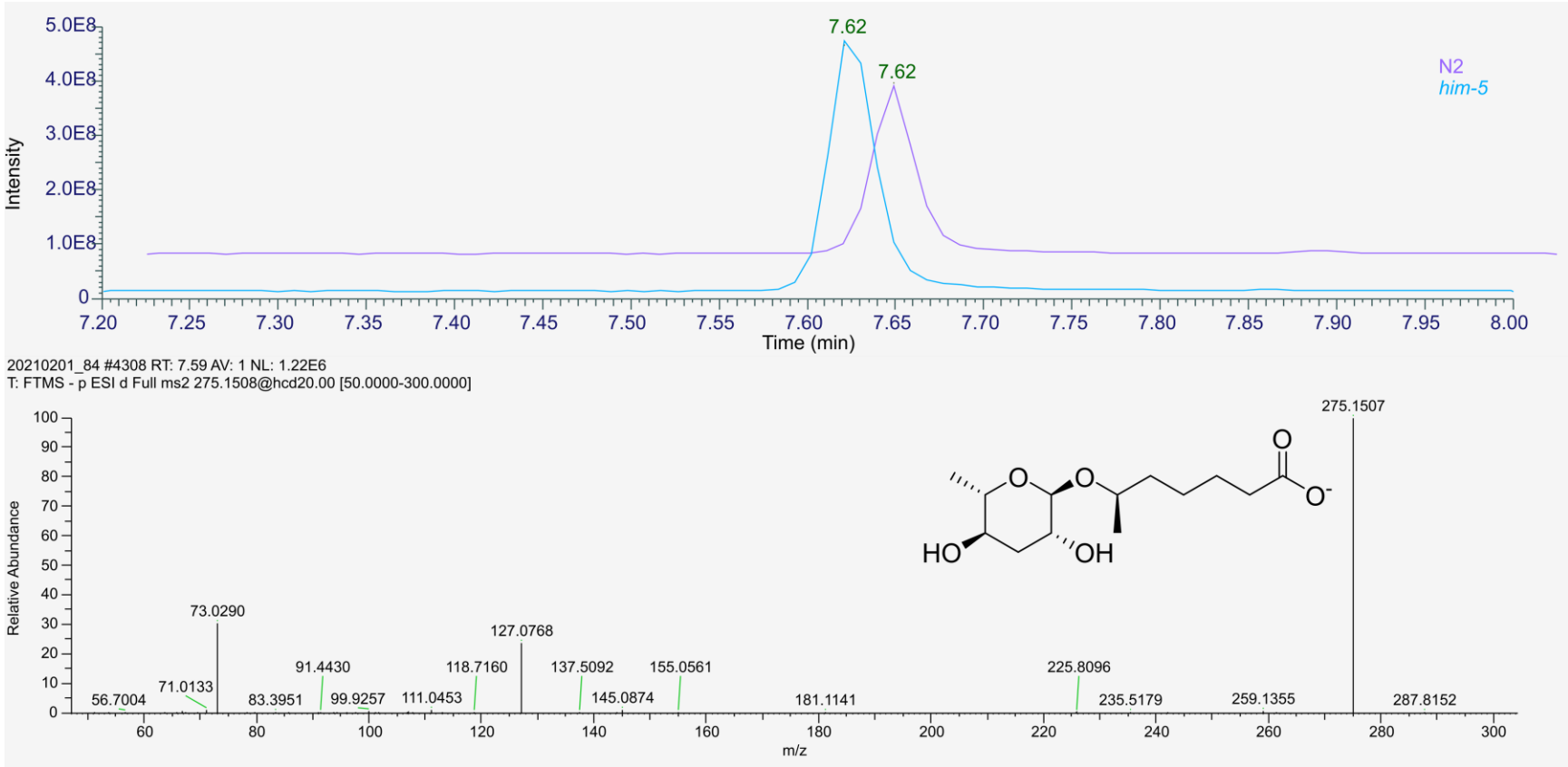

Supplemental Figure 4.8. MS and MS2 spectra of ascr#1 (4.8). EIC of *m/z* 275.1500 in N2 and *him-5* exo-metabolome samples showing peaks for ascr#1 and MS2 spectrum for ascr#1 acquired from a *him-5* exo-metabolome sample.

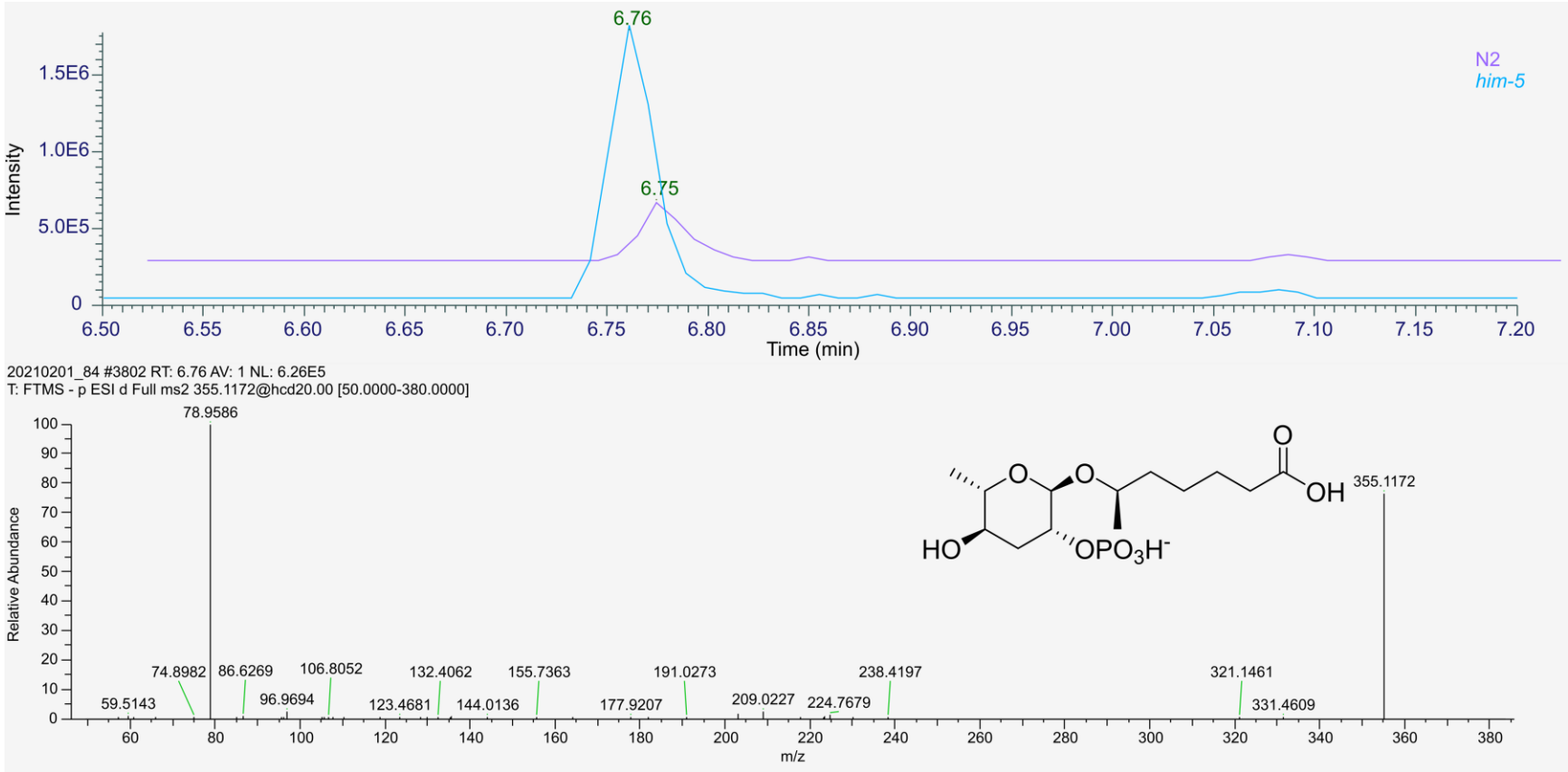

Supplemental Figure 4.9. MS and MS2 spectra of phascr#1 (4.9). EIC of *m/z* 355.1168 in N2 and *him-5* exo-metabolome samples showing peaks for phascr#1 and MS2 spectrum for phascr#1 acquired from a *him-5* exo-metabolome sample.

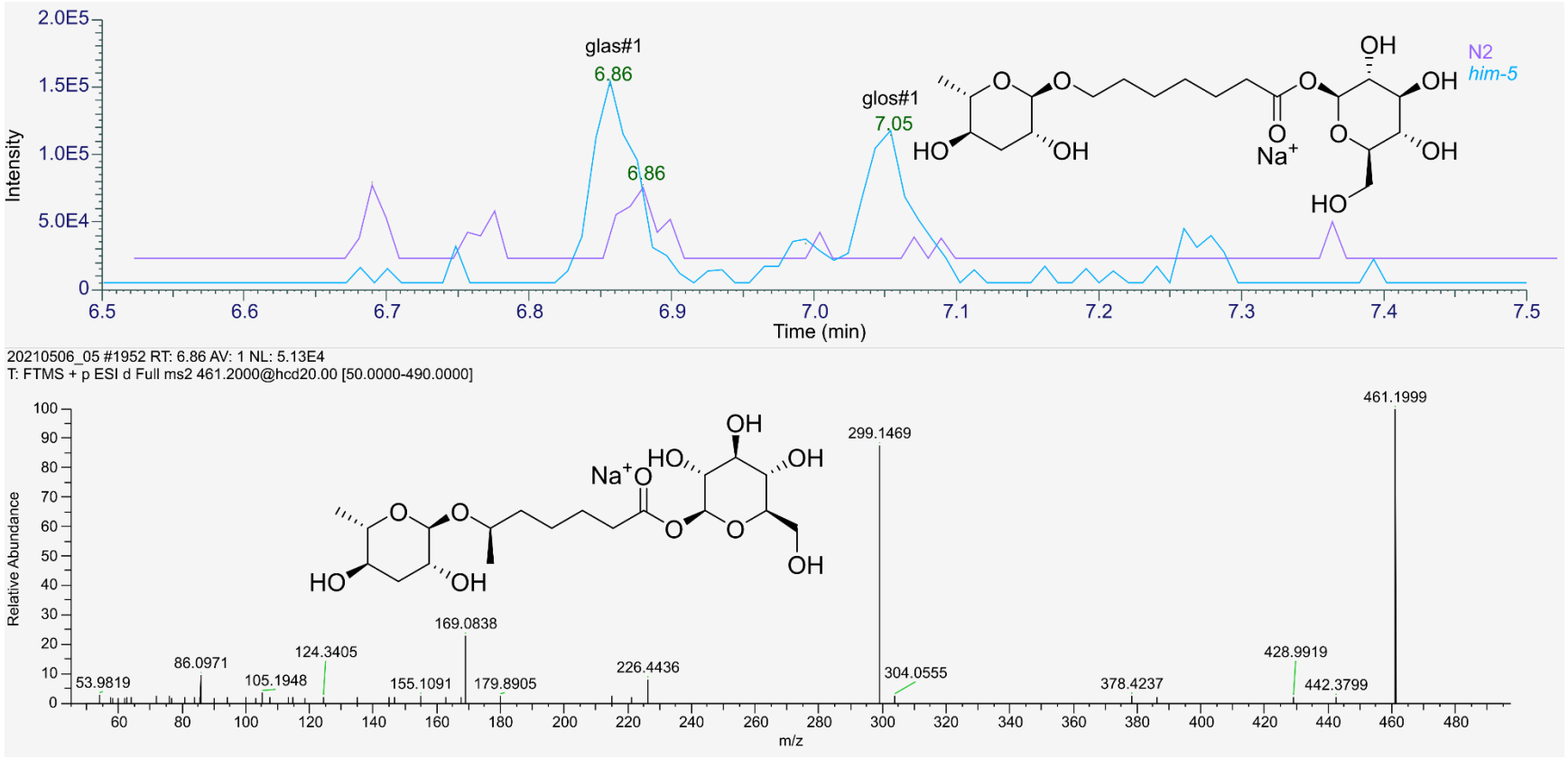

Supplemental Figure 4.10. MS and MS2 spectra of glas#1 (4.10) and glos#1 (4.11). EIC of *m/z* 461.1995 in N2 and *him-5* endo-metabolome samples showing peaks for glas#1 and glos#1 and MS2 spectrum for glas#1 acquired from a *him-5* endo-metabolome sample.

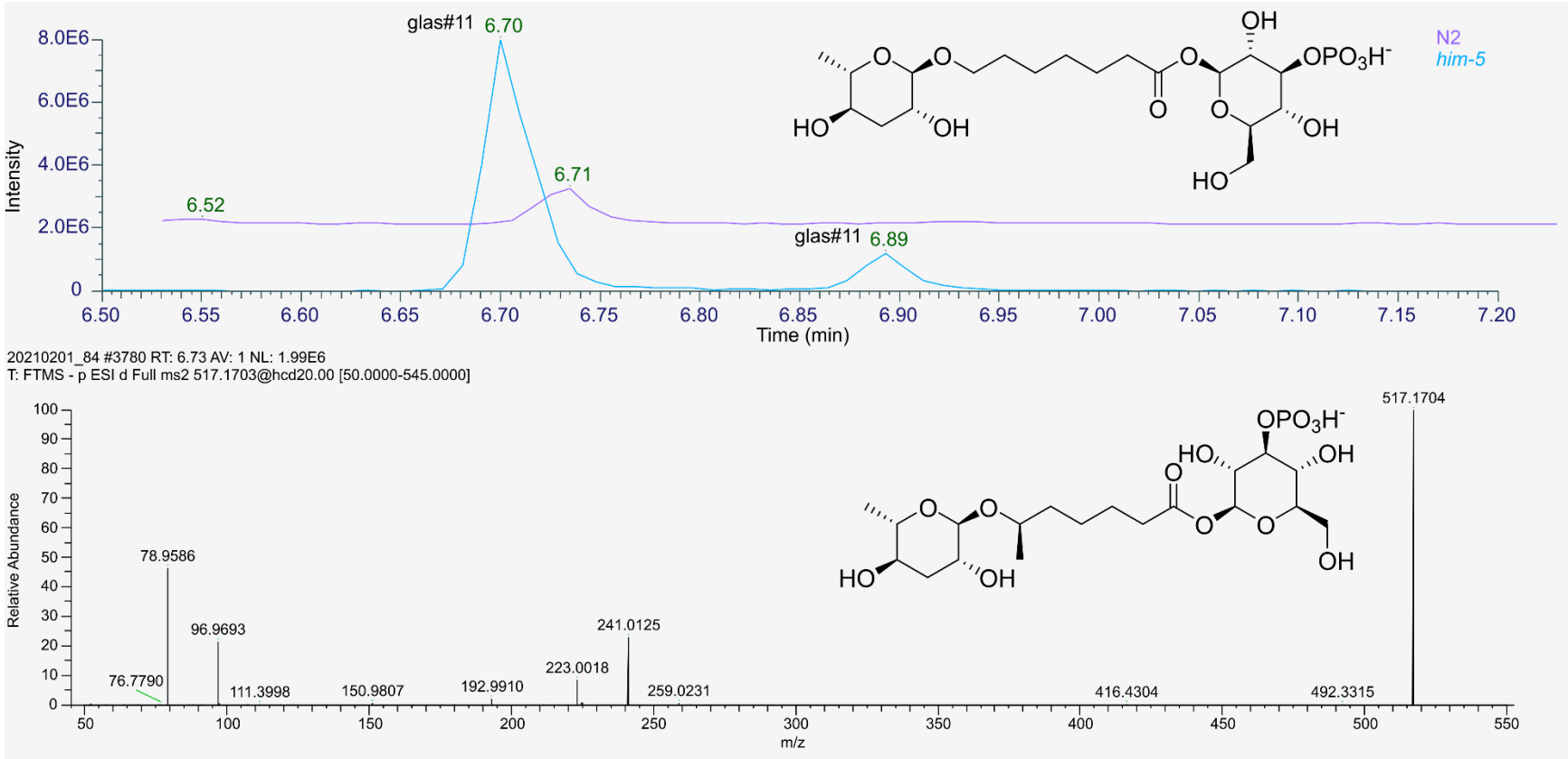

Supplemental Figure 4.11. MS and MS2 spectra of glss#11 (4.12) and glos#11 (4.13). EIC of *m/z* 517.1669 in N2 and *him-5* exo-metabolome samples showing peaks for glas#11 and glos#11 and MS2 spectrum for glas#11 acquired from a *him-5* exo-metabolome sample.

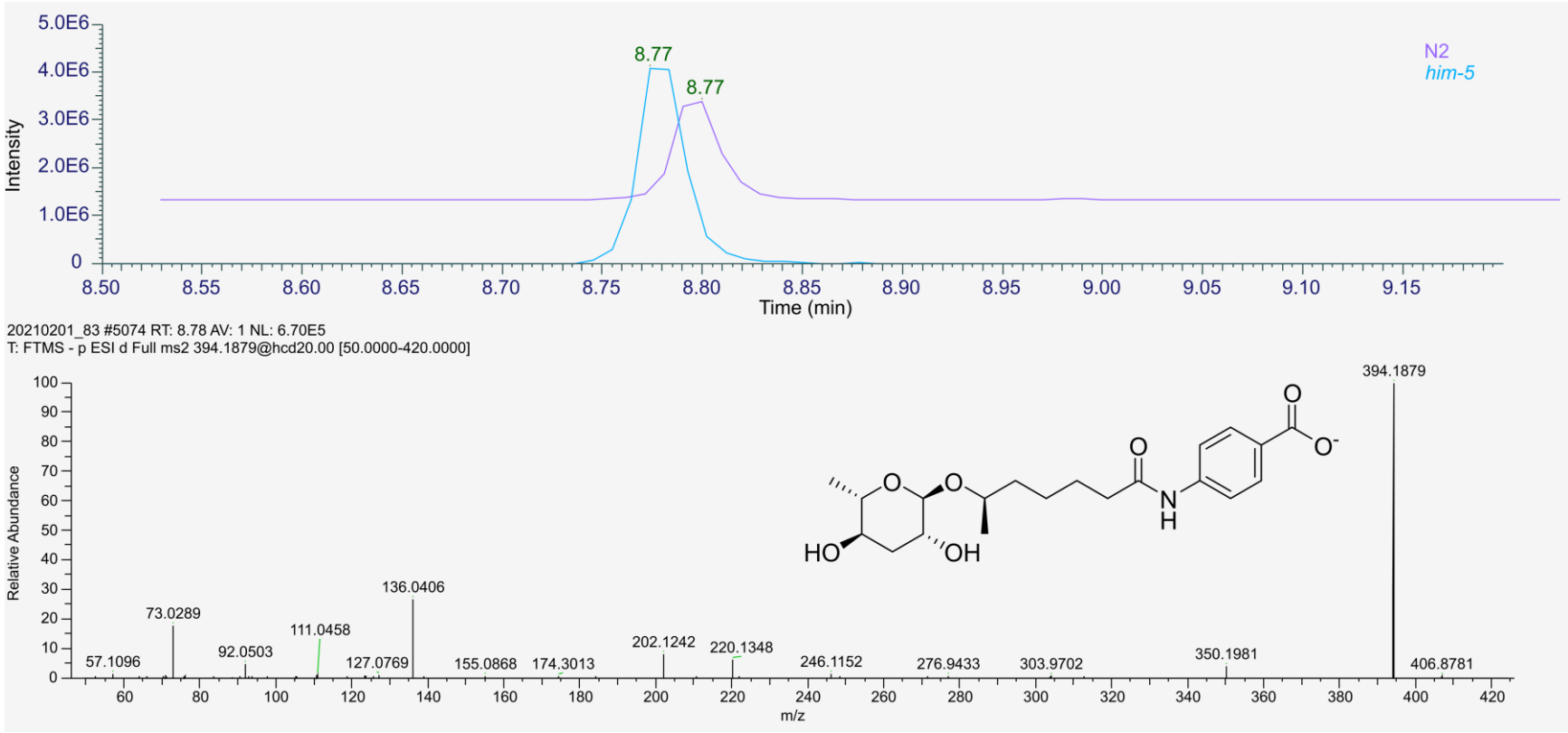

Supplemental Figure 4.12. MS and MS2 spectra of ascr#801 (4.14). EIC of *m/z* 394.1875 in N2 and *him-5* exo-metabolome samples showing peaks for ascr#801 and MS2 spectrum for ascr#801 acquired from a *him-5* exo-metabolome sample.

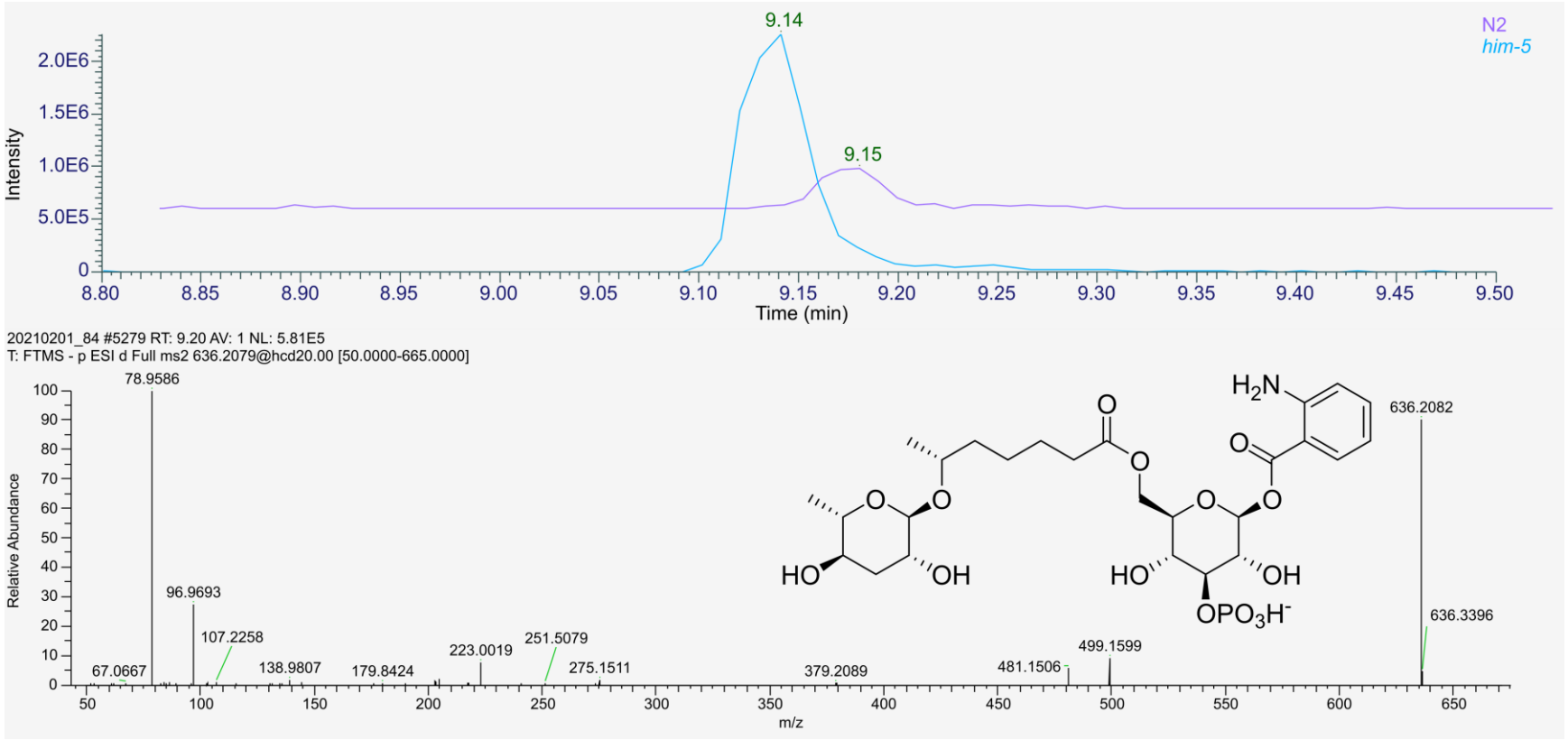

Supplemental Figure 4.13. MS and MS2 spectra of anglas#2 (4.15). EIC of *m/z* 636.2070 in N2 and *him-5* endo-metabolome samples showing peaks for anglas#2 and MS2 spectrum for anglas#2 acquired from a *him-5* endo-metabolome sample.

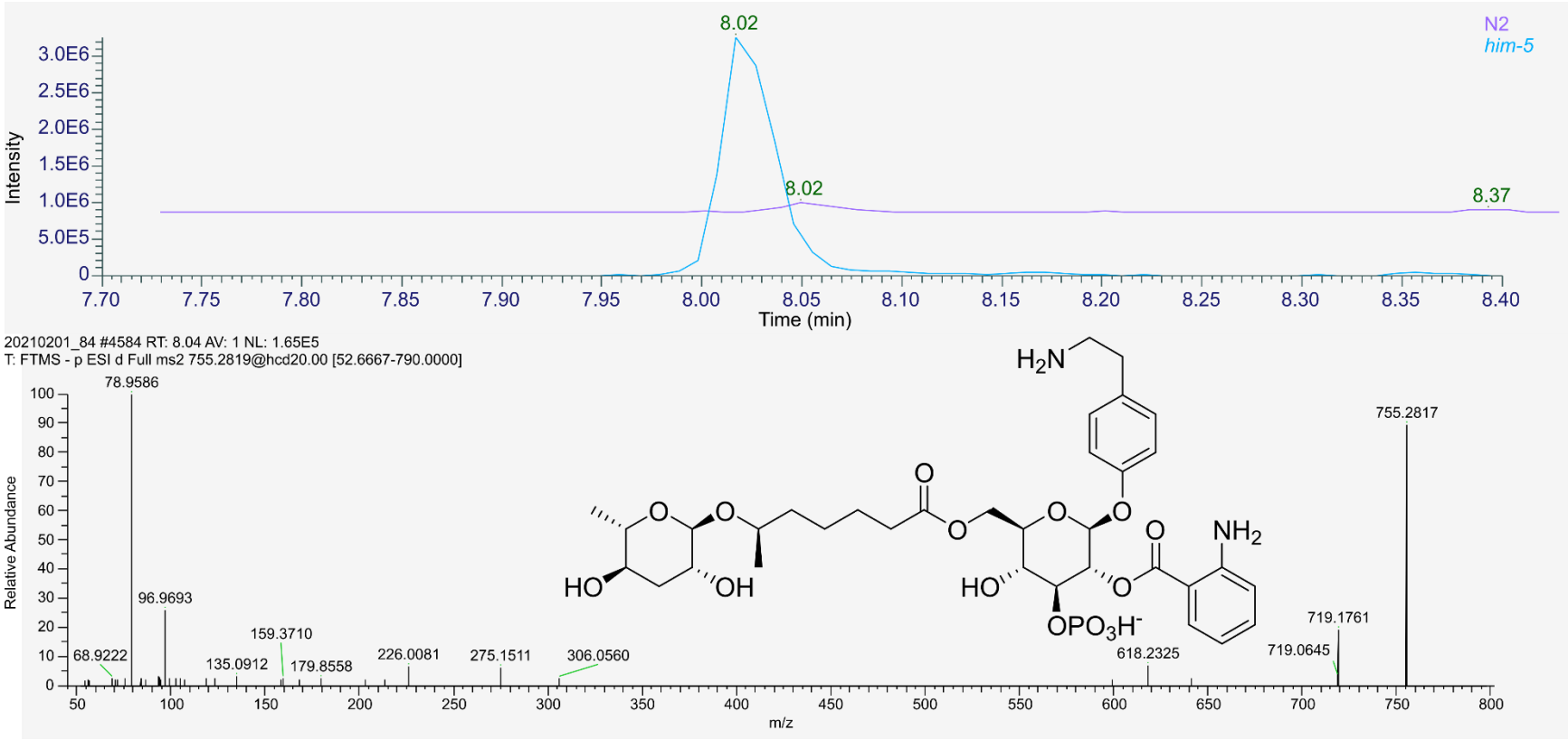

Supplemental Figure 4.14. MS and MS2 spectra of tyglas#1 (4.16). EIC of *m/z* 755.2807 in N2 and *him-5* endo-metabolome samples showing peaks for tyglas#1 and MS2 spectrum for tyglas#1 acquired from a *him-5* endo-metabolome sample.

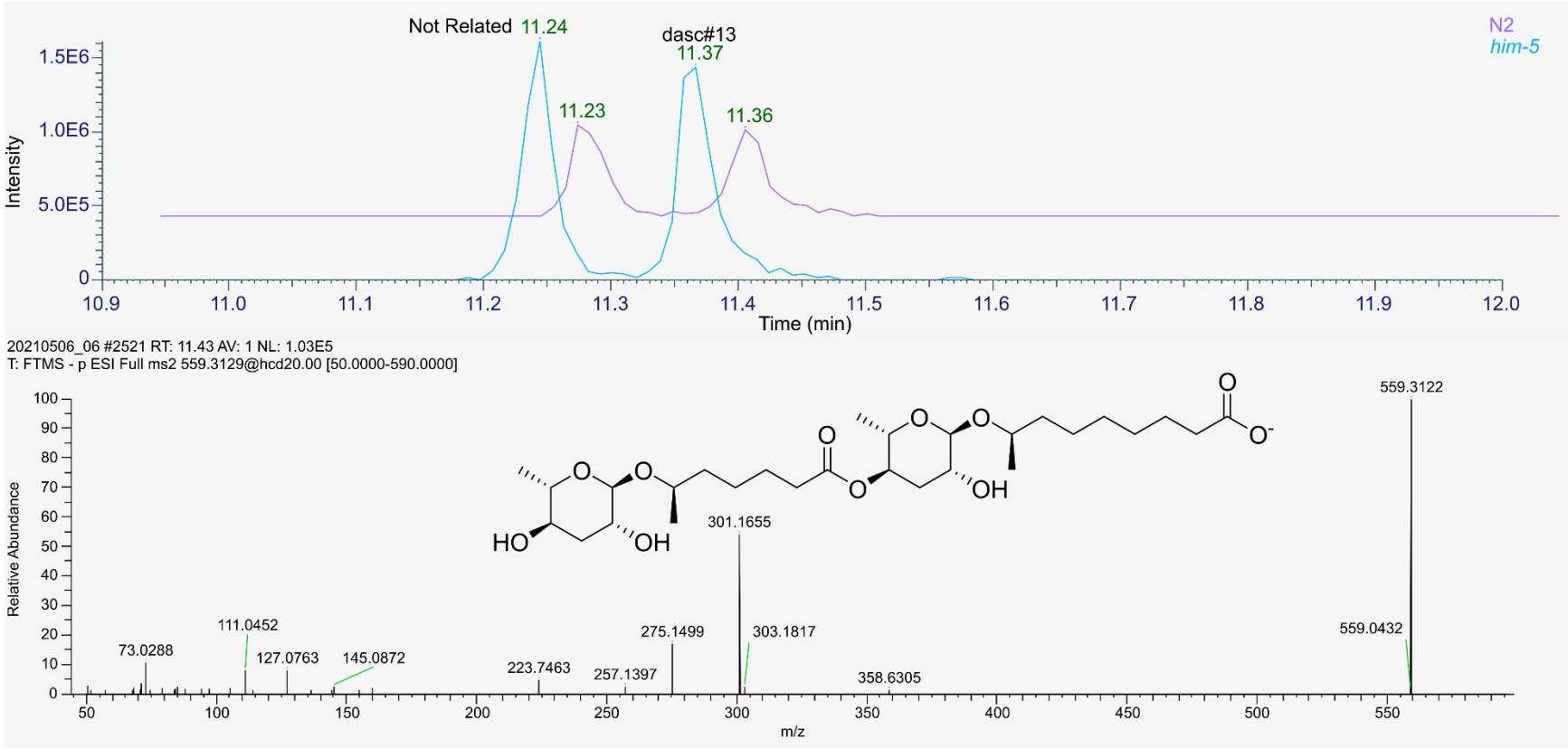

Supplemental Figure 4.15. MS and MS2 spectra of dasc#13 (4.17). EIC of *m/z* 559.3129 in N2 and *him-5* exo-metabolome samples showing peaks for dasc#13 (11.37 min) and MS2 spectrum for dasc#1 acquired from a *him-5* exo-metabolome sample.

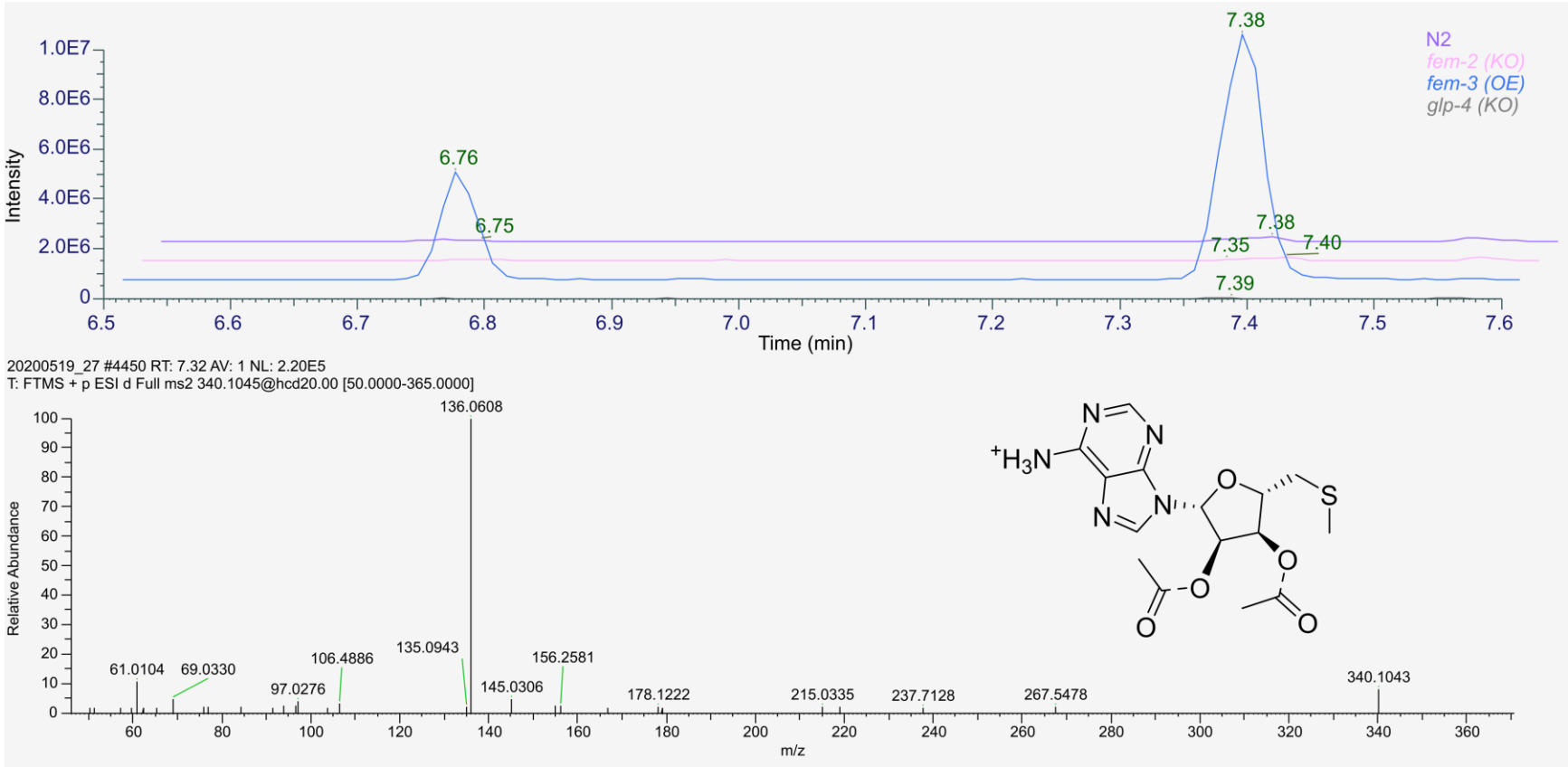

Supplemental Figure 4.16. MS and MS2 spectra of amta#1 and amta#2. EIC of *m/z* 340.1074 in N2 and *him-5* endo-metabolome samples showing peaks for amta#1 and amta#2 and MS2 spectrum for amta#2 acquired from a *fem-3* (OE) endo-metabolome sample.

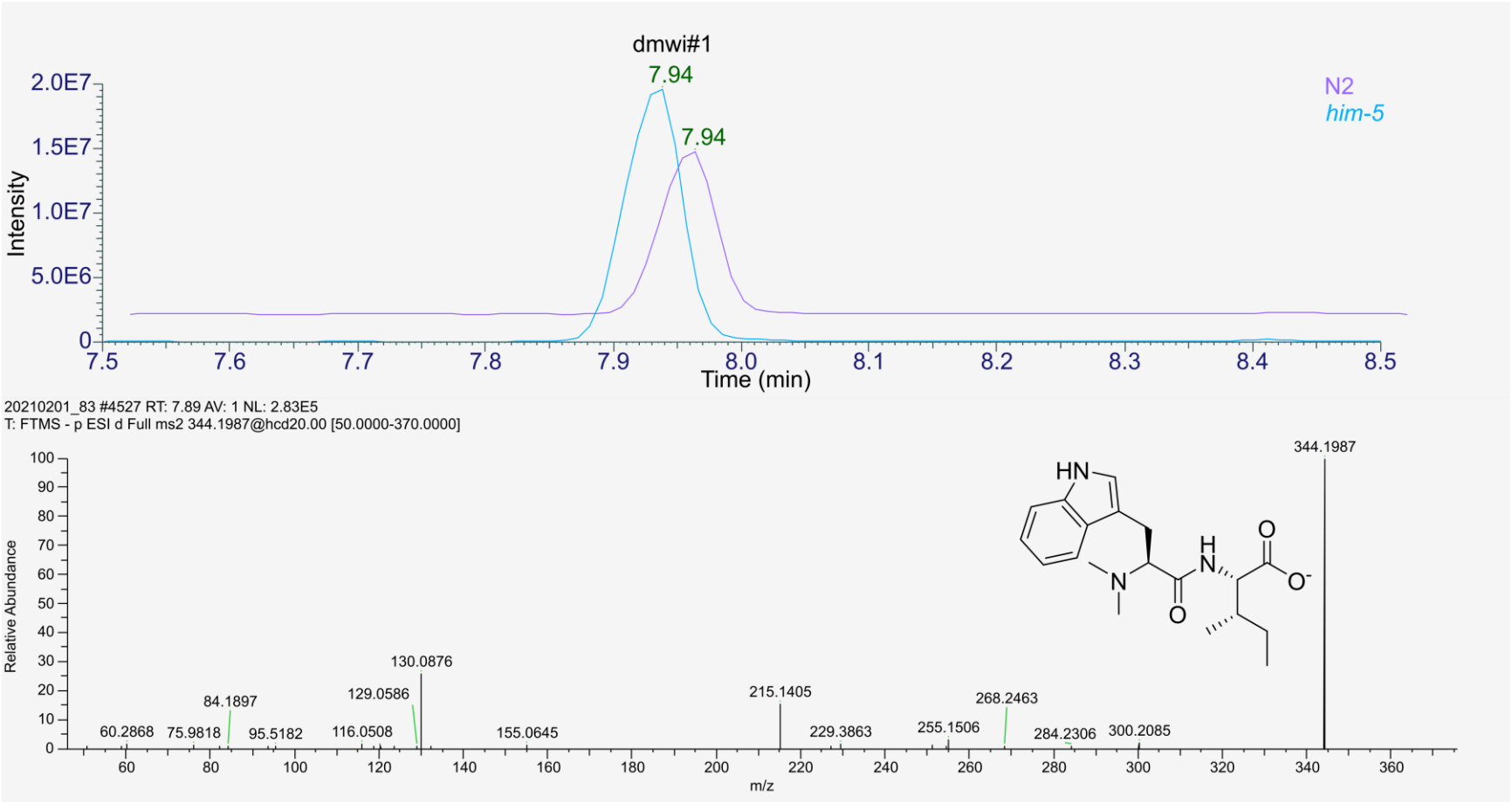

Supplemental Figure 4.17. MS and MS2 spectra of dmwi#1 (4.21). EIC of *m/z* 346.2125 in N2 and *him-5* exo-metabolome samples showing peaks for dmwi#1 and MS2 spectrum for dmwi#1 acquired from a *fem-3* (OE) endo-metabolome sample.

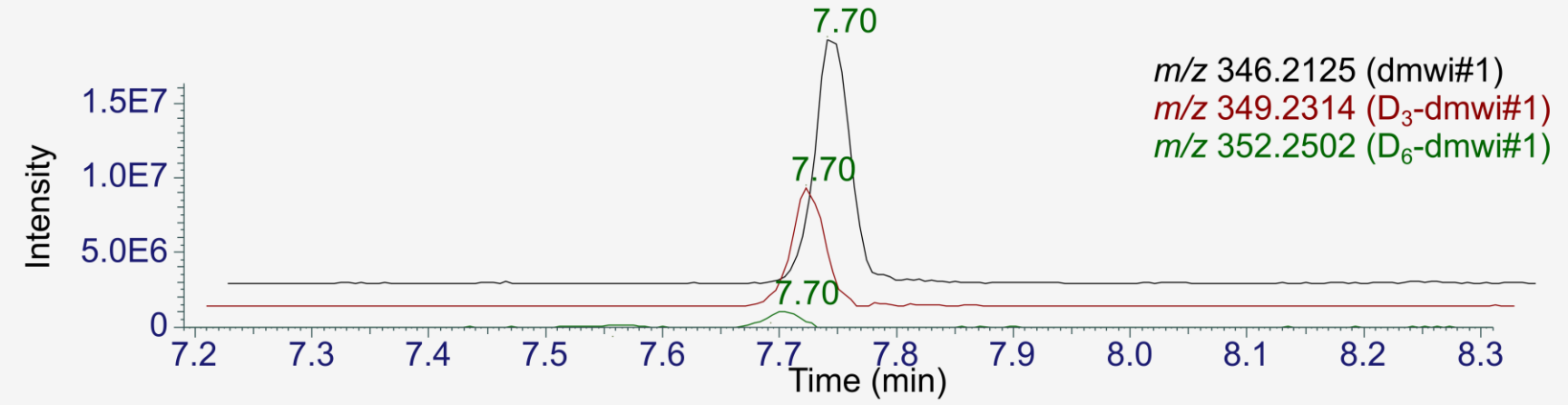

Supplemental Figure 4.18. D_3-Methionine labeling of dmwi#1. EIC of dmwi#1, D_3-dmwi#1, D_6-dmwi#1 in the exo-metabolome of *him-5* fed D_3-methionine.

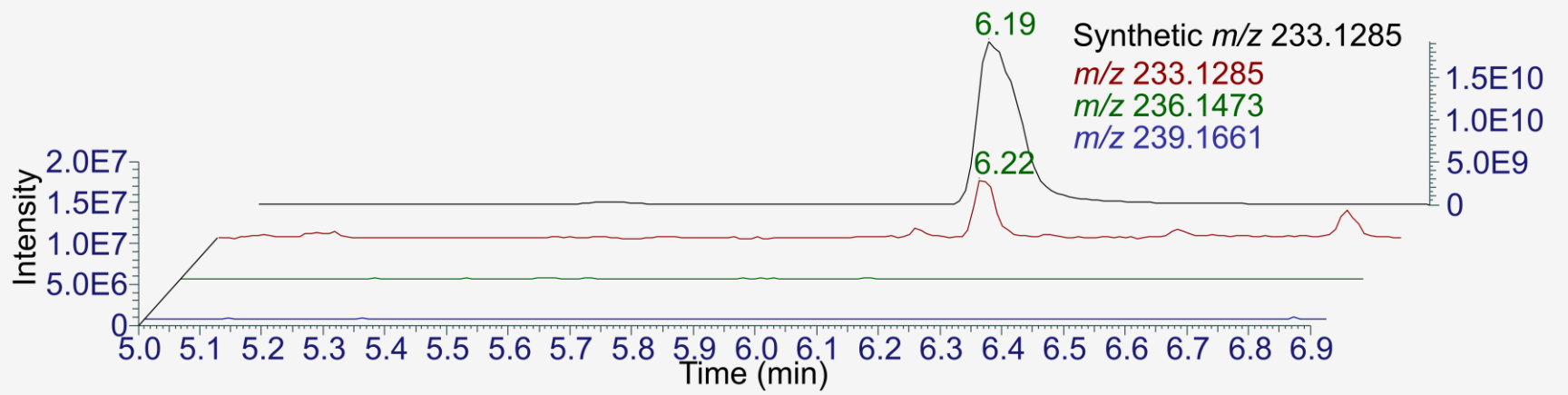

Supplemental Figure 4.19. D_3-Methionine feeding does not label DMW. EIC of synthetic DMW (black), a naturally co-eluting peak from a sample of *him-5* exo-metabolome (brown), the trace for D_3-DMW lacking a co-eluting peak (green), and the trace for D_6-DMW, also lacking a co-eluting peak.

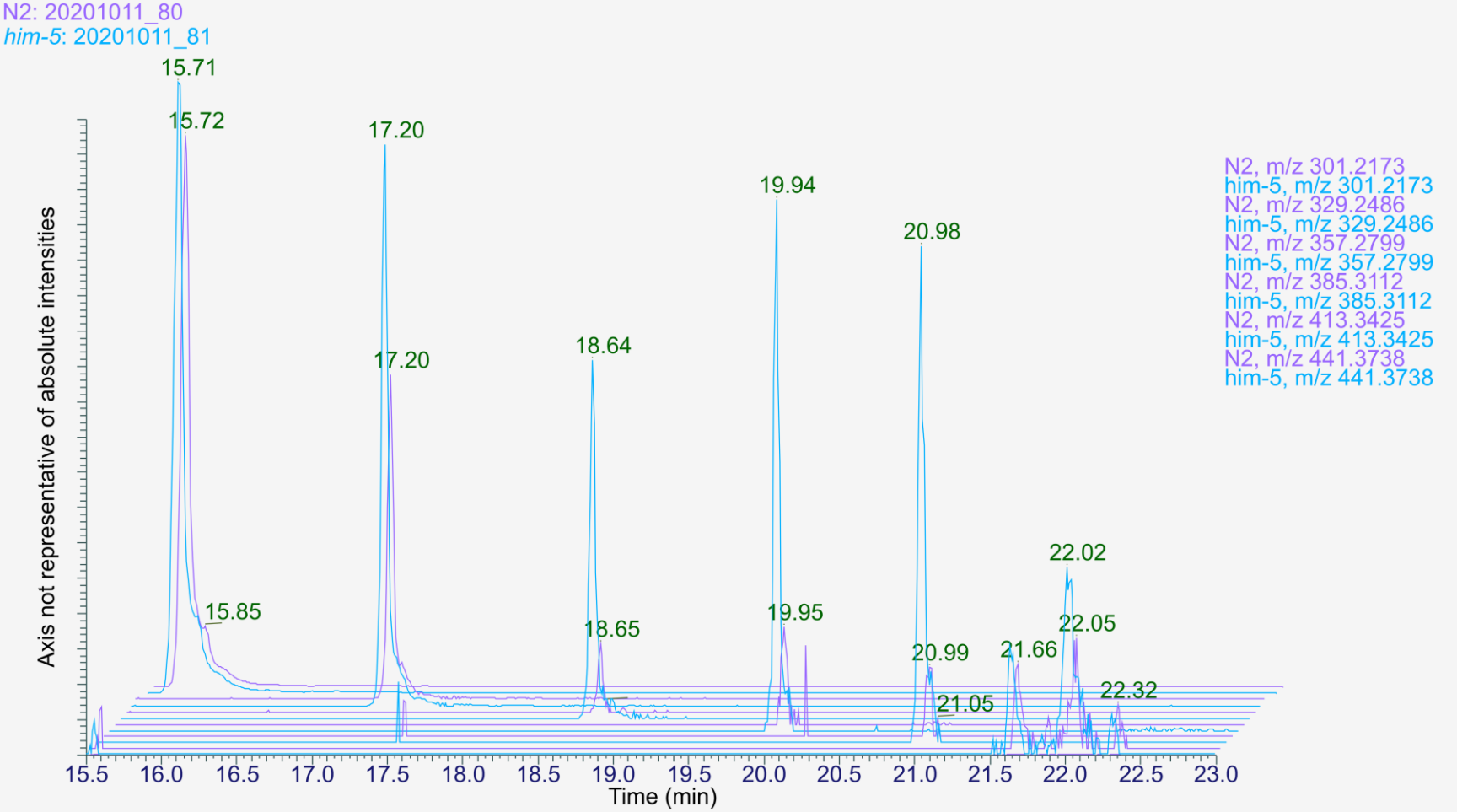

Supplemental Figure 4.20. Chromatography of the VLCPUFA series. EIC of VLCPUFAs from C_{20}-C_{30} in N2 and *him-5* endo-metabolome samples.

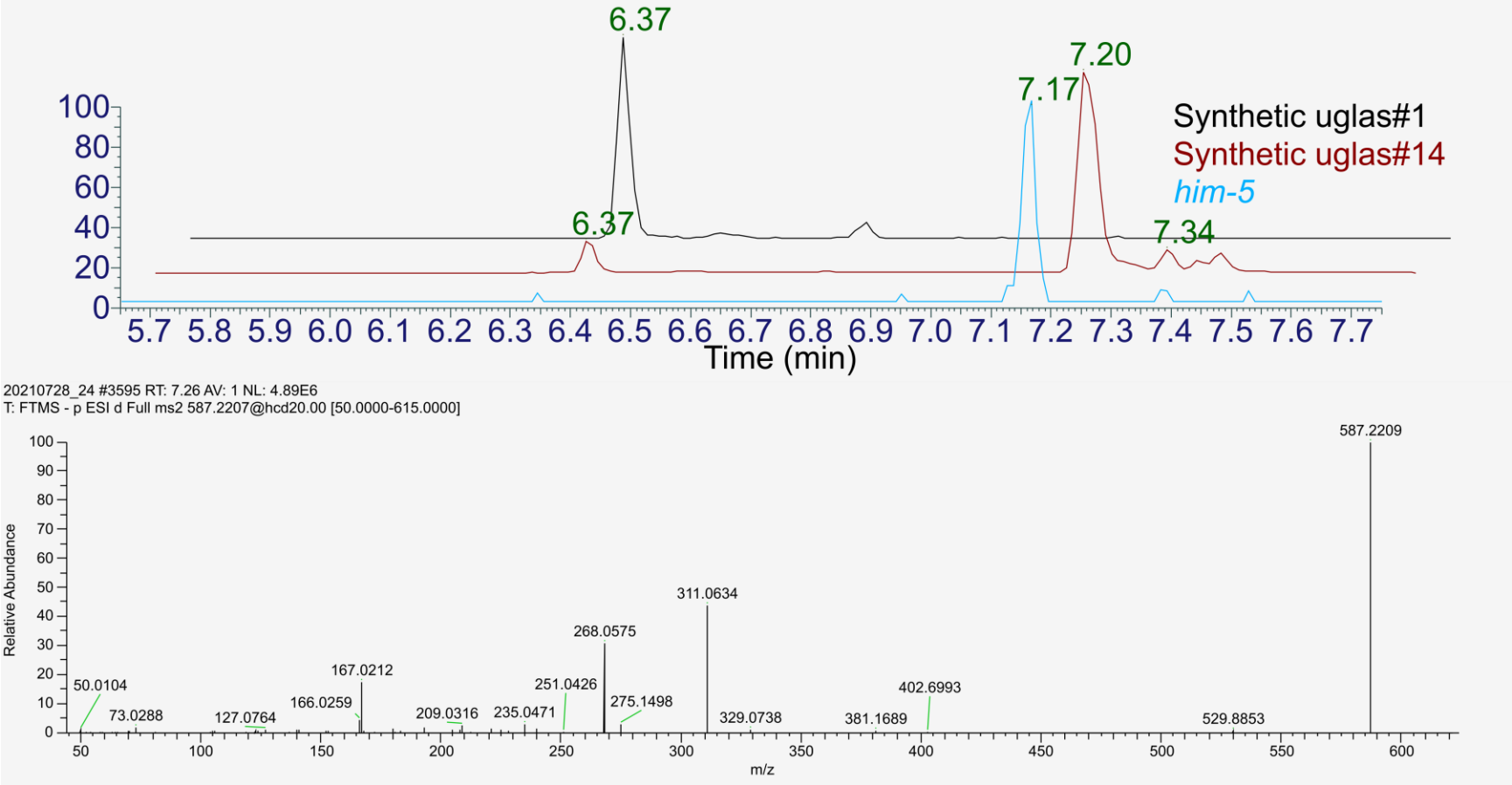

Supplemental Figure 4.21. MS and MS2 spectra for synthetic uglas#14. EIC of *m/z* 587.2211 in synthetic samples for uglas#1 and uglas#14 and a *him-5* endo-metabolome sample showing peaks for uglas#1 and uglas#2 and MS2 spectrum for synthetic uglas#14.

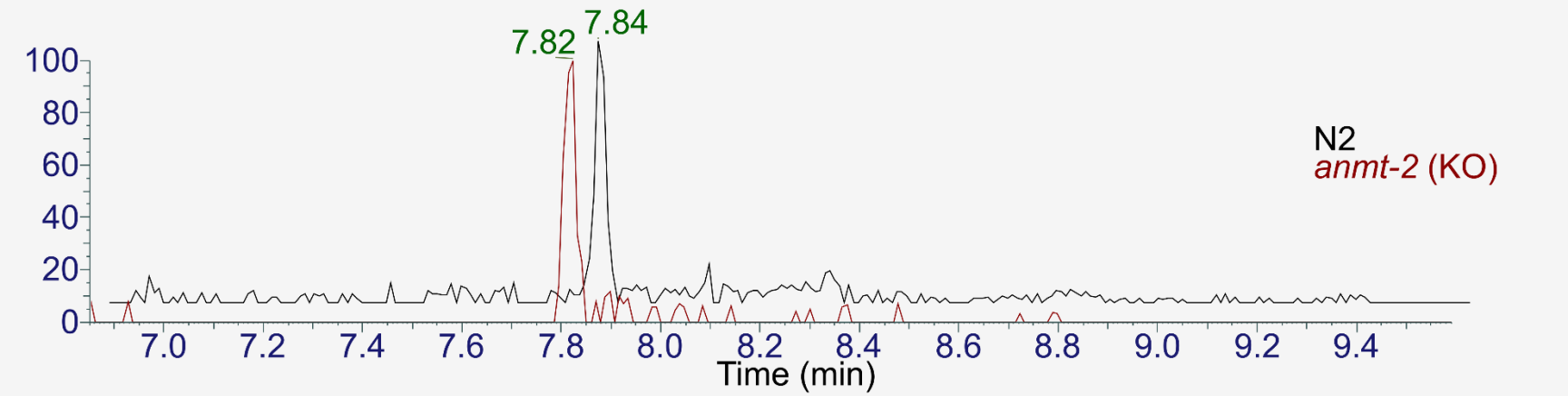

Supplemental Figure 4.22. Production of dmwi#1 is independent of ANMT-2. EIC of *m/z* 587.2211 in N2 and *anmt-2(gk3185)* endo-metabolome sample showing peaks for dmwi#2 shows it is still present in the absence of a functional ANMT-2 protein.

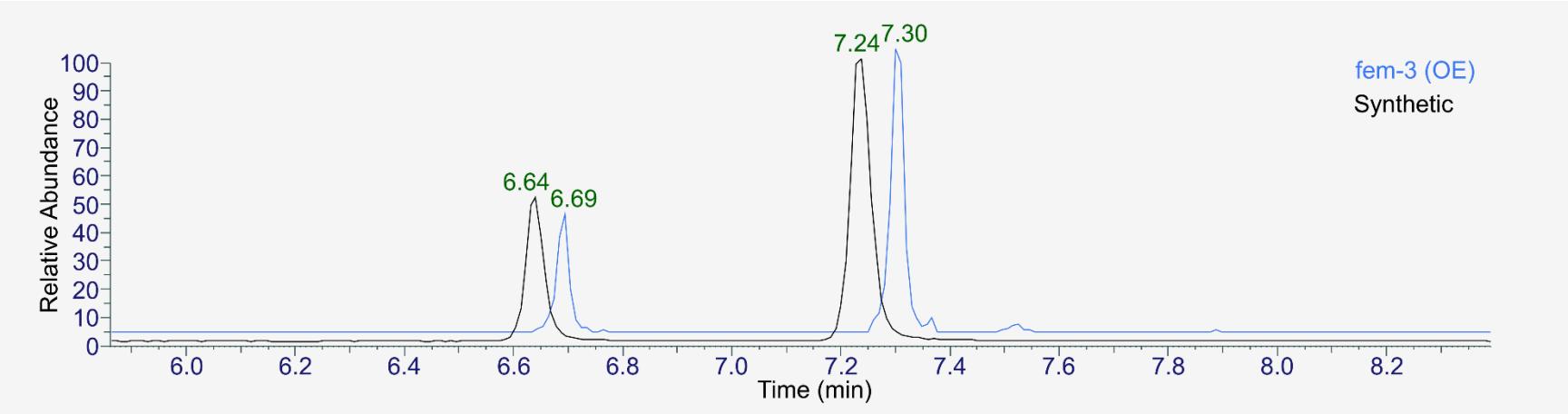

Supplemental Figure 4.23. MS spectra of natural and synthetic amta#1 and amta#2. EIC of *m/z* 340.1074 in a *fem-3* (OE) endo-metabolome sample (blue) and a synthetic standard of amta#1 and amta#2 (black).

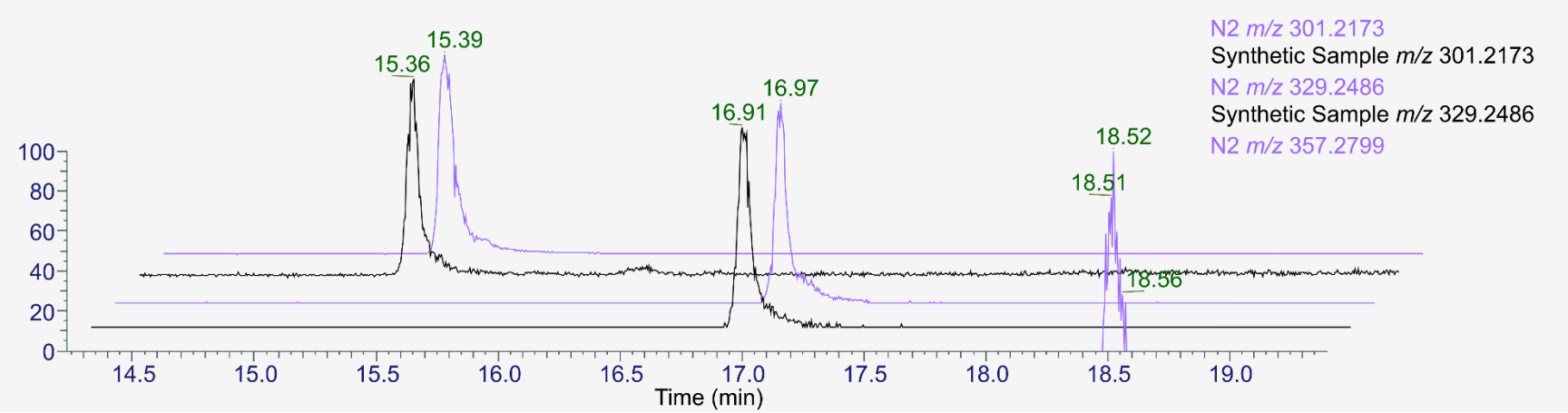

Supplemental Figure 4.24. MS spectra of natural and synthetic VLCPUFAs. EIC traces for eicosapentaenoic acid (*m/z* 301.2173) and docosapentaenoic acid (*m/z* 329.2486) in N2 endo-metabolome (purple) and a mixture of synthetic standards (black) and the EIC trace for tetracosapentaenoic acid (*m/z* 257.2799) in the endo-metabolome of N2.

Synthetic Procedures

panglu#1 (4.1). Synthetic protocols for panglu#1 will be reported in the dissertation of Brian Curtis, but NMR spectroscopic data for panglu#1 are included below.

uglas#1 and uglas#14. Synthetic protocols for the preparation of uglas#1 and uglas#14 are reported by Brian Curtis *et al.* but NMR spectroscopic data for both are reported below.

uglas#1[1]**:**

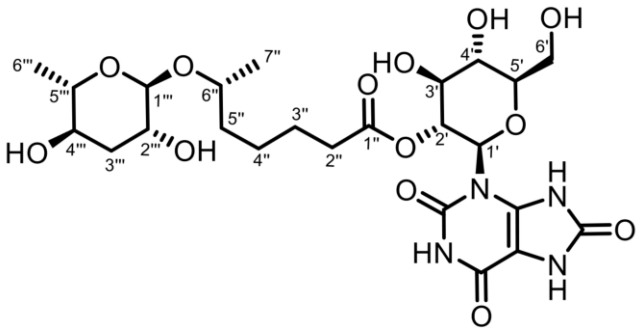

Supplemental Table 4.1 NMR spectroscopic data for uglas#1. ^{1}H (800 MHz), ^{13}C (201 MHz), CD_3OD. 13C NMR chemical shift data for uric acid carbons: δ 155.0 154.1, 150.6, 100.7. One of the uric acid carbons expected at ~134 ppm could not be observed due to line broadening.

Position	^{13}C [ppm]	^{1}H [ppm]	$J_{H,H}$ couplings [Hz}	HMBC correlations
1’	82.5	5.91	-	-
2’	72.2	5.20	-	-
3’	76.1	3.71	-	C-4’
4’	69.9	3.77	-	-
5’	81.7	3.56	$J_{5',6'}$ = 2.5	-
6’	61.5	3.89, 3.90	-	C-4’, C-5’
1’’	174.1	-	-	-
2’’	34.5	2.29	$J_{2'',3''}$ = 9.1	C-1’’, C-3’’
3’’	25.6	1.52	-	-
4’’	25.9	-	-	-
5’’	37.6	1.43, 1.52	$J_{5'',6''}$ = 6.8	C-3’’, C-4’’, C-6’’, C-7’’
6’’	71.9	3.75	$J_{6'',7''}$ = 6.1	C-5’’, C-1’’’
7’’	19.1	1.10	-	C-5’’, C-6’’
1’’’	97.3	4.65	$J_{1''',2'''}$ = 2.7	C-6’’, C-2’’’, C-3’’’, C-5’’’
2’’’	69.7	3.71	$J_{2''',3'''a}$ = 3.0, $J_{2''',3'''b}$ = 3.1	C-1’’’, C-3’’, C-4’’’

3’’’	35.6	1.76 (a), 1.94 (b)	$J_{3'''a,3'''b}$ = 13.1, $J_{3'''a,4'''}$ = 11.3 $J_{3'''b,4'''}$ = 4.6	C-1’’’ (b), C-2’’’ (a,b), C-4’’’ (a,b), C-5’’’ (a,b)
4’’’	68.1	3.51	$J_{4''',5'''}$ = 9.6	C-3’’’, C-5’’’, C-6’’’
5’’’	70.9	3.60	$J_{5''',6'''}$ = 6.2	C-1’’’, C-3’’’, C-4’’’, C-6’’’
6’’’	17.8	1.22	-	C-4’’’, C-5’’’

uglas#14[1]**:**

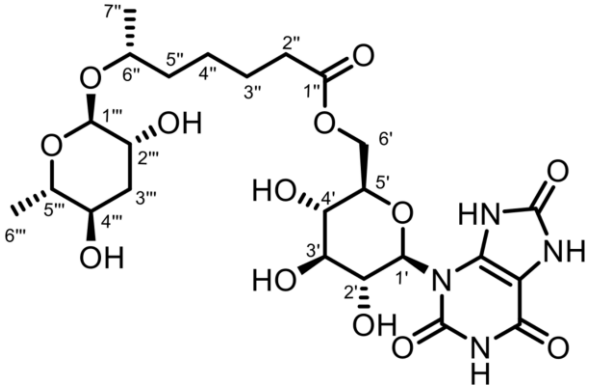

Supplemental Table 4.2 NMR spectroscopic data for uglas#14. ^{1}H (800 MHz), ^{13}C (201 MHz), CD_3OD. 13C NMR chemical shift data for uric acid carbons: δ 154.6, 154.1, 150.7, 134.8, 100.7.

Position	**^{13}C [ppm]**	**^{1}H [ppm]**	**$J_{H,H}$ couplings [Hz}**	**HMBC correlations**
1’	85.1	5.62 (broad)	-	-
2’	70.9	3.86	$J_{2',3'}$ = 9.2	-
3’	78.3	3.49	$J_{3',4'}$ = 9.5	C-1’, C-2’, C-4’, C-5’
4’	70.8	3.58	$J_{4',5'}$ = 10.5	C-3’, C-5’, C-6’, C-1’’
5’	79.0	3.71	$J_{5'6'a}$ = 7.5, $J_{5',6'b}$ = 2.0	C-3’
6’	64.7	4.30 (a), 4.48 (b)	$J_{6'a,6'b'}$ = 12.1	C-4’(a,b), C-5’ (a)
1’’	175.0	-	-	-
2’’	34.5	2.37	$J_{2'',3''}$ = 7.4	C-1’’, C-3’’
3’’	25.7	1.61	-	C-1’’, C-2’’, C-4’’, C-5’’
4’’	25.9	1.37, 1.43	-	C-2’’, C-3’’, C-5’’, C-6’’
5’’	37.6	1.43 (a), 1.5(b)	$J_{5''a,6''}$ = 7.4, $J_{5''b,6''}$ = 4.7	C-3’’, C-4’’, C-6’’, C-7’’
6’’	72.0	3.72	$J_{6'',7''}$ = 6.1	C-4’’, C-5’’, C-1’’’
7’’	19.0	1.09	-	C-5’’, C-6’’
1’’’	97.3	4.61	$J_{1''',2'''}$ = 2.6	C-6’’, C-2’’’, C-3’’’, C-5’’’

2’’’	69.7	3.70	$J_{2'''3'''a}$ = 3.4, $J_{2'''3'''b}$ = 3.2	C-1’’’, C-3’’
3’’’	35.7	1.75 (a), 1.93 (b)	$J_{3'''a,3'''b}$ = 13.1, $J_{3''a',4'''}$ = 11.0 $J_{3'''b,4'''}$ = 3.7	C-1’’’ (b), C-2’’’ (b), C-4’’’ (a,b), C-5’’’ (a,b)
4’’’	68.1	3.49	$J_{4'''5'''}$ = 9.6	C-3’’’, C-5’’’, C-6’’’
5’’’	71.0	3.58	$J_{5'''6'''}$ = 6.2	C-1’’’, C-3’’’, C-4’’’, C-6’’’
6’’’	17.8	1.19	-	C-4’’’, C-5’’’

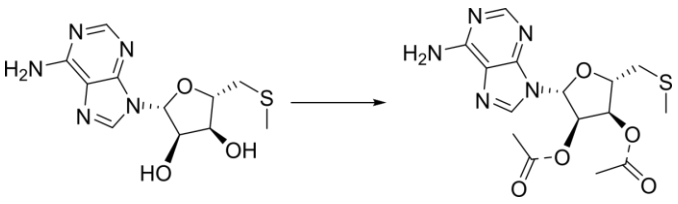

***(2O)*- and *(3O)*-acetyl-*S*-methylthioadenosine.** *S*-methylthioadenosine (MTA) (10 mg, 0.0336 mmol) was dissolved in pyridine (150 µL) and stirred at ambient temperature. Acetic anhydride (34 µL, 0.0336 mmol) was added and the reaction stirred. After 2 h methanol (2 mL) was added and the reaction stirred 30 min. The reaction was diluted with $CHCl_3$ and washed with 2% aqueous acetic acid (1×4 mL) and saturated sodium bicarbonate (1×6 mL) then dried over $MgSO_4$, filtered, and concentrated under reduced pressure. The resulting oil was purified by flash chromatography on silica. Elution with a gradient of 0-40% DCM/MeOH yielded the diacetylated product (10 mg, 74.9%) and a 1:3 mixture of the (2*O*)- and (3*O*)-acetylated products (2.5 mg, 20.9%).

***(3O)*-acetyl:**

^{1}H NMR ($CDCl_3$, 500 MHz) δ (ppm) 8.25 (s, 1H), 8.02 (s, 1H), 5.94 (d, 6.7 Hz, 1H), 5.38 (dd, 5.8, 2.8 Hz, 1H), 4.97 (t, 6.3 Hz, 1H), 4.48 (td, 5.6, 2.8 Hz, 1H), 2.90 (t, 5.5 Hz, 2H), 2.21 (s, 3H), 2.16 (s, 3H).

^{13}C NMR ($CDCl_3$, 125 MHz) δ (ppm) 170.6, 155.6, 152.7 (2C), 139.3, 89.5, 83.5, 75.0, 73.8, 37.1, 21.1, 17.0.

***(2O)*-acetyl:**

^{1}H NMR ($CDCl_3$, 500 MHz) δ (ppm) 8.31 (s, 1H), 7.98 (s, 1H), 6.09 (d, 3.4 Hz, 1H), 5.75 (dd, 5.6, 3.4 Hz, 1H), 4.83 (t, 6.3 Hz, 1H), 4.25 (q, 6.0 Hz, 1H), 2.99 (dd, 14.2, 5.2 Hz, 1H), 1.85-2.95 (m, 1H), 2.17 (s, 3H), 2.15 (s, 3H).

^{13}C NMR ($CDCl_3$, 125 MHz) δ (ppm) 170.4, 155.5, 153.1, 149.5, 139.7, 120.0, 87.2, 83.2, 76.1, 72.2, 36.4, 20.9, 16.9.

HRMS (ESI) *m/z*: Calculated: $(M+H)^+$ 340.1074. Actual: 340.1049. Δ ppm: -7.30.

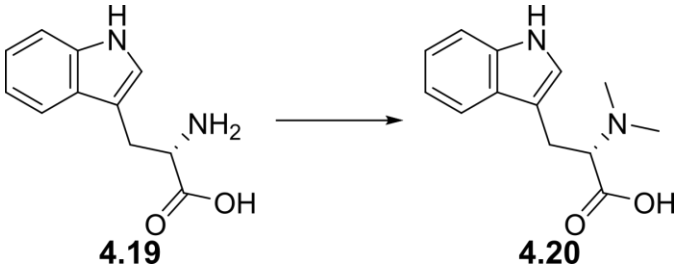

4.19 **4.20**

***N*,*N*-Dimethyltryptophan (4.20).** Based on a synthesis for *N*,*N*-dimethyltryptamine, tryptophan (1.0 g, 4.9 mmol) was stirred in MeOH (30 mL) at 0 °C under an atmosphere of argon[2]. Addition of sodium cyanoborohydride (1.5 g, 24 mmol) was added followed by formaldehyde (1.54 mL 36%, 20 mmol) and the reaction was stirred for 36 h. The reaction was concentrated and recrystallized from MeOH to yield white crystals (636 mg, 56%) that were used without further purification.

^{1}H NMR (D_6-DMSO, 500 MHz) δ (ppm) 10.83 (s, 1H), 7.54 (d, 7.8 Hz, 1H), 7.32 (d, 7.8 Hz, 1H), 7.06 (td, 7.2, 1.0 Hz, 1H), 6.97 (td, 7.2, 1.0 Hz, 1H), 3.47 (dd, 8.0, 6.1 Hz, 1H), 3.34 (dd, 14.8, 7.9 Hz, 1H), 2.97 (dd, 14.7, 6.2 Hz), 2.41 (s, 6H).

^{13}C NMR (D_6-DMSO, 125 MHz) δ (ppm) 171.0, 136.1, 127.2, 123.4, 120.9, 118.3, 118.2, 111.3, 110.5, 68.4, 41.3, 24.3.

HRMS (ESI) *m/z*: Calculated: $(M+H)^+$ 233.1289. Actual: 233.1270 . Δ ppm: 4.27.

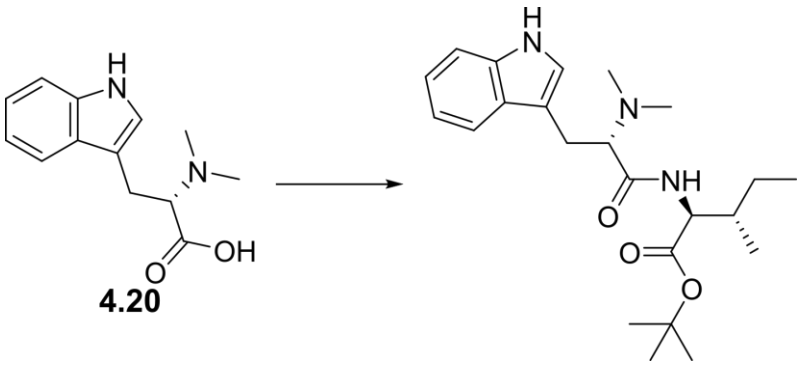

dmwi#1-*tert*-butyl ester. HOBt (11 mg, 0.0647 mmol), triethylamine (15 µL, 0.108 mmol), DCC (11.6 mg, 0.056 mmol), and isoleucine-*tert*-butyl ester (20 mg, 0.086 mmol) were added to a solution of *N*,*N*-dimethyltryptophan (10 mg, 0.043 mmol) in DCM (1 mL) and DMF (1 mL) and stirred overnight. The reaction was quenched with water (1 mL), extracted with DCM (3×5 mL), dried over $MgSO_4$, filtered, and concentrated under reduced pressure. The resulting solid was purified via flash chromatography on silica gel. Elution with a gradient of 0-10% DCM/MeOH yielded a mixture of dmwi#1-*tert*-butyl ester and isoleucine-*tert*-butyl ester (27.8 mg), which was used without further purification.

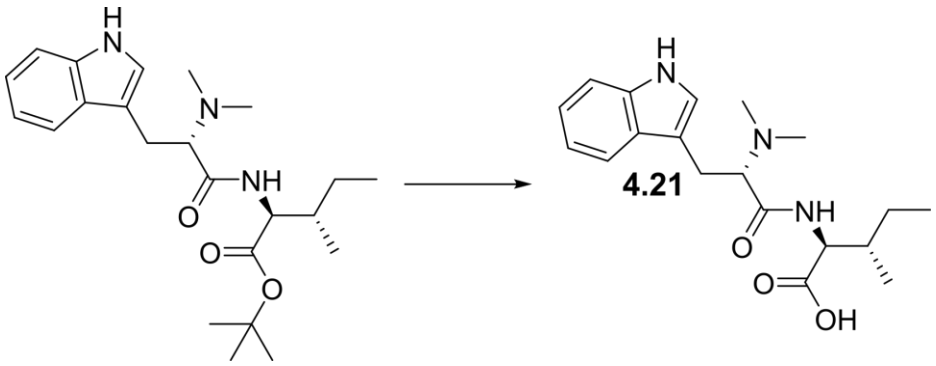

dmwi#1 (4.21). TFA (530 µL, 6.88 mmol) was added to a stirring solution of dmwi#1-*tert*-butyl ester and isoleucine-*tert*-butyl ester (27.8 mg) in DCM (530 µL) and stirred for 4 h. The reaction was then concentrated under reduced pressure. The resulting oil was purified via flash chromatography on silica gel. Elution with a gradient of 0-20% DCM/MeOH yielded dmwi#1 as a white solid (14.9 mg, ~100%).

^{1}H NMR (CD_3OD, 500 MHz) δ (ppm) 7.59 (d, 8.0 Hz, 1H), 7.36 (d, 8.1 Hz, 1H), 7.22 (s, 1H), 7.12 (td, 7.3, 1 Hz, 1H), 7.05 (td, 7.3, 1 Hz, 1H), 4.29 (d, 5.5 Hz, 1H), 4.22 (dd, 8.9, 5.3 Hz, 1H), 3.50 (dd, 14.6, 5.2 Hz, 1H), 3.42 (dd, 14.6, 8.9 Hz, 1H), 2.98 (s, 6H), 1.78-1.89 (m, 1H), 1.35-1.48 (m, 1H), 1.08-1.18 (m, 1H), 0.89 (t, 7.5 Hz, 3H), 0.88 (d, 6.8 Hz, 3H).

^{13}C NMR (CD_3OD, 125 MHz) δ (ppm) 173.2, 168.5, 138.1, 128.2, 125.6, 120.3, 118.8, 112.6, 107.2, 69.5, 58.4, 54.8, 42.4, 38.4, 26.2, 25.7, 15.9, 11.7.

HRMS (ESI) *m/z*: Calculated: $(M+H)^+$ 346.2125. Actual: 346.2102. Δ ppm: 6.77.

NMR Spectra of Synthetic Compounds

uglas#1, ^{1}H NMR spectrum (800 MHz, CD_3OD)[1]

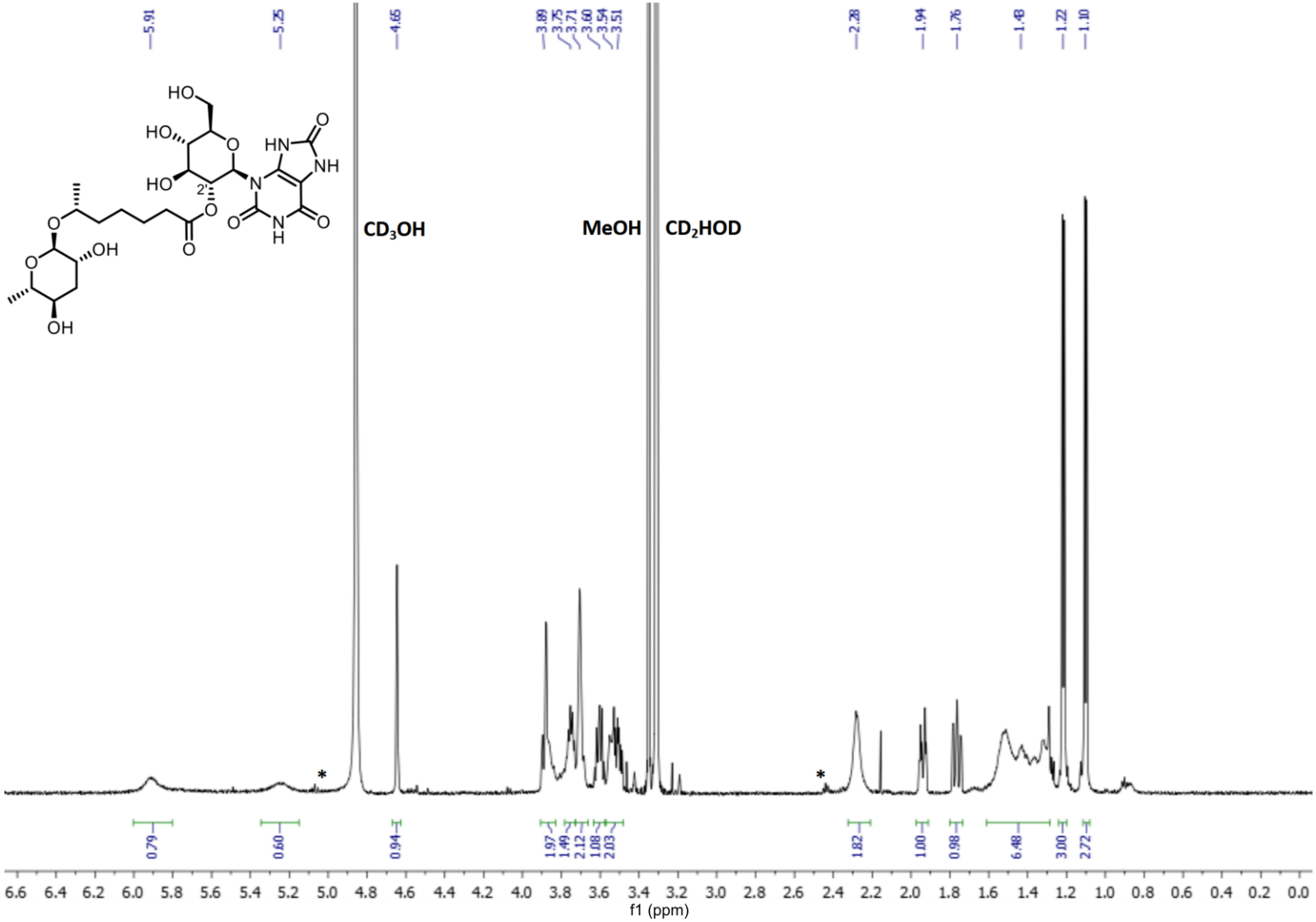

uglas#1, ^{13}C NMR spectrum (206 MHz, CD_3OD)[1]

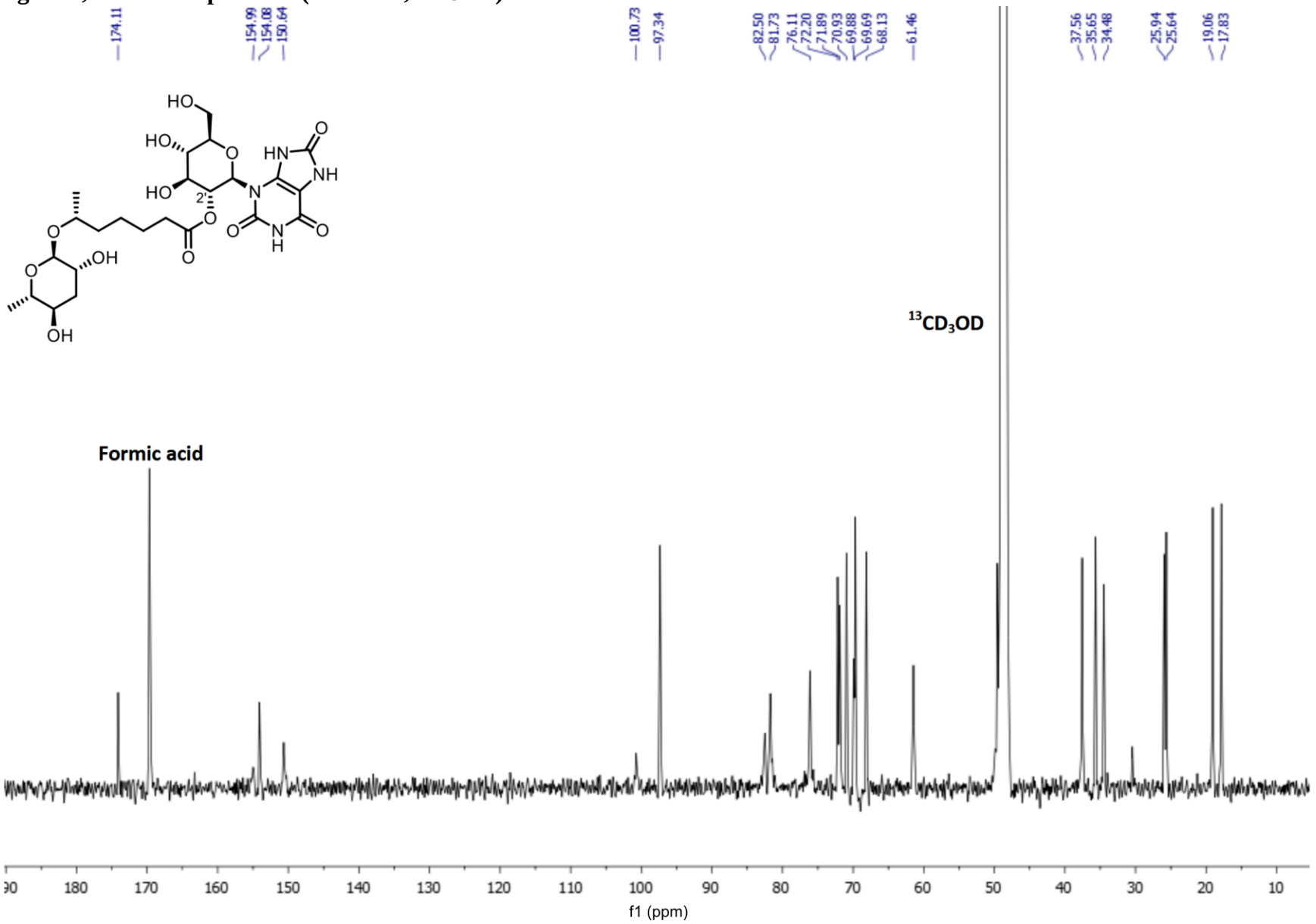

uglas#14, ^{1}H NMR spectrum(800 MHz, CD_3OD)[1]

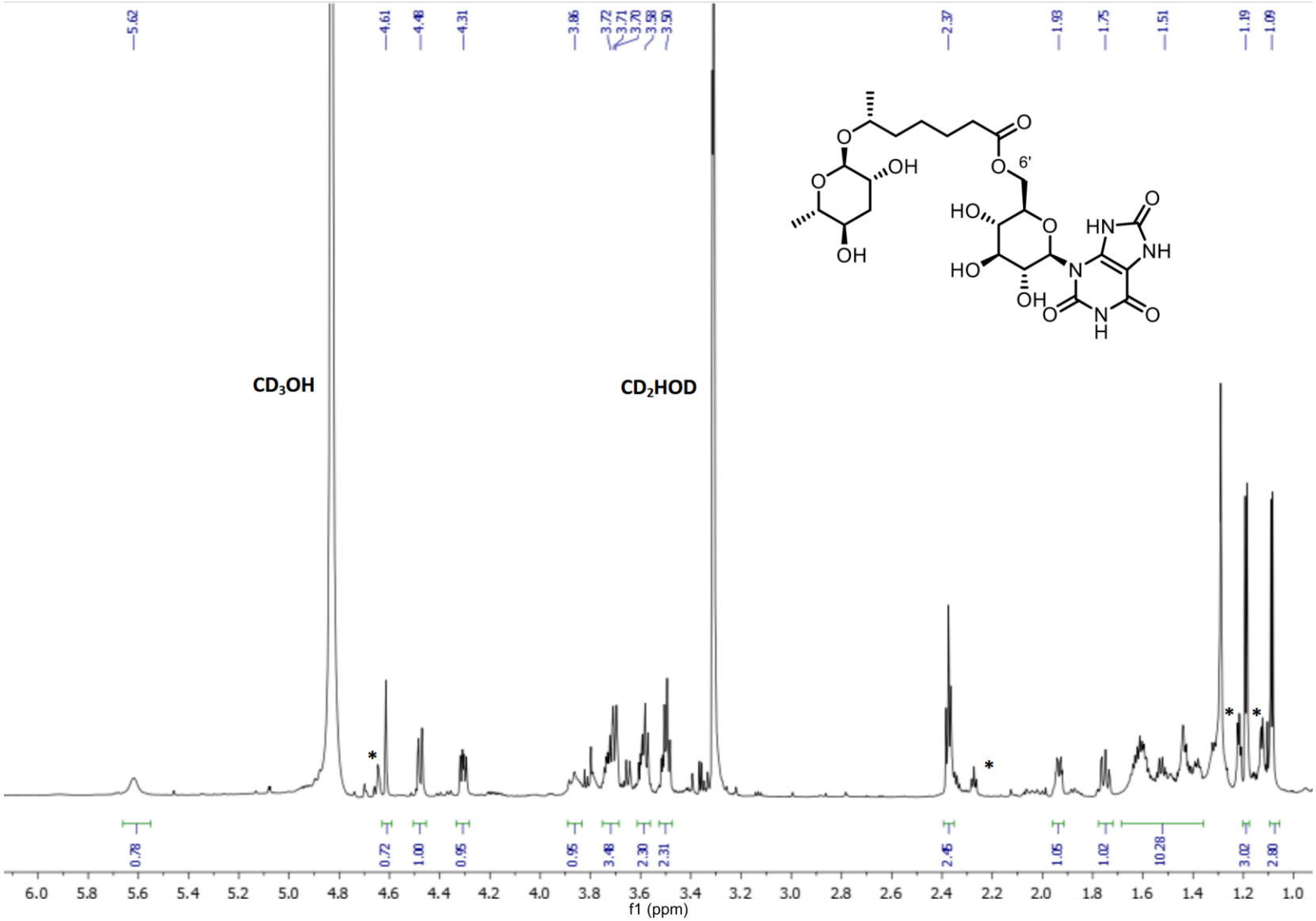

uglas#14, ^{13}C NMR spectrum (201 MHz, CD_3OD)[1]

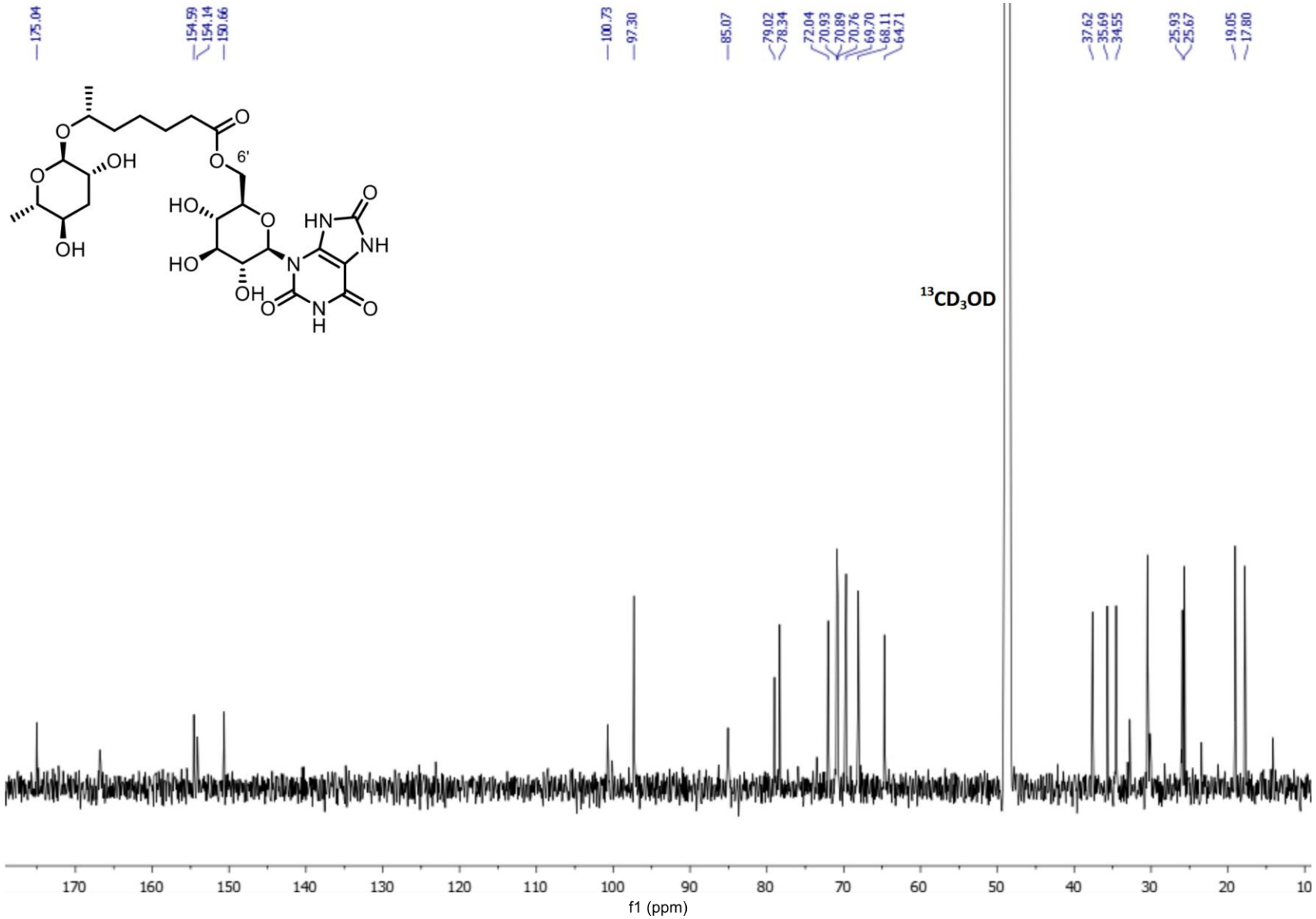

(2*O*)- and (3*O*)-acetyl-*S*-methylthioadenosine (amta#1 and amta#2), ^{1}H NMR spectrum (500 MHz, $CDCl_3$)

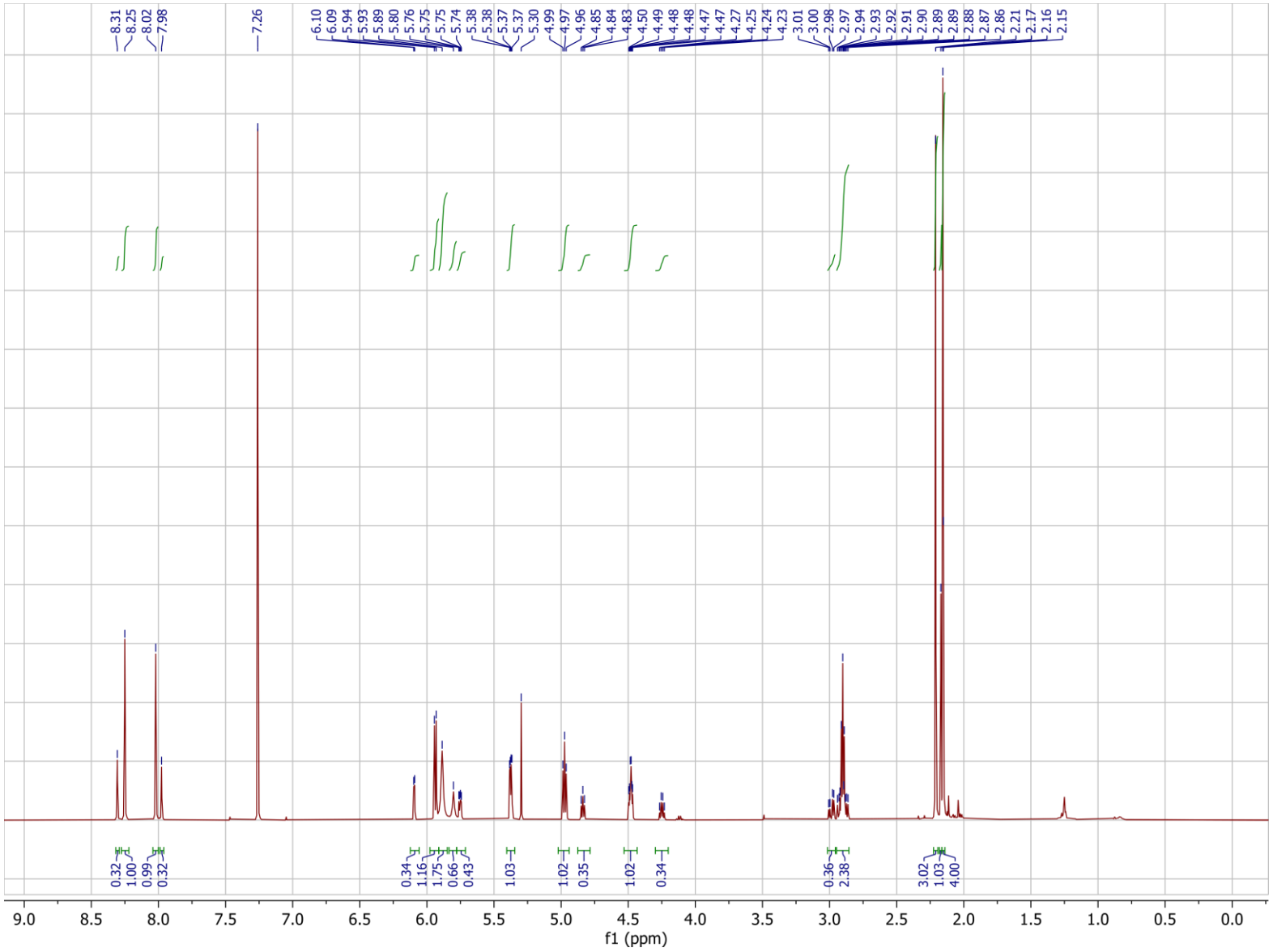

amta#1 and amta#2, ^{13}C NMR spectrum (125 MHz, $CDCl_3$)

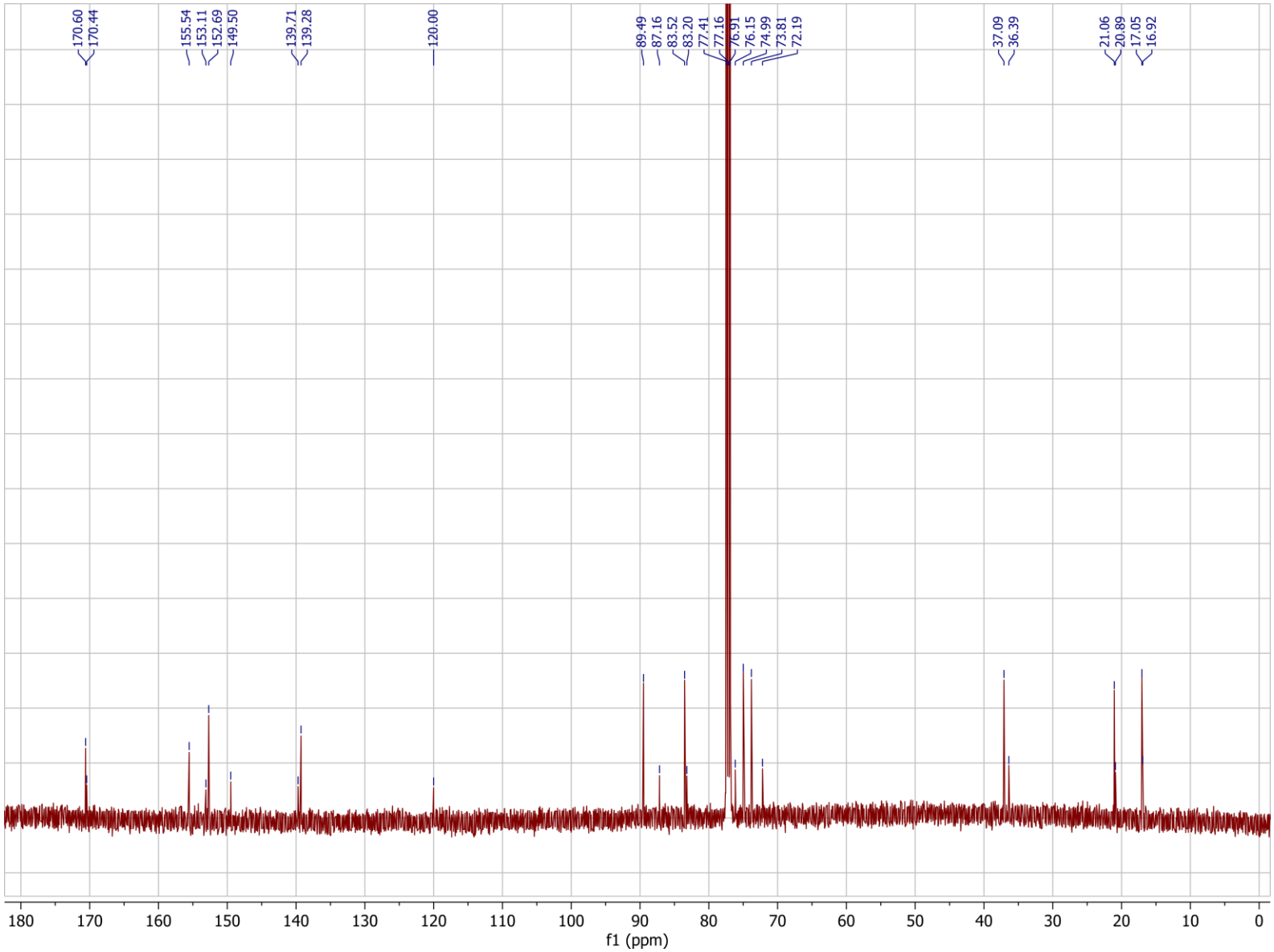

***N*,*N*-Dimethyltryptophan (4.19), ^{1}H NMR spectrum (500 MHz, D_6-DMSO)**

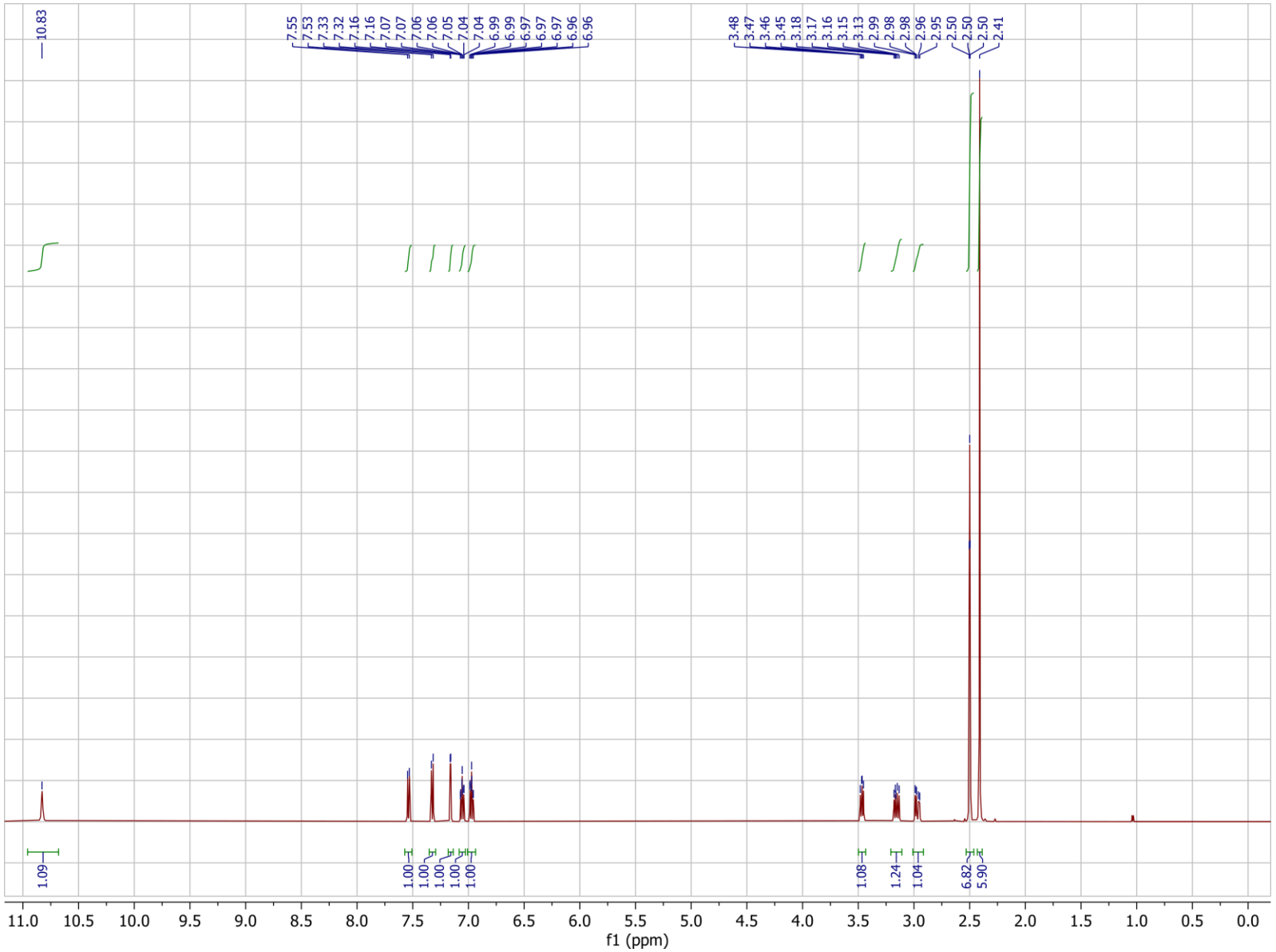

***N,N*-Dimethyltryptophan (4.19), ^{13}C NMR spectrum (125 MHz, D$_6$-DMSO)**

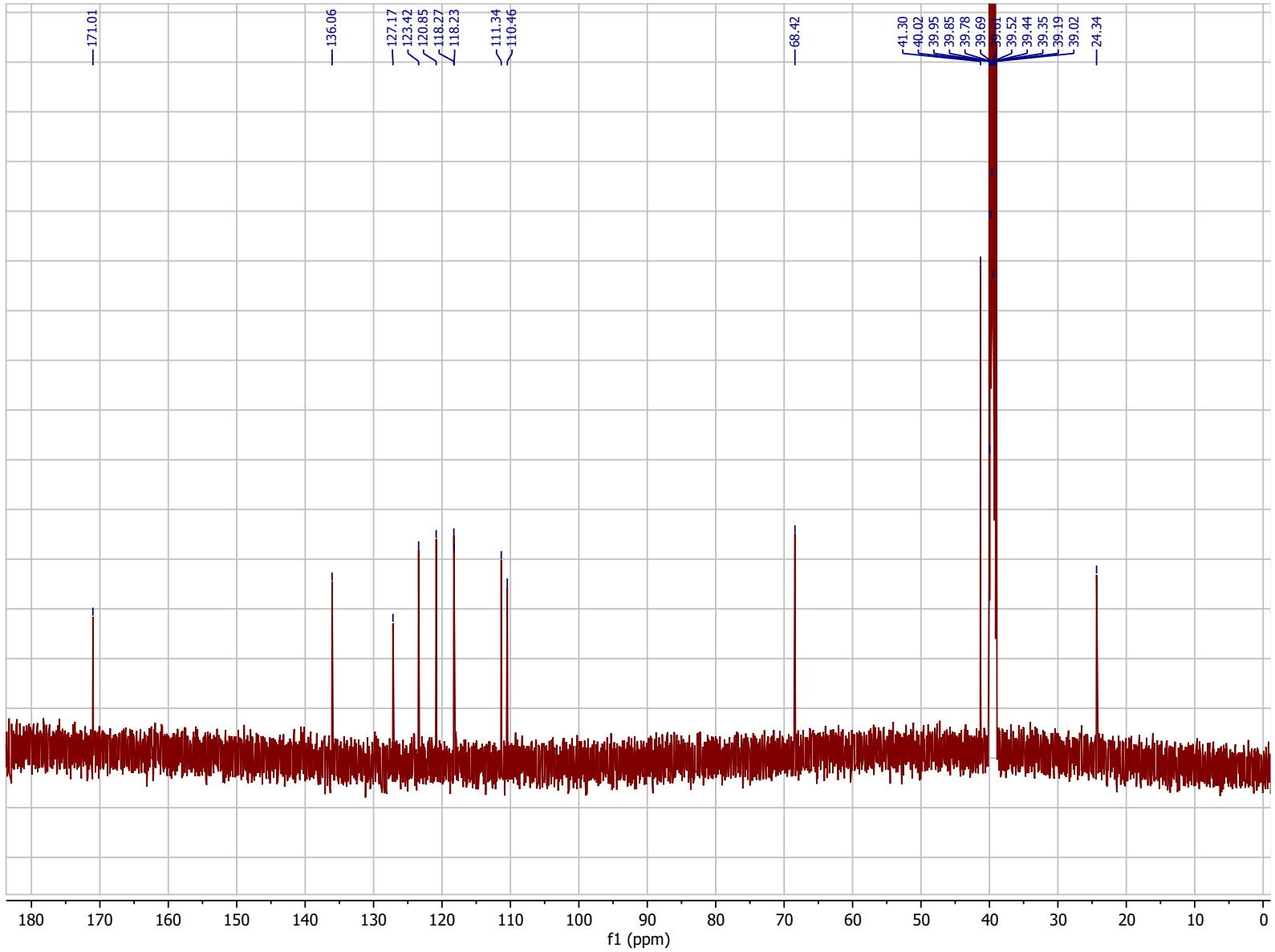

dmwi#1, ^{1}H NMR spectrum (500 MHz, CD_3OD)

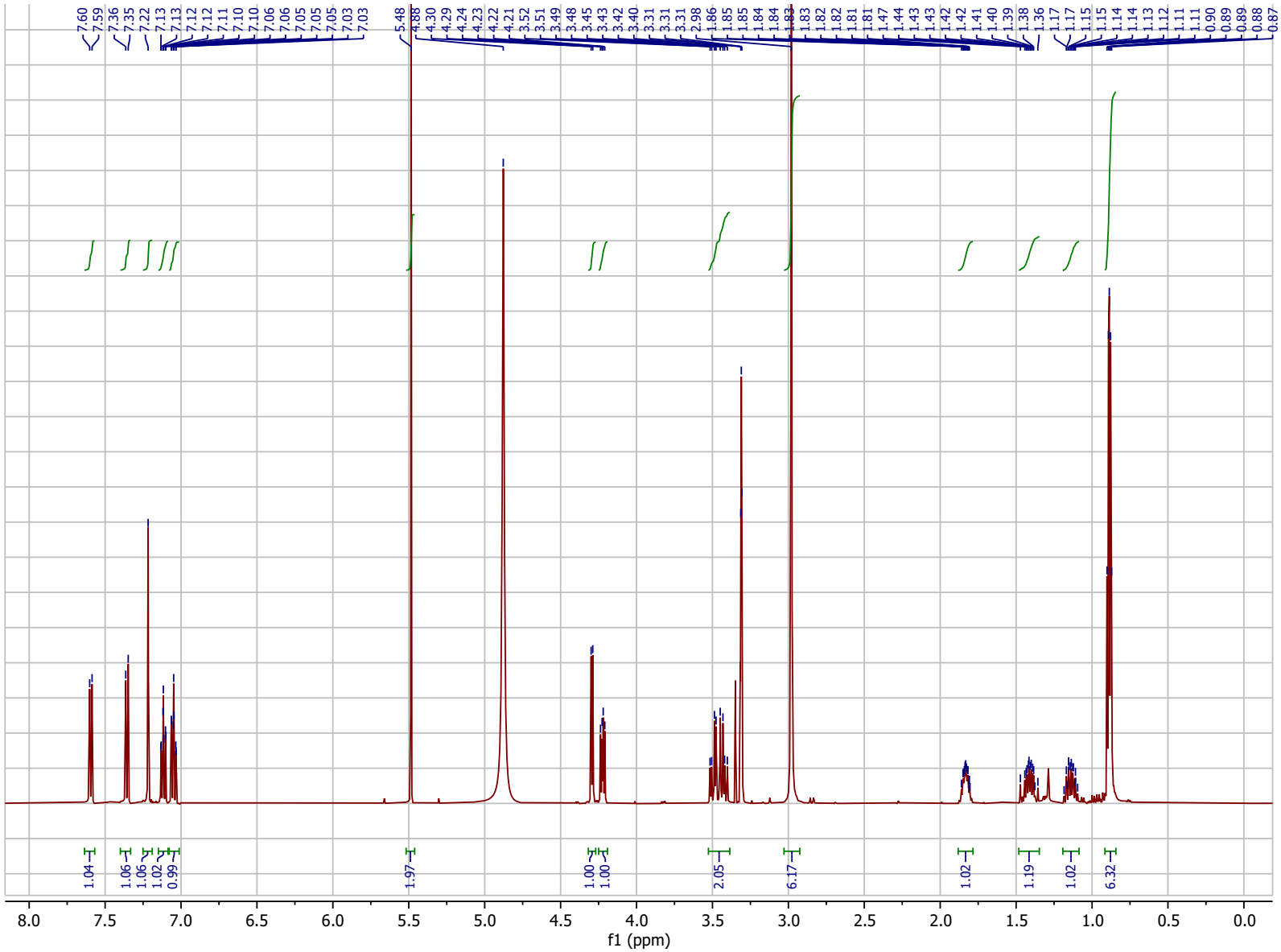

dmwi#1, ^{13}C NMR spectrum (104 MHz, CD_3OD)

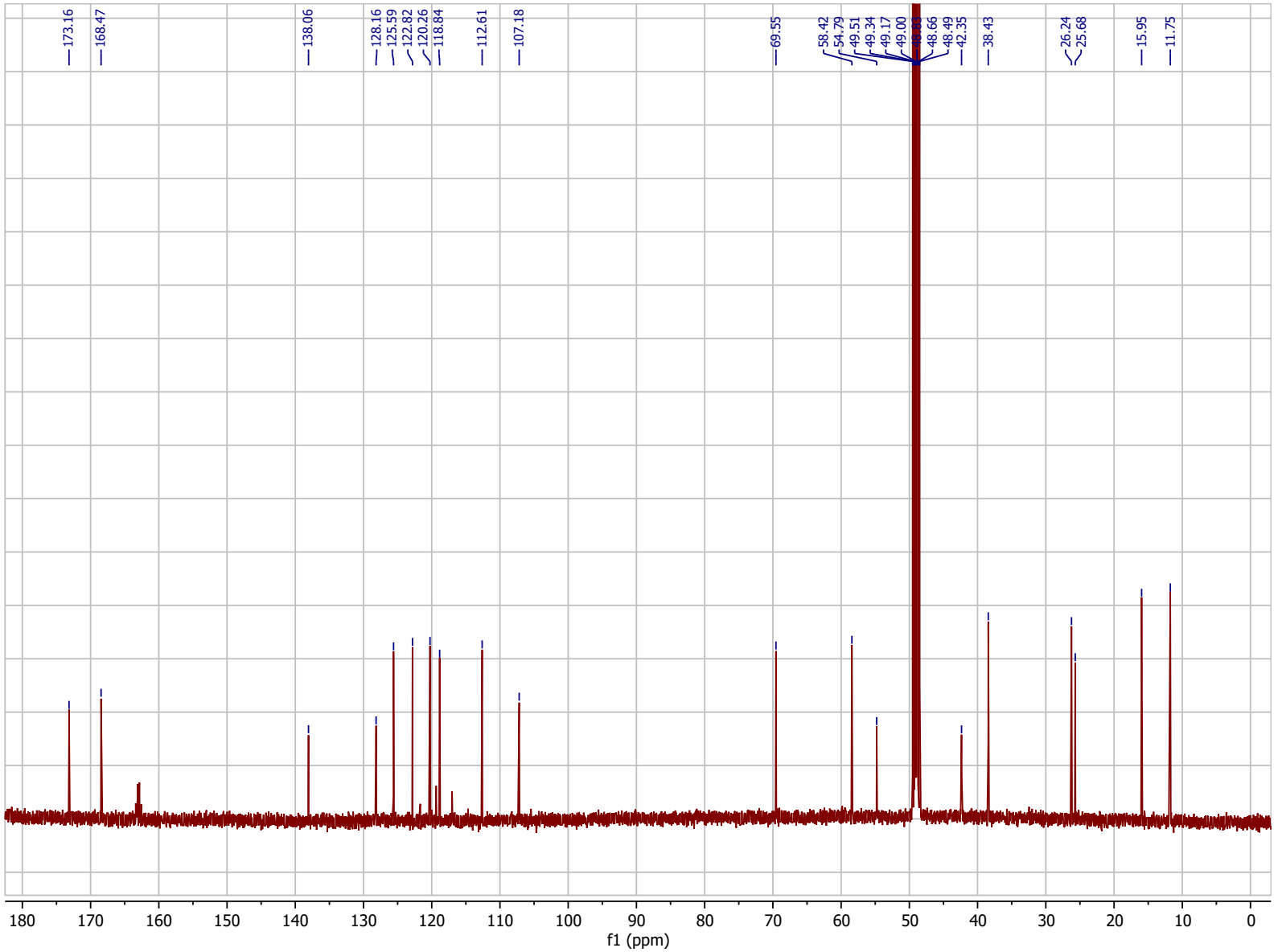

Supplemental Citations

(1) Curtis, B. J., Kim, L. J., Wrobel, C. J. J., Eagan, J. M., Smith, R. A., Burch, J. E., Le, H. H., Artyukhin, A. B., Nelson, H. M., Schroeder, F. C. Identification of uric acid gluconucleoside-ascaroside conjugates in *Caenorhabditis elegans* by combining synthesis and MicroED. *Org. Lett.* **22**: 6724-6728. **2020.**

(2) Brandt, S. D., Moore, S. A., Freeman, S., Kanu, A. B. Characterization of the synthesis of *N*,*N*-dimethyltryptamine by reductive amination using gas chromatography ion trap mass spectrometry. *Drug Test. Anal*. **2**: 330-338. **2010.**

APPENDIX E

Supplemental Information for Chapter 5

Experimental

General Procedures

Unless stated otherwise, all reactions were performed under argon in flame-dried glassware. All commercially available reagents were used as purchased unless otherwise stated. All solvents were dried over activated 3Å sieves for a minimum of 24 hours unless used in reactions where aqueous reagents were involved. Thin-layer chromatography (TLC) was performed with J.T. Baker Silica Gell IB2-F plastic-backed plates. Reverse-phase column chromatography was performed using Teledyne ISCO CombiFlash Rf and Rf+ systems with Teledyne ISCO RediSep Rf and Rf Gold silica columns. Nuclear Magnetic Resonance (NMR) spectra were recorded on a Varian INOVA 600 (600 MHz) or Bruker AV 500 (500 MHz) in the Cornell University NMR Facility. ^{1}H NMR chemical shifts are reported in ppm (δ) relative to the residual solvent peaks (7.26 ppm for $CDCl_3$) and ^{13}C NMR shifts relative to their respective residual solvent peaks (77.16 for $CDCl_3$).

Synthetic Procedures

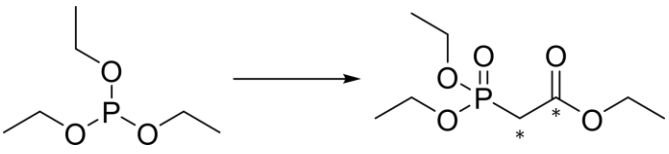

Triethyl phosphonoacetate-1,2-$^{13}C_2$. Triethyl phosphite (305 µL, 1.78 mL) and ethyl bromoacetate-$^{13}C_2$ (250 mg, 1.48 mmol) were stirred to reflux under argon. After 3 hours the

reaction was concentrated under reduced pressure to remove remaining starting material and bromoethane, yielding ethyl bromoacetate-$^{13}C_2$ (260 mg, 97%) which was used without further purification[1].

^{1}H NMR ($CDCl_3$, 600 MHz) δ (ppm) 4.14-4.21 (m, 6H), 3.06 (dd, 21.5, 7.5, 1H), 2.84 (dd, 21.5, 7.5, 1H), 1.34 (t, 7.1 Hz, 6 H), 1.28 (t, 7.1 Hz, 3H).

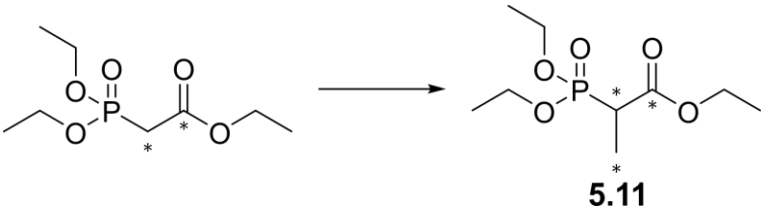

5.11

Triethyl 2-phosphonopropionate-1,2,3-$^{13}C_3$ (5.11). Triethyl phosphonoacetate-$^{13}C_2$ (260 mg, 1.3 mmol) and methyl iodide-^{13}C (97.4 µL, 1.56 mmol) were added to a solution of tetrabutyl ammonium fluoride (6.5 mL, 1M) and the reaction wrapped in foil. The reaction was vortexed for 180 s, poured into 100 mM aqueous NH_4OAc w/ 0.5% AcOH (10 mL), and extracted with EtOAc (3×10 mL). The combined organics were washed with water (1×10 mL), dried over $MgSO_4$, filtered, and concentrated under reduced pressure. The resulting liquid was purified by flash chromatography with silica gel. Elution with a gradient of 0-20% DCM/MeOH yielded triethyl 2-phosphonopropionate-1,2,3-$^{13}C_3$ (**5.11**, 227.0 mg, 72.5%)[2].

^{1}H NMR ($CDCl_3$, 300 MHz) δ (ppm) 4.10-4.22 (m, 6H), 3.12-3.30 (m, 0.5H), 2.69-2.87 (m, 0.5H), 1.60-1.70 (m, 1.5H), 1.17-1.35 (m, 10.5 H).

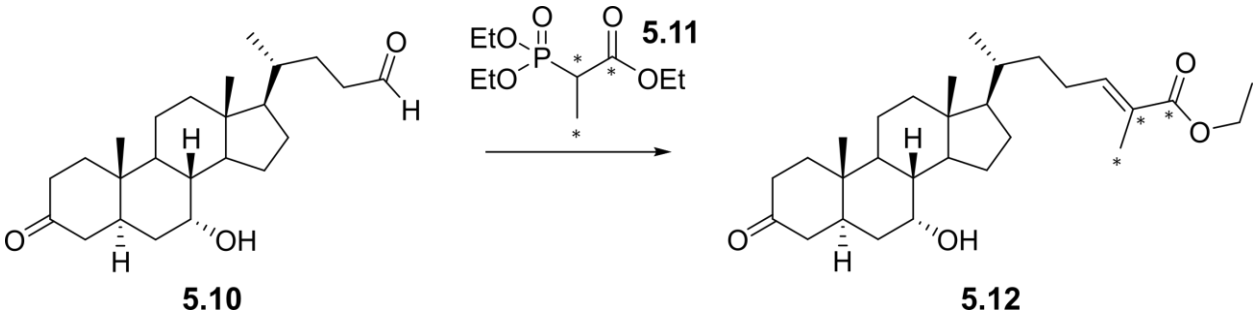

Ethyl *(E)*-3-oxo-5α-7α-hydroxy-cholest-25-enoate-25,26,27-$^{13}C_3$ (5.12). Based on the synthesis of dafa#2 by Dr. Joshua Judkins, triethyl 2-phosphonopropionate-1,2,3-$^{13}C_3$ (227 mg, 0.941 mmol) was added to a stirring solution of LiCl (100 mg, 2.36 mmol) and diisopropyl ethylamine (547 µL, 3.14 mmol) in MeCN (8 mL) and stirred under argon for 1 h[3]. Aldehyde **5.10** (292 mg, 0.785 mmol) was dissolved in MeCN (12 mL) and added to the reaction. After 36 hours the reaction was diluted with saturated aqueous NaCl (30 mL) and extracted with DCM (3×30 mL). The combined organics were dried over $MgSO_4$, filtered, concentrated under reduced pressure, and purified via flash chromatography on silica gel. Elution with a gradient of 0-100% EtOAc/hexanes yielded α-β unsaturated ester-$^{13}C_3$ **5.12** (217.2 mg, 60.3%).

^{1}H NMR ($CDCl_3$, 300 MHz) δ (ppm) 6.74 (m, 1H), qd (4.19, 7.2, 3.2 Hz, 2H), 3.87 (bs, 1H), 1.10-2.45 (m, 37H), 1.00 (s, 3H), 0.96 (d, 6.4 Hz, 3H), 0.69 (s, 3H).

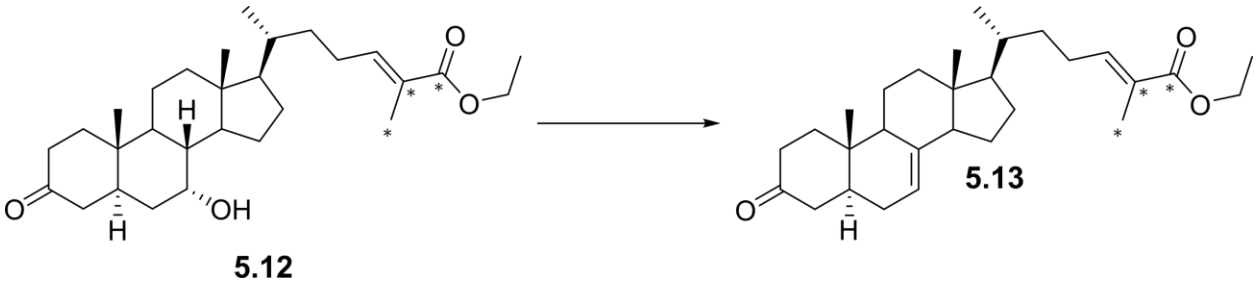

Ethyl *(E)*-3-oxo-5α-cholest-7,25-enoate-25,26,27-$^{13}C_3$ (5.13). Alcohol **5.12** (208 mg, 0.452 mmol) and Burgess reagent (323 mg, 1.36 mmol) were dissolved in toluene (30 mL) and stirred

at reflux under argon[3]. After 2 h the reaction was poured into saturated aqueous NaCl (30 mL) and extracted with EtOAc (3×30 mL). The combined organics were dried over $MgSO_4$, filtered, concentrated under reduced pressure, and purified via flash chromatography on silica gel. Elution with a gradient of 0-100% EtOAc/hexanes yielded diene **5.13** (154 mg, 77%).

^{1}H NMR ($CDCl_3$, 600 MHz) δ (ppm) 6.74 (m, 1H), 5.18 (m, 1H), qd (7.1, 2.9 Hz, 2H), 1.10-2.45 (m, 35H), 1.01 (s, 3H), 0.98 (d, 6.6 Hz, 3H), 0.57 (S, 3H).

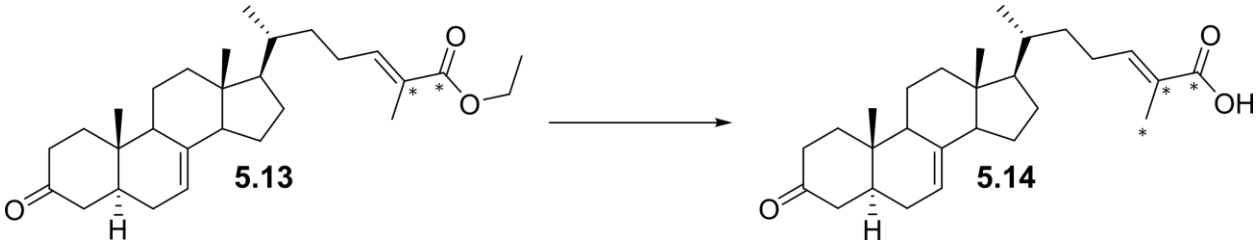

Ethyl *(E)*-3-oxo-5α-cholest-7,25-enoic acid-25,26,27-$^{13}C_3$ (5.14). The α-β unsaturated ester **5.13** (91.1 mg, 0.205 mmol) was added to a solution of LiOH (204 mg, 4.87 mmol) in 1:2:2 water:MeOH:THF (4.5 mL) and stirred at ambient temperature[3]. After 27 hours the reaction was acidified with aqueous 1M HCl and extracted with DCM (3×10 mL). The combined organics were dried over $MgSO_4$, filtered, and concentrated to yield acid **5.14** (84.7 mg, 99.6%) which was used in the next step without further purification.

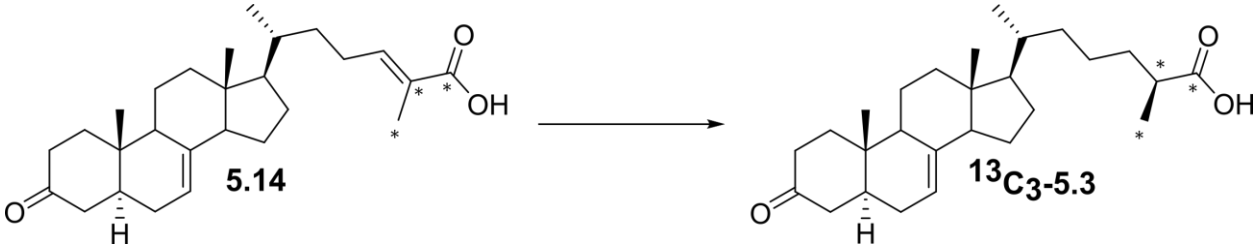

***(25S)*-Δ7-dafachronic acid-25,26,27-$^{13}C_3$ ($^{13}C_3$-dafa#2, $^{13}C_3$-5.3).** The α-β unsaturated acid **5.14** (84.7 mg, 0.204 mmol) was stirred in MeOH (10 mL) and purged with argon three times[3]. *(S)*-$Ru(OAc)_2[H_8$-BINAP] (18 mg) was suspended in MeOH (8 mL), purged with argon three

times, and added to the acid. The reaction was purged with argon three times, purged with H_2 three times, and stirred at 50 °C under an atmosphere of H_2. After 24 hours the reaction was purged with argon, concentrated under reduced pressure, and purified via flash chromatography on silica gel. Elution with a gradient of 0-30% EtOAc/hexanes w/ 0.25% AcOH yielded 83.3 mg impure $^{13}C_3$-dafa#2. Further purification via reverse phase preparatory HPLC yielded pure $^{13}C_3$-dafa#2, with a typical run with 1.3 mg crude dafachronic acid yielding 0.9 mg pure dafachronic acid.

^{1}H NMR ($CDCl_3$, 600 MHz) δ (ppm) 5.18 (bs, 1H), 2.54-2.62 (m, 0.5H), 2.43 (td, 14.6, 6.0 Hz, 1H), 2.33-2.39 (m, 0.5H), 2.30-2.31 (m, 3H), 2.09-2.16 (m, 1H), 2.03-2.07 (m, 1H), 1.18-1.92 (m, 22H), 1.03-1.11 (m, 2H), 1.01 (s, 3H), 0.93 (d, 6.4 Hz, 3H), 0.56 (s, 3H).

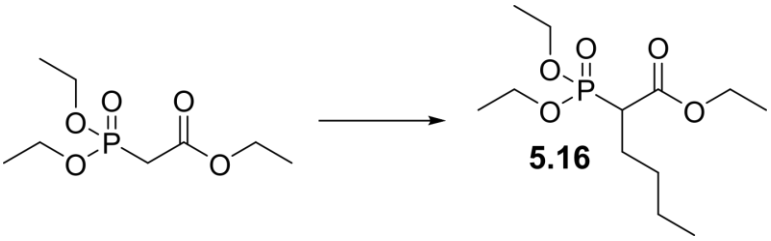

Triethyl 2-phosphonohexanoate (5.16). Sodium iodide (75 mg, 0.5 mmol) and potassium carbonate (276 mg, 2 mmol) were added to a stirring solution of bromobutane (101 µL, 1.2 mmol) and triethyl phosphonoacetate (200 µL, 1 mmol) under an atmosphere of argon[4]. The reaction was heated to 60 °C and stirred for 22 h. The reaction was diluted with saturated aqueous NaCl (2 mL) and extracted with Et_2O (4×2 mL). The combined organics were dried over $MgSO_4$, filtered, and concentrated under reduced pressure. The resulting oil was purified via flash chromatograph on silica gel. Elution with a gradient of 0-100% EtOAc/hexanes yielded triethyl phosphonohexanoate (**5.16**) (146 mg, 52.1%).

^{1}H NMR ($CDCl_3$, 600 MHz) δ (ppm) 4.17-4.25 (m, 2H), 4.10-4.17 (m, 4H), 2.91 (ddd, 22.5, 11.2, 3.8 Hz, 1H), 1.94-2.01 (m, 1H), 1.78-1.87 (m, 1H), 1.32 (td, 7.1, 3.0 Hz, 6H), 1.28 (t, 7.2 Hz, 3H), 1.23-1.37 (m, 4H), 0.88 (t, 6.8 Hz, 3H).

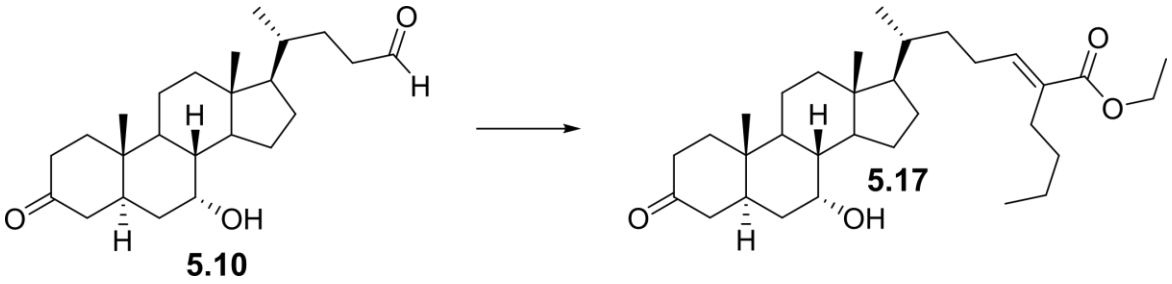

Ethyl (*E*)-3-oxo-5α-7α-hydroxy-26-propylcholest-25-enoate (5.17). Triethyl phosphonohexanoate (71 mg, 0.25 mmol) was added to a stirring solution of LiCl (16.1 mg, 0.38 mmol) and diisopropylethylamine (87 µL, 0.51 mmol) in MeCN (1 mL) and stirred for 3 hours[3]. 3-Oxo-5α-7α-hydroxy-cholan-24-al (**5.10**, 47 mg, 0.126 mmol) was dissolved in MeCN (2.5 mL) and added to the reaction and stirred for 5 days. The reaction was diluted with saturated aqueous NaCl (10 mL) and extracted with EtOAc (4×10 mL), dried over $MgSO_4$, filtered, and concentrated under reduced pressure. The resulting oil was purified via flash chromatography on silica gel. Elution with a gradient of 0-100% EtOAc/hexanes yielded a mixture of ethyl ester **5.17** and triethyl phosphonohexanoate (25.8 mg, 41.0%) and used without further purification.

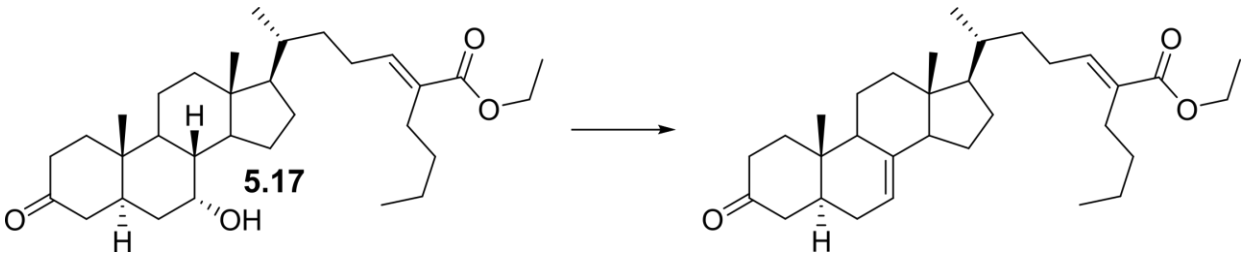

Ethyl (*E*)-3-oxo-5α-26-propylcholest-7,25-enoate. The product of the above reaction was combined with Burgess reagent (36.8 mg, 0.156 mmol) and toluene (3 mL) and heated to reflux

and stirred 4 h then cooled to ambient temperature, diluted with saturated aqueous NaCl (5 mL), and extracted with EtOAc (4×10 mL)[3]. The organics were dried over $MgSO_4$, filtered, and concentrated under reduced pressure. The resulting oil was purified via flash chromatography on silica gel. Elution using a gradient of 0-60% EtOAc/hexanes yielded a mixture of the *cis*- and *trans*-isomers of the desired unsaturated ethyl ester (2.8 mg, 59.6%).

***trans*: ^{1}H NMR ($CDCl_3$, 400 MHz)** δ (ppm) 6.71 (t, 7.65 Hz, 1H), 5.19 (bs, 1H), 4.18 (q, 7.1 Hz, 2H), 1.10-2.48 (m, 38H), 1.01 (s, 3H), 0.97 (d, 6.6 Hz, 3H), 0.57 (s, 3H).

***cis*: ^{1}H NMR ($CDCl_3$, 400 MHz)** δ (ppm) 5.80 (t, 7.5 Hz, 1H), 5.19 (bs, 1H), 4.18 (q, 7.2 Hz, 2H), 1.10-2.48 (m, 38H), 0.96 (s, 3H), 0.93 (d, 6.3 Hz, 3H), 0.56 (s, 3H).

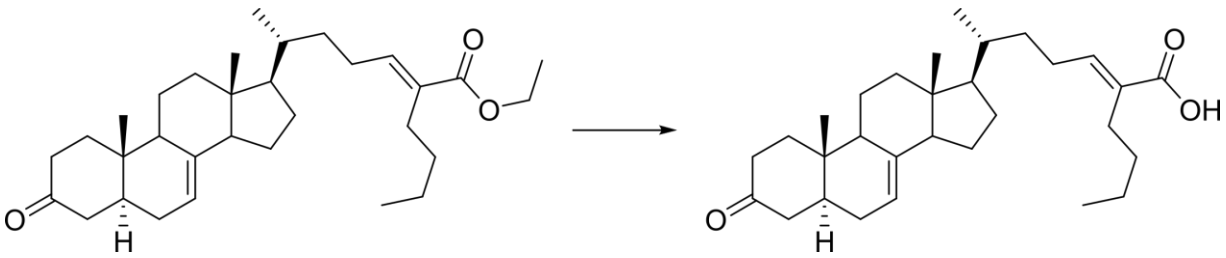

(*E*)-3-oxo-5α-26-propylcholest-7,25-enoic acid. Lithium hydroxide (4.9 mg, 0.116 mmol) was added to a stirring solution of ethyl (*E*)-3-oxo-5α-26-propylcholest-7,25-enoate (2.8 mg, 0.006 mmol) in 1:2:2 water:MeOH:THF (100 µL)[3]. The reaction was stirred for 16 hours, acidified with 1M aqueous HCl, diluted with saturated aqueous NaCl (5 mL), and extracted with DCM (4×10 mL). The combined organics were dried over $MgSO_4$, filtered, and concentrated under reduced pressure. The resulting α-β unsaturated acid (1.4 mg, 53.6%) was used in the next step without further purification.

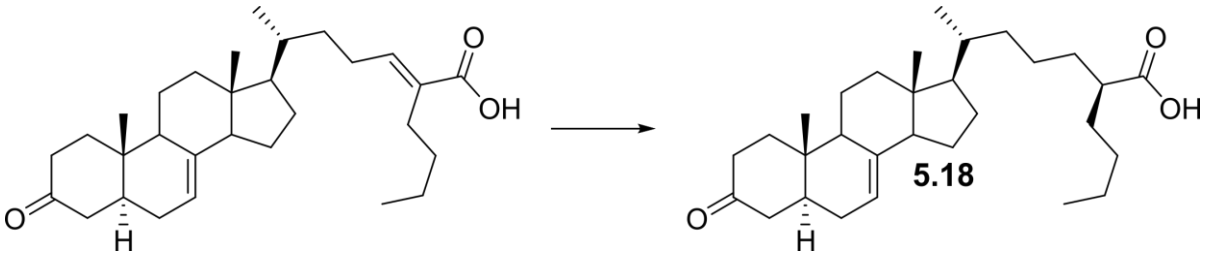

***(25S)*-butyl-Δ^7-dafachronic acid (butyl-dafa#2) (5.18).** Ethyl (*E*)-3-oxo-5α-26-propylcholest-7,25-enoic acid (1.4 mg, 0.0031 mmol) was stirred in MeOH (400 µL) and purged with argon three times[3]. *(S)*-Ru(OAc)$_2$[H$_8$-BINAP] (0.9 mg) was suspended in MeOH (300 µL), transferred to the stirring solution, and the reaction purged with argon three times, purged with H_2 three times, and stirred at 50 °C under an atmosphere of H_2 for 3 h. The reaction was cooled to ambient temperature and concentrated under reduced pressure, then purified via flash chromatography on silica gel. Elution with a gradient of 0-60% EtOAc/hexanes with 0.25% acetic acid yielded butyl-dafa#2 (**5.18**, 1.1 mg, 78.6%) which was further purified via reverse phase preparatory HPLC to yield pure butyl-dafa#2 (0.8 mg, 57.2%).

^{1}H NMR (CDCl$_3$, 500 MHz) δ (ppm) 5.18 (bs, 1H), 2.42 (td, 14.7, 6.0 Hz, 1H), 2.35-2.40 (m, 1H), 2.20-2.30 (m, 3H), 2.12 (ddd, 13.4, 5.9, 2.5 Hz, 1H), 2.04 (dt, 12.9, 3.2 Hz, 1H), 1.78-1.92 (m, 4H), 1.70-1.77 (m, 1H), 1.18-1.66 (m, 23H), 1.01 (s, 3H), 0.92 (d, 6.5 Hz, 3H), 0.89 (t, 7.0 Hz, 3 H), 0.55 (s, 3H).

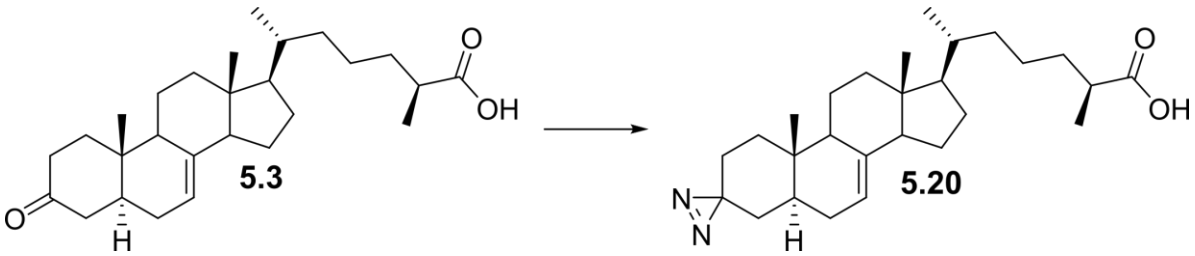

***(25S)*-3,3-azi-Δ^7-dafachronic acid (diazo-dafa#2, 5.20).** Based on the preparation of diazirines reported by Dr. Ying Zhang, ammonia (7.5 µL, 7 N, 0.053 mmol) was added to a stirring

solution of dafa#2 (3 mg, 0.007 mmol) in MeOH (500 µL) at 0 °C and stirred at ambient temperature for 3 h then cooled to 0 °C[2]. Hydroxylamine-*O*-sulfonic acid in MeOH (1 mg, 0.009 mmol, 8 µL) was added and the reaction stirred overnight. The reaction was diluted with MeOH (3 mL), filtered, concentrated under reduced pressure, and resuspended in MeOH (500 µL) in a foil-wrapped vial. Triethylamine (2 µL, 0.017 mmol) was added and the solution stirred for 10 min. I_2 crystals (~1.5 mg) were added to the solution until color persisted for 10 minutes of additional stirring. The reaction was diluted with EtOAc (10 mL), washed with 1 M aqueous HCl (1×5 mL), saturated aqueous sodium thiosulfate (1×5 mL), dried over $MgSO_4$, filtered, concentrated under reduced pressure, and purified via flash chromatography on silica gel. Elution with 0-100% EtOAc/hexanes yielded the diazirine (1.0 mg, 32.3%).

^{1}H NMR ($CDCl_3$, 600 MHz) δ (ppm) 5.15 (bs, 1H), 2.49 (q, 6.8 Hz, 1H), 2.35 (t, 7.6 Hz, 1H), 2.1-1.0 (m, 24H), 1.19 (d, 7.0 Hz, 3H), 0.92 (d, 6.4 Hz, 3H), 0.85 (s, 3H), 0.54 (s, 3H), 0.33 (m, 1H), 0.28 (m, 1H).

NMR Spectra of Synthetic Compounds, Triethyl phosphonoacetate-1,2-^{13}C, ^{1}H NMR spectrum (600 MHz, $CDCl_3$)

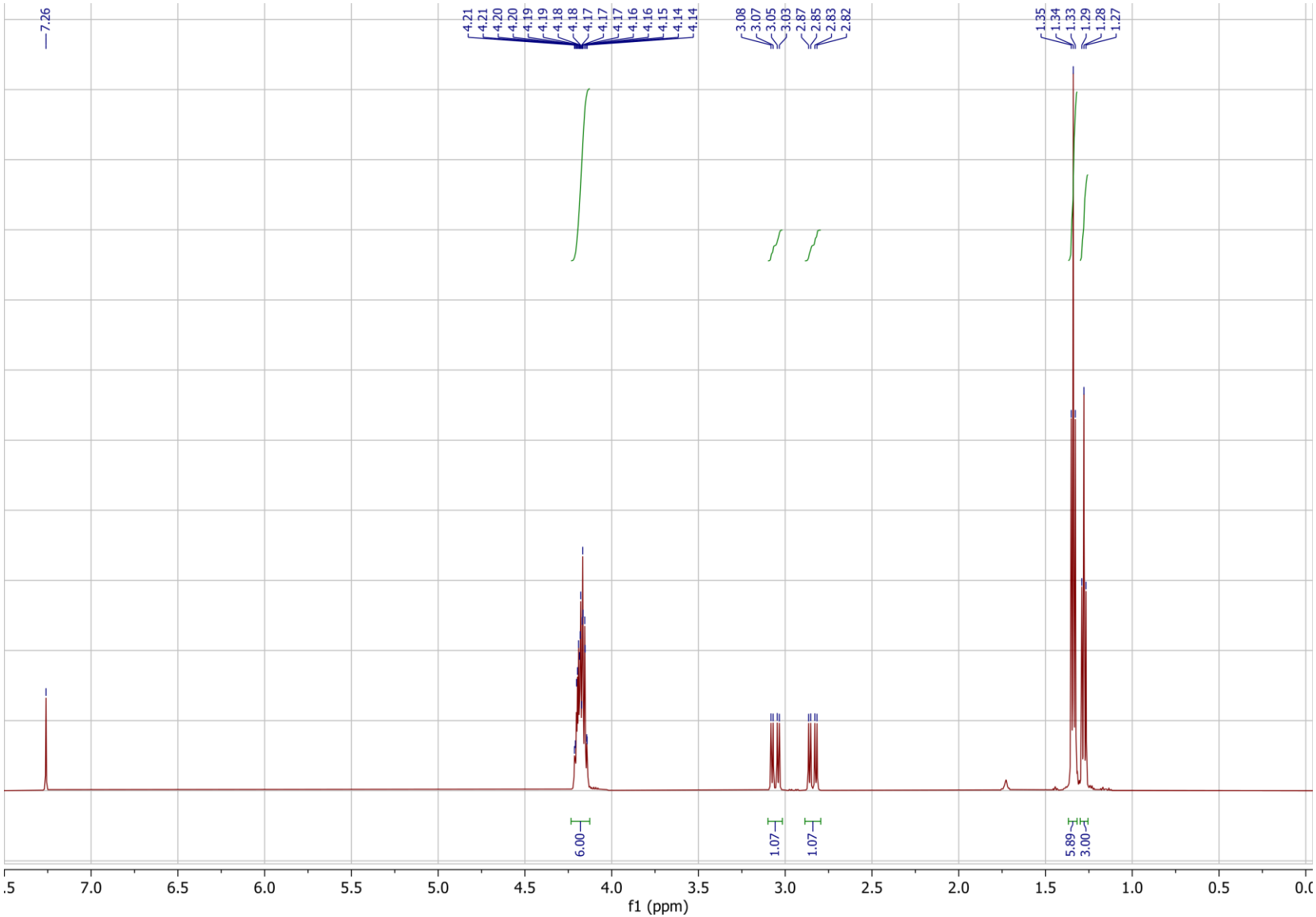

Triethyl 2-phosphonopropionate-1,2,3-$^{13}C_3$ (5.11), ^{1}H NMR spectrum (300 MHz, $CDCl_3$)

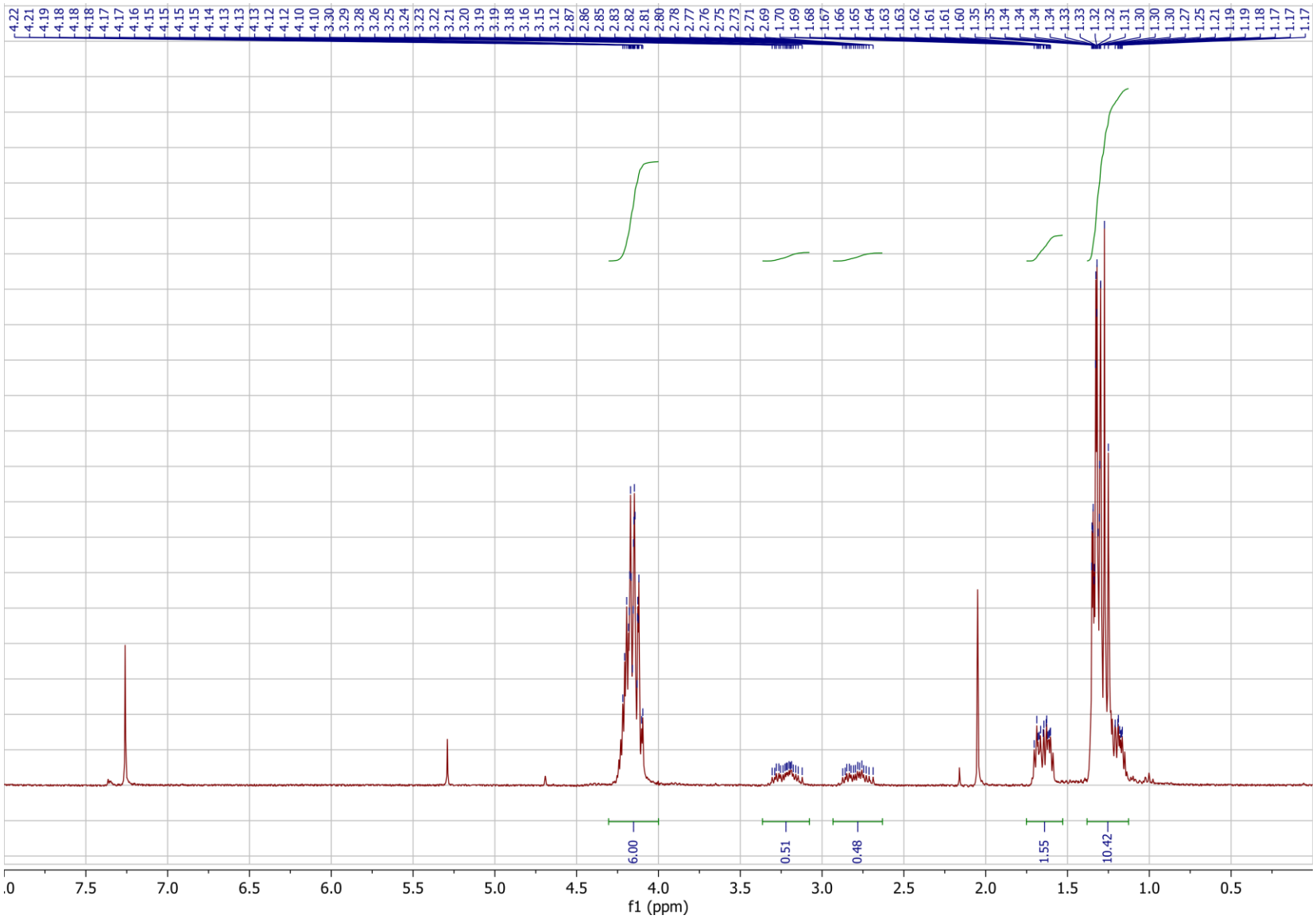

Ethyl *(E)*-3-oxo-5α-7α-hydroxy-cholest-25-enoate-25,26,27-$^{13}C_3$ (5.12), ^{1}H NMR spectrum (300 MHz, $CDCl_3$)

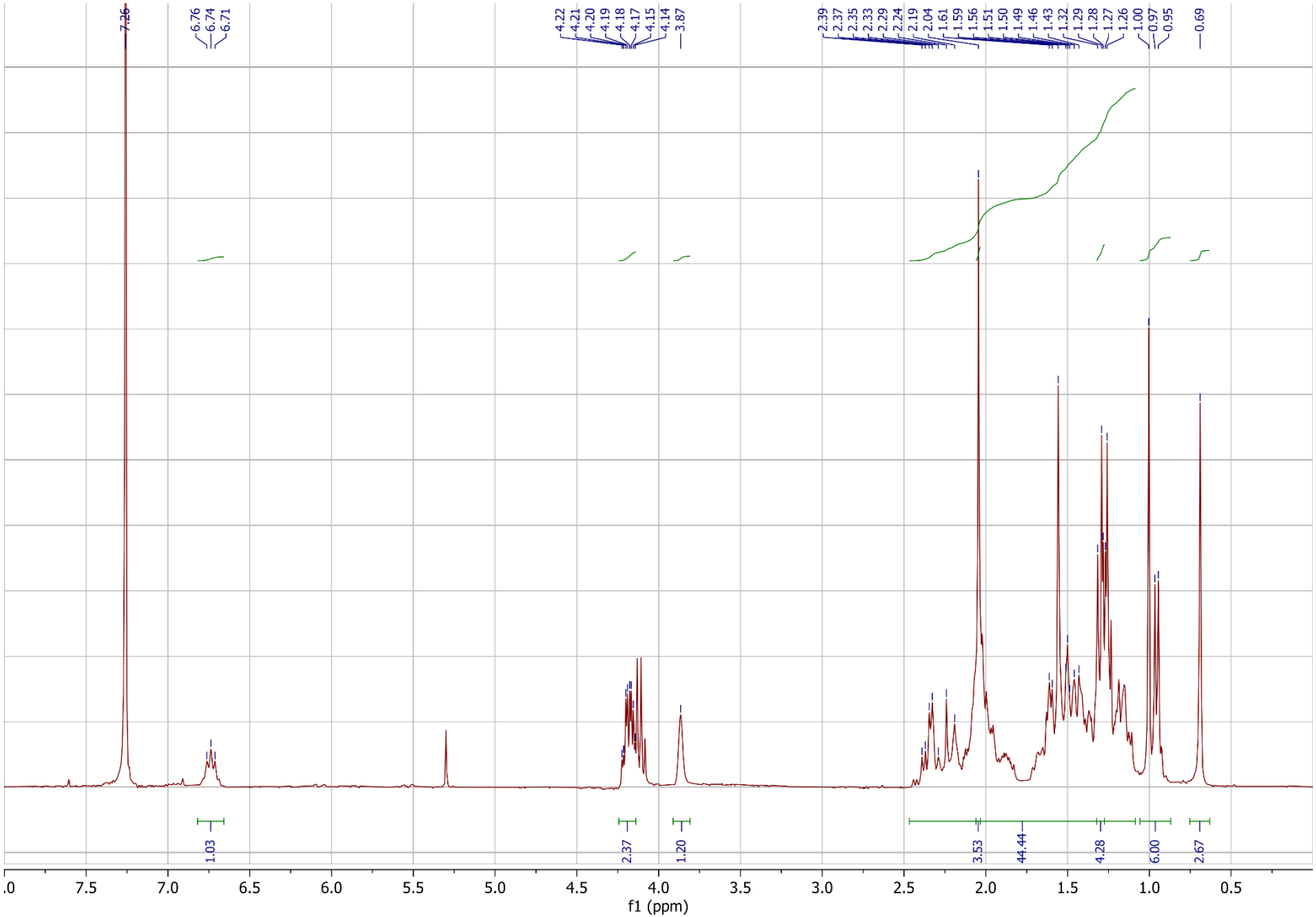

Ethyl *(E)*-3-oxo-5α-cholest-7,25-enoate-25,26,27-$^{13}C_3$ (5.13), ^{1}H NMR spectrum (600 MHz, $CDCl_3$)

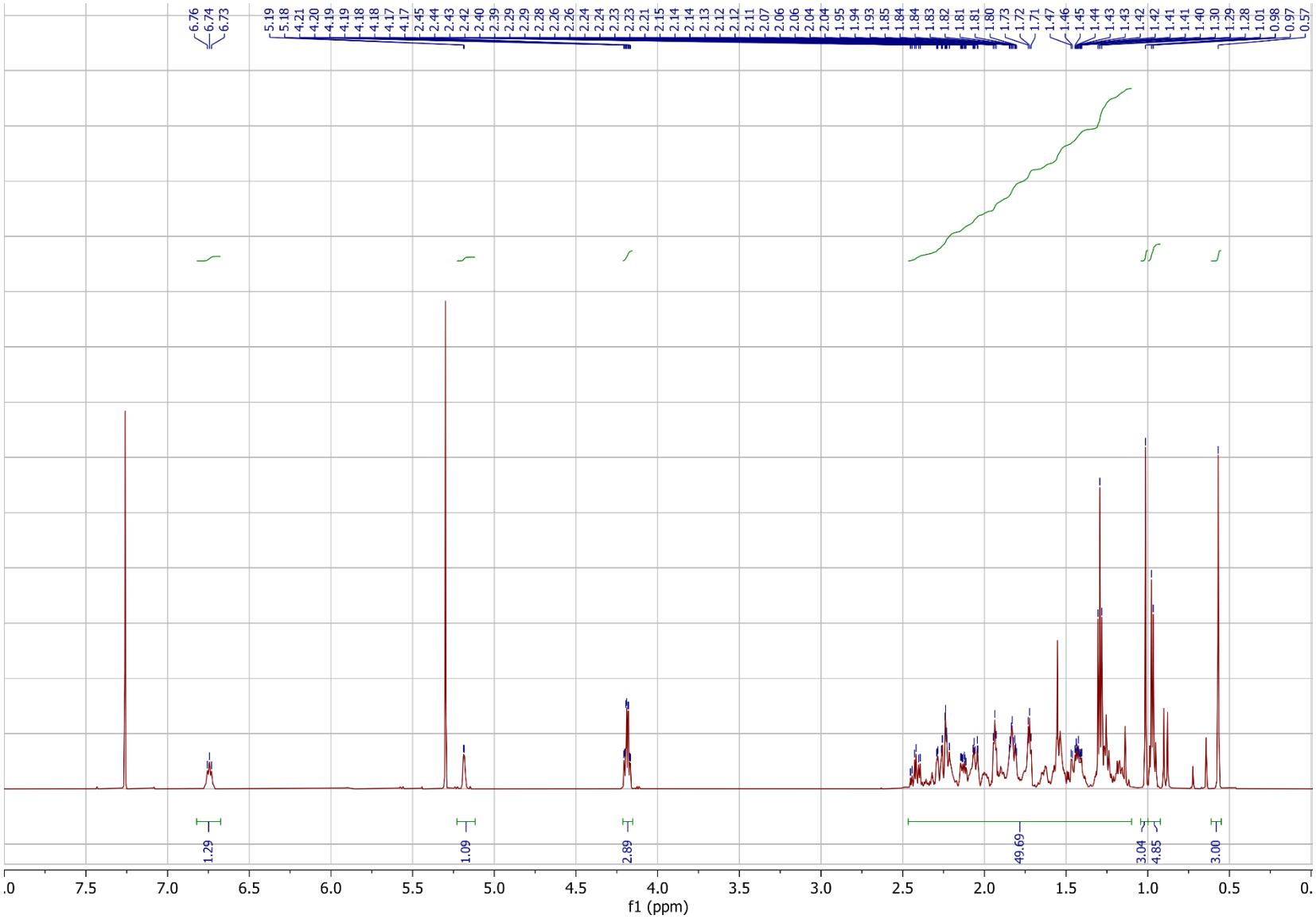

***(25S)*-Δ7-dafachronic acid-25,26,27-$^{13}C_3$ ($^{13}C_3$-dafa#2, $^{13}C_3$-5.3), ^{1}H NMR spectrum (600 MHz, $CDCl_3$)**

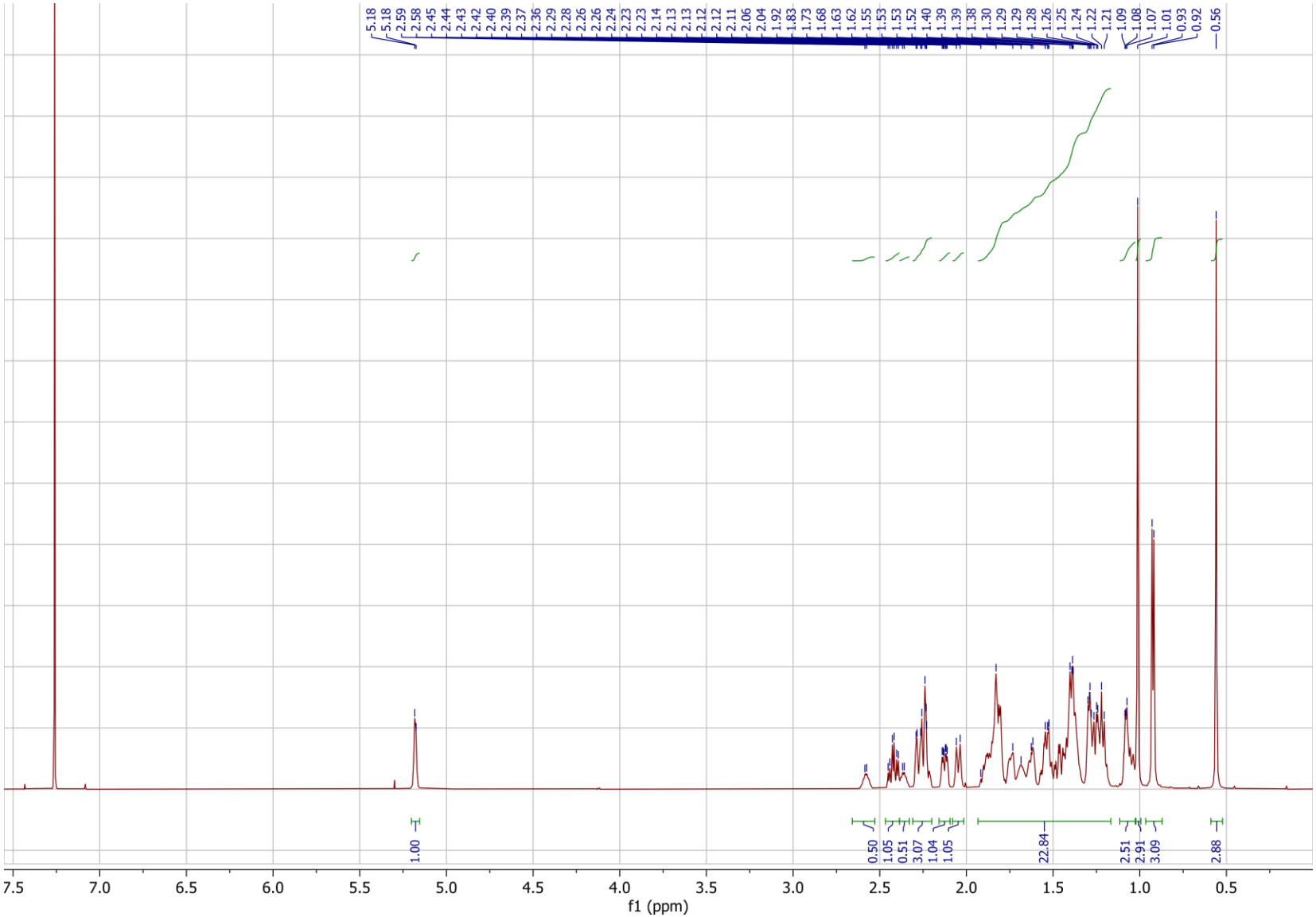

Triethyl 2-phosphonohexanoate (5.16), ^{1}H NMR spectrum (600 MHz, $CDCl_3$)

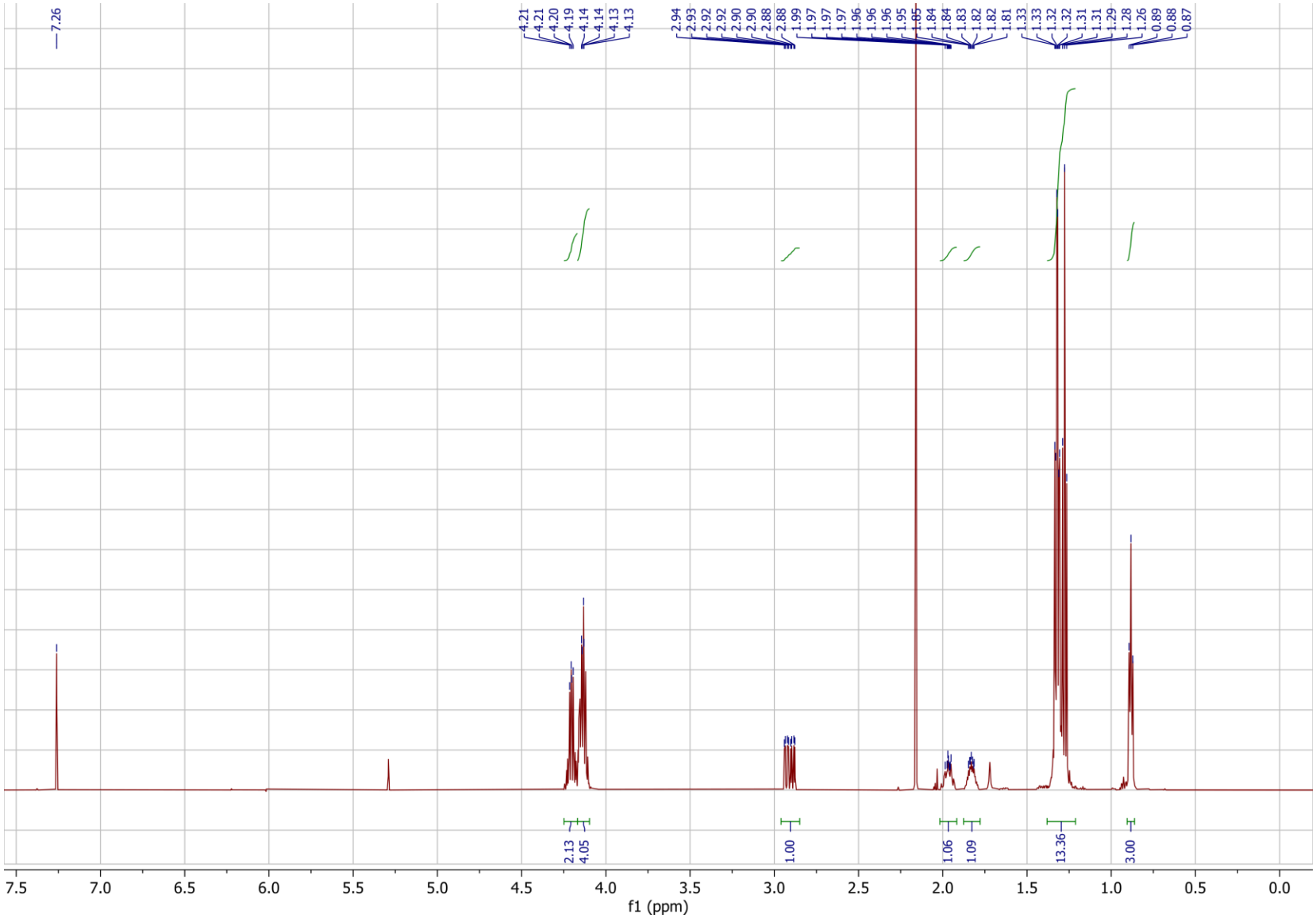

Ethyl (*E*)-3-oxo-5α-26-propylcholest-7,25-enoate, ^{1}H NMR spectrum (400 MHz, $CDCl_3$)

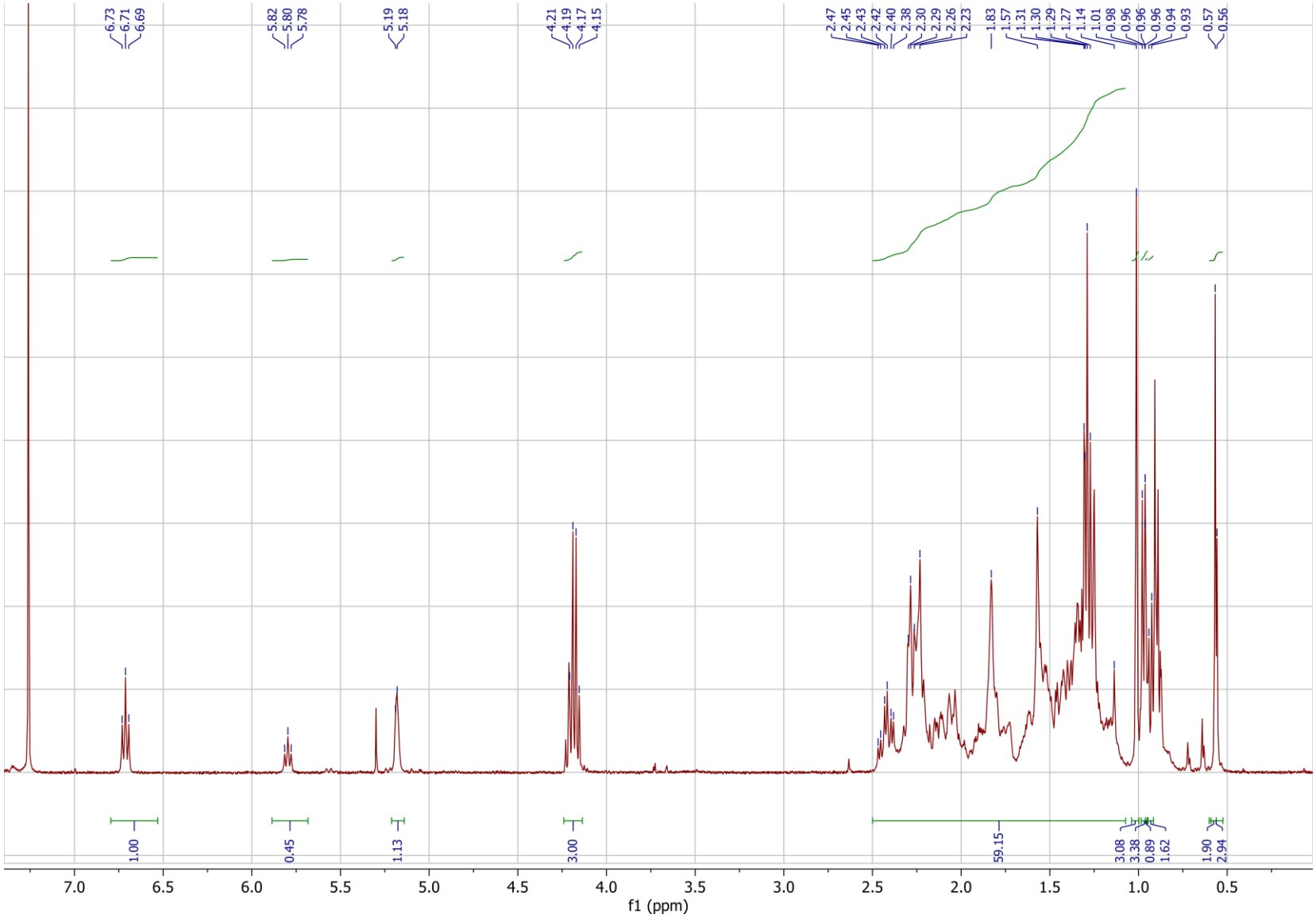

***(25S)*-butyl-Δ^7-dafachronic acid (butyl-dafa#2) (5.18), ^{1}H NMR spectrum (500 MHz, $CDCl_3$)**

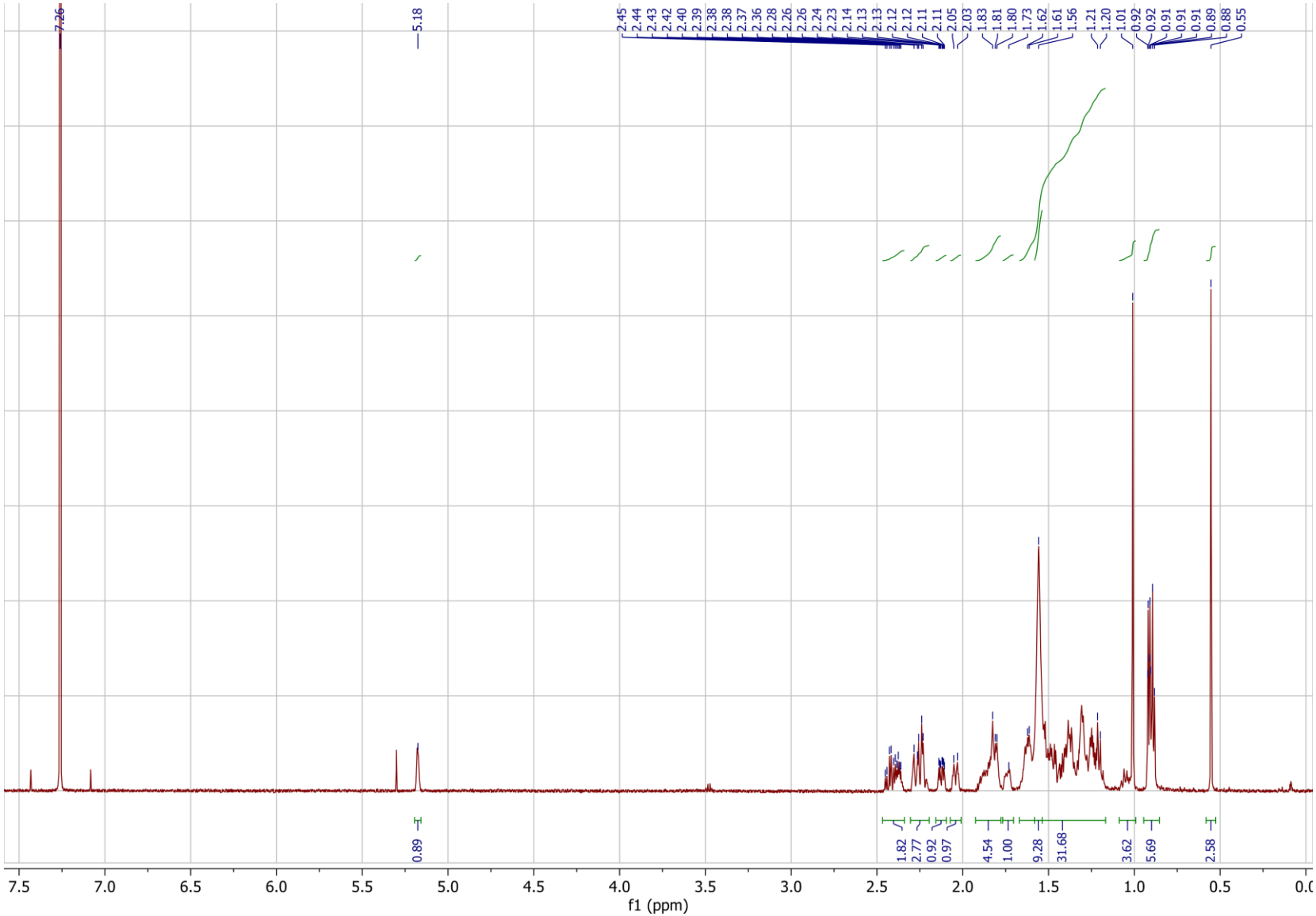

***(25S)*-3,3-azi-Δ^7-dafachronic acid (diazo-dafa#2, 5.20), ^{1}H NMR spectrum (500 MHz, $CDCl_3$)**

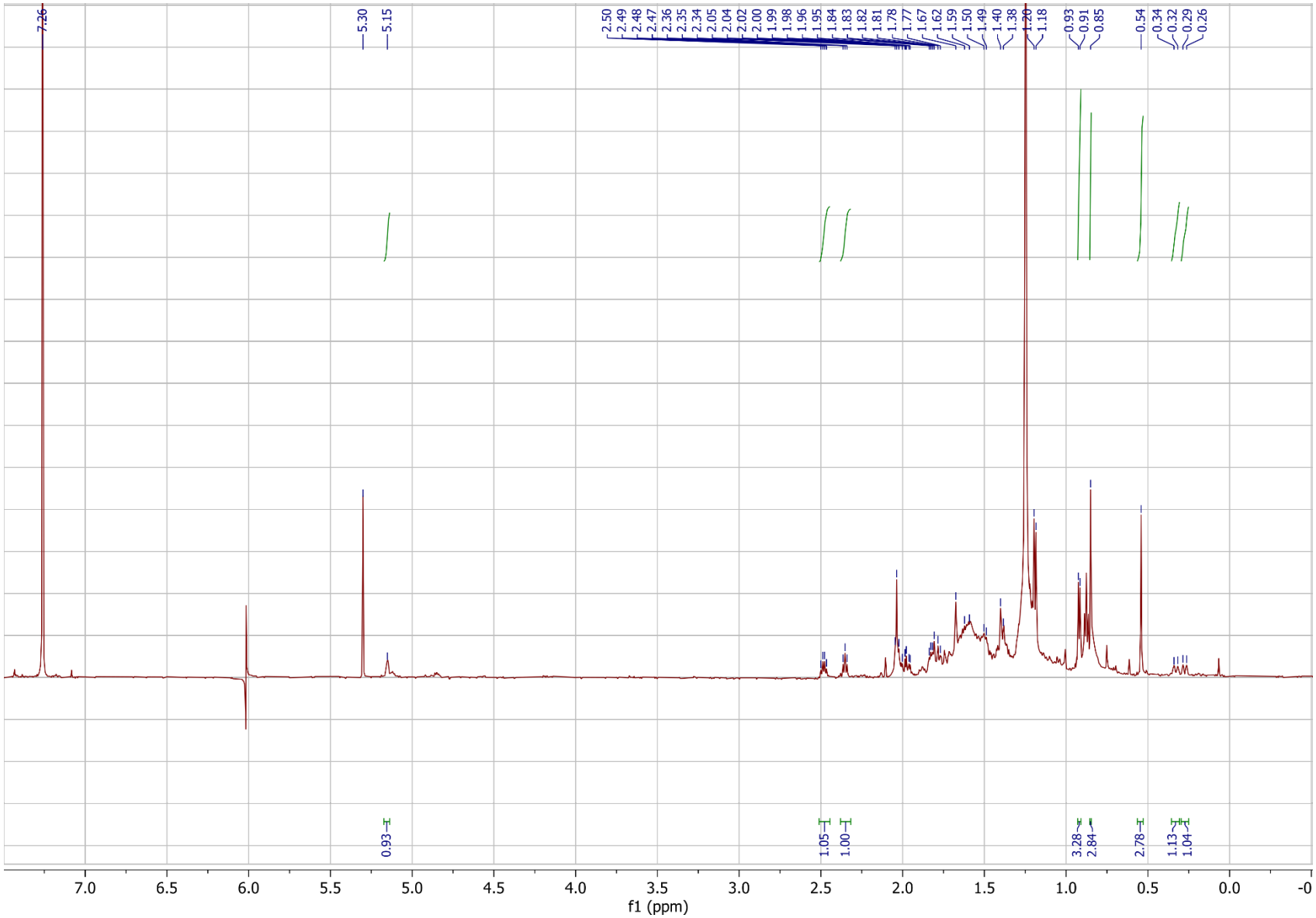

Supplemental Citations

(1) Van Der Klei, A., De Jong, R. L. P., Lugtenburg, J., Tielens, A. G. M. Synthesis and Spectroscopic Characterization of [1'-^{14}C]Ubiquinone-2, [1'-^{14}C]-5-Demethoxy-5-hydroxyubiquinone-2, and [1'-^{14}C]-5-Demethoxyubiquinone-2. *Euro. J. Org. Chem.* **17**: 3015-3023. **2002**.

(2) Takashima, M., Kato, K., Ogawa, M., Magata, Y. One-pot sequential reaction for the synthesis of versatile 11C-labeled olefin frameworks. *RSC Advances*. **44**: 21275-21279. **2013**.

(3) Judkins, J. Synthesis, Biosynthesis, and Function of Small Molecules Regulating Behavior and Development in *C. elegans*. *Doctoral dissertation, Cornell University*. **2014**.

(4) Kirschleger, B., Queignec, R. Heterogenous mediated alkylation of ethyl diethylphosphonoacetate. A "One Pot" Access to α-Alkylated Acrylic Esters. *Synthesis*. **11**: 926-928. **1986**.

(5) Zhang, Y. K. Synthesis of Nematode Signaling Molecules. *Doctoral dissertation, Cornell University*. **2019**.